Gold(I)-Catalyzed Hydrofunctionalizations of Allenes with Nitrogen and Oxygen Nucleophiles

by

Alethea Nikeisha Duncan

Department of Chemistry
Duke University

Date:_____

Approved:

_____
Ross A. Widenhoefer, Supervisor

_____
Stephen L. Craig

_____
Jiyong Hong

_____
Barbara Ramsay Shaw

Dissertation submitted in partial fulfillment of
the requirements for the degree of Doctorate of Philosophy in the Department of Chemistry in the Graduate School
of Duke University

2011

ABSTRACT

Gold(I)-Catalyzed Hydrofunctionalizations of Allenes with Nitrogen and Oxygen Nucleophiles

by

Alethea Nikeisha Duncan

Department of Chemistry
Duke University

Date:_____

Approved:

_____
Ross A. Widenhoefer, Supervisor

_____
Stephen L. Craig

_____
Jiyong Hong

_____
Barbara Ramsay Shaw

An abstract of a dissertation submitted in partial fulfillment of the requirements for the degree of Doctorate of Philosophy in the Department of Chemistry in the Graduate School of Duke University

2011

Abstract

The importance of nitrogen-containing compounds in human life has drawn us to focus on the preparation of amine derivatives, combined with the limitations associated with traditional methods for the formation of C-N bonds has prompted us to develop new and efficient syntheses, of amine and ether derivatives and explore the mechanisms of the gold(I)-catalyzed reactions.

A mixture of AuCl[P(*t*-Bu)$_2$-biphenyl] (5 mol %) and AgOTf (5 mol %) served as an effective catalyst for the intermolecular hydroamination of allenes with arylamines to form *N*-prenylaniline and *N*,*N*-diprenylaniline derivatives. This gold(I)-catalyzed protocol was effective for the formation of arylamines at non-forcing conditions with wide substrate scope in both allene and aniline, in high yields with good regioselectivity diastereoselectivity.

The mechanism of the gold(I)-catalyzed hydroalkoxylation and hydroamination of alcohols and carbamates with allenes, catalyzed by AuIPrCl (IPr= 1,3-bis(2,6-diisopropylphenyl)imidazol-2-ylidine) and AgOTf was investigated. The experimental rate laws for both reactions indicate first-order behavior in nucleophile and catalyst and zero-order behavior in catalyst. We propose an outer-sphere mechanism with turnover limiting protonolysis for the gold(I)-catalyzed hydrofunctionalization of allenes with

alcohols or carbamates based on kinetic isotope effect, saturation behavior, and stereochemical analysis of hydroalkoxylation.

The mechanism of gold(I)-catalyzed hydroamination of allenes with arylamines was examined. Specifically, we explored the hydroamination of 3-methy-1,2-butadiene with aniline catalyzed by AuCl[P(*t*-Bu)$_2$*o*-biphenyl] (5 mol %) and AgOTf (5 mol %) in dioxane at 45 °C to form *N*-prenylaniline and *N*,*N*-diprenylaniline. The kinetics of this reaction were determined to be first-order in aniline, allene, and catalyst. We have concluded that the mechanism for the gold(I)-catalyzed intermolecular hydroamination of allenes with arylamines involves outer-sphere attack of aniline on the gold-π-allene complex based on stereochemical analysis of the hydroamination product from the reaction of an enantiomerically enriched allene, (*R*)-1-phenyl-1,2-butadiene, with 3-bromoaniline.

Dedication

I would like to dedicate this doctoral dissertation to love: love of life, love of chemistry, and love of friends.

Contents

List of Tables

List of Figures

List of Schemes

Acknowledgements

Regardless of what we achieve in life there is always someone that helps us along the way. I have been fortunate enough to have several people assist me in this journey over the past 5 years. I am extremely grateful to each and every one of them for the role they have played in my life. Without their support I would not be here today. Above all I would like to thank Professor Ross A. Widenhoefer for motivating me to do everything to the best of my ability. He has provided me with invaluable insight into this field. Under his guidance I have grown as a professional making me better able to analyze both experiments and situations.

My family members have also played a crucial role in getting me to this day. I thank my mother for always being available to provide her own unique perspective to whatever issue I was facing. My father on the other hand assisted on the day to day trouble shooting. My elder sister, Thea, acted as my personal cheerleader always convinced of my own capabilities. Even my little brother Aeon helped out, since I've always wanted to be a good role model to him. My other sisters, Zinzi and Laura, for making sure I keep my "eye on the prize" and distracting me with entertaining stories about life in the real world.

Then of course, I would like to thank my Duke Family, the people near and dear to me who have made Duke and Durham home. "The Girls" always being there for me

from running columns late Friday nights, Gossip Girl night, yoga/gym time, trips to Greensboro, and our many weekend adventures. Not to be outdone, “My Boys” always came through, from Wishful Wednesdays to road-side emergencies to slip-and-slide, and of course BYA. I would like to thank my chemistry mom, Dr. Tonya Gerald, who always stepped in for mom-like duties and advice, both chemistry and non-chemistry related, as well as my GSA family and key administrators. I will always have fond memories of Duke because of my friends, co-workers, faculty and staff who embraced me through my journey. I am forever grateful for everything you’ve done. FOREVER DUKE!

1 Gold (I)-Catalyzed Intermolecular Hydroamination of Allenes with Arylamines

Portions of this chapter have been published: Duncan, A. N.; Widenhoefer, R.A. *Synlett* **2010**, 419-422.

1.1 Introduction

Hydroamination is the formal addition of the N-H bond of an amine derivative across a C-C multiple bond. This reaction has attracted considerable attention due to the importance of carbon-nitrogen bonds in biological systems and it is an atom economical and highly desirable process for the preparation of amine derivatives. [1-4] As a result, considerable effort has been directed toward the development of hydroamination reactions using alkenes, alkynes, and allenes. [5, 6] The majority of hydroamination reactions found in literature are intramolecular reactions as opposed to intermolecular protocols because of the unfavorable entropy associated with intermolecular hydroamination processes and the modest enthalpy of both processes.

In 1973, Coulson and coworkers developed a transition metal-catalyzed reaction of allene with various amines or carboxylic acids employing catalytic amounts of group VIII metal complexes to form derivatives of 2,3-dialkyl-1,3-butadienes. [7] For example, allene and methylamine are treated with bis(triphenyl phosphine)(maleic anhydride)-palladium in THF at 120 °C for 6 h to form *N*-3-dimethyl-2-methylene-3-butenylamine in 42 % yield (eq 1.1). [7]

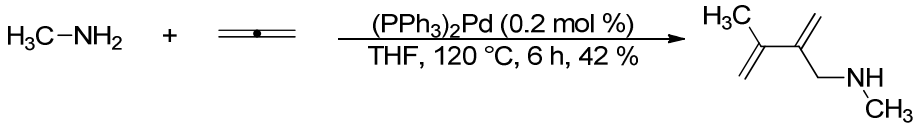

(eq 1.1)

In 1995, Cazes and coworkers reported the palladium-catalyzed hydroamination of allenes to form substituted allylic amines in the presence of triethylammonium iodide.

In one experiment, phenylallene and pyrolidine were treated with a catalytic amount of $Pd(dba)_2$ [dba = dibenzylideneacetone] (5 mol %) and PPh_3 (10 mol%) in THF at 60 °C for 32 h to form *N*-(3-phenyl-2-propenyl) pyrolidine in 89 % yield (eq 1.2). [8]

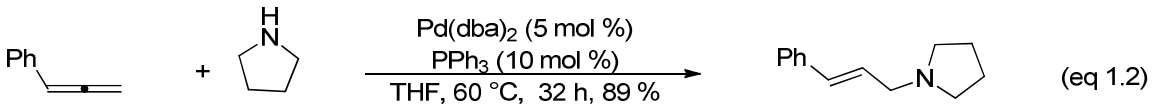

(eq 1.2)

Yamamoto improved Cazes' procedure by employing $Pd_2(dba)_3$ and dppf [1,1'-bis(diphenylphosphino ferrocene] as the catalyst. In one experiment, phenylallene and diethyl 2,2'-iminodiacetate were treated with catalytic amounts of $Pd_2(dba)_3$ (5 mol %), dppf (5 mol %) and acetic acid as an additive in THF at 80 °C for 8 h to form *N*-[(*E*)-3-phenyl-2-propen-1-yl]-ethyl ester glycine in 98 % yield (eq 1.3). [9] Yamamoto's catalytic system was restricted for the intermolecular hydroamination of mono-substituted allenes with protected amines.

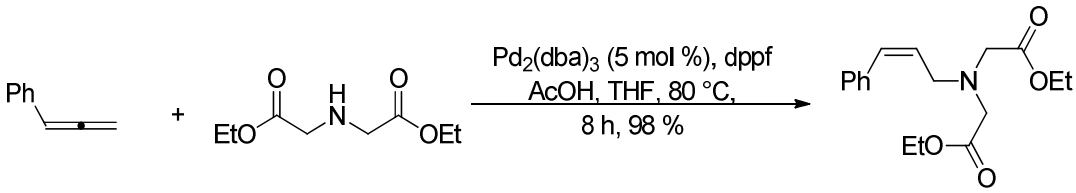

(eq 1.3)

Bergman and coworkers developed a zircocene bis(amide) [$Cp_2Zr(NH\text{-}2,6\text{-}Me_2C_6H_3)_2$] catalyst for the hydroamination of alkynes and allenes with aniline derivatives. For example, allene and 2,6-dimethylaniline are treated with $Cp_2Zr(NH\text{-}2,6\text{-}Me_2C_6H_3)_2$ (2.7 mol %) in C_6H_6 at 90 °C for 6 days to form 2,6-dimethylimine of acetone in 83 % yield (eq 1.4). [10]

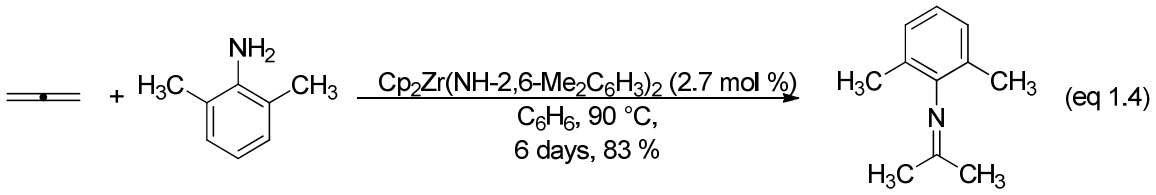

(eq 1.4)

Bergman and coworkers completed a kinetic investigation for the reaction of 2,6-dimethylaniline to diphenylacetylene catalyzed by zircocene bis(amide). They concluded that the reaction was first-order with respect to [catalyst] and [alkyne], but inverse first-order in [amine]. [10] This was the first example of a group IV metal complex catalyzing the hydroamination of a C-C multiple bond; however, amines that are sterically less bulky than 2,6-dimethylaniline could not undergo intermolecular hydroamination with alkynes or allenes. Additional experiments conducted by Bergman and coworkers revealed that titanium-based imido complexes like Cp_2TiMe_2 function as a catalyst precursor for hydroamination reactions of allenes and alkynes with arylamines, alkylamines, and hydrazine. [11] For instance, reaction of allene with 2,6-dimethylaniline and Cp_2TiMe_2 (10 mol %) in C_6D_6 at 90 °C for 2 h formed 2,6-dimethylimine of acetone in 87 % yield, an improvement from 6 days to 2 h in comparison to the zircocene bis(amide) complex (eq 1.5). [11]

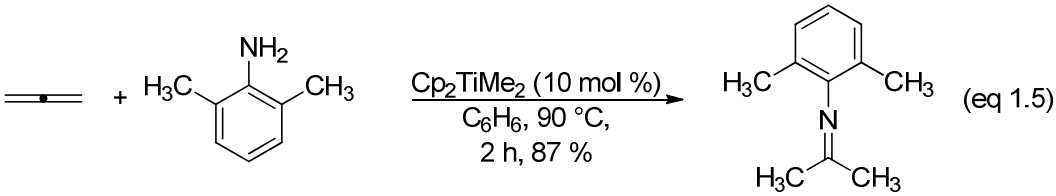

(eq 1.5)

Kinetic studies of the above reaction with varying concentrations of catalyst, pyridine, and amine revealed that the reaction is zero-order in [amine], inverse first-order in [pyridine], and first-order in [catalyst]. This result contrasts the previously studied zircocene bis(amide) catalytic system that exhibited an inverse first-order dependence on [amine]. The proposed mechanism for the intermolecular hydroamination of 2,6-dimethylaniline and allene catalyzed by imidotitanium complex is outlined in Scheme 1.1. [11, 12]

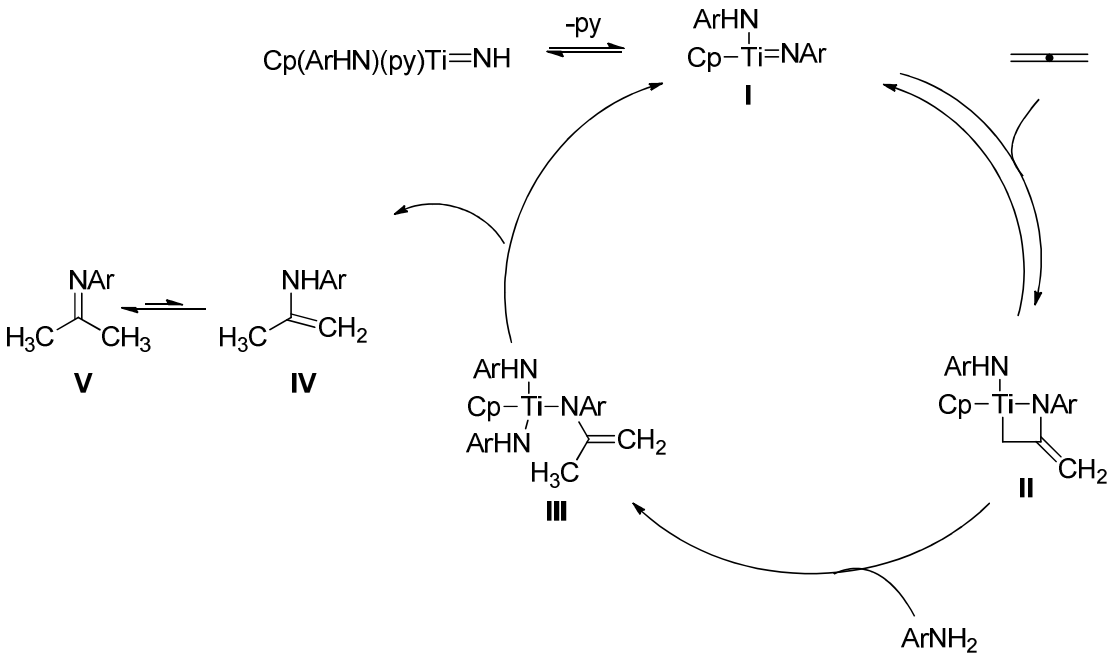

Scheme 1.1. Proposed mechanism for the intermolecular hydroamination of 2,6-dimethylaniline and allene catalyzed by an imidotitanium complex.

Pyridine reversibly dissociates from the mono (Cp) complex to generate **I**, the Lewis base-free imido complex. **I** undergoes formal [2+2] cycloaddition with allene to form azametallacyclobutane, **II**. Complex **II** is rapidly protonated by amide to generate a

tris(amido) titanium-complex, **III**. Elimination expels the enamine product, **IV**, which then tautomerizes to the thermodynamically stable imine, **V**, and regenerates the active catalyst **I**. [12, 13]

Shafer and coworkers have employed a bis(amidate)-bis(amido) titanium complex for the intermolecular hydroamination of alkynes with alkylamines. [14] The bis(amidate)-bis(amido) titanium complex catalyzes the intermolecular hydroamination of substituted allenes with arylamines and alkylamines; however, reactions with alkylamines required a higher catalyst loading and high temperature than reactions with arylamines. For example, a mixture of phenylallene and 2,6-dimethylaniline are treated with bis[*N*-[bis(isopropyl)phenyl]benzimidate]bis[*N*-(ethyl)ethanaminato]titanium (bis(amidate)-bis(amido) titanium complex) (5 mol %) in toluene-d_8 at 90 °C for 7 h to form 2,6-dimethylimine of acetone in 76 % yield (eq 1.6). In contrast, the reaction of phenylallene and isopropylamine requires a 10 mol % of bis(amidate)-bis(amido) titanium complex in C_6D_5Br at 120 °C for 24 h to form *N*-[(*E*)-1-methyl-2-phenylethylidene] propan-2-amine in 65 % yield (eq 1.7). [15]

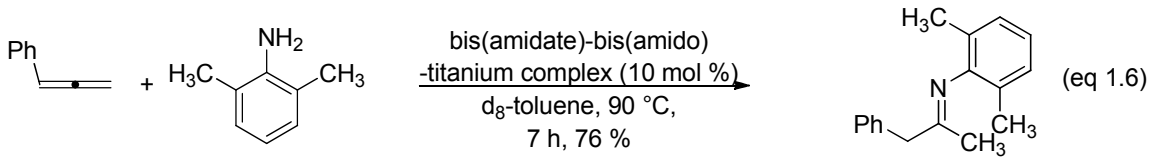

(eq 1.6)

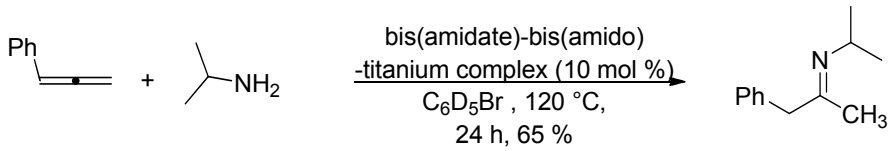

(eq 1.7)

Intramolecular and intermolecular hydroamination methods have been developed employing group IV metal complexes as catalyst, with a metal-imido (M=NR) proposed as a key intermediate. [13, 16-19] Bergman and coworkers develop an intermolecular hydroamination protocol for alkynes and allenes using an imido complex of tantalum. [20] In one experiment, a mixture of allene and 2,6-dimethylaniline are treated with $[(PhCH_2)Ta{=}NCMe_3)]^+$ (5 mol %) and $KB(C_6F_5)_4$ (5 mol %) in C_6D_6 at 135 °C for 24 h to form 2,6-dimethylimine of acetone in greater than 95 % yield (eq 1.8).

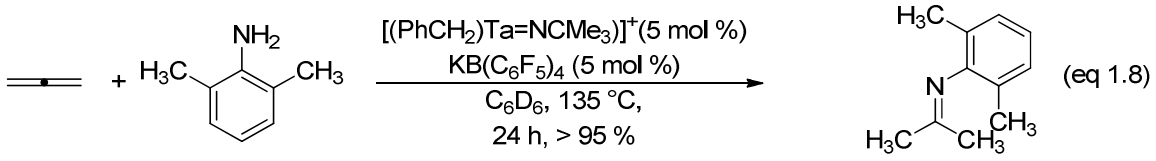

(eq 1.8)

Yamamoto and coworkers have developed an intermolecular hydroamination catalyst system for the reaction of allenes with arylamines at ambient temperature, which is not based on a group IV or group V metal. In lieu of a group IV or group V metal, Yamamoto employed a gold(III)-catalyst system for the intermolecular

hydroamination of allenes with aniline in THF at ambient temperature, which also allowed for the transfer of chirality from allenes to the hydroamination product with high enantiomeric enrichment. [21] In one experiment, a mixture of phenylallene and aniline are treated with a catalytic amount of $AuBr_3$ (10 mol %) in THF at 30 °C for 1-5 h to form *N*-[(2*E*)-3-phenylprop-2-en-1-yl]aniline in 78% yield (eq 1.9). In a second experiment, a mixture of (*R*)-1-phenyl-1,2-butadiene (94 % ee) and two equivalents of aniline was treated with a catalytic amount of $AuBr_3$ (10 mol %) in THF at 30 °C to form *N*-[(1*S*,2*E*)-1-methyl-3-phenylprop-2-en-1-yl]aniline in 68% yield and 88 % ee (eq 1.10).

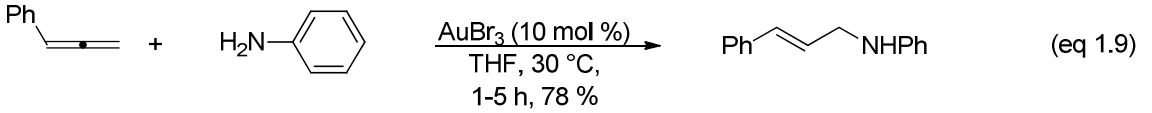

(eq 1.9)

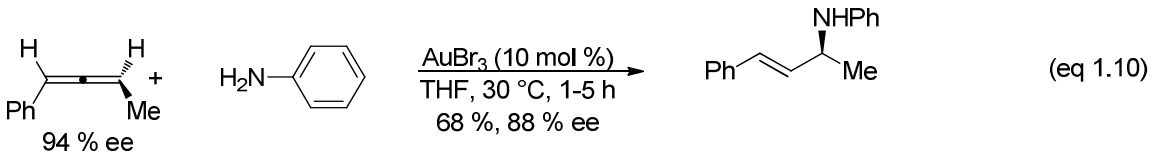

(eq 1.10)

Although Yamamoto's gold(III)-catalyzed protocol is effective at catalyzing the hydroamination of mono substituted allenes, it gave poor yields for 1,1 and 1,3-disubstituted allenes. For instance, a mixture of 3-phenyl-1,2-butadiene and aniline are treated with a catalytic amount of $AuBr_3$ (10 mol %) in THF at 30 °C for 1-5 h to form *N*-[(2*E*)-3-phenylbut-2-en-1-yl]aniline in 9% yield (eq 1.11)

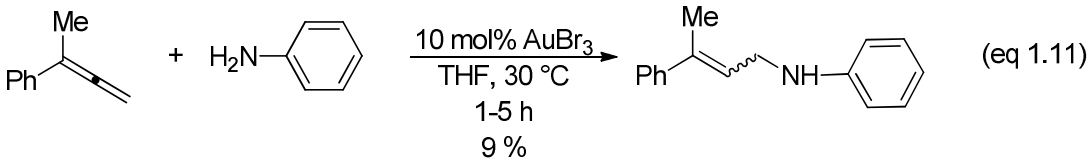

(eq 1.11)

The mechanism for the gold(III)-catalyzed intermolecular hydroamination of allenes with aniline was proposed in Scheme 1.2 based on experimental data obtained with the use of chiral allenes (*R*)-1-methyl-3-phenylallene and (*R*)-1-pentyl-3-pentylallene. Yamamoto proposed an inner-sphere pathway because of the stereoselectivity and regioselectivity observed in the formation of *N*-[(1*S*,2*E*)-1-methyl-3-phenylprop-2-en-1-yl]aniline (eq 1.10). These results point towards the formation of a gold-amine complex, followed by addition to the allene. The catalytic cycle is probably initiated by the coordination of allene to the gold-amine complex, **VI,** to form the gold-π-allenyl complex, **VII**. Amino auration of **VII** gives **VIII**. Protonation of **VIII** gives the hydroamination product and regenerates the catalyst, $AuBr_3$.

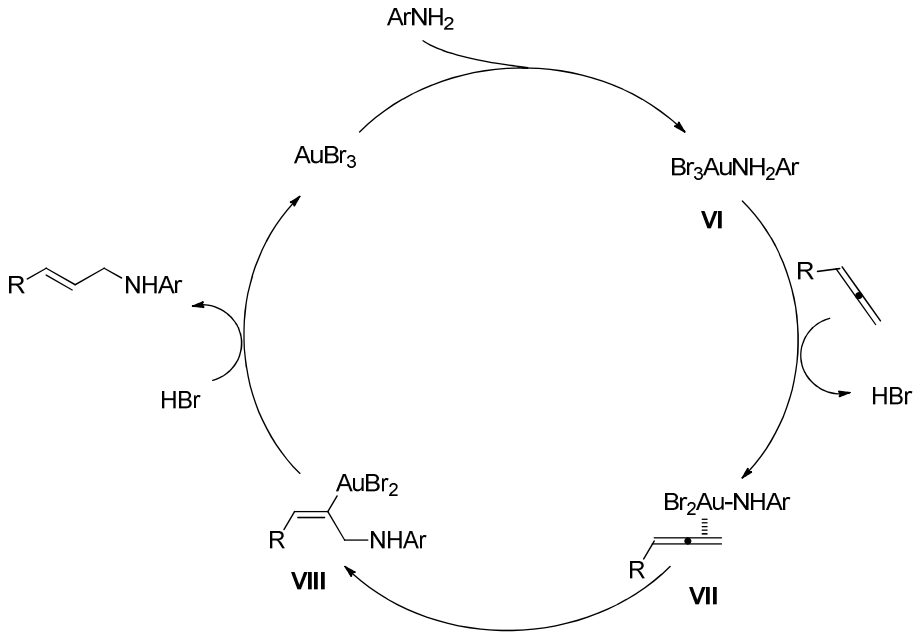

Scheme 1.2. The proposed mechanism for the gold(III)-catalyzed intermolecular hydroamination of allenes with anilines

Gold(III) and gold(I)-catalytic system catalyze the intermolecular hydroamination of allenes with secondary and primary amines. [22-24] In particular, Yamamoto and coworkers employed morpholine with allene catalyzed by a cationic gold(I) complex with AgOTf in toluene to give the corresponding allylic amines. As an example, phenylallene and morpholine were treated with (Cl)Au[PPh_2(*o*-tolyl)] (10 mol %) and AgOTf (10 mol %) in toluene at 80 °C for 24 h to give 4-[(*E*)-3-phenylprop-2-en-1-yl]morpholine in 66 % yield (eq 1.12). [23] It should be noted, that morpholine possesses unusually low basicity (pKa 8.36) relative to other alkyl amines (piperidine 11.32 and dimethylamine 10.64) , which may be responsible for the effectiveness for the effectiveness of morpholine in this reaction. [25]

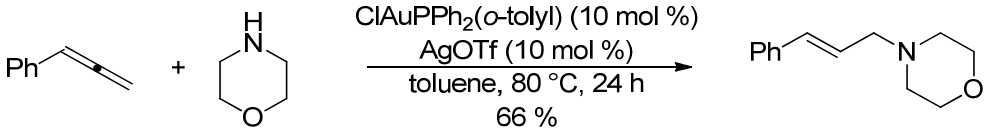

(eq 1.12)

In an effort to increase the scope with respect to the nucleophile for the intermolecular hydroamination reaction with allenes, Bertrand and coworkers developed a cationic gold(I) complex supported by a cyclic(alkyl)(amino)carbine (CAAC) ligand to catalyze the addition of ammonia to a variety of unactivated alkynes and allenes. For example, a mixture of tetraphenylallene and ammonia are treated with a catalytic mixture of **Cat1** (5 mol %) in C_6D_6 at 175 °C for 44 h to give 1,1,3,3-tetraphenylprop-1-en-2-amine in 79 % yield (eq 1.13). Bertrand's (CAAC)gold(I) complex was also able to promote the addition

of all types of nontertiary amines to a variety of allenes, affording allylic amines in good to excellent yields. *N*-methylaniline and 3-methyl-1,2-butadiene are treated with a catalytic amount of **Cat1** (5 mol %) in C_6D_6 at 70 °C for 12 h to form *N*-methyl-*N*-(3-methylbut-2-en-1-yl)aniline in 98 % yield (eq 1.4).

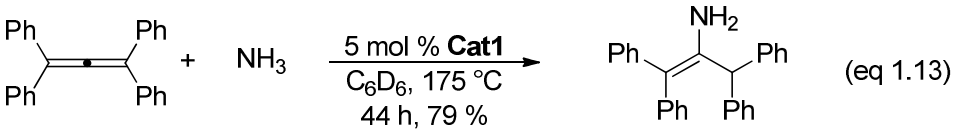

(eq 1.13)

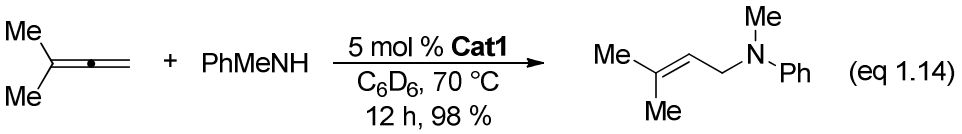

(eq 1.14)

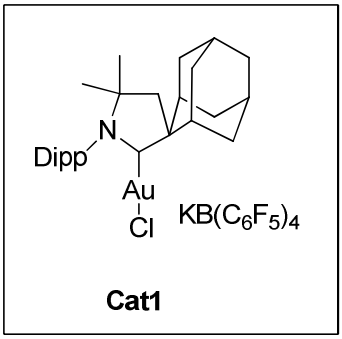

To gain insight into the mechanism of gold(I)-catalyzed hydroamination of allenes, Bertrand and coworkers conducted two experiments to evaluate the complexation of allene and amine to **Cat2** (Scheme 1.3). In one experiment, excess allene is added to **Cat2** in deuterated benzene at room temperature and the solution was heated at 50 °C; however, the desired allene gold complex was not formed. In another experiment, diethylamine is treated with **Cat2** in deuterated benzene at room temperature to form amine gold complex, **IX**. This complex was then treated with excess allene in C_6D_6 at 70

°C for 16 h to form complex **X**. These observations suggested an inner-sphere mechanism with transient formation of a tricoordinated gold complex. [22]

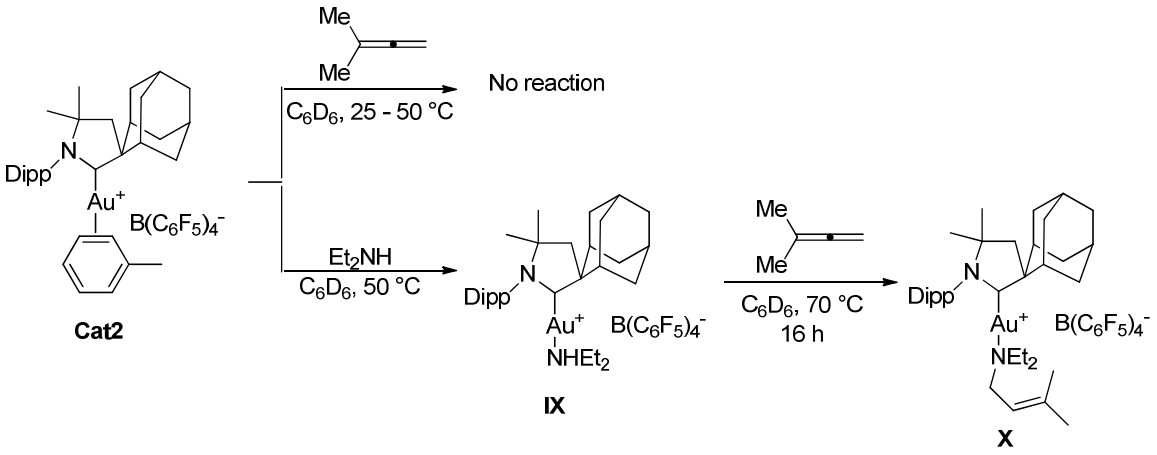

Scheme 1.3. Experiments to approach the reaction mechanism for the gold(I) catalyzed intermolecular hydroamination of allenes with secondary amines. [22]

Toste and coworkers have developed a gold(I)-catalyzed protocol for the intermolecular hydroamination of allenes with hydrazides. [26] For example, a mixture of 1,7-diphenylhepta-3,4-diene and methyl carbazate (2.5 equivalents) are treated with a catalytic amount of $(Ph_3P)AuNTf_2$ (9 mol %) in $MeNO_2$ at 45 °C for 12 h to form 2-[5-phenyl-1-(2-phenylethyl)-2-penten-1-yl]-hydrazine carboxylic acid methyl ester in > 95 % conversion (eq 1.14). [26]

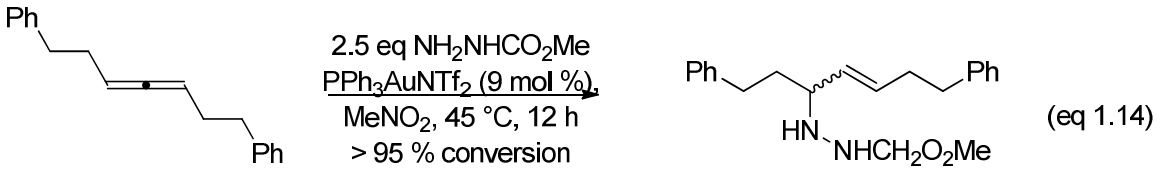

Kinetic and mechanistic studies were conducted for the reaction above, and it was concluded that the reaction was first-order in [gold] and [allene], but zero-order in [nucleophile]. Toste and coworkers also concluded that allene activation was the rate limiting step. [26] Computational studies supported an outer-sphere mechanism and a two-step mechanism with no intermediates. [26] Scheme 1.3 shows the proposed mechanism for the hydroamination of 1,7-diphenylhepta-3,4-diene with hydrazine catalyzed by $Ph_3PAuNTf_2$.

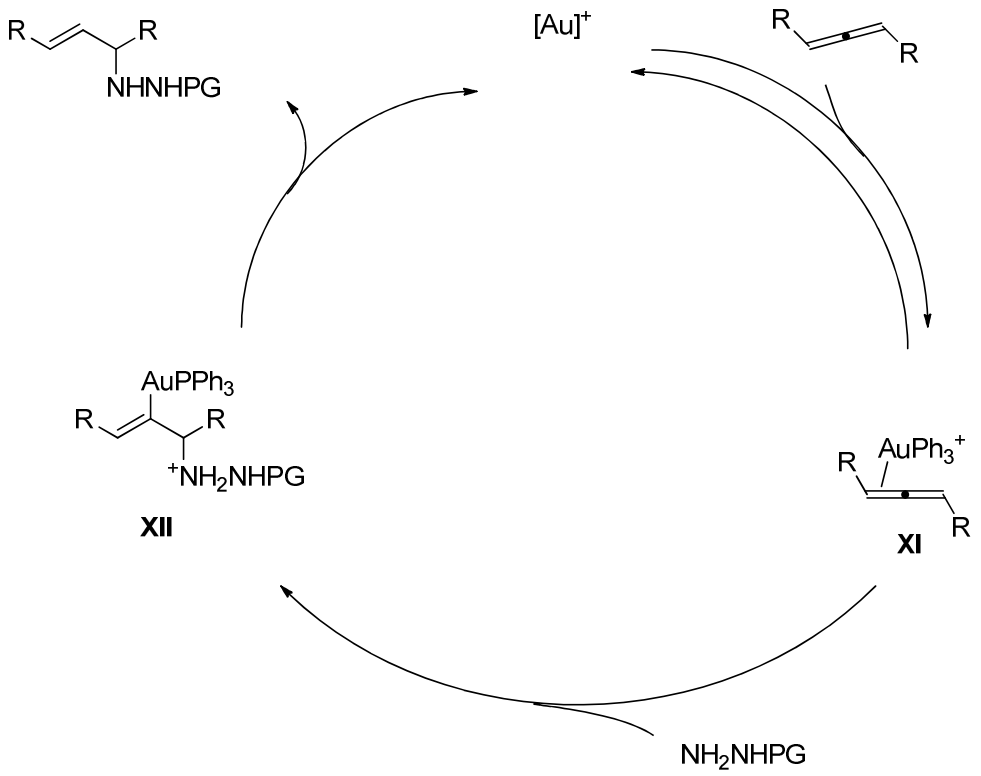

Allene undergoes reversible coordination to the cationic gold(I) complex to form **XI**. Rate-limiting formation of an η^1-Au-allene complex followed by fast irreversible nucleophilic addition occurs from an outer-sphere attack to form **XII**, followed by

irreversible protodemetalation of **XII** to form the hydroamination product and regenerate the cationic gold(I) complex.

As noted above, group IV, cationic gold(I) phosphine, and gold cyclic(alkyl)(amino)carbene complexes have been shown to catalyze intermolecular hydroamination reactions with secondary alkylamines and primary amines, but these reactions have been restricted to morpholine as the alkylamine or required forcing reaction temperatures. Widenhoefer and coworkers developed a platinum(II)-catalyzed intermolecular hydroamination system of monosubstituted allenes with secondary alkylamines at non-forcing conditions. Treatment of benzyl methyl amine with dimethyl 2,3-butadienyl malonate and a 1:1 mixture of (dppf)$PtCl_2$ and AgOTf in toluene at 80 °C for 24 h led to the isolation of dimethyl (4-(benzyl(methyl)amino)-2-butenyl)malonate in 86 % yield (eq 1.15). [27]

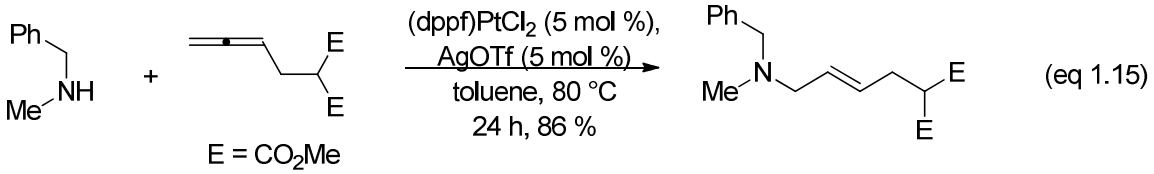

(eq 1.15)

The catalytic systems noted in the preceding paragraphs do not include protocols for the hydroamination of both mono and di-substituted allenes with arylamines at moderate temperatures with good to excellent yields. In response to this limitation, and motivated by biological and pharmaceutical importance of *N*-allyl aniline derivatives, [28, 29] Widenhoefer and coworkers developed gold(I)-catalyzed protocols for the

intermolecular hydroamination of ethylene and 1-alkenes with cyclic ureas [30] and the intermolecular hydroamination of allenes with *N*-unsubstituted carbamates. [31] For example, treatment of 1-methyl-imidazolidin-2-one with ethylene (60 psi) and a 1:1 catalytic mixture of [P(*t*-Bu)$_2$*o*-biphenyl]AuCl and AgOTf in dioxane at 60 °C for 20 h led to isolation of 1-ethyl-3-methyl-imidazolidin-2-one in 99% yield (eq 1.16).

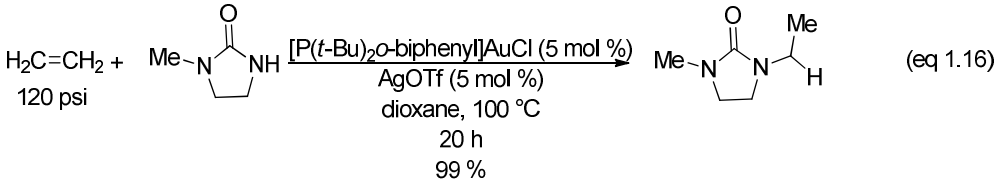

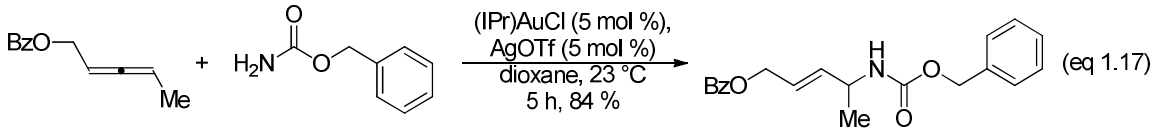

Additionally, the reaction of 2,3-pentadienyl benzoate with benzyl carbamate catalyzed by a 1:1 mixture of (IPr)AuCl [IPr = 1,3-bis(2,6-diisopropylphenyl)imidazol-2-ylidene] and AgOTf in dioxane at 23 °C for 5 h led to isolation of (*E*)-4-(benzyloxycarbonylamino)-2-pentenyl benzoate in 84% yield as a single regioisomer and diastereomer (eq 1.17). This gold(I)-catalyzed hydroamination protocol proceeded under mild reaction conditions and demonstrated wide substrate scope, high yields, good regioselectivity, and good diastereoselectivity. Based on these encouraging results, we sought to further extend the synthetic utility of gold(I)-catalyzed hydroamination to include the intermolecular reaction of arylamines with allenes. In particular, the goals of

my project were to develop a gold(I)-catalyzed protocol for the intermolecular hydroamination of allenes with arylamines and to explore the substrate scope of Au(I)-catalyzed intermolecular hydroamination of allenes with arylamines. This chapter describes our efforts, which have led to the realization of these goals.

1.2 Results and Discussion

1.2.1 Optimization

Widenhoefer and coworkers developed effective protocols for (1) the intramolecular hydroamination of *N*-γ- and δ-allenyl carbamates [32] catalyzed by a mixture of the gold phosphine complex [P(*t*-Bu)$_2$*o*-biphenyl]AuCl and AgOTf; (2) the intermolecular hydroalkoxylation of allenes with alcohols [33] catalyzed by a mixture of the gold (NHC) complex [(IPr)AuCl] and AgOTf; and (3) intermolecular hydroamination of allenes with *N*-unsubstituted carbamates [24] catalyzed by a mixture of (IPr)AuCl and AgOTf. We therefore targeted [P(*t*-Bu)$_2$*o*-biphenyl]AuCl and (IPr)AuCl as precatalysts for the intermolecular hydroamination of allenes with arylamines. In an initial experiment, the gold(I)-carbene complex, (IPr)AuCl, was employed as a precatalyst for the intermolecular hydroamination of allenes with arylamines. Treatment of two equivalents of 3-methyl-1,2-butadiene (**1**) with one equivalent of aniline and a catalytic 1:1 mixture of (IPr)AuCl and AgOTf (5 mol %) in dioxane at room temperature for 24 h led to the formation of the hydroamination product, *N*-prenylaniline (**2a**), as the exclusive product in 17 % yield (Table 1.1, entry 1).

Subsequent efforts to optimize the gold(I)-catalyzed hydroamination transformation revealed that the yield of **2a** decreased when the solvent was changed from dioxane to toluene (Table 1.1, entry 2). However, the yield of **2a** improved when the solvent changed from dioxane to dichloromethane (30 % yield) and when the catalyst changed from (IPr)AuCl to (**3**)AuCl [**3** = P(*t*-Bu)$_2$*o*-biphenyl] (35 % yield) (Table 1.1, entry 3 and 4). Dichloromethane and (**3**)AuCl were employed in subsequent reactions because of the increase in the yield of **2a**. Two equivalents of **1** was reacted with aniline and a catalytic mixture of (**3**)AuCl (5 mol %) and AgOTf (5 mol %) in dichloromethane for 24 h at room temperature to give **2a** in 66% yield (Table 1.1, entry 5). Complete consumption of aniline was not achieved in the previous reaction, thus dioxane was employed as the solvent so that the catalytic reaction could be heated. A solution of **1**, aniline, (**3**)AuCl (5 mol %), and AgOTf (5 mol %) in dioxane was heated at 45 °C for 12 h to give **2a** and *N*,*N*-diprenylaniline (**2b**) in a ratio of 4.1:1 with 100% conversion (Table 1.1, entry 6).

Table 1.1. Effect of catalyst and solvent on the gold(I)-catalyzed intermolecular reaction of 3-methyl-1,2-butadiene (1) with aniline

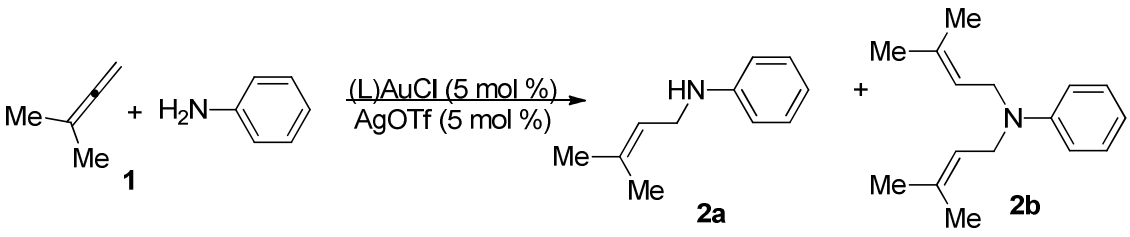

entry	catalyst[a]	solvent	temp (°C)	time (h)	convn (%)	Ratio **2a**/**2b**
1	(IPr)AuCl/AgOTf	dioxane	25	24	17	>25:1
2	(IPr)AuCl/AgOTf	toluene	25	24	10	>25:1
3	(IPr)AuCl/AgOTf	DCM	25	24	30	>25:1
4	(**3**)AuCl/AgOTf	dioxane	25	24	35	>25:1
5	(**3**)AuCl/AgOTf	DCM	25	24	66	>25:1
6	(**3**)AuCl/AgOTf	dioxane	45	12	100	4.1:1

[a](IPr) =1,3-bis(2,6-diisopropylphenyl)imidazol-2-ylidene and (**3**) = (1,1'-biphenyl-2-yl)di-*tert*-butylphosphine). Conversion and product ratio determined by GC analysis versus hexadecane internal standard. Reaction conditions: 3-methyl-1,2-butadiene (**1**) (0.4 mmol), aniline (0.2 mmol), AuCl/AgOTf (0.01 mmol) in solvent (0.5 mL) was stirred at indicated temperature and time

1.2.2 Control experiments

A series of control experiments were performed to rule out the possibility of catalysis via silver triflate, silver(I)-phosphine complex, or a triflic acid phosphine complex (Table 1.2). In one experiment, two equivalents of **1** was treated with aniline and AgOTf (5 mol %) in dioxane at 45 °C and stirred for 12 h. GC analysis of the crude reaction mixture indicated no detectable formation of **2a** or **2b**, or consumption of aniline (Table 1.2, entry 1). In a second experiment, two equivalents of **1** was treated with aniline, AgOTf (5 mol%), and P(*t*-Bu)$_{20}$-biphenyl (5 mol%) in dioxane at 45 °C and stirred for 12 h. GC analysis of the crude reaction mixture indicated no detectable formation of **2a** or **2b**, or consumption of aniline (Table 1.2, entry 2). In a third experiment, two equivalents of **1** was treated with aniline P(*t*-Bu)$_{20}$-biphenyl (5 mol%), and HOTf (5 mol%) in dioxane at 45 °C and stirred for 12 h. GC analysis of the crude reaction mixture indicated no detectable formation of **2a** or **2b**, or consumption of aniline (Table 1.2, entry 3). These experiments show that both (**3**)AuCl and AgOTf are required for catalysis and Bronsted acid-catalyzed hydroamination does not occur under reaction conditions. For these reasons, (**3**)AuCl and AgOTf were employed as the catalyst for the subsequent intermolecular hydroamination of allenes with arylamines.

Table 1.2. Control reactions for the gold(I)-catalyzed intermolecular reaction of 3-methyl-1,2-butadiene (1) with aniline in dioxane at 45 °C

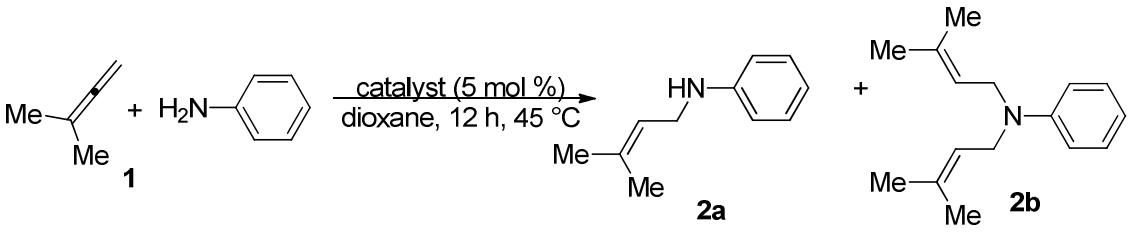

entry	catalyst	convn (%)	Ratio 2a/2b
1	AgOTf	0	-
2	**3**/AgOTf	0	-
3	**3**/HOTf	0	-

(**3**) = (1,1'-biphenyl-2-yl)di-*tert*-butylphosphine)
Conversion and product ratio determined by GC analysis versus hexadecane internal standard
Reaction conditions: 3-methyl-1,2-butadiene (**1**) (0.4 mmol), aniline (0.2 mmol), catalyst (0.01 mmol) in dioxane (0.5 mL) was stirred at 45 °C for 12 h

1.2.3 Reaction Scope

1.2.3.1 Anilines

With the optimized reaction conditions in hand, we probed the substrate scope of the gold(I)-catalyzed intermolecular hydroamination of allenes with arylamines. Gold(I)-catalyzed hydroamination of 3-methyl-1,2-butadiene (**1**) with aniline catalyzed by (**3**)AuCl (5 mol %) and AgOTf (5 mol %) in dioxane at 45 °C formed *N*-prenylaniline (**2a**), in 73% isolated yield and *N*,*N*-diprenylaniline (**2b**) in 18% isolated yield (Table 1.3, entry 1). Noteworthy, the intermolecular hydroamination of **1** with anilines tolerated

ortho, meta, and para substitution on the anilines (Table 1.3, entry 2-5, 7, 8, and 9). The reaction of **1** with ortho-substituted anilines gave only the mono addition product while reaction of **1** with para-substituted anilines gave a higher ratio of the bis addition product relative to the mono addition product. To further explore the effects of ortho-and-para substitution on the mono:bis addition product ratio, 4-chloro-2-methylaniline was reacted with two equivalents of **1** and a catalytic mixture of (**3**)AuCl (5 mol %) and AgOTf (5 mol %) at 45 °C for 12 h, which formed exclusively (4-chloro-2-methylphenyl)-(3-methyl-2-butenyl)amine in 86% isolated yield (Table 1.3, entry 10).

Since we were able to selectively form the mono addition product, we wanted to explore conditions that would produce only the bis addition product. In one experiment, a mixture of para-nitroaniline and two equivalents of **1** were treated with a catalytic amount of (**3**)AuCl (5 mol %) and AgOTf (5 mol %) was heated in dioxane at 45 °C for 12 h, to produce a 1:3 ratio of (3-methyl-2-butenyl)-(4-nitrophenyl)amine and bis-3-methyl-2-butenyl)-(4-nitrophenyl)amine in 99 % yield (Table 1.3, entry 4). In a second experiment, a mixture of para-bromoaniline and two equivalents of **1** were treated with a catalytic amount of (**3**)AuCl (5 mol %) and AgOTf (5 mol %) in dioxane at 45 °C for 12 h, to form a ~1:1 ratio of (4-bromophenyl)-(3-methyl-2-butenyl)amine and (4-bromophenyl)-bis-(3-methyl-2-butenyl)amine in 96 % (Table 1.3, entry 8). In a third experiment, a mixture of para-(trifluoromethyl)aniline and two equivalents of **1** were treated with a catalytic amount of (**3**)AuCl (5 mol %) and AgOTf (5 mol %) was heated in

dioxane at 45 °C for 12 h, to form a 1:2 ratio of *N*-(3-methylbut-2-en-1-yl)-4-(trifluoromethyl)aniline and *N*,*N*-bis(3-methylbut-2-en-1-yl)-4-(trifluoromethyl)aniline in 76 % yield (Table 1.3, entry 5).

To increase the formation of the bis-addition product, para-nitroaniline and para-bromoaniline were each reacted with three equivalents of **1**. In the first experiment, para-nitroaniline and three equivalents of **1** were treated with a catalytic amount of (**3**)AuCl (5 mol %) and AgOTf (5 mol %) in dioxane at 45 °C for 12 h to produce exclusively bis-3-methyl-2-butenyl)-(4-nitrophenyl)amine in 99% isolated yield (Table 1.3, entry 12). In a second experiment, para-bromoaniline and three equivalents of **1** were treated with a catalytic amount of (**3**)AuCl (5 mol %) and AgOTf (5 mol %) in dioxane at 45 °C for 24 h to form exclusively (4-bromophenyl)-bis-(3-methyl-2-butenyl)amine in 99% isolated yield (Table 1.3, entry 11).

After studying the effect of the substitution pattern and electron donating/withdrawing groups on the mono:bis selectivity, we sought to explore the effects of ortho, meta, and para substitution on aniline on the mono:bis ratio. *Ortho*-bromoaniline, *meta*-bromoaniline, and *para*-bromoaniline were each reacted with two equivalents of **1** and a catalytic mixture of (**3**)AuCl (5 mol %) and AgOTf (5 mol %) at 45 °C for 24 h, 12 h and 12 h, respectively; each reaction formed varying ratios of mono to bis addition hydroamination products (Table 1.3, entry 2, 8 and 9). Specifically, the reaction of **1** with ortho-bromoaniline and a catalytic mixture of (**3**)AuCl (5 mol %) and

AgOTf (5 mol %) in dioxane at 45 °C for 24 h formed exclusively (2-bromophenyl)-(3-methyl-2-butenyl)amine in 87 % yield (Table 1.3, entry 2). In another experiment, a mixture of **1** and meta-bromoaniline were reacted with a catalytic mixture of (**3**)AuCl (5 mol %) and AgOTf (5 mol %) in dioxane at 45 °C for 12 h to form a 3:1 mixture of (3-bromophenyl)-(3-methyl-2-butenyl)amine and (3-bromophenyl)-bis-(3-methyl-2-butenyl)amine in 95 % isolated yield (Table 1.3, entry 8). As previously discussed, the reaction of **1** and para-bromoaniline formed 1:1.4 mixtures of mono:bis addition products in 96 % isolated yield (Table 1.3, entry 8). From these results it can be concluded that the location of substitution on the aniline affects the ratio of mono:bis addition products in the gold(I)-catalyzed hydroamination of **1**.

We then sought to evaluate the effect of the size of the substituent at the ortho position of the aniline on the gold(I)-catalyzed hydroamination of **1**. The size of the group at the ortho position of the aniline had a greater effect on the isolated yield of the reaction than did the presence of an electron donating or electron withdrawing groups on the aniline (Table 1.3, entry 2,3, and 7). As an example, ortho-isopropylaniline was treated with two equivalents of **1** and a catalytic mixture of (**3**)AuCl (5 mol %) and AgOTf (5 mol %) in dioxane at 45 °C for 24 h to form (2- isopropylphenyl)-(3-methyl-2-butenyl)amine in 82% yield (eq 2.5). In another experiment, ortho-*tert*-butylaniline was treated with two equivalents of **1** and (**3**)AuCl (5 mol %) and AgOTf (5 mol %) in dioxane at 45 °C for 36 h to form (2-*tert*-butylphenyl)-(3-methyl-2-butenyl)amine in 66%

yield (eq 2.6). However, when a slightly electron withdrawing group like ortho-bromoaniline was treated with two equivalents of **1** and (**3**)AuCl (5 mol %) and AgOTf (5 mol %) in dioxane at 45 °C in 12 h to produce (2-bromophenyl)-(3-methyl-2-butenyl)amine in 87% yield (eq 2.4). From the previously described experimental results, it can be concluded that the size of the group on the ortho position of the aniline has an affect on the yield and reaction time for gold(I)-catalyzed hydroamination of allenes with arylamines.

Table 1.3. Gold(I)-catalyzed intermolecular hydroamination of 1 with arylamines: substrate scope with respect to aniline catalyzed by a mixture of (3)AuCl (5 mol %) and AgOTf (5 mol %) in dioxane at 45 °C.

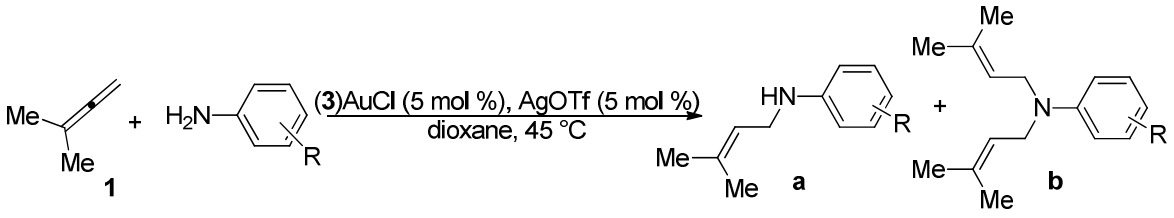

entry	R	time (h)	**a**/**b**[a]	yield of **a** (%)[b]	yield of **b** (%)[b]
1	H	12	4.1:1	73	18
2	*o*-Br	24	>99:1	87	
3	*o*-*i*-Pr	24	>99:1	82	
4	*p*-NO_2	12	1:2	33	66
5	*p*-CF_3	12	1:5.3	12	64
6	3,4,5 = OMe	36	>99:1	58	
7	*o*-*t*-Bu	36	>99:1	66	
8	*p*-Br	12	1:1.4	40	56
9	*m*-Br	12	3.1:1	72	23
10	*o*-Me, *p*-Cl	16	>99:1	86	
11[c]	*p*-Br	24	>1:99		99
12[c]	*p*-NO_2	12	>1:99		99

(**3**) = (1,1'-biphenyl-2-yl)di-*tert*-butylphosphine. Reaction conditions: 3-methyl-1,2-butadiene (**1**) (0.4 mmol), arylamine (0.2 mmol), (**3**)AuCl/AgOTf (0.01 mmol) in dioxane (0.5 mL) was stirred at 45 °C at indicated time. [a] Product ratio (**a**/**b**) was determined from the ratio of the isolated yields of product **a** and **b**. GC analysis versus hexadecane internal standard [b] Isolated yield [c] 3-Methyl-1,2-butadiene (**1**) (0.6 mmol), arylamine (0.2 mmol), (**3**)AuCl/AgOTf (0.01 mmol) in dioxane (0.5 mL) was stirred at 45 °C at indicated time.

1.2.3.2 *N*-Alkyl Anilines

Table 1.3 demonstrates the efficiency and generality of the gold(I)-catalyzed hydroamination of **1** as a function of aniline. We next explored the intermolecular hydroamination of **1** with *N*-alkyl anilines. Gold(I)-catalyzed intermolecular hydroamination of allenes tolerated substitution on the nitrogen of the aniline as well as arylamines with fused aromatic rings system, such as 1-naphthylamine. For example, reaction of *N*-methylaniline with two equivalents of **1** and a catalytic mixture of (**3**)AuCl (5 mol %) and AgOTf (5 mol %) at 45 °C for 24 h produced *N*-methyl-*N*-(3-methylbut-2-en-1-yl)aniline in 86% isolated yield (Table 1.4, entry 1). Similarly, reaction of 4-bromo-*N*-methylaniline with two equivalents of **1** catalyzed by (**3**)AuCl (5 mol %) and AgOTf (5 mol %) at 45 °C for 12 h produced 4-bromo-*N*-methyl-*N*-(3-methylbut-2-en-1-yl)aniline in excellent yield (94 %) (Table 1.4, entry 2). We then investigated the effect of electron donating groups such as methoxy on the aromatic ring. Reaction of 4-methoxy-*N*-methylaniline with two equivalents of **1** and (**3**)AuCl (5 mol %) and AgOTf (5 mol %) at 45 °C for 36 h produced 4-methoxy-*N*-methyl-*N*-(3-methylbut-2-en-1-yl)aniline in 36 % isolated yield (Table 1.4, entry 3). We concluded from these experiments with electron withdrawing and electron donating groups on aniline that electron donating groups inhibit the intermolecular hydroamination reaction of allenes with anilines. The effect of a fused aromatic system on the intermolecular hydroamination of allenes was explored. The reaction of 1-naphthylamine with two equivalents of **1** and a catalytic mixture of

(**3**)AuCl (5 mol %) and AgOTf (5 mol %) in dioxane at 45 °C for 22 h formed *N*-(3-methylbut-2-en-1-yl)naphthalen-1-amine in good yield (84 %) (Table 1.4, entry 1, 4).

Table 1.4. Gold(I)-catalyzed intermolecular hydroamination of allenes with arylamines catalyzed by a mixture of (3)AuCl (5 mol %) and AgOTf (5 mol %) in dioxane at 45 °C

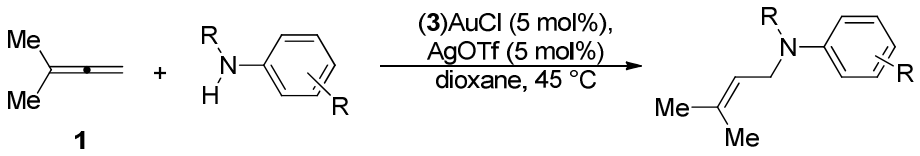

entry	Aniline	Product	time (h)	yield (%)
1	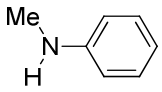	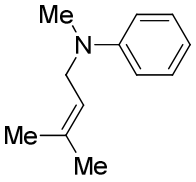	24	86
2	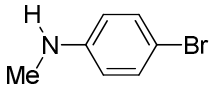	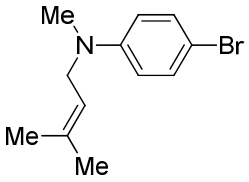	12	94
3	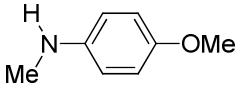	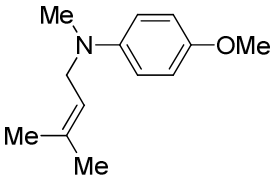	36	36
4	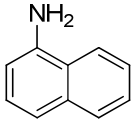	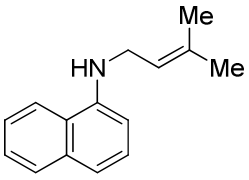	22	84

(**3**) = (1,1'-biphenyl-2-yl)di-*tert*-butylphosphine. Reaction conditions: 3-methyl-1,2-butadiene (**1**) (0.4 mmol), arylamine (0.2 mmol), (**3**)AuCl/AgOTf (0.01 mmol) in dioxane (0.5 mL) was stirred at 45 °C at indicated time.

1.2.3.3 Substituted Allenes

We then sought to explore the effect of various substituents and substitution patterns on the allene on the intermolecular hydroamination reaction of allenes with arylamines. We previously showed that **1** underwent gold(I)-catalyzed intermolecular hydroamination with various arylamines, ranging from 1-naphthylamine to *N*-methylaniline to 4-bromoaniline. However, the allene used throughout the previously mentioned experiments was restricted to **1**. Here we describe experiments that explore the scope of the intermolecular hydroamination of allenes with arylamines as a function of allene substitution. In one experiment, two equivalents of cyclohexylallene was reacted with 3-bromoaniline, (**3**)AuCl (5 mol %), and AgOTf (5 mol %) in dioxane at 45 °C for 12 h to form (3-bromophenyl)-(3-cyclohexyl-allyl)-amine in 91% isolated favoring the *E*-isomer (*E:Z* = 5.2:1) (Table 1.5, entry 1). We also explored the effect of the ester functionality on the monosubstituted allene. To this end, dimethyl-2(2,3-butadienyl)malonate (two equivalents) was reacted with 3-bromoaniline, (**3**)AuCl (5 mol %), and AgOTf (5 mol %) in dioxane at 45 °C for 12 h to form dimethyl-[4-(3-bromophenylamino)-but-2-enyl]-malonate (in 72 % isolated yield) favoring the E-isomer (*E:Z* = 8.6:1) (Table 1.5, entry 2). The intermolecular hydroamination of allenes with arylamines also tolerated 1,3-disubstituted allenes. For example, 6,7-tridecadiene (two equivalents) was treated with 3-bromoaniline and a catalytic amount of (**3**)AuCl (5 mol

%) and AgOTf (5 mol %) in dioxane at 45 °C for 36 h to form (3-bromophenyl)-(1-pentyl-2-octenyl)amine in 87 % isolated yield (Table 1.5, entry 3). In another experiment, 1-phenyl-1,2-butadiene (two equivalents) was treated with 3-bromoaniline and a catalytic amount of (**3**)AuCl (5 mol %) and AgOTf (5 mol %) in dioxane at 45 °C for 24 h to form (3-bromophenyl)-(1-methyl-3-phenyl-allyl)-amine in 86 % isolated yield with > 25:1 *E*/*Z* selectivity (Table 1.5, entry 4). Lastly, we explored the effect of the ester functionality on a 1,1-differentially disubstituted allene. To this end, ethyl 3-ethenylidenenonanoate (two equivalents) was reacted with 3-bromoaniline catalyzed by (**3**)AuCl (5 mol %) and AgOTf (5 mol %) in dioxane at 45 °C for 12 h formed ethyl (3*Z*)-3-{2-[(3-bromophenyl)amino]ethylidene}nonanoate in 93 % isolated yield (Table 1.5, entry 5).

As shown in Table 1.5, the regioselectivity of the hydroamination product was not affected by electron donating groups or electron withdrawing groups on the allene. For example, 1-phenyl-1,2-butadiene, dimethyl-2(2,3-butadienyl)malonate, and ethyl 3-ethenylidenenonanoate each underwent gold(I)-catalyzed hydroamination to form the hydroamination product in greater than 72 % yield (Table 1.5, entries 2,4, and 5). These results demonstrate that the intermolecular hydroamination reaction of allenes with arylamines tolerated monosubstituted, 1,1-disubstituted, 1,1-differentially substituted, 1,3- disubstituted, and 1,3-differentially disubstituted allenes, as well as ester functional groups. Additionally, it can be concluded that the substitution pattern on the allene (mono-substitution, 1,1-disubstiution, and 1,3-disubstition) had a greater effect on the

reaction time and yield than the presence of electron withdrawing or electron donating groups on the allene.

Table 1.5. Gold (I)-catalyzed intermolecular hydroamination of various allenes with arylamines catalyzed by a mixture of (3)AuCl (5 mol %) and AgOTf (5 mol %) in dioxane at 45 °C.

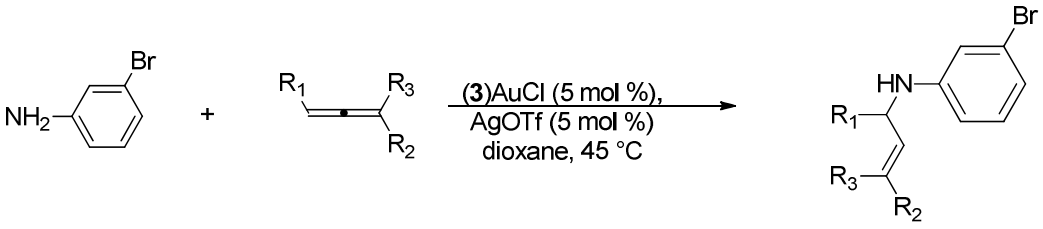

entry	allene	product	time (h)	yield (%)	*E*:*Z*
1	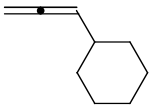	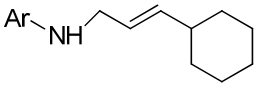	12	91	5.2:1
2	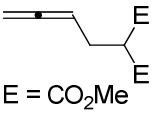	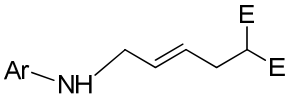	12	72	8.6:1
3	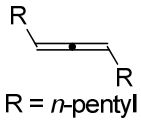	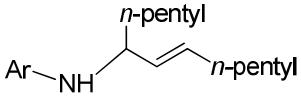	36	87	7.7:1
4	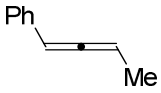	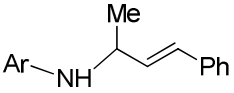	24	86	>25:1
5	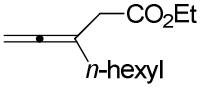	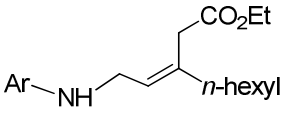	12	93	1:4.4

(**3**) = (1,1'-biphenyl-2-yl)di-*tert*-butylphosphine
Reaction conditions: 3-methyl-1,2-butadiene (**1**) (0.4mmol), 3-bromoaniline (0.2mmol), (**3**)AuCl/AgOTf (0.01 mmol) in dioxane (0.5 mL) was stirred at 45 °C at indicated time.

1.3 Summary

We have developed a mild and effective gold(I)-catalyzed protocol for the intermolecular hydroamination of allenes with arylamines. Monosubstituted and 1,1- and 1,3-disubsituted allenes underwent gold(I)-catalyzed hydroamination to form *N*-allylic aniline derivatives under mild reaction conditions, with wide substrate scope, high yields, good regioselectivity, and good diastereoselectivity.

1.4 Experimental procedures, analytical and spectroscopic data for aryl amines.

1.4.1 General Methods

Catalytic reactions were performed in sealed glass tubes under an atmosphere of dry nitrogen unless noted otherwise. NMR spectra were obtained on a Varian spectrometer operating at 500 MHz for ^{1}H NMR and 125 MHz for ^{13}C NMR in $CDCl_3$ unless noted otherwise. IR spectra were obtained on a Bomen MB-100 FT IR spectrometer. Gas chromatography was performed on a Hewlett-Packard 5890 gas chromatograph equipped with a 25 m polydimethylsiloxane capillary column employing FID detection. Chiral HPLC was performed on a Hewlett-Packard chromatograph equipped with a 0.46 cm × 25 cm Chiralpak AD-H column. Column chromatography was performed employing 200-400 mesh silica gel (EM). Thin layer chromatography (TLC) was performed on silica gel 60 F254. Elemental analyses were performed by Complete Analysis Laboratories (Parsippany, NJ).

Aryl amines, 3-methyl-1,2-butadiene (**1**), (1,2-propadienyl)cyclohexane, [P(*t*-Bu)$_2$-biphenyl]AuCl [(**3**)AuCl], and silver trifluoromethanesulfonate were purchased from major chemical suppliers and were used as received. Dioxane (Aldrich) was dried using the PureSolv™ solvent purification system. 6,7-Tridecadiene, [34] 1-phenyl-1,2-butadiene, [35] dimethyl 2-(2,3-butadienyl)malonate, [36] and ethyl 3-ethenylidenenonanoate were synthesized employing published procedures.

1.4.2 Catalytic Hydroamination of Allenes

General Procedure. Dioxane was added to a mixture of arylamine (**3**)AuCl, and AgOTf and the resulting suspension was stirred for 10 minutes at room temperature. Allene was added via syringe and the resulting mixture was stirred at 45 °C for the indicated time. Column chromatography of the reaction mixture (hexanes–EtOAc) gave the hydroamination product.

(2-Bromophenyl)-(3-methyl-2-butenyl)amine (Table 1.3, entry 2a). Dioxane (0.50 mL) was added to a mixture of 2-bromoaniline (39.4 mg, 0.23 mmol), (**3**)AuCl (5.8 mg, 1.1×10^{-2} mmol), and AgOTf (2.8 mg, 1.1×10^{-2} mmol) and the resulting suspension was stirred for 10 minutes at room temperature. Methyl-1,2-butadiene (29 mg, 0.43 mmol) was added via syringe and the resulting mixture was stirred at 45 °C for 24 h. Column chromatography of the reaction mixture (hexanes–EtOAc = 15:1) gave (2-bromophenyl)-(3-methyl-2-butenyl)amine (Table 1.3, entry 2) (48 mg, 87%) as a pale amber oil. ^{1}H NMR: δ 7.41 (dd, J = 1.5, 8.5 Hz, 1 H), 7.17 (dt, J = 1.5, 7.8 Hz, 1 H), 6.62

(dd, *J* = 1.0, 8.3 Hz, 1 H), 6.55 (dt, *J* = 1.5, 7.5 Hz, 1 H), 5.35-5.31 (m, 1 H), 4.23 (br s, 1 H), 3.72 (d, *J* = 6.8 Hz, 2 H), 1.76 (d, *J* = 1.0 Hz, 3 H), 1.72 (s, 3 H). $^{13}C\{^{1}H\}$ NMR: δ 45.1, 136.1, 132.3, 128.4, 121.1, 117.5, 111.4, 109.7, 41.9, 25.7, 18.1. HRMS calcd (found) for $C_{11}H_{14}BrN$ (M^+): 239.0310 (239.0313).

All remaining *N*-allyl anilines were synthesized employing a procedure analogous to that used to synthesize (2-bromo-phenyl)-(3-methyl-but-2-enyl)-amine):

***N*-(3-Methyl-2-butenyl)aniline (2a; Table 1.3, entry 1a).**[37] ^{1}H NMR: δ 7.21 (td, *J* = 1.0, 8.5 Hz, 2 H), 6.73 (tt, *J* = 1.0, 7.5 Hz, 1 H), 6.64 (dd, *J* = 1.2, 8.4 Hz, 2 H), 5.38-5.34 (m, 1 H), 3.67 (d, *J* = 6.8 Hz, 2 H), 1.73 (s, 3 H), 1.69 (s, 3 H). $^{13}C\{^{1}H\}$ NMR: δ 148.4, 135.6, 129.2, 121.6, 117.3, 112.9, 42.0, 25.7, 18.0.

***N,N*-Bis-(3-methyl-2-butenyl)aniline (3a; Table 1.3, entry 1b)**.[37] ^{1}H NMR: δ 7.21-7.16 (m, 2 H), 6.71-6.68 (m, 3 H), 5.23-5.20 (m, 2 H), 3.85 (d, *J* = 6.5 Hz, 4 H), 1.72 (s, 6 H), 1.70 (s, 6 H). $^{13}C\{^{1}H\}$ NMR: δ 148.9, 133.9, 129.0, 121.7, 115.9, 112.7, 48.1, 25.7, 17.8.

(2-Isopropylphenyl)-(3-methyl-2-butenyl)amine (Table 1.3, entry 3a). Amber oil, 83%. TLC (ether–hexanes = 1:2): R_f = 0.91. ^{1}H NMR: δ 7.11 (m, 2 H), 6.73 (t, *J* = 7.6 Hz, 1 H), 6.64 (d, *J* = 8.1 Hz, 1 H), 5.39-5.36 (m, 1 H), 3.71 (d, *J* = 6.6 Hz, 2 H), 3.58 (br s, 1 H), 2.85 (septet, *J* = 6.8 Hz, 1 H), 1.76 (s, 3 H), 1.71 (s, 3 H), 1.24 (d, *J* = 6.8 Hz, 6 H). $^{13}C\{^{1}H\}$ NMR: δ 145.1, 135.8, 132.2, 126.7, 124.8, 121.9, 117.2, 110.6, 42.2, 27.1, 22.3, 15.8, 18.1. IR (neat, cm^{-1}): 3434, 2972, 1598, 1505, 1449, 1373, 1300, 1253, 1065, 742. HRMS

calcd (found) for $C_{14}H_{21}N$ (M^+): 203.1674 (203.1670). Anal. calcd (found) for $C_{14}H_{21}N$: C, 82.70 (82.49); H, 10.41 (10.18).

(3-Methyl-2-butenyl)-(4-nitrophenyl)amine (Table 1.3, entry 4a).[38] Yellow solid, 33%. ^{1}H NMR: δ 8.06 (d, *J* = 9.5 Hz, 2 H), 6.49 (d, *J* = 9.0 Hz, 2 H), 5.29-5.25 (m, 1 H), 4.44 (br s, 1 H), 3.75 (br s, 2 H), 1.75 (d, *J* = 1.0 Hz, 3 H), 1.71 (s, 3 H). ^{13}C{^{1}H} NMR: δ153.3, 137.9, 137.5, 126.4, 119.7, 111.1, 25.7, 18.1. IR (neat, cm^{-1}): 3667, 3396, 2975, 1590, 1506, 1450, 1280, 1189, 1068, 820, 645. HRMS calcd (found) for $C_{11}H_{14}N_2O_2$ (M^+): 206.1055 (206.1058).

Bis-(3-methyl-2-butenyl)-(4-nitrophenyl)amine (Table 1.3, entry 4b and 12b). Yellow solid, 99%. TLC (ether–hexanes = 1:2): R_f = 0.70. ^{1}H NMR: δ 8.05 (d, *J* = 9.5 Hz, 2 H), 6.53 (d, *J* = 9.5 Hz, 2 H), 5.13-5.10, (m, 2 H), 3.94 (d, *J* = 1.2 Hz, 4 H), 1.72 (d, *J* = 1.2 Hz, 6 H), 1.71 (s, 6 H). ^{13}C{^{1}H} NMR: δ 153.3, 136.0, 126.3, 119.7, 119.5, 48.6, 25.7, 18.0. IR (neat, cm^{-1}): 3674, 2975, 1585, 1467, 1287, 1193, 1085, 1028, 910, 829, 746. HRMS calcd (found) for $C_{16}H_{22}N_2O_2$ (M^+): 274.1681 (274.1692). Anal. calcd (found) for $C_{16}H_{22}N_2O_2$: C, 70.04 (69.62); H, 8.08 (8.37).

***N*- (3-methylbut-2-en-1-yl)-4-(trifluoromethyl)aniline (Table 1.3, entry 5a).**[39] Yellow solid, 12%. ^{1}H NMR: δ 7.37 (d, *J* = 8.0 Hz, 2 H), 6.57 (d, *J* = 9.0 Hz, 2 H), 5.32-5.26 (m, 1 H), 3.92 (br s, 1 H), 3.69 (d, *J* = 6.5 Hz, 2 H), 1.74 (d, *J* = 1.0 Hz, 3 H), 1.70 (s, 3 H). ^{13}C{^{1}H} NMR: δ 150.7, 136.5, 126.6, 120.8, 120.7, 111.8, 41.5, 29.7, 25.7, 18.1

***N,N*-bis(3-methylbut-2-en-1-yl)-4-(trifluoromethyl)aniline (Table 1.3, entry 5b).** Yellow solid, 64%. TLC (ether–hexanes = 1:2): R_f = 0.84. ^{1}H NMR: δ 7.39 (d, *J* = 9.0 Hz, 2 H), 6.64 (d, *J* = 9.0 Hz, 2 H), 5.17-5.14 (m, 2 H), 3.89 (d, J = 6.0 Hz, 4 H), 1.72 (d, *J* = 1.0 Hz, 6 H), 1.70 (s, 6 H). ^{13}C{^{1}H} NMR: δ 149.9, 133.9, 125.4, 119.8, 110.3, 47.2, 24.7, 16.8 IR (neat, cm^{-1}): 3670, 2928, 1614, 1324, 1105, 815 . HRMS calcd (found) for $C_{17}H_{22}F_3N$ (M^+): 297.3584 (297.1710).

(3-Methyl-but-2-enyl)-(3,4,5-trimethoxy-phenyl)-amine (Table 1.3, entry 6a) Pale brown oil, 58%. TLC (ether–hexanes = 1:2): R_f = 0.58. ^{1}H NMR: δ 5.83 (s, 2 H). 5.32-5.28, (m, 1 H), 3.80 (s, 6 H), 3.74 (s, 1 H), 3.64 (d, *J* = 7.0, Hz, 2 H), 1.73 (d, *J* = 0.5 Hz, 3 H), 1.70 (s, 3 H), ^{13}C{^{1}H} NMR: δ 152.9, 144.2, 134.7, 129.0, 120.5, 89.3, 60.1, 54.9, 24.7, 17.0. IR (neat, cm^{-1}) 3671, 3379, 2974, 1602, 1508, 1453, 1224, 1116, 1022, 798, 630. HRMS calcd (found) for $C_{14}H_{21}NO_3$ (M^+): 251.32 (251.1530).

(2-*tert*-Butylphenyl)-(3-methyl-2-butenyl)amine (Table 1.3, entry 7a). Amber oil, 66%. TLC (ether–hexanes = 1:2): R_f = 0.84. ^{1}H NMR: δ 7.23 (dd, *J* = 1.5, 8.0 Hz, 1 H), 7.13 (dt, *J* = 1.5, 7.2 Hz, 1 H), 6.70-6.65 (m, 2 H), 5.42-5.40, (m, 1 H), 3.80 (br s, 1 H), 3.74 (d, *J* = 6.6 Hz, 2 H), 1.77 (d, *J* = 0.5 Hz, 3 H), 1.72 (d, *J* = 0.5 Hz, 3 H), 1.41 (s, 9 H). ^{13}C{^{1}H} NMR: δ 146.6, 136.0, 133.2, 127.1, 126.1, 121.8, 116.8, 111.9, 42.6, 34.2, 29.9, 25.7, 18.0. IR (neat, cm^{-1}): 3670, 2970, 1593, 1497, 1446, 1390, 1249, 1060, 879, 742. HRMS calcd (found) for $C_{15}H_{23}N$ (M^+): 217.1830 (217.1825). Anal. calcd (found) for $C_{15}H_{23}N$: C, 82.89 (82.86); H, 10.67 (10.70).

(4-Bromophenyl)-(3-methyl-2-butenyl)amine (Table 1.3, entry 8a).[40] Amber oil, 40%. ^{1}H NMR: δ 7.15 (d, *J* = 7.2 Hz, 2 H), 6.38 (d, *J* = 7.6 Hz, 2 H), 5.22-5.18, (m, 1 H), 3.55 (d, *J* = 6.8 Hz, 2 H), 3.52 (br s, 1 H), 1.65 (s, 3 H), 1.61 (s, 3 H). ^{13}C{^{1}H} NMR: δ 147.4, 136.0, 131.9, 121.6, 114.4, 108.8, 42.0, 25.7, 18.0.

(4-Bromophenyl)-bis-(3-methyl-2-butenyl)amine (Table 1.3, entry 8b and 11b). [40] Amber oil, 99%. ^{1}H NMR: δ 7.18-7.16 (m, 2 H), 6.47 (d, *J* = 7.1 Hz, 2 H), 5.10-5.07, (m, 2 H), 3.75 (d, *J* = 6.4 Hz, 4 H), 1.64 (d, *J* = 1.0 Hz, 6 H), 1.61 (s, 6 H).^{13}C{^{1}H} NMR: δ 143.7, 130.2, 127.5, 127.3, 116.9, 110.1, 103.5, 44.1, 21.4, 13.7.

(3-Bromophenyl)-(3-methyl-2-butenyl)amine (Table 1.3, entry 9a).[40] Amber oil, 72%. ^{1}H NMR: δ 6.99 (t, *J* = 8.1 Hz, 1 H), 6.78 (dd, *J* = 1.0, 7.9 Hz, 1 H), 6.71 (t, *J* = 2.2 Hz, 1 H), 6.49 (d, *J* = 2.2, 8.1 Hz, 1 H), 5.28 (tt, *J* = 1.2, 6.6 Hz, 1 H), 3.63 (d, *J* = 6.9 Hz, 2 H), 1.74 (s, 3 H), 1.70 (s, 3 H), N*H* proton not observed. ^{13}C{^{1}H} NMR: δ 147.7, 134.3, 128.5, 121.3, 119.0, 118.0, 113.3, 109.7, 39.9, 23.8, 16.1.

(3-Bromophenyl)-bis-(3-methyl-2-butenyl)amine (Table 1.3, entry 9b).[40] Amber oil, 23%. ^{1}H NMR: δ 6.99 (t, *J* = 8.0 Hz, 1 H), 6.77 (t, *J* = 2.2 Hz, 1 H), 6.73 (d, *J* = 7.8 Hz, 1 H), 6.55 (dd, *J* = 2.4, 8.3 Hz, 1 H), 5.14 (tt, *J* = 1.5, 6.4 Hz, 2 H), 3.81 (d, *J* = 6.5, Hz, 4 H), 1.70 (d, *J* = 0.7 Hz, 6 H), 1.68 (s, 6 H). ^{13}C{^{1}H} NMR: δ 148.3, 132.7, 128.3, 121.5, 119.1, 116.6, 113.4, 109.3, 46.3, 27.8, 23.8, 16.0.

(4-Chloro-2-methylphenyl)-(3-methyl-2-butenyl)amine (Table 1.3, entry 10a). Amber oil, 86%. TLC (ether–hexanes = 1:2): R_f = 0.78. ^{1}H NMR: δ 7.05 (dd, *J* = 2.7, 8.5

Hz, 1 H), 7.01-7.00 (m, 1 H), 6.50 (d, *J* = 8.6 Hz, 1 H), 5.36-5.32, (m, 1 H), 3.69 (d, *J* = 6.6 Hz, 2 H), 3.38 (br s, 1 H), 2.09 (s, 3 H), 1.76 (s, 3 H), 1.72 (s, 3 H). $^{13}C\{^{1}H\}$ NMR: δ 140.6, 131.7, 125.4, 122.4, 122.2, 119.3, 117.0, 106.4, 37.7, 21.4, 13.7, 13.0. IR (neat, cm^{-1}): 3423, 3056, 2921, 2857, 1580, 1525, 1466, 1405, 1279, 1109, 969, 770. HRMS calcd (found) for $C_{12}H_{16}ClN$ (M^+): 209.0971 (209.0975). Anal. calcd (found) for $C_{12}H_{16}ClN$: C, 68.73 (68.62); H, 7.61 (7.56).

***N*-(3-Methyl-2-butenyl)-*N*-methylaniline (Table 1.4, entry 1).**[41] Pale amber oil, 86%. ^{1}H NMR: δ 7.27 (dt, *J* = 1.0, 7.5 Hz, 2 H), 6.78 (d, *J* = 8.3 Hz, 2 H), 6.75 (t, *J* = 7.1 Hz, 1 H), 5.24-5.27 (m, 1 H), 3.93 (d, *J* = 6.4 Hz, 2 H), 2.93 (s, 3 H), 1.76 (s, 6 H). $^{13}C\{^{1}H\}$ NMR: δ 148.8, 133.6, 128.1, 119.8, 115.4, 111.9, 49.5, 36.9, 24.8, 16.9.

(4-Bromophenyl)-methyl-(3-methyl-2-butenyl)amine (Table 1.4, entry 2). Amber oil, 94%. TLC (ether–hexanes = 1:2): R_f = 0.82. ^{1}H NMR: δ 7.26 (d, *J* = 9.0 Hz, 2 H) 6.57 (d, *J* = 9.2 Hz, 2 H), 5.16-5.12 (m, 1 H), 3.84 (d, *J* = 6.4 Hz, 2 H), 2.85 (s, 3 H), 1.71 (d, *J* = 1.2 Hz, 3 H), 1.70 (s, 3 H). $^{13}C\{^{1}H\}$ NMR: δ 144.4, 130.7, 127.5, 116.0, 110.1, 103.9, 46.2, 33.8, 21.5, 13.0. IR (neat, cm^{-1}): 2920, 1673, 1592, 1496, 1367, 1249, 1193, 1098, 929, 807. $C_{12}H_{16}BrN$ (M^+): 253.0466 (253.0457). Anal. calcd (found) for $C_{12}H_{16}BrN$: C, 56.71 (56.96); H, 6.35 (6.35).

4-(Methoxymethyl)-*N*-methyl-*N*-(3-methylbut-2-en-1-yl)aniline (Table 1.4, entry 3)[42] Amber oil, 36%. ^{1}H NMR: δ 1.67 (s, 3 H), 1.69 (d, *J* = 1.5 Hz, 3 H), 2.79 (s, 3

H), 3.74 (s, 3 H), 3.77 (d, *J* = 6.5 Hz, 2 H) 5.18-5.21 (m, 1 H), 6.74 (d, *J* = 9 Hz, 2 H), 6.81 (d, *J* = 9.0 Hz, 2H). $^{13}C\{^{1}H\}$ NMR: δ 113.7, 112.7, 53.8, 50.0, 36.9, 27.8, 23.8, 16.0.

(3-Methyl-2-butenyl)-naphthalen-1-yl-amine (Table 1.4, entry 4).[43] Amber oil, 84%. TLC (ether–hexanes = 1:2): R_f = 0.77. ^{1}H NMR (400 MHz): δ 7.80 (t, *J* = 7.4 Hz, 2 H), 7.47-7.41 (m, 2 H), 7.37 (t, *J* = 8.0 Hz, 1 H), 7.25 (d, *J* = 8.1 Hz, 1 H), 6.63 (d, *J* = 7.3 Hz, 1 H), 5.51-5.48 (m, 1 H), 4.36 (br s, 1 H), 3.86 (d, *J* = 6.8, Hz, 2 H), 1.81 (s, 3 H), 1.77 (s, 3 H). $^{13}C\{^{1}H\}$ NMR (100 MHz): δ 141.6, 134.4, 132.4, 126.7, 124.7, 123.8, 122.7, 119.5, 118.0, 115.4, 102.6, 40.4, 27.8, 23.9, 16.2.

E-(3-Bromophenyl)-(3-cyclohexyl-allyl)-amine (Table 1.5, entry 1). Amber oil, 91%; *E:Z* = 5.2:1. TLC (ether–hexanes = 1:2): R_f = 0.76. ^{1}H NMR (E isomer): δ 6.98 (t, *J* = 8.0 Hz, 1 H), 6.79 (td, *J* = 1.0, 7.5 Hz, 1 H), 6.73 (t, *J* = 2.0 Hz, 1 H), 6.49 (ddd, *J* = 0.5, 2.5, 7.0 Hz, 1 H), 5.63 (dd, *J* = 6.5, 15.5 Hz, 1 H), 5.46 (dtd, *J* = 1.0, 6.0, 16.0 Hz, 1 H), 3.75 (br s, 1 H), 3.64 (br s, 2 H), 1.98-1.91 (m, 1 H), 1.73-1.67 (m, 4 H), 1.31-1.02 (m, 6 H). $^{13}C\{^{1}H\}$ NMR (E isomer): δ 147.6, 137.8, 128.5, 121.6, 121.3, 118.1, 113.5, 109.8, 50.0, 44.1, 38.5, 30.9, 24.1. IR (neat, cm^{-1}): 3670, 2974, 2916, 1592, 1395, 1244, 1061, 883, 760, 677. HRMS calcd (found) for $C_{15}H_{20}BrN$ (M^+): 293.0779 (293.0793). Anal. calcd (found) for $C_{15}H_{20}BrN$: C, 61.23 (61.51); H, 6.85 (6.77).

Dimethyl-[4-(3-Bromophenylamino)-but-2-enyl]-malonate (Table 1.5, entry 2). Pale amber oil, 72%; E:Z = >25:1. TLC (ether–hexanes = 1:2): R_f = 0.45. ^{1}H NMR: δ 6.98 (t, *J* = 8.1 Hz, 1 H), 6.78 (ddd, *J* = 1.0, 2.3, 8.0 Hz, 1 H), 6.69 (t, *J* = 2.3 Hz, 1 H), 6.46 (ddd, *J*

= 1.0, 2.2, 8.5 Hz, 1 H), 5.63-5.62 (m, 2 H), 3.80 (br s, 1 H), 3.70 (s, 6 H), 3.66-3.64 (m, 2 H), 3.41 (t, *J* = 7.6 Hz, 1 H), 2.63-2.61 (m, 2 H). $^{13}C\{^{1}H\}$ NMR: δ167.3, 147.3, 128.6, 127.9, 126.2, 121.3, 118.3, 113.5, 109.7, 50.7, 49.6, 43.4, 29.6. IR (neat, cm^{-1}): 3408, 2969, 2669, 1734, 1592, 1491, 1438, 1235, 1160, 1060, 977, 840, 766, 680. HRMS calcd (found) for $C_{15}H_{18}BrNO_4$ (M^+): 355.041920 (355.0426).

(3-Bromophenyl)-(1-pentyl-2-octenyl)amine (Table 1.5, entry 3). Pale amber oil, 87%; E:Z = 7.7:1. TLC (ether–hexanes = 1:2): R_f = 0.74. ^{1}H NMR (E isomer): δ 6.95 (t, *J* = 8.1 Hz, 1 H) , 6.73 (td, *J* = 1.0, 8.6 Hz, 1 H), 6.70 (t, *J* = 2.0 Hz, 1 H), 6.46 (dd, *J* = 1.0, 8.5 Hz, 1 H), 5.57 (td, *J* = 6.8, 15.4 Hz, 1 H), 5.22 (dd, *J* = 6.6, 15.4 Hz, 1 H), 3.64-3.69 (m, 2 H), 1.98 (q, *J* = 7.0 Hz, 2 H), 1.56-1.48 (m, 2 H), 1.39-1.20 (m, 12 H), 0.87-0.83 (m, 6 H). $^{13}C\{^{1}H$ NMR (E isomer): δ 147.1, 130.2, 129.3, 128.3, 121.2, 117.6, 114.0, 110.1, 53.5, 48.9, 34.2, 30.3, 29.3, 27.1, 23.7, 20.7, 20.6, 12.2. IR (neat, cm^{-1}): 3407, 2928, 2860, 1726, 1564, 1485, 1321, 1159, 1071, 975, 840, 757, 679. HRMS calcd (found) for $C_{19}H_{30}BrN$ (M^+): 351.1562 (351.1565).

The configuration of the major diastereomer of (3-bromophenyl)-(1-pentyl-2-octenyl)amine was established by interpreting J_{HH} coupling constants.

***E*-(3-Bromophenyl)-(1-methyl-3-phenyl-allyl)-amine (Table 1.5, entry 4).** Amber oil, 86%; E:Z = >25:1. TLC (ether–hexanes = 1:2): R_f = 0.85. ^{1}H NMR : δ 7.39 (m, 2 H), 7.34 (t, *J* = 7.6 Hz, 2 H), 7.26 (tt, *J* = 1.2, 7.3 Hz, 1 H), 7.03 (t, *J* = 8.1 Hz, 1 H), 6.84-6.81 (m, 2 H), 6.61-6.57 (m, 2 H), 6.21 (dd, *J* = 5.6, 16.1 Hz, 1 H), 4.15 (doublet of quintets, *J* =

1.2, 6.6 Hz, 1 H), 3.68 (br s, 1 H) 1.43 (d, *J* = 6.6 Hz, 3 H). $^{13}C\{^{1}H\}$ NMR: δ 148.6, 136.8, 132.3, 130.5, 128.6, 127.5, 126.4, 123.2, 120.1, 116.0, 112.0, 50.7, 22.0, 19.6, IR (neat, cm^{-1}): 3407, 3030, 2962, 1590, 1490, 1320, 1160, 1076, 971, 841, 753, 684. HRMS calcd (found) for $C_{16}H_{16}NBr$ (M^+): 301.0466 (301.0475).

Ethyl (3*Z*)-3-{2-[(3-bromophenyl)amino]ethylidene}nonanoate (Table 1.5, entry 5). Amber oil, 93%. E:Z = 1: 4.4 TLC (ether–hexanes = 1:2): R_f = 0.85.^{1}H NMR: δ 6.98 (t, *J* = 8.0 Hz, 1H), 6.78 (d, *J* = 7.5 Hz, 1H), 6.72 (t, *J* = 2.0 Hz, 1H), 6.49 (dd, *J* = 2.5, 8.0 Hz, 1H), 5.55 (t, *J* = 7.0 Hz, 1H), 4.13 (q, *J* = 7.0 Hz, 2H), 3.92 (br s, 1H), 3.67 (d, *J* = 7.0 Hz, 2H), 3.09 (s, 2H), 2.08 (t, *J* = 7.5 Hz, 2H), 1.41-1.37 (m, 2H), 1.30-1.22 (m, 9H), 0.86 (t, *J* = 7.0 Hz, 3H). $^{13}C\{^{1}H\}$ NMR: δ 171.4, 149.6, 137.1, 130.5, 124.8, 123.3, 120.1, 115.4, 111.7, 61.0, 41.5, 37.7, 36.5, 31.7, 30.7, 28.9, 27.5, 22.6, 14.2. IR (neat, cm^{-1}): 3394, 2930, 2856, 1725, 1594, 1479, 1414, 1254, 1163, 1031. HRMS calcd (found) for $C_{19}H_{28}BrNO_2$ (M^+): 382.1303 (381.1296)

The configuration of the major diastereomer of ethyl (3*Z*)-3-{2-[(3-bromophenyl)amino]ethylidene}nonanoate was established as Z through 1D-NOE analysis. In particular, irradiation of the allylic methylene protons of the n-hexyl group of the major diastereomer of ethyl (3*Z*)-3-{2-[(3-bromophenyl)amino]ethylidene}nonanoate led to enhancement of the alkenyl proton. Conversely, irradiation of the allylic methylene protons of the carboethoxymethyl group of the major diastereomer of ethyl (3*Z*)-3-{2-[(3-bromophenyl)amino]ethylidene}nonanoate led to no enhancement of the alkenyl proton.

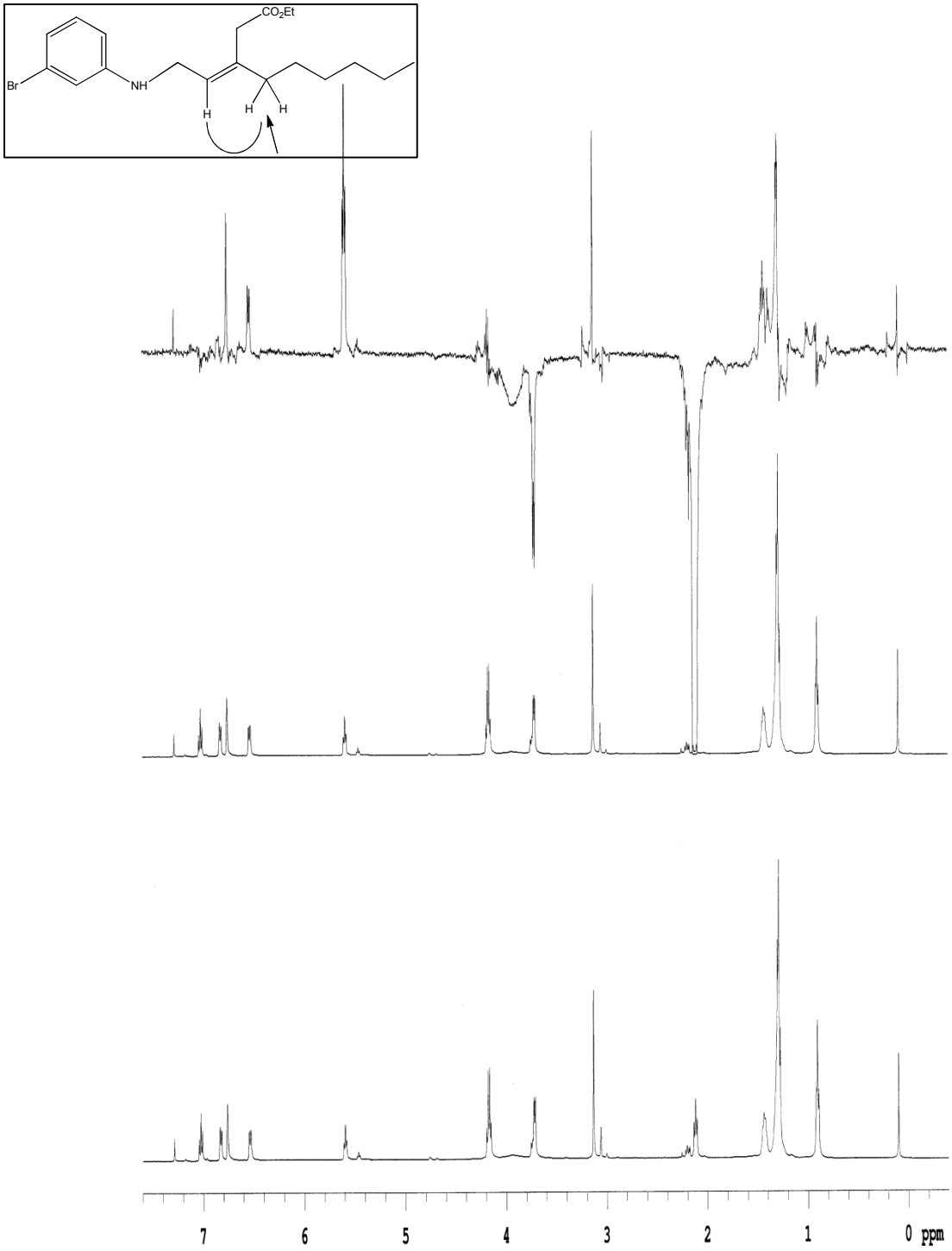

Figure 1.1. 1D-NOE analysis of ethyl (3*Z*)-3-{2-[(3-bromophenyl)amino]ethylidene}nonanoate. Irradiation of the allylic methylene protons of the *n*-hexyl group of the major diastereomer of ethyl (3*Z*)-3-{2-[(3-bromophenyl)amino]ethylidene}nonanoate led to enhancement of the alkenyl proton.

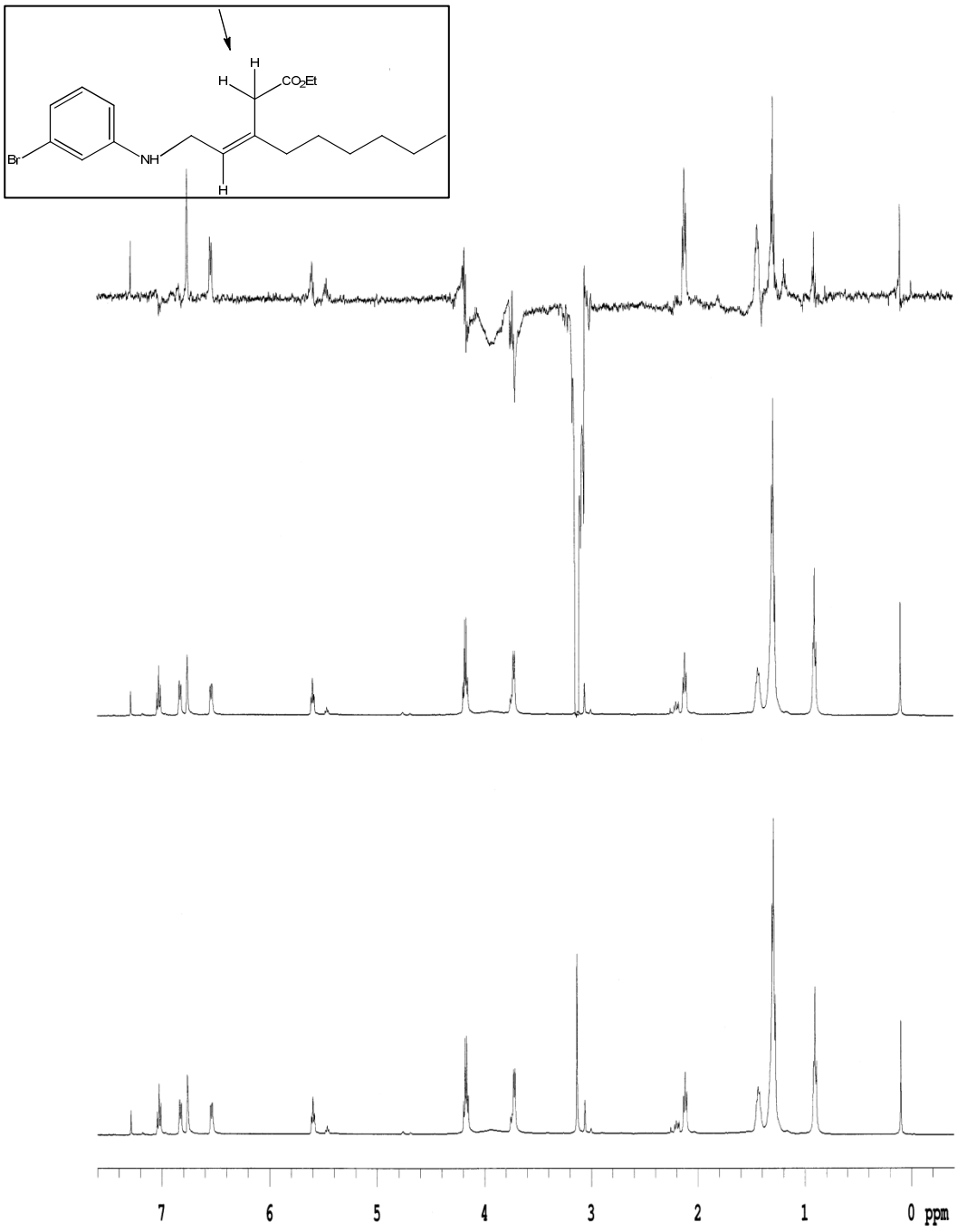

Figure 1.2. 1D-NOE analysis of ethyl (3*Z*)-3-{2-[(3-bromophenyl)amino]ethylidene}nonanoate. Irradiation of the allylic methylene protons of the carboethoxymethyl group of the major led to no enhancement of the alkenyl proton.

1.4.3 Control Reactions

1) Silver only (Table 1.2, entry 1). Dioxane (0.50 mL) was added to a mixture of aniline (22 mg, 0.23 mmol) and AgOTf (2.9 mg, 0.011 mmol) and stirred for 10 minutes at room temperature. **1** (28 mg, 0.41 mmol) was added via syringe and the resulting mixture was stirred at 45 °C for 12 h. GC analysis of the crude reaction mixture revealed no detectable consumption of aniline and no detectable formation of **2a** or **2b**.

2) Silver/ligand (Table 1.2, entry 2). Dioxane (0.50 mL) was added to a mixture of aniline (19.4 mg, 0.21 mmol), AgOTf (3.3 mg, 0.013 mmol), **3** (3.1 mg, 0.010 mmol) and stirred for 10 minutes at room temperature. **1** (30 mg, 0.44 mmol) was added via syringe and the resulting mixture was stirred at 45 °C for 12 h. GC analysis of the crude reaction mixture revealed no detectable consumption of aniline and no detectable formation of **2a** or **2b**.

3) HOTf/ligand (Table 1.2, entry 3). Dioxane (0.50 mL) was added to a mixture of aniline (20.3 mg, 0.22 mmol), HOTf (2.1 mg, 0.014 mmol), and **3** (3.2 mg, 0.011 mmol) and stirred for 10 minutes at room temperature. **1** (30 mg, 0.44 mmol) was added via syringe and the resulting mixture was stirred at 45 °C for 12 h. GC analysis of the crude reaction mixture revealed no detectable consumption of aniline and no detectable formation of **2a** or **2b**.

2 Kinetic Studies of Gold(I)-Catalyzed Hydroalkoxylation and Hydroamination of Allenes with Alcohols and Carbamates

2.1 Introduction

Gold catalyzed activation of C-C multiple bonds is a rapidly growing area in organic synthesis. These efforts have focused primarily on nucleophilic additions to C-C multiple bonds catalyzed by gold(I)-complexes including the hydroamination, [31, 44-61] hydroalkoxylation, [62-67] and hydroarylation [68-75] of alkenes, allenes, and alkynes. In particular, hydroamination and hydroalkoxylation of allenes are effective methods for the synthesis of allylic amines and allylic ethers, respectively. Allylic ethers and amides have generated considerable interest in the field of organic chemistry because of their bioactivity [76-78] and their utility as building blocks in synthesis. [79, 80] A detailed review of hydroamination reactions with allenes can be found in the introduction of chapter one.

2.1.1 Intramolecular Hydroalkoxylations of Allenes and Alkynes

Hydroalkoxylation is the formal addition of the O-H bond of an alcohol across a carbon-carbon multiple bond. These reactions can be performed intramolecularly to form oxygen containing heterocycles or intermolecularly to form acyclic ethers. Previously, hydroalkoxylation reactions have been catalyzed by bases like phosphine and dimethylamino pyridine. [81-84] In an example of a base catalyzed intramolecular hydroalkoxylation reaction, a catalytic amount of cesium hydroxide was reacted with 6-(phenylthio)hex-5-yn-1-ol in *N*-methyl-2-pyrrolidnone (NMP) forming 7-(phenylthio)-2,3,4,5-tetrahydrooxepine, a functionalized enol ethers in 74 % yield (eq 2.1). [82]

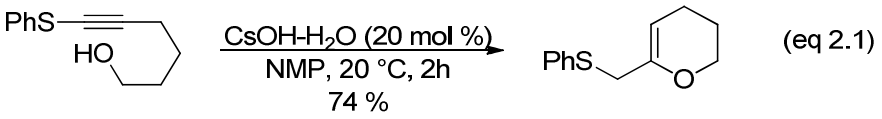

(eq 2.1)

More recent efforts in intramolecular hydroalkoxylation reactions have focused on transition metals and post-transition metals. Intramolecular hydroalkoxylation reactions continue to attract interest as a means to synthesize oxygen heterocycles with substitution patterns that mimic those of natural products. Acetogenins and polyether antibiotics are two examples of oxygen-containing heterocycles that are naturally occurring and biologically active. For these reasons, alkenes, [64, 85] alkynes, [67] and allenes [32, 67] have been used in metal-catalyzed hydroalkoxylation reactions. Marks and coworkers showed that lanthanide triflates dissolved in 1-ethyl-3-methylimidazolium trifluoromethanesulfonate ([C_2mim][OTf]) solutions serve as efficient catalysts for the intramolecular hydroalkoxylation of 2-allylphenol to form 2-methyl-2,3-dihydro-1-benzofuran (eq 2.2). [64] Cyclizations were effective for the formation of five-membered oxygen heterocycles with Markovnikov selectivity.

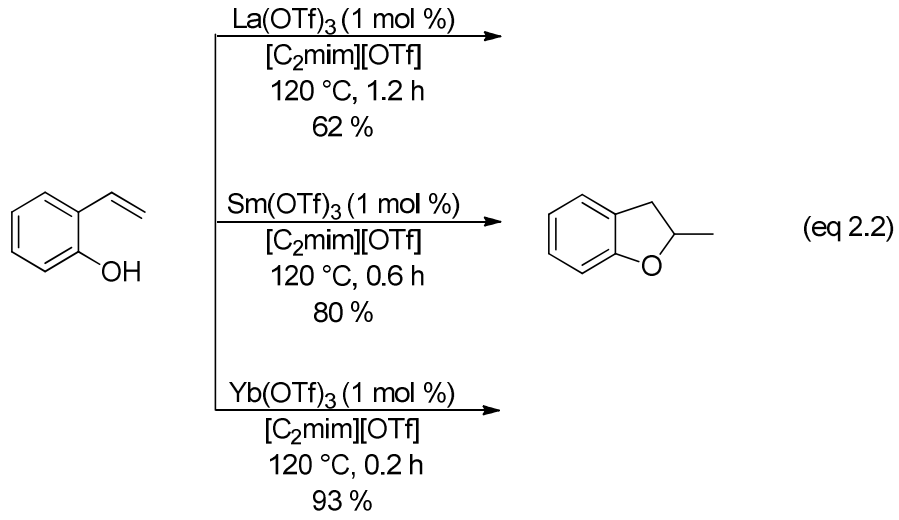

(eq 2.2)

Bismuth(III) salts have been also shown to catalyze the intramolecular hydroalkoxylation of alkenes. For instance, substituted tetrahydrofurans were synthesized from unactivated olefins using bismuth(III) triflate as a catalyst. More specifically, 1-phenylpent-4-en-1-ol was treated with $Bi(OTf)_3$ (10 mol %) in dichloroethane at 80 °C for 50 min to form (2*S*,5*R*)-2-methyl-5-phenyltetrahydrofuran in 94 % yield as a 2.4:1 mixture of trans/cis isomers (eq 2.3). [85]

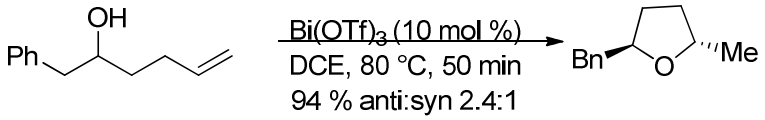

(eq 2.3)

Efforts to increase the functionality and diversity of the oxygen heterocycles generated via intramolecular hydroalkoxylation led to utilization of alkynes as substrates. Diéguez-Vásquez and coworkers demonstrated tandem intramolecular/intermolecular double hydroalkoxylations of conjugated 7-hydroxyheptynoates to form six-membered cyclic acetals using gold(III) chloride as a catalyst (eq 2.4). Presumably these

transformations occur via initial formation of a 6-exo-dig cyclization followed by intermolecular addition of methanol to the resulting enolether. Double intramolecular hydroalkoxylations catalyzed by a iridium(I) cyclooctadiene BAr_F (BAr_F = tetrakis(3,5-di-trifluoromethylphenyl)borate) were also used to form a variety of spiroketals motifs from aliphatic alkyne diols (eq 2.5). Widenhoefer and coworkers γ-Hydroxy and δ-hydroxy allenes underwent gold(I)-catalyzed intramolecular hydroalkoxylation within minutes at room temperature to form the corresponding oxygen heterocycles in good yield with high exo-selectivity. For example, reaction of 2,2-diphenylhexa-4,5-dien-1-ol with a catalytic mixture of Au[P(*t*-Bu)$_2$(*o*-biphenyl)]Cl (5 mol %) and AgOTs (5 mol%) in toluene at room temperature for 3 min led to the formation of 4,4-diphenyl-2-vinyltetrahydrofuran in 96% yield, subsequent chromatography gave 4,4-diphenyl-2-vinyltetrahydrofuran in 91% isolated yield (eq 2.6). [32]

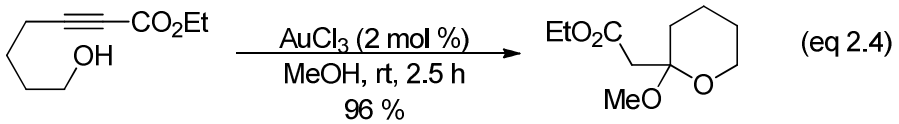

(eq 2.4)

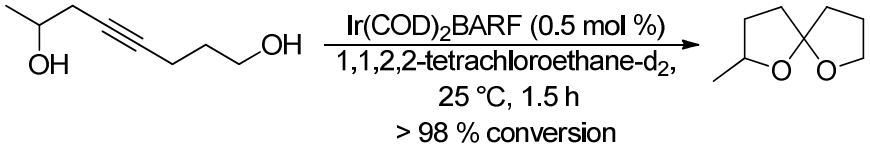

(eq 2.5)

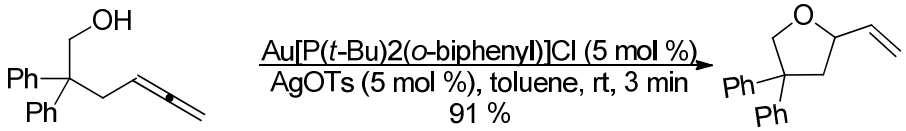

(eq 2.6)

2.1.2 Intermolecular Hydroalkoxylation

Transition metal-catalyzed intermolecular hydroalkoxylation reactions offer the potential for C-O bond formation under mild conditions with control of selectivity. As such, early and late transition metal complexes and lanthanide salts have been applied as catalysts for the hydroalkoxylation of C-C multiple bonds including activated alkenes, [66, 86, 87] unactivated alkenes, [88-92] alkynes, [93-106] and allenes. [32, 36, 107-111]

2.1.2.1 Alkenes

Electron deficient alkenes have been used for intermolecular hydroamination reactions because of their enhanced reactivity compared to their unactivated counterparts. A monomeric copper *N*-heterocylic carbene complex was used to catalyze the addition of the O-H bond of ethanol (1 equiv) bond across the C=C bond of acrylonitrile (eq 2.7).[86] Abu-Omar and Toste independently developed catalytic systems to transform enones into β-alkoxy ketones via C=C hydroalkoxylation. Abu-Omar and coworkers employed palladium(II) complexes (eq 2.8) to achieve this transformation, while Toste and coworkers used a trialkyl phosphine in the absence of a transition metal. This system was discovered while attempting to develop a transition-metal catalyzed hydration protocol for alkene hydroalkoxylation(eq 2.9). [66, 87]

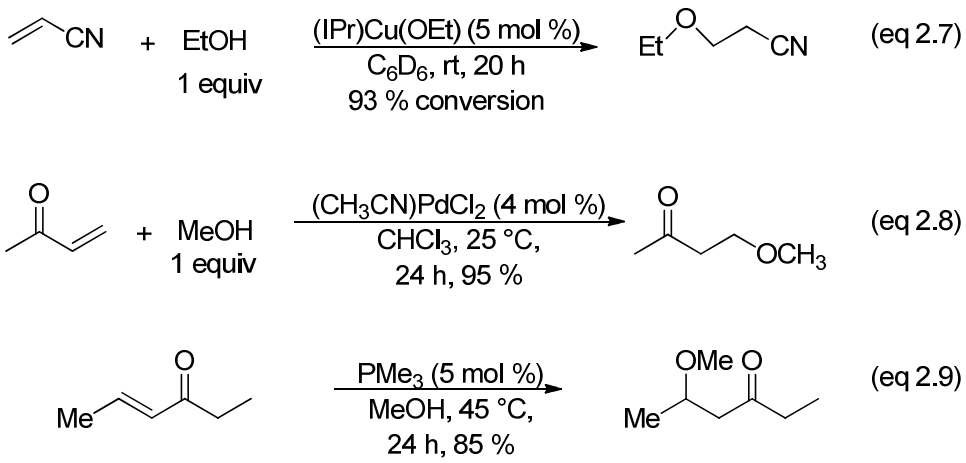

The examples of catalytic alkene hydroalkoxylation noted in the previous paragraph employed Michael acceptors as substrates to facilitate the Nucleophilic addition. In an effort to develop a metal-catalyzed protocol for the intermolecular hydroalkoxylation of non-conjugated alkenes with alcohols, methylenecyclopropanes have been utilized. For example, in the presence of catalytic amounts of tetrakis(triphenylphosphine)palladium (5 mol %) and tri-*o*-tolylphosphine (10 mol %) the reaction of octylidenecyclopropane with benzyl alcohol in THF at 100 °C gave a ring-opened allylic ether, {[(2-methyleneundecyl)oxy]methyl}benzene, in 69 % yield (eq 2.10). [112] Extension of alkene hydroalkoxylation to include electronically unactivated C=C bonds was achieved independently by Wang and Oe. [113, 114] An example of this hydroalkoxylation dehydration is the reaction of 1-phenylbut-3-en-1-ol in the presence of catalytic amounts of palladium(II) chloride (10 mol %) at 30 °C for 3 h gave (3-methoxybut-1-en-1-yl)benzene in 84 % yield (eq 2.11). [113] Alternatively, Oe showed that treatment of styrene with 2-phenylethanol and a catalytic amount of $Cp^*RuCl_2(PPh_3)$

(Cp* = C_5Me_5) (20 mol %) and AgOTf (20 mol %) in toluene at 70 °C for 48 h led to isolation of [1-(2-phenylethoxy)ethyl]benzene in 83 % yield (eq 2.12). [114]

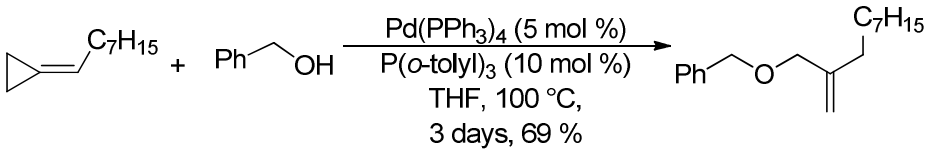

(eq 2.10)

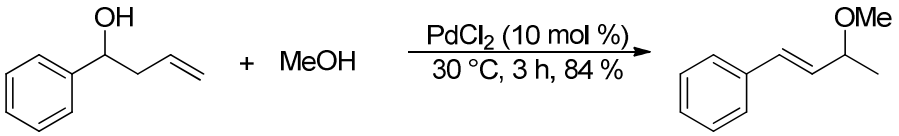

(eq 2.11)

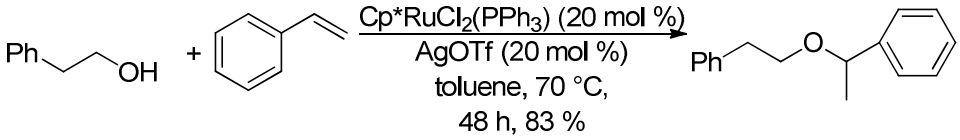

(eq 2.12)

2.1.2.2 Alkynes and Allenes

Hydroalkoxylation protocols of alkynes and alkenes have been developed because they offer the potential for additional functionality and milder reaction conditions. As an example of intermolecular alkyne hydroalkoxylation, 1-phenyl-1-propyne was treated with 1.2 equivalents of benzyl alcohol and a catalytic amount of $Pd(PPh_3)_4$ (10 mol %) and benzoic acid (10 mol %) in dioxane at 100 °C for 3 days to from benzyl cinnamyl ether in 96 % yield (eq 2.13). [115] Yamamoto and co-workers developed a gold(I)-catalyzed intermolecular hydroalkoxylation protocol of allenes with alcohols that permitted substitution on the allene. [116] For instance, a mixture of propa-1,2-dien-1-ylbenzene and isopropyl alcohol was treated with a catalytic amount of

ClAu(PPh3) (5 mol %) and AgOTf (5 mol %) for 2.5 h to form (3*E*)-4-phenylbut-3-en-1-ol - isobutene (eq 2.14). [116] Cui and coworkers developed a gold-catalyzed protocol for the hydroalkoxylation of alkoxyallenes with alcohols to form allylic acetals. [111] For example, reaction of 3,4-dimethoxybenzyoxylallene with methanol in the presence of a catalytic amount of (PPh3)Au(NO3) (2 mol %) in dichloroethane at -15 °C to room temperature for 3 h formed 4-[3-(benzyloxy)pent-4-en-1-yl]-1,2-dimethoxybenzene in 90 % isolated yield (eq 2.15). [111]

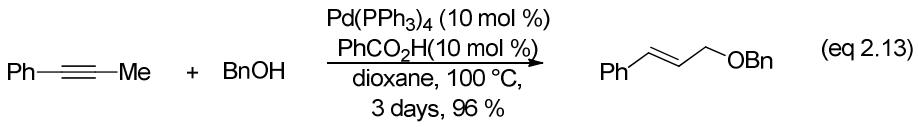

(eq 2.13)

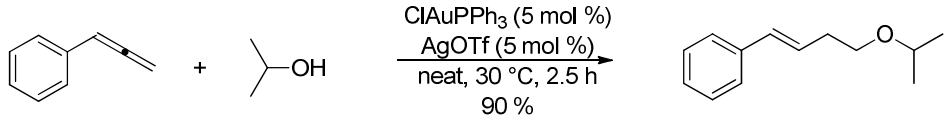

(eq 2.14)

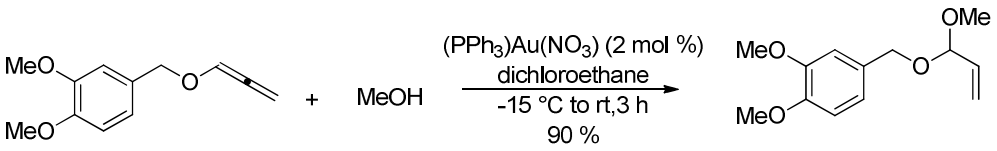

(eq 2.15)

Widenhoefer and coworkers have reported that (IPr)AuCl [IPr= 1,3-bis(2,6-diisopropylphenyl)imidazol-2-ylidine], activated with AgOTf, catalyzes the intermolecular hydroalkoxylation of allenes with alcohols. [117] For example, a mixture of 1-phenylpropan-1-ol (**1**) and 3-methyl-1,2-butadiene (**2**) were treated with a catalytic amount of (IPr)AuCl (5 mol %) and AgOTf (5 mol %) in toluene at 23 °C for 4 h to form {1-[(3-methylbut-2-en-1-yl)oxy]propyl}benzene (**3**) in 88 % yield (eq 2.16).

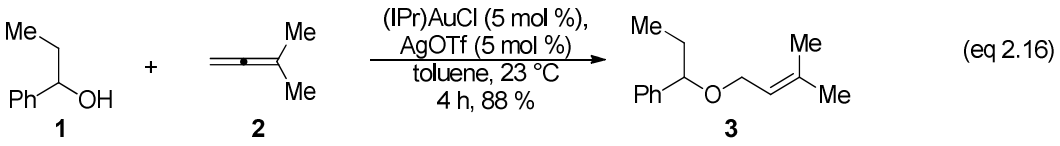

(eq 2.16)

2.1.3 Mechanism of Hydroalkoxylation

Intramolecular reaction mechanisms have been proposed for lanthanide-catalyzed (La, Sm, and Y) hydroalkoxylation with alkenes [64] and alkynes. [63] Available evidence suggests the mechanism of gold(I)-catalyzed allene hydroalkoxylation is quite different. Widenhoefer and coworkers have evaluated the stereochemistry of gold(I)-catalyzed intramolecular and intermolecular hydroalkoxylation and hydroamination of allenes with alcohols and carbamates, which point towards an outer-sphere mechanisms for these transformations. [32, 36] The reaction of (*S*)-nona-4,5-dien-1-ol catalyzed by Au[P(*t*-Bu)$_2$(*o*-biphenyl)]Cl (5 mol %) and AgOTs (5 mol %) in toluene-d$_8$ at room temperature for 2 h led to the formation of (*R,E*)-2-(pent-1-en-1-yl)tetrahydrofuran in 81 % ee and (*R,Z*)-2-(pent-1-en-1-yl)tetrahydrofuran in 84 % ee in 87 % yield by ^{1}H NMR (E:Z 5.3:1) (eq 2.17). [32] The reaction of (*S*)-benzyl nona-4,5-dien-1-ylcarbamate catalyzed by Au[P(*t*-Bu)$_2$(*o*-biphenyl)]Cl (5 mol %) and AgOTf (5 mol %) in dioxane at room temperature for 45 min led to the isolation of (*R,E*)-benzyl 2-(pent-1-en-1-yl)pyrrolidine-1-carboxylate in 74 % ee in 96 % yield by ^{1}H NMR (eq 2.18). [32] The reaction of (*S*)-penta-2,3-dien-1-yl benzoate with benzyl alcohol catalyzed by (IPr)AuCl/AgOTf (5 mol %) in toluene at room temperature for 20 min led to the isolation of (*R,E*)-4-[1-(benzyloxy)ethoxy]but-2-en-1-yl benzoate in 83 % yield and 79 %

ee (eq 2.19).[36] For these reasons we considered an outer-sphere mechanism for the gold(I)-catalyzed intermolecular hydroamination of allenes with alcohols.

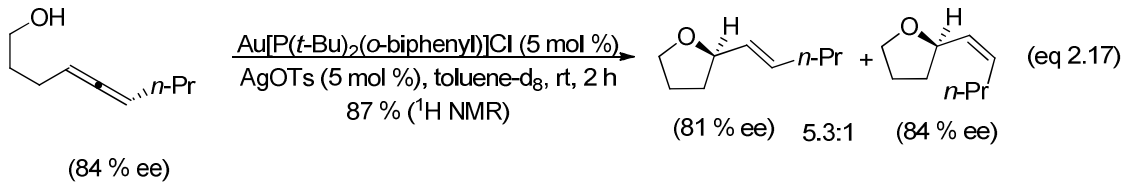

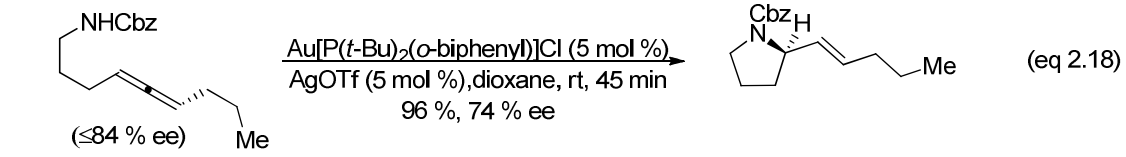

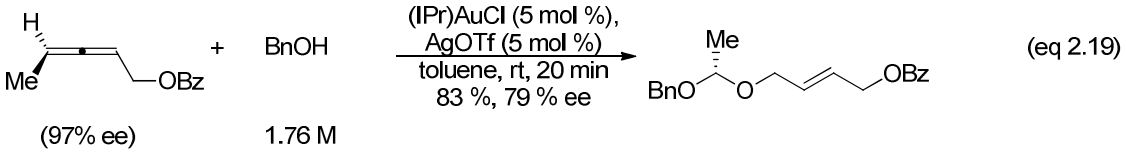

2.1.4 Scope of Study

The goals of this project were: (1) to elucidate the reaction order and mechanism for the gold(I)-catalyzed hydroalkoxylation of alcohols with allenes catalyzed by (IPr)AuCl and AgOTf, and (2) explore the reversibility of hydroalkoxylation. Widenhoefer and coworkers also reported that (IPr)AuCl with AgOTf, catalyzes the intermolecular hydroamination of allenes with carbamates. [31] For example, benzyl carbamate and **2** were treated with a catalytic amount of (IPr)AuCl (5 mol %) and AgOTf (5 mol %) in dioxane at 23 °C for 24 h to form benzyl (2-methylbut-3-en-2-yl)carbamate (**5**) in 93 % yield (eq 2.20). [31] We also investigated the kinetics of gold(I)-catalyzed intermolecular hydroamination because of the similarities between the intramolecular

hydroalkoxylation and hydroamination reactions and their proposed mechanisms. Also, we chose to study gold(I)-catalyzed intermolecular hydroamination because of the similarities in its catalytic system to that of the intermolecular hydroalkoxylation reaction despite the differences in regioselectivity of the reaction. We also studied the competition between nucleophilic attack by alcohols and carbamates on allenes. The rate behavior for the gold(I)-catalyzed hydroalkoxylation and hydroamination was elucidated by evaluating the absolute concentrations of nucleophile (alcohol or carbamate), allene, and (IPr)AuCl in relation to the change in nucleophile concentration over time.

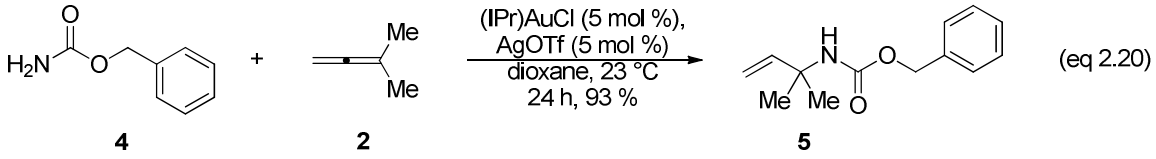

4 2 5 (eq 2.20)

2.2 Kinetics of Hydroalkoxylation.

2.2.1 Rate dependence on alcohol concentration

We sought to establish the rate behavior of the gold(I)-catalyzed intermolecular hydroalkoxylation of an allene with an alcohol under catalytic conditions that approximated the relative and absolute concentrations of alcohol, allene, and catalyst used in preparatory scale reactions. [36] To this end, kinetic studies of the hydroalkoxylation of 1-phenylpropanol (**1**) and 3-methyl-1,2-butadiene (**2**) catalyzed by (IPr)AuCl and AgOTf in toluene at room temperature were performed because of the

ability to monitor the reaction progress by GC (eq 2.16). Reaction mixtures were monitored periodically by removing aliquots (10 μL) at regular time intervals and analyzing the aliquots by gas chromatography. The concentration of **1** was determined from the integration of the GC peak of **1** relative to that of *n*-tetradecane, internal standard. The pseudo first-order rate constants for the intermolecular hydroamination of **1** and **2** catalyzed by (IPr)AuCl and AgOTf in toluene as a function of [allene], [alcohol], and [catalyst] are shown in Table 2.1.

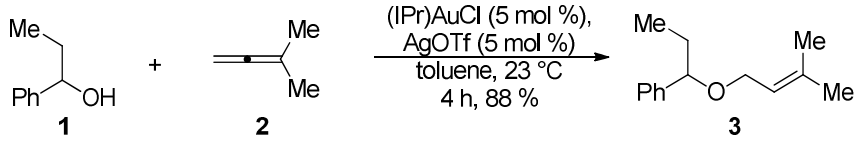

(eq 2.16)

We sought to determine the rate dependence on alcohol concentration in gold(I)-catalyzed hydroalkoxylation. To this end, the reaction order in alcohol was determined by evaluating the change in concentration of **1** (0.24 M) in reaction with **2** as a function of time under pseudo first-order conditions employing excess allene (3.0 M), a constant concentration of catalyst (15 mM) at room temperature. Alcohol concentration was monitored until > 90% conversion (Table 2.1, entry 3). A plot of [**1**] versus time displayed curvature, consistent with non-zero-order dependence of [**1**] on the rate of conversion of **1** to **3** (Figure 2.1). Indeed, a plot of ln[**1**] versus time was linear to > 3 half-lives, consistent with the first-order dependence of [**1**] on the rate of conversion of **1** to **3** (Figure 2.1) (k_{obs} = 5.1 ± 0.1 x 10^{-4} s^{-1}). In a similar manner, the reaction order in alcohol

was determined for the reaction of **1** (0.14 M) and **2** (1.7 M) catalyzed by (IPr)AuCl and AgOTf (15 mM) at 24 °C under pseudo first-order conditions. A plot of ln[**1**] versus time was linear to > 3 half-lives, consistent with the first-order dependence of [**1**] on the rate of conversion of **1** to **3** (Figure 2.2) (k_{obs} = 4.6 ± 0.1 x 10^{-4} s^{-1}). In a third experiment, the reaction order in alcohol was determined for the reaction of **1** (0.48 M) and **2** (5.2 M) catalyzed by (IPr)AuCl and AgOTf (15 mM) at 24 °C. A plot of ln[**1**] versus time was linear to > 3 half-lives, which established the first-order dependence of [**1**] on the rate of conversion of **1** to **3** (Figure 2.3) (k_{obs} = 5.1 ± 0.1 x 10^{-4} s^{-1}). Comparison of these pseudo first-order rate constants and a plot of k_{obs} versus $[alcohol]_0$ revealed that these rate constants differed by ~ 20 % (Figure 2.4), implying first-order dependence of the rate on [alcohol] over the range of 0.14 M to 0.48 M (Table 2.1).

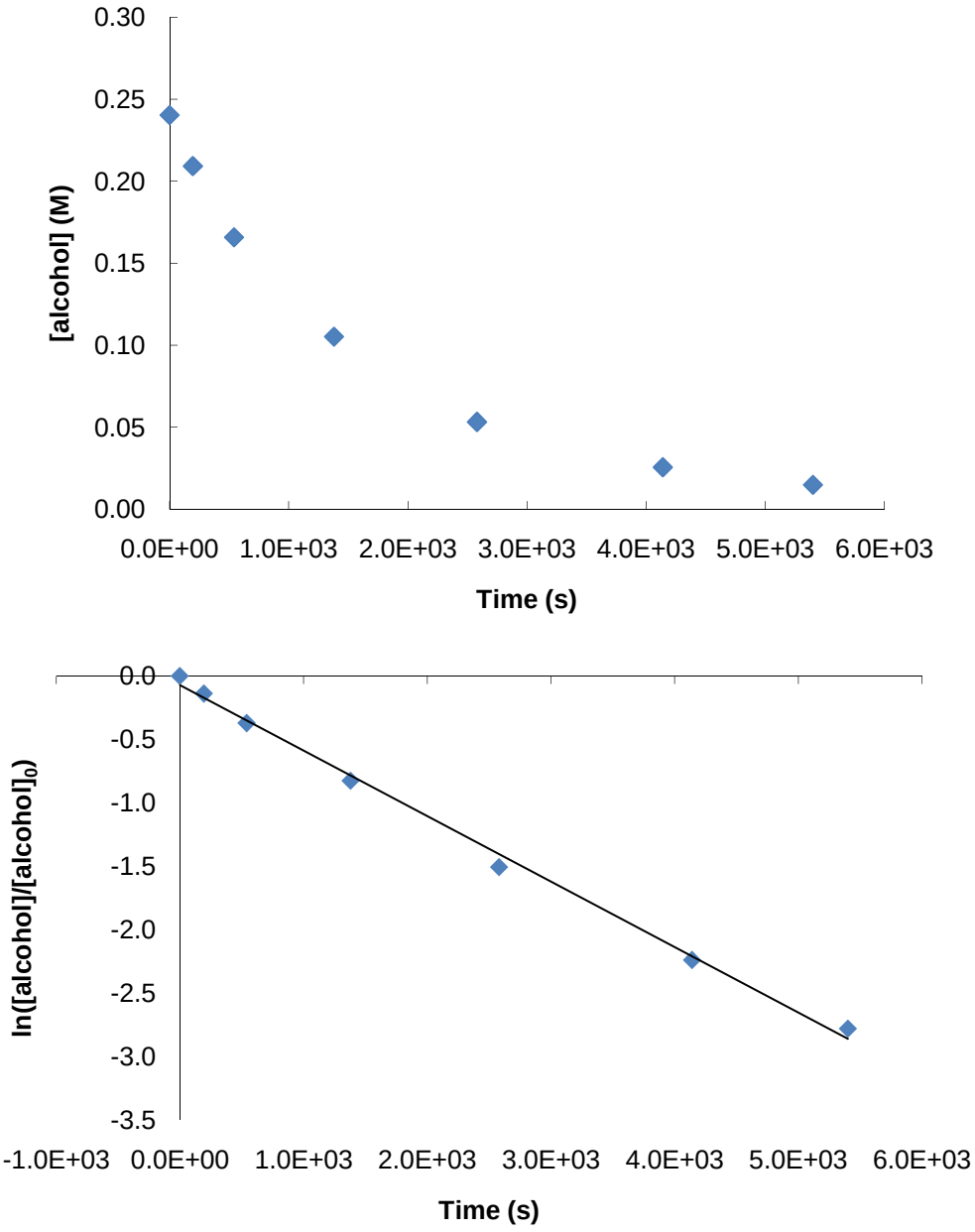

Figure 2.1. Concentration versus time (top) and pseudo first-order (bottom) plots for the intermolecular hydroalkoxylation of [3-methyl-1,2-butadiene]= 3.0 M with [1-phenylpropanol] = 0.24 M using [(IPr)AuCl/AgOTf] = 15 mM as the catalyst in toluene. The non-linear slope is indicative of the non zero-order dependence of 1-phenylpropanol (k_{obs} = 5.1 ± 0.1 x 10^{-4} s^{-1}). (Table 2.1, entry 3)

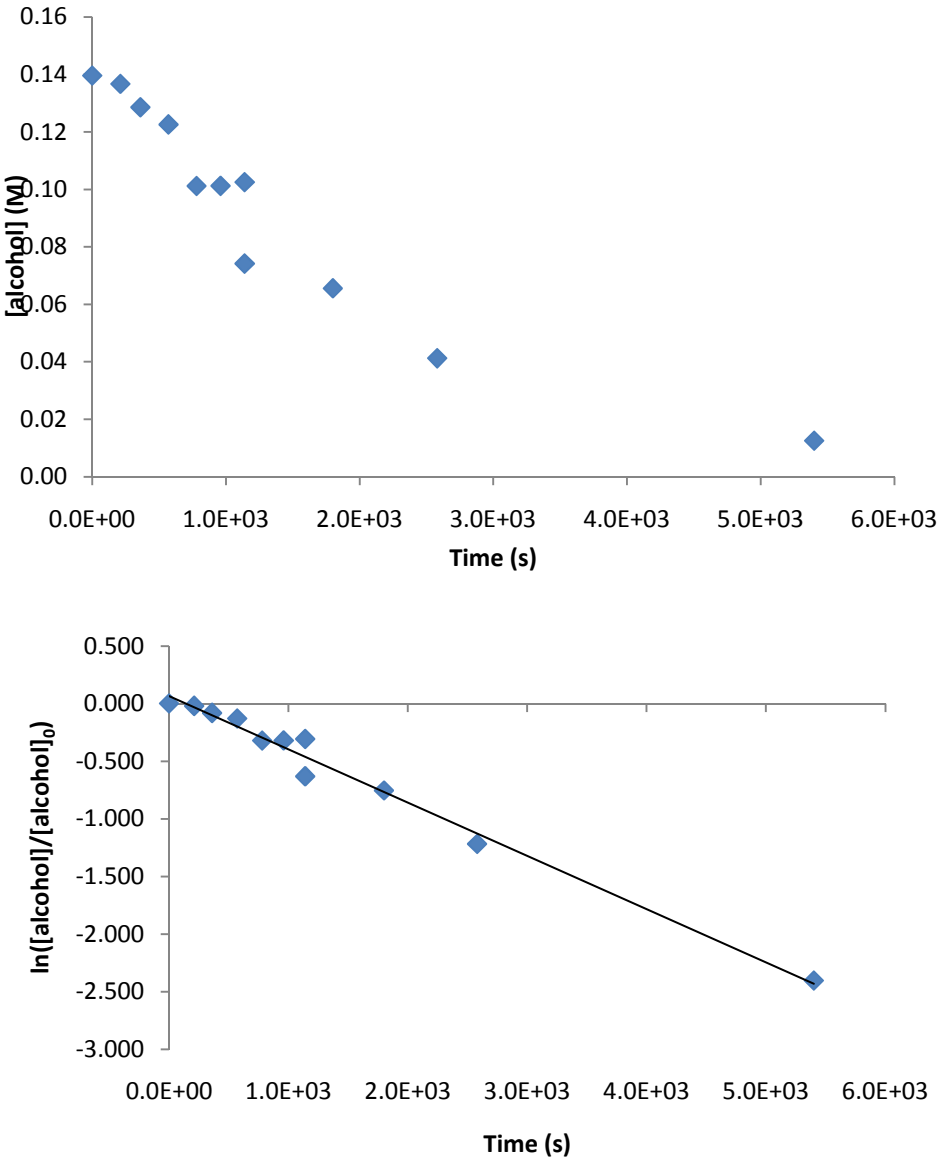

Figure 2.2. Concentration versus time (top) and pseudo first-order (bottom) for the gold(I)-catalyzed intermolecular hydroalkoxylation of 3-methyl-1,2-butadiene with 1-phenylpropanol in toluene at room temperature. [2] = 1.7 M, [1] = 0.14 M, [(IPr)AuCl/AgOTf] = 15 mM (k_{obs} = 4.6 ± 0.1 x 10^{-4} s^{-1}) (Table 2.1, entry 1)

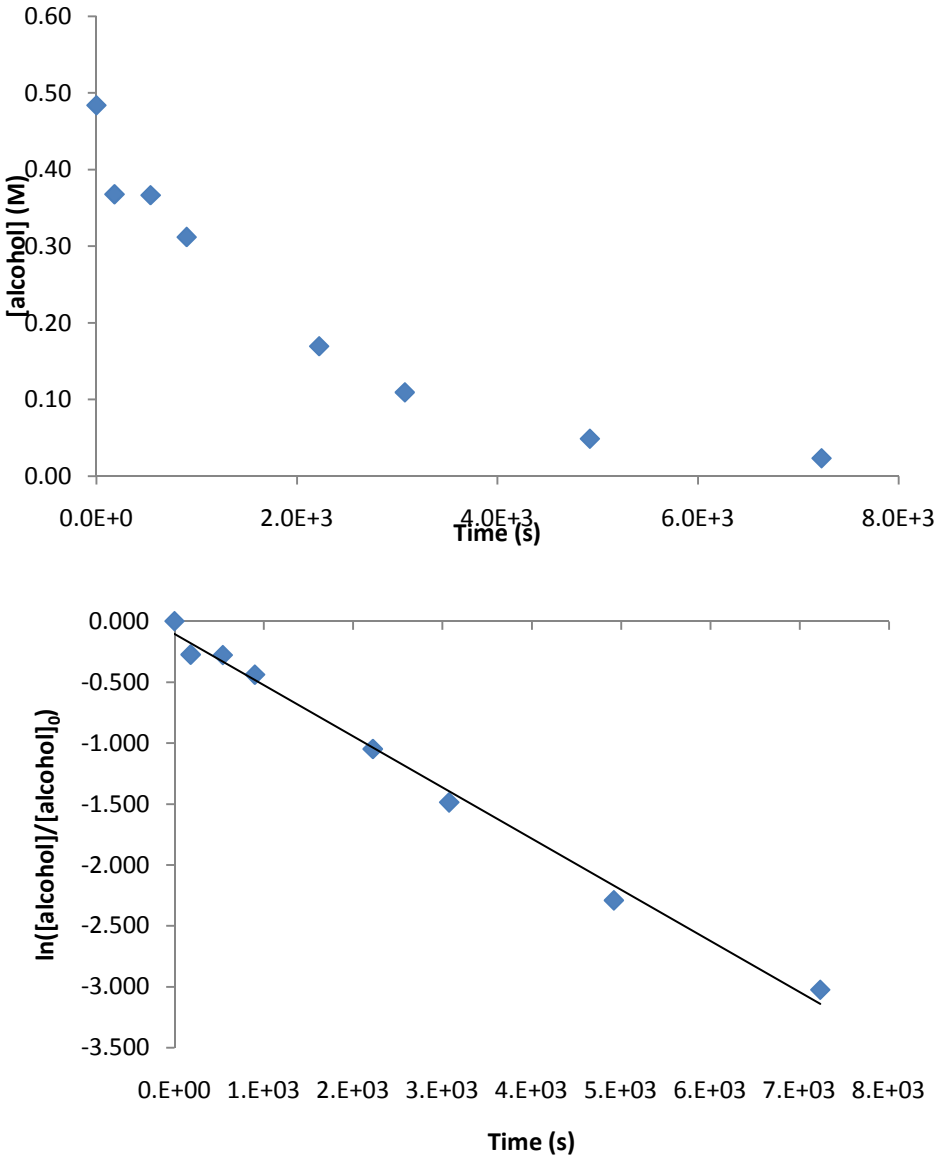

Figure 2.3. Concentration versus time (top) and pseudo first-order (bottom) for the gold(I)-catalyzed intermolecular hydroalkoxylation of 3-methyl-1,2-butadiene with 1-phenylpropanol in toluene at room temperature. [2] = 5.2 M, [1] = 0.48 M, [(IPr)AuCl/AgOTf] = 15 mM k_{obs} = 4.2 ± 0.1 x 10^{-4} s^{-1} (Table 2.1, entry 2)

Table 2.1. Observed rate constants for the intermolecular hydroalkoxylation of 1-phenylpropanol (1) and 3-methyl-1,2-butadiene (2) catalyzed by (IPr)AuCl and AgOTf in toluene as a function of [allene], [alcohol], and [catalyst].

Entry	[allene] (M)	[alcohol] (M)	[catalyst] (mM)	k_{obs} (s^{-1}) (10^{-4})[a]	Temp (°C)
1	1.7	0.14	15	4.6 ± 0.1	24
2	5.2	0.48	15	4.2 ± 0.1	24
3	3.0	0.24	15	5.1 ± 0.1	24
4	0.32	0.34	15	0.5 ± 0.1	24
5	0.65	0.35	15	1.8 ± 0.1	24
6	1.9	0.34	15	4.1 ± 0.5	23
7	1.0	0.38	14	3.1 ± 0.1	24
8	1.4	0.37	14	3.3 ± 0.1	23
9	0.87	0.35	14	2.9 ± 0.1	24
10	2.4	0.38	15	5.0 ± 0.1	24
11	3.4	0.35	14	5.3 ± 0.1	24
12	2.7	0.34	15	5.3 ± 0.1	24
13	3.7	0.34	15	5.3 ± 0.1	24
14	2.7	0.34	15	5.3 ± 0.1	24
15	2.5	0.37	28	6.3 ± 0.1	24
16	2.5	0.37	57	10. ± 0.5	24
17	2.6	0.36	43	7.9 ± 0.2	24
18	2.5	0.33	10	2.2 ± 0.2	24
19	2.6	0.35	5	1.2 ± 0.1	24
20	2.5	0.34	15	2.8 ± 0.1	24

[a] Error in k_{obs} values determined from the standard deviation of the slope for the plot of ln[alcohol] versus time

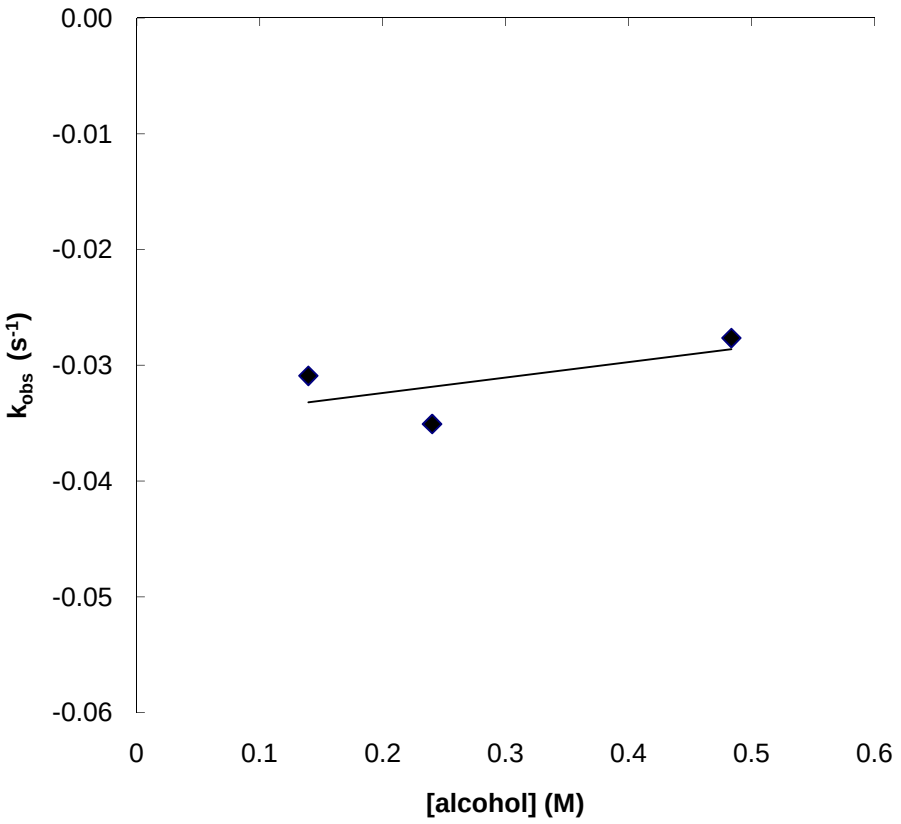

Figure 2.4. Plot of the observed rate versus alcohol concentration for the intermolecular hydroalkoxylation of 1-phenylpropanol (1) with 3-methyl-1,2-butadiene (2) using (IPr)AuCl/AgOTf as the catalyst in toluene. The slope (0.013) confirms the first-order dependence in alcohol from 0.14 to 0.48 M.

2.2.2 Rate dependence on gold concentration

After establishing the first-order dependence of [**1**] on the rate of gold(I)-catalyzed intermolecular hydroalkoxylation, we sought to determine the rate dependence on catalyst concentration. To this end, the rate was evaluated as a function of catalyst concentration maintaining a 1:1 ratio of (IPr)AuCl/AgOTf from 5 mM to 57 mM, under pseudo first-order conditions at constant $[\mathbf{1}]_0$ (0.35 M) and $[\mathbf{2}]_0$ (2.5 M). For each reaction, pseudo first-order decay of [**1**]was observed to ~3 half-lives (Table 2.1, entry 15 - 20; Figure 2.37 - Figure 2.42). A plot of pseudo first-order rate constants of the six experiments versus the concentration of (**1**)AuCl and AgOTf was linear which established the apparent first-order dependence of the rate on [catalyst] (Figure 2.5). The pseudo second-order rate constant was found to be $0.018 \pm 0.004\ M^{-1}s^{-1}$ and the pseudo second order rate law was determined to be rate = k_2 [**1**][catalyst] in the presence of excess allene. To verify this linear relationship, a van't Hoff plot of $\ln(k_{obs})$ versus ln[catalyst] gave a slope of 0.8 ± 0.2 consistent with first-order dependence on the rate on [catalyst] (Figure 2.6).

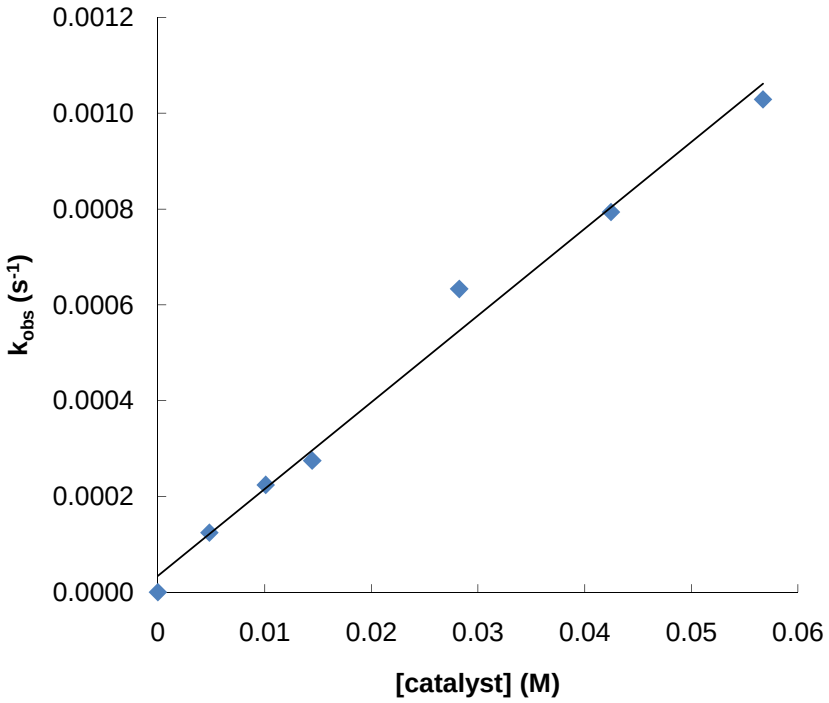

Figure 2.5. Plot of observed rate versus time for the intermolecular hydroalkoxylation of 1 (~0.35 M) with 2 (~2.5 M) using (IPr)AuCl/AgOTf as the catalyst in toluene. The plot indicates first-order behavior with respect to catalyst. The pseudo second order rate constant was determined to k_2 = be 0.018 ± 0.004 $M^{-1}s^{-1}$.

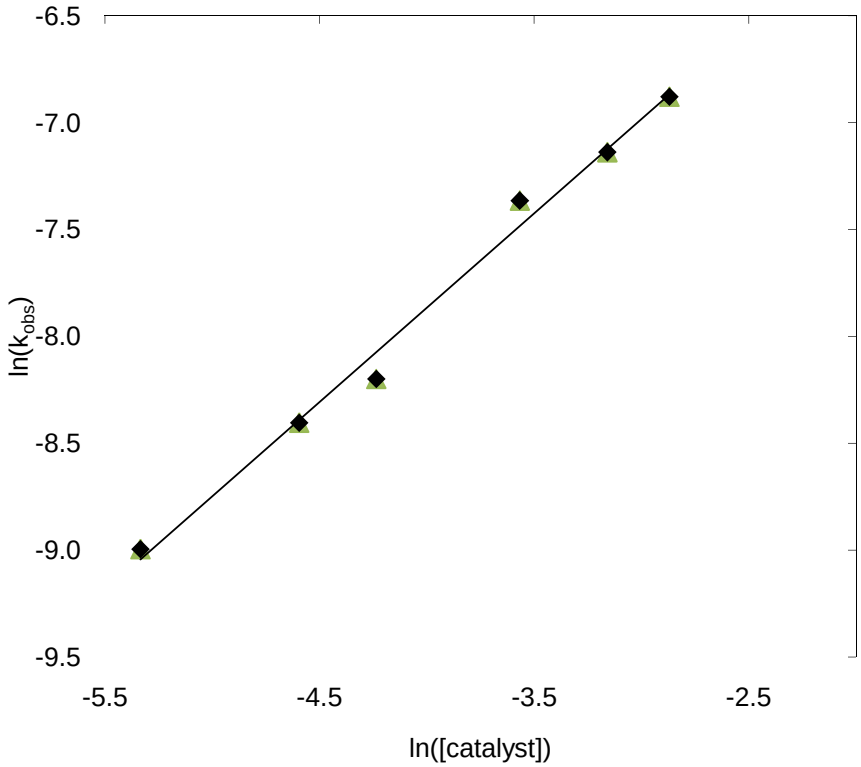

Figure 2.6. Van't Hoff plot of the hydroalkoxylation of 1-phenylpropanol with 3-methyl-1,2-butadieneusing (IPr)AuCl/AgOTf as the catalyst in toluene at room temperature. The slope of the line was found to be 0.8 ± 0.2.

2.2.3 Rate dependence of hydroalkoxylation on allene concentration

Having established the first-order dependence of both [**1**] and [catalyst] on the hydroalkoxylation of **1** with **2** catalyzed by (IPr)AuCl/AgOTf under pseudo first-order conditions (excess allene), we sought to determine the rate dependence of gold(I)-catalyzed hydroalkoxylation on **2**. We evaluated the rate as a function of **2** from 0.32 M to 3.7 M at a constant [**1**] (0.35 M) and [catalyst] (15 mM). Reactions in which pseudo first-order conditions were not maintained were monitored until ~ 10% conversion. In these cases, reactions were monitored throughout complete conversion, and the plots include the linear portion of the data (Table 2.1, entry 4 – 14; Figure 2.26 - Figure 2.36). A plot of pseudo first-order rate constants versus [allene] (Figure 2.7) revealed non-linear dependence of the rate on [allene]. The rate increased approximately linearly with increasing [allene] at low allene concentrations (0 – 1 M), and then more slowly as [allene] was increased from 1 – 3 M with saturation achieved at ~ 2 M. Overall, the empirical rate law can be expressed as: rate = k_3[**1**]^1[allene]^1[catalyst]^1 at low concentrations of allene, with a third order rate of k_3 = 0.0244 ± 0.004 M^{-2} s^{-1} under these conditions. At high concentrations of allene, the rate can be expressed as: rate = k_{sat} [**1**]^1[catalyst]^1 with a second-order rate of k_{sat} = 0.018 ± 0.004 $M^{-1}s^{-1}$.

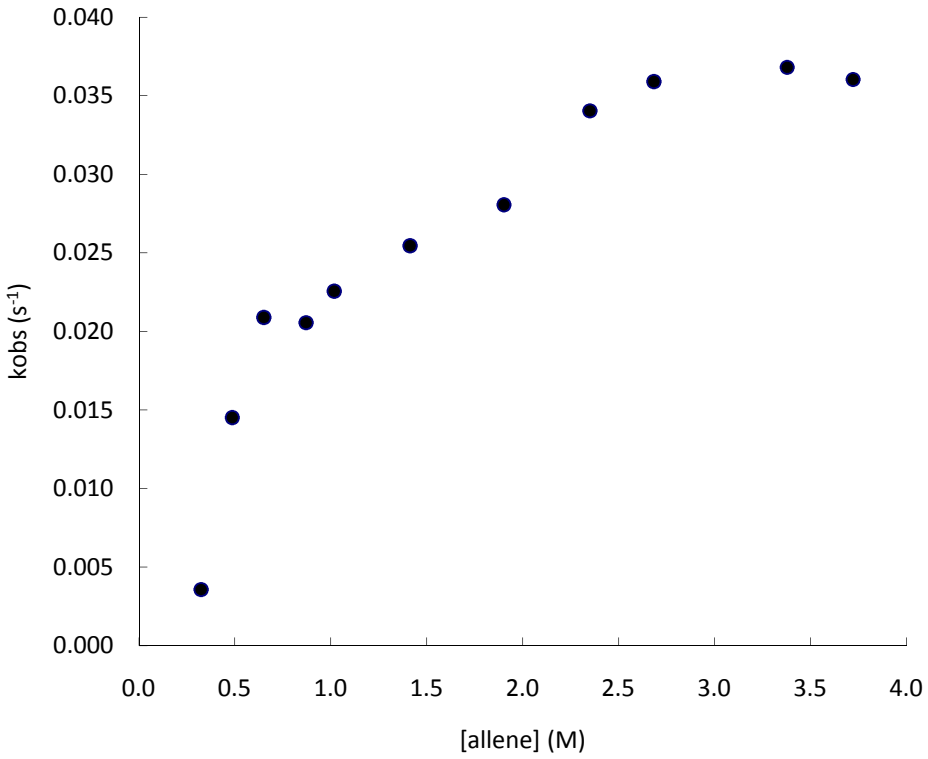

Figure 2.7. Plot of pseudo first-order rate constants versus [2] = 0.32 – 3.7 M for the intermolecular hydroalkoxylation of 1 (~ 0.35 M) with 2 employing (IPr)AuCl/AgOTf (~14 mM) as the catalyst in toluene at room temperature. The pseudo third order rate constant was determined to be $k_3 = 0.0244 \pm 0.004\ M^{-2}\ s^{-1}$.

2.2.4 Effect of excess triflate on the gold(I)-catalyzed hydroalkoxylation of allenes with alcohols

AgOTf is required in the gold(I)-catalyzed hydroalkoxylation of allenes to abstract the chloride ligand from (IPr)AuCl and generate the active gold cationic catalyst, (IPr)Au-OTf. Because triflate is a potential coordinating ligand for gold, we sought to evaluate the effect of [TfO^-] on the rate of gold(I)-catalyzed hydroalkoxylation. Therefore, the effect of excess triflate on the rate of gold(I)-catalyzed hydroalkoxylation was evaluated by determining the pseudo first-order rate constants for the reaction of **1** with **2** catalyzed by a 1:1 mixture of (IPr)AuCl and AgOTf in toluene at room temperature as a function of [OTf^-], employing tetrabutylammonium trifluoromethanesulfonate (0.25 M) as a source of soluble triflate anion. To this end, reaction of [**1**] (0.25 M), [**2**] (2.0 M) and [(IPr)AuCl/AgOTf] (11 mM) that contained OTf^- (25 mM) at room temperature was monitored by GC.

A plot of $[\mathbf{1}]_t$ versus time displayed curvature, consistent with non-zero-order dependence of [**1**] on the rate of conversion of **1** to **3**. Conversely, a plot of ln[**1**] versus time was linear to > 3 half-lives, consistent with the first-order dependence of the rate on [**1**] (Table 2.2, entry 2; Figure 2.43). The pseudo first-order rate constant for the reaction with excess triflate was found to be $k_{obs} = 2.9 \times 10^{-5}\ s^{-1}$, this value was compared with the observed rate constant for the reaction of [**1**] (0.34 M), [**2**] (2.5 M) and [(IPr)AuCl/AgOTf] (14 mM) in toluene at room temperature, $k_{obs} = 2.8 \times 10^{-4}\ s^{-1}$ (Table 2.2, entry 1; Figure 2.42). From these values we conclude that the presence of excess triflate slowed the

reaction by approximately 93 %. The inhibition of the catalytic reaction by excess triflate by approximately one order of magnitude is shown graphically in Figure 2.8.

Table 2.2. Observed rate constant for the intermolecular hydroalkoxylation of alcohol with allene catalyzed by (IPr)AuCl and AgOTf in toluene at 24 °C as a function of [allene], [alcohol], [catalyst], and [Bu_4NOTf].

Entry	[allene] (M)	[alcohol] (M)	[catalyst] (mM)	[Bu_4NOTf] (M)	k_{obs} (s^{-1}) (10^{-4})[a]
1	2.5	0.34	15	0.00	2.8 ± 0.1
2	2.0	0.25	11	0.25	0.29 ± 0.01

[a] Error in k_{obs} values determined from the standard deviation of the slope for the plot of ln[alcohol] versus time

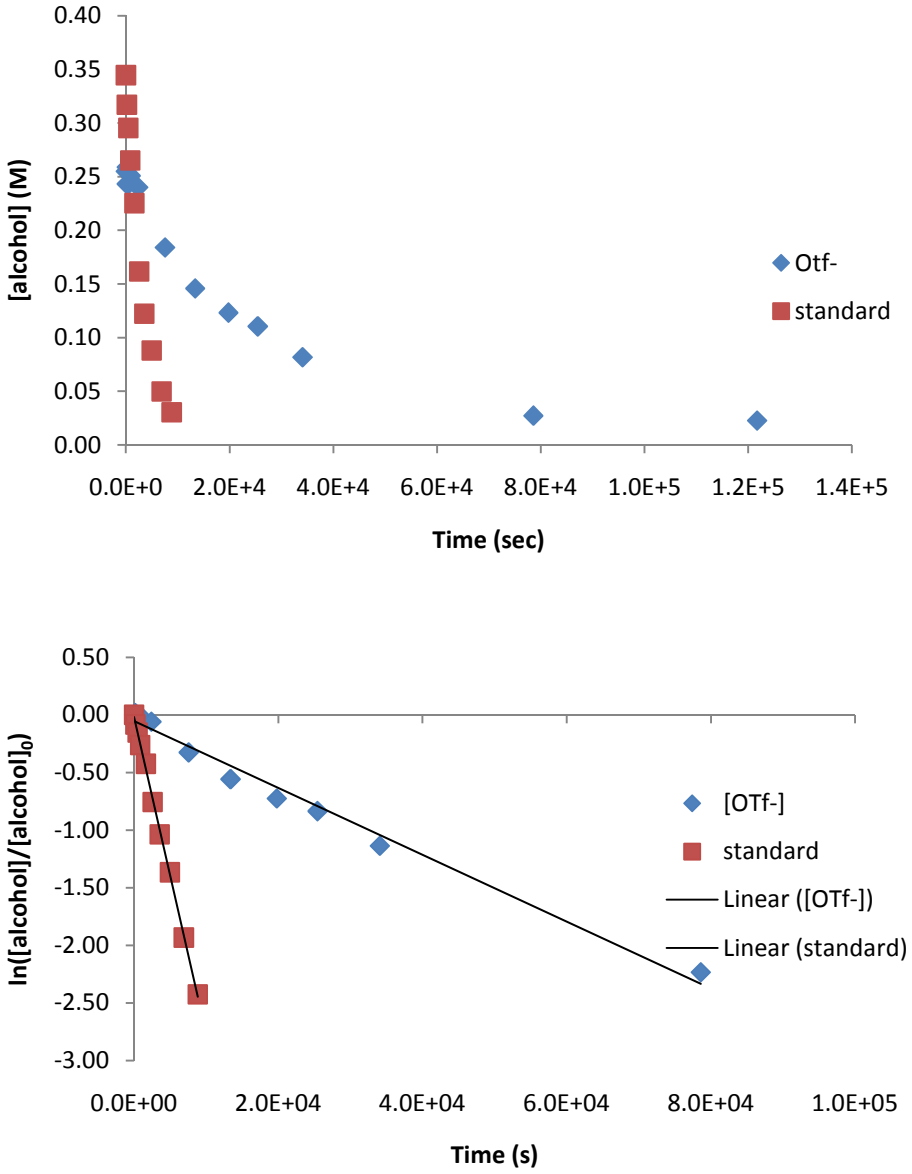

Figure 2.8. Concentration versus time (top) and pseudo first-order (bottom) plots for the reaction of 1 (0.34 M and 0.25 M) and 2 (2.5 M and 2.0 M) catalyzed by (IPr)AuCl/AgOTf (15 mM and 11 mM) in the absence of Bu_4NOTf and in the presence of 0.25 M Bu_4NOTf. Pseudo first-order rate constants were 2.82 ± 0.08 x 10^{-4} s^{-1} and 0.29 ± 0.01 x 10^{-4} s^{-1}, respectively, indicating a ~ 10 fold decrease in reaction rate (Table 2.2, entry 1 and 2).

2.2.5 Reversibility

Gold(I)-catalyzed intermolecular hydroalkoxylation of 1,1-disubstituted allenes has been shown to produce primary allylic ethers.[36, 108, 116] However, gold(I)-catalyzed intermolecular hydroamination of 1,1-disubstituted allenes with carbamates has been shown to produce the tertiary amine. [24, 118] Maseras proposed from DFT studies that nucleophilic attack of an Au(I)-coordinated allene occurs reversibly for the Au(I)-catalyzed intermolecular hydroalkoxylation of allenes and that the Au(I)-catalyzed mechanism allows the facile interconversion of regioisomeric allylic ether products.[119] Lee and coworkers developed a highly regioselective gold(I)-catalyzed system to form tertiary allylic ethers by (presumably) preventing the isomerization of the tertiary allylic ether product to a primary allylic ether product.[109]

For the reasons outlined above, we sought to evaluate the potential reversible formation of the tertiary alkyl ether (**6**) in the gold(I)-catalyzed conversion of **1** and **2** to **3**. To this end, we synthesized **6** and treated this compound with (IPr)AuCl (5 mol %) and AgOTf (5 mol %) in toluene for two hours at room temperature (eq 2.21). The reaction mixture was loaded onto a silica gel-filled pipet and eluted with $CDCl_3$ to remove the catalyst. The ^1H NMR spectrum of the crude reaction mixture was taken to evaluate the conversion of **6** to **7**. The alkenyl region (δ 4.5 to 6.5) of the spectrum was compared to the alkenyl region of the ^1H NMR spectrum of **6**. It was determined via ^1H

NMR that only the starting material was present and that **6** does not isomerizes to form **7** with (IPr)AuCl (5 mol %) and AgOTf (5 mol %) in toluene at room temperature in 2 h.

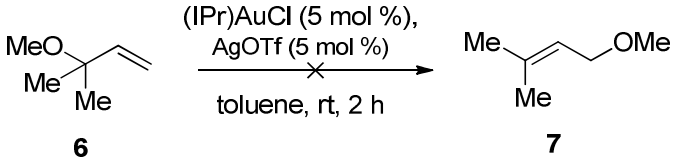

6 **7** (eq 2.21)

Then, we explored the potential conversion of **6** to **7** in the presence of alcohol. To this end, **6** was reacted with MeOH (1 equiv), (IPr)AuCl (5 mol %) and AgOTf (5 mol %) in toluene for two hours at room temperature (eq 2.22). ^{1}H NMR analysis of the alkenyl region (δ 4.5 - 6.5) of the crude of the reaction mixture was compared to the alkenyl region of the starting material, **6**. It was determined from ^{1}H NMR spectroscopy that only the starting material was present and that **6** does not isomerizes to form **7** when reacted with one equivalent of methanol and (IPr)AuCl (5 mol %) and AgOTf (5 mol %) in toluene at room temperature for 2 h. From these experiments we concluded that product **3** formed in the gold(I)-catalyzed hydroalkoxylation of **1** with **2** is not formed through a reversible process involving initial formation of the tertiary allylic ether.

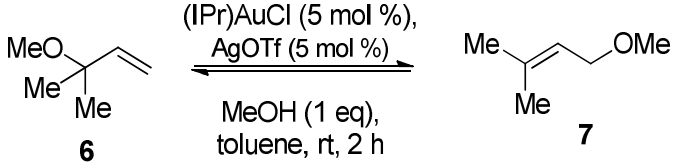

6 **7** (eq 2.22)

2.2.6 Deuterium Labeling Studies

To further probe the mechanism of the gold(I)-catalyzed intermolecular hydroamination of **2** with **1** catalyzed by (IPr)AuCl and AgOTf, we evaluated the rate of hydroalkoxylation employing 1-phenyl-1-propanol-OD (**1**-d_1). To this end, a mixture of **2** (1.4 M), **1-*d*$_1$** (0.37 M) (≥95% d), (IPr)AuCl and AgOTf (15 mM) and *n*-tetradecane in toluene was stirred at room temperature and the disappearance of **1-*d*$_1$** was monitored by GC analysis, which presumably formed {1-[(3-methylbut-2-en-1-yl)oxy]propyl}benzene-d_1 (3- d_1), it should be noted that deuterium incorporation into the product was not confirmed, but a similar experiment employing CH_3OD led to ~80% deuterium incorporation into the vinylic position of the allylic ether (eq 2.23) (Table 2.3). [36]

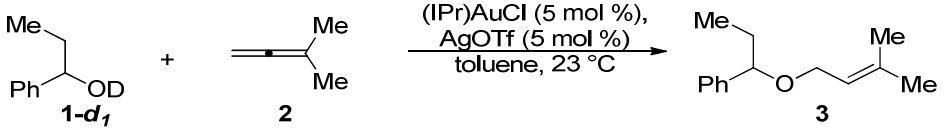

(eq 2.23)

A plot of the ln [**1-*d*$_1$**] versus time gave a straight line with a slope of k_{obs} = 1.6 ± 0.1 x 10^{-4} s^{-1} (Figure 2.9). As a point of comparison, the reaction of **2** (1.4 M) was reacted with **1** (0.36 M) with (IPr)AuCl and AgOTf (15 mM) in toluene at room temperature. A plot ln [**1**] versus time gave a straight line with a slope of k_{obs} = 2.8 ± 0.1 x 10^{-4} s^{-1} (Figure 2.9), which corresponds to a primary KIE of k_H/k_D = 1.8 ± 0.2 (Table 2.3).

Kinetic isotope effects occur because of the difference in zero-point vibrational energy between bonds to different isotopes. The replacement of hydrogen by deuterium

increases the reduced mass, which in turn decreases the vibrational frequency. Thus the vibrational energy levels associated with deuterium are lower to those of hydrogen when bonded to the same element. Therefore, separation of a deuterium bond requires more energy than does the removal of a hydrogen bond when bonded to the same element because deuterium has a lower zero point energy, so complete dissociation requires more energy. [120-123] Primary deuterium kinetic isotope effects can be as large as 7-8 for k_H/k_D at 30 °C for rate limiting hydrogen transfer through a linear transition state having the hydrogen/deuterium atom symmetrically located between the donor and acceptor atoms. [124] Small values of $k_H/k_D < 1.5$ usually indicate that the hydrogen transfer step is not rate determining. [120, 124-126] Since the experimentally determined kinetic isotope effect for the gold(I)-catalyzed intermolecular hydroalkoxylation of **1** with **2** was greater than 1, we can conclude that protonolysis is involved in the rate determining step for the gold(I)-catalyzed intermolecular hydroalkoxylation of **2** with **1** catalyzed by (IPr)AuCl and AgOTf in toluene at room temperature. [63, 66]

Table 2.3. Observed rate constants for the intermolecular hydroalkoxylation of 3-methyl-1,2-butadiene (1.4 M) with proteo and deutero 1-phenylpropanol (0.3 M) catalyzed by (IPr)AuCl/AgOTf (15 mM) in toluene at 24 °C as a function of [alcohol].

Entry	[alcohol] (M)	k_{obs} (s^{-1})(10^{-4})[a]
1	OH - 0.36	2.8 ± 0.1
2	OD - 0.37	1.6 ± 0.1

[a] Error in k_{obs} values determined from the standard deviation of the slope for the plot of ln[alcohol] versus time

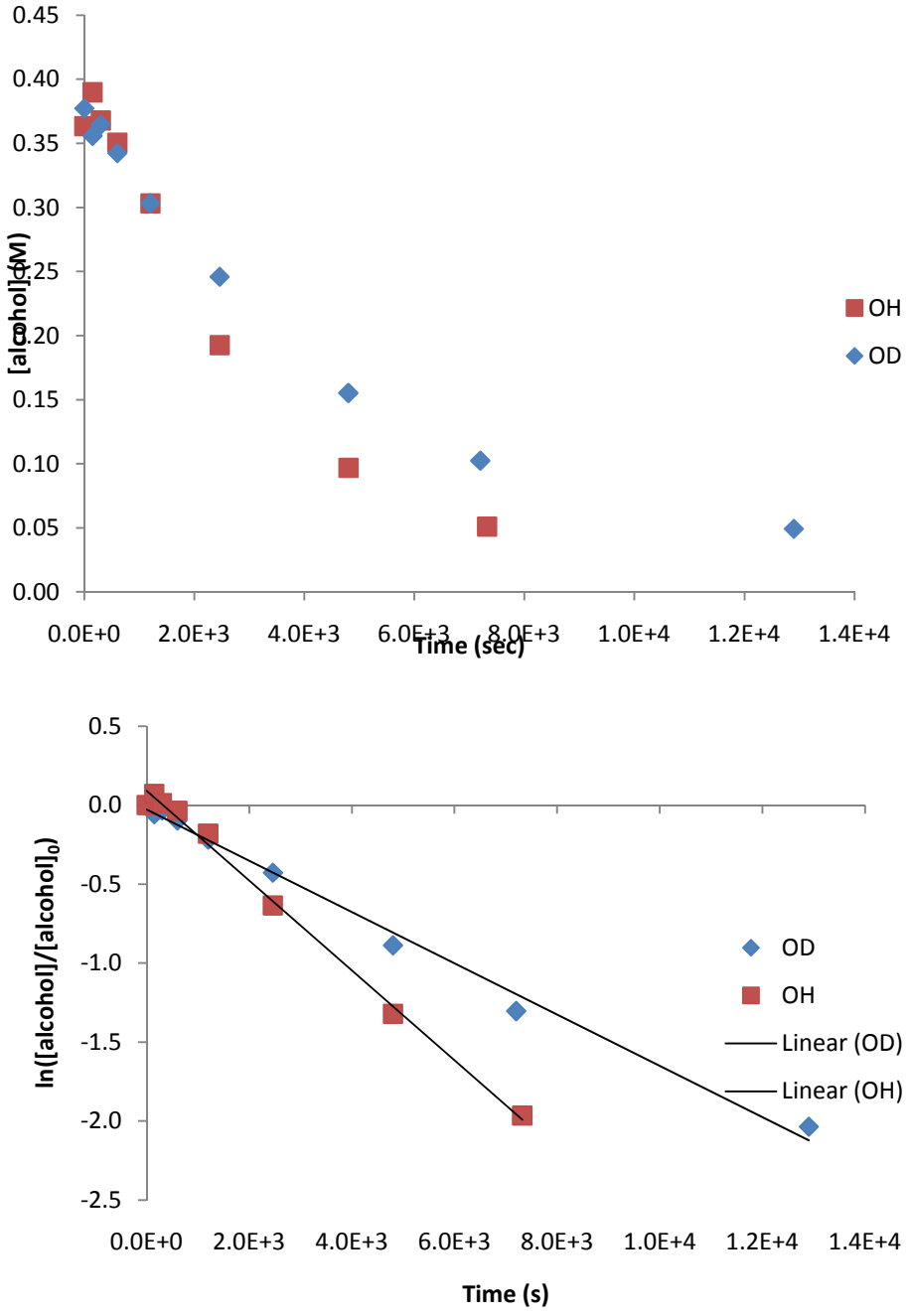

Figure 2.9. Concentration versus time (top) and pseudo first-order (bottom) plots for the reaction of 1 (0.36 M) and 1-d_1 (0.37 M) with 2 (1.4 M) catalyzed by (IPr)AuCl and AgOTf (15 mM) in toluene at 24 ° C. (k_{obs} = 2.8 ± 0.1 x 10^{-4} s^{-1} of 1 and k_{obs} = 1.6 ± 0.1 x 10^{-4} s^{-1} 1-*d*) (Table 2.3, entry 1 & 2).

2.3 Kinetic and Mechanistic Studies of Hydroamination.

2.3.1 Rate dependence on carbamate concentration

To evaluate the effects of nucleophile on the kinetics and mechanism of gold(I)-catalyzed allene hydrofunctionalization, we performed a kinetic analysis of the hydroamination of 3-methyl-1,2-butadiene (**2**) with benzyl carbamate (**4**) catalyzed by (IPr)AuCl/AgOTf to form benzyl (2-methylbut-3-en-2-yl)carbamate (**5**) (eq 2.20). We sought to establish the rate behavior of the gold(I)-catalyzed hydroamination of **4** with **2** catalyzed by (IPr)AuCl and AgOTf under catalytic conditions that approximate the relative and absolute concentrations of carbamate, allene, and catalyst in preparatory scale reactions and gain information regarding the reversal of regioselectivity compared to the gold(I)-catalyzed hydroalkoxylation reaction. [24] To gain insight into the mechanism of gold(I)-catalyzed intermolecular hydroamination kinetic studies of the hydroamination of **4** and **2** catalyzed by (IPr)AuCl and AgOTf were carried out at various concentrations in dioxane at room temperature. The extent of reaction was determined by removing aliquots (10 μL) at regular time intervals and analyzing the aliquots by gas chromatography. The concentration of **4** was determined from the integration of the GC peak of **4** relative to that of *n*-tetradecane, internal standard. The pseudo first-order rate constants for the intermolecular hydroamination of **4** with **2** catalyzed by (IPr)AuCl and AgOTf I dioxane as a function of [allene], [carbamate], and [catalyst] are shown in Table 2.4.

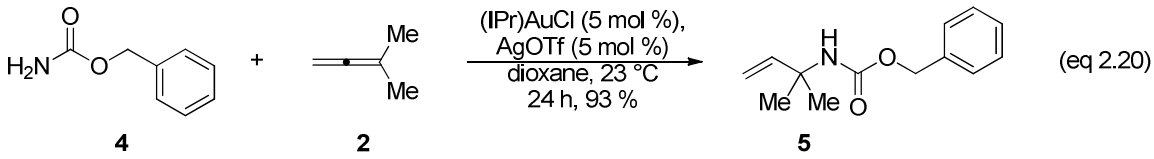

(eq 2.20)

We first sought to determine the rate dependence on carbamate concentration in gold(I)-catalyzed hydroamination. To this end, the reaction order in carbamate was determined by evaluating the concentration of **4** (0.42 M) as a function of time under pseudo first-order conditions employing excess allene (4.2 M) at a constant concentration of catalyst (19 mM) (Table 2.4, entry 1), the reaction was monitored until > 90% conversion. A plot of [**4**] versus time, displayed curvature, which is consistent with non-zero-order dependence of the rate on [**4**] on the conversion of **4** to **5** (Figure 2.10). Conversely, a plot of ln[**4**] versus time was linear to > 3 half-lives, consistent with the first-order dependence of[**4**] on the rate of conversion of **4** to **5** with a pseudo first-order rate constant of k_{obs} = 6.85 ± 0.01 x 10^{-5} s^{-1} (Figure 2.10) .

We evaluated the rate dependence on [carbamate] as a function of initial carbamate concentration. In a similar manner, the reaction order in carbamate was determined for the reaction of **4** (0.21 M) and **2** (4.2 M) catalyzed by (IPr)AuCl and AgOTf (19 mM) in dioxane at 24 °C (Table 2.4, entry 2). A plot of ln[**4**] versus time was linear to > 3 half-lives, consistent with the first-order dependence of [**4**] on the rate of conversion of **4** to **5** with a pseudo first-order rate constant of k_{obs} = 8.27 ± 0.05 x 10^{-5} s^{-1} (Figure 2.11). In a third experiment, the reaction order in carbamate was determined for

the reaction of **4** (0.10 M) and **2** (4.2 M) catalyzed by (IPr)AuCl and AgOTf (19 mM) in dioxane at 24 °C (Table 2.4, entry 3). A plot of ln[**4**] versus time was linear to > 3 half-lives, consistent with the first-order dependence of [**4**] on the rate of conversion of **4** to **5** with a pseudo first-order rate constant of $k_{obs} = 9.10 \pm 0.05 \times 10^{-5}$ s^{-1} (Figure 2.12).

Analysis of these pseudo first-order rate constants and a plot of k_{obs} versus [carbamate] revealed that the rate decreased slightly with increasing [carbamate], suggesting modest inhibition of the rate with increasing [carbamate] consistent with complexation of carbamate to gold(Figure 2.13), and apparent first-order dependence of the rate on [carbamate] over the range of 0.10 M to 0.42 M (Table 2.4, entry 1-3).

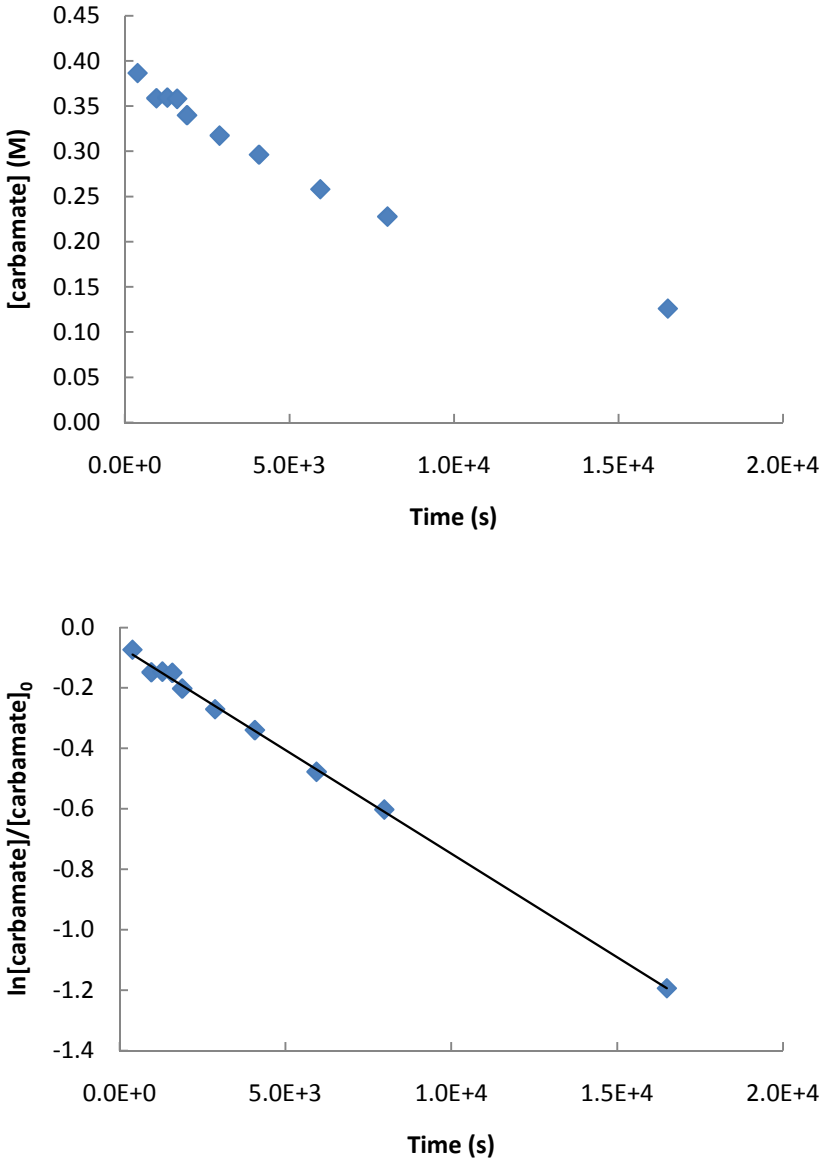

Figure 2.10. Concentration versus time (top) and pseudo first-order (bottom) plots for the intermolecular hydroamination of [2] = 4.2 M with [4] = 0.42 M catalyzed by [(IPr)AuCl/AgOTf] = 19 mM in dioxane at 24 °C (k_{obs} = 6.85 ± 0.01 x 10^{-5} s^{-1}) (Table 2.4, entry 1).

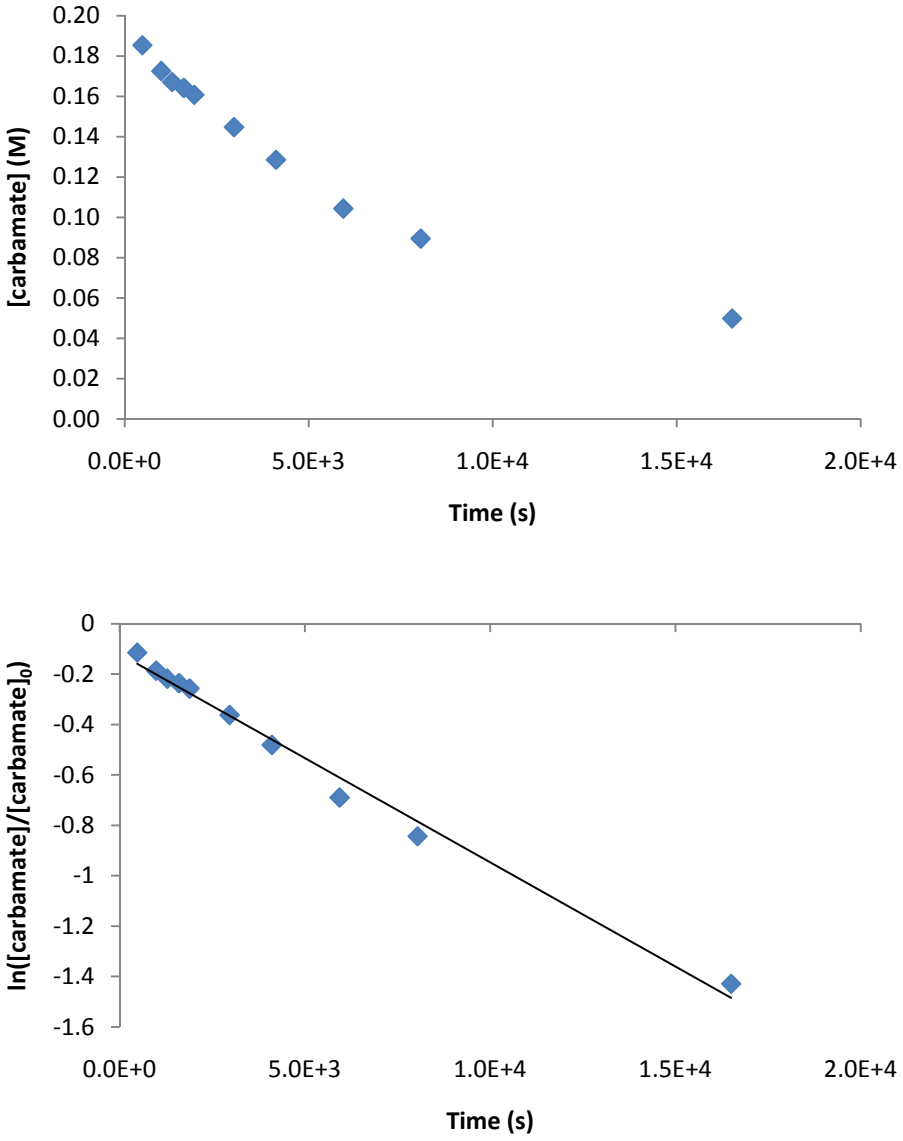

Figure 2.11. Concentration versus time (top) and pseudo first-order (bottom) plots for the gold(I)-catalyzed intermolecular hydroamination of benzyl carbamate with 3-methyl-1,2-butadiene in dioxane at room temperature. [2] = 4.2 M, [4] = 0.21 M, [(IPr)AuCl/AgOTf] = 19 mM (k_{obs} = 8.27 ± 0.05 x 10^{-5} s^{-1}) (Table 2.4, entry 2)

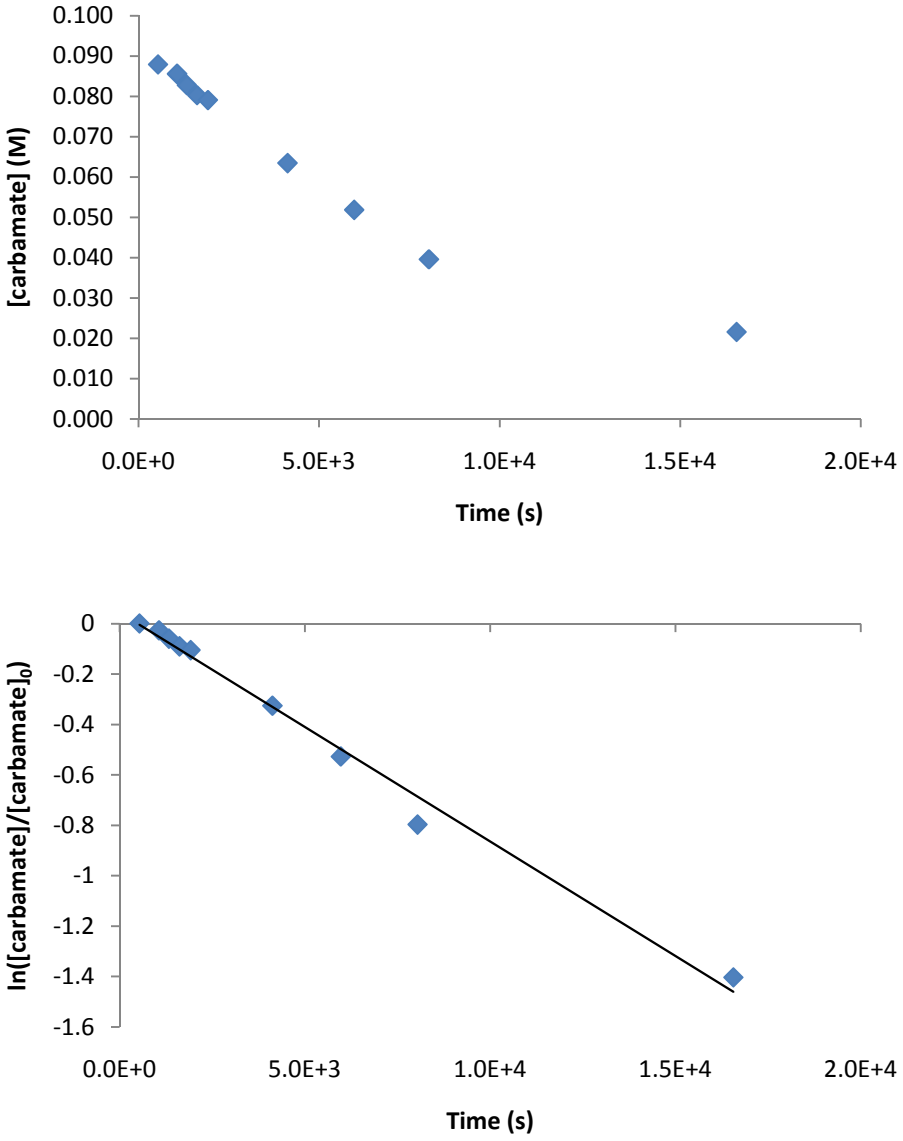

Figure 2.12. Concentration versus time (top) and pseudo first-order (bottom) plots for the gold(I)-catalyzed intermolecular hydroamination of benzyl carbamate with 3-methyl-1,2-butadiene in dioxane at room temperature. [2] = 4.2 M, [4] = 0.10 M, [(IPr)AuCl/AgOTf] = 19 mM (k_{obs} = 9.10 ± 0.05 x 10^{-5} s^{-1}) (Table 2.4, entry 3)

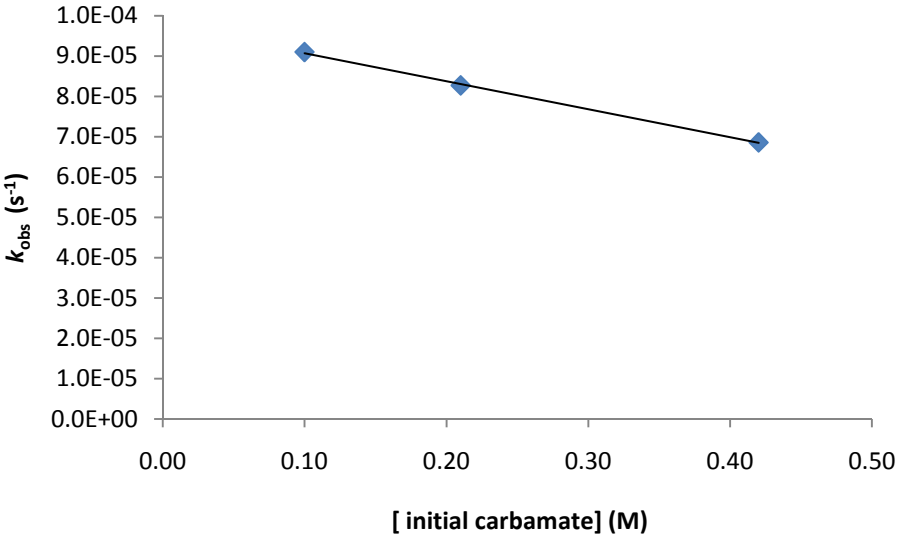

Figure 2.13. Plot of k_{obs} versus initial carbamate concentration in for the gold(I)-catalyzed intermolecular hydroamination of benzyl carbamate with 3-methyl-1,2-butadiene using (IPr)AuCl/AgOTf as the catalyst in dioxane. The slope (7.0 x 10^{-5} $M^{-1}s^{-1}$) suggests that the rate is somewhat less than pure first-order dependence in 4 from 0.10 to 0.42 M

Table 2.4. Observed rate constants for the intermolecular hydroamination of benzyl carbamate (4) with 3-methyl-1,2-butadiene (2) catalyzed by (IPr)AuCl and AgOTf as a function of [allene], [carbamate], and [catalyst].

Entry	[allene] (M)	[carbamate] (M)	[catalyst] (mM)	k_{obs} (s^{-1}) (10^{-5})[a]	Temperature (°C)
1[b]	4.2	0.42	19	6.85 ± 0.01	25
2[b]	4.2	0.21	19	8.27 ± 0.05	25
3[b]	4.2	0.10	19	9.10 ±0.05	25
4	0.88	0.24	20	5.7 ± 0.1	24
5	0.32	0.20	19	0.87 ± 0.02	24
6	0.52	0.20	19	2.08 ± 0.05	24
7	0.65	0.23	19	1.25 ± 0.05	24
8	3.8	0.21	19	14.5 ± 0.5	25
9	3.4	0.23	20	15.3 ± 0.7	25
10	3.0	0.24	22	16.1 ± 0.8	25
11	2.5	0.21	19	14.2 ± 0.3	25
12	1.2	0.19	18	4.76 ± 0.05	25
13	1.4	0.19	18	8.0 ± 0.1	24
14	1.4	0.22	21	6.7 ± 0.1	24
15	1.9	0.20	21	11.2 ± 0.1	24
16	2.7	0.28	15	14.9 ± 0.1	24
17	2.8	0.29	15	12.7 ± 0.1	24
18	2.2	0.22	47	80.5 ± 0.9	24
19	2.2	0.23	22	31.3 ± 0.3	24
20	2.3	0.23	37	56.0 ± 1.2	24

[a] Error in k_{obs} values determined from the standard deviation of the slope for the plot of ln[carbamate] versus time

[b] Experiment conducted by Robert E. Kinder

2.3.2 Rate dependence on gold concentration

After determining the approximate first-order dependence on [**4**] for the gold(I)-catalyzed hydroamination, we sought to determine the rate dependence of catalytic hydroamination on [catalyst]. The rate was evaluated as a function of catalyst concentration from 15 mM to 47 mM under pseudo first-order conditions at constant [**4**] (0.2 M) and [**2**] (2 M) (Table 2.4, entry 16 – 20 ; Figure 2.60 – Figure 2.64). A plot of pseudo first-order rate constants versus the concentration of (IPr)AuCl and AgOTf was linear over the concentration range 15 - 47 mM, which established the apparent first-order dependence of the rate on [catalyst] and the pseudo second-order rate law: rate = k_2 [**4**][catalyst] in the presence of excess allene, where $k_2 = 0.0204 \pm 0.0001$ $M^{-1}s^{-1}$ (Figure 2.14). To verify the first-order dependence of the rate on [catalyst], a van't Hoff of ln[k_{obs}] versus ln[catalyst] was linear with a slope of 1.53 ±0.013, consistent with first-order dependence of the rate on (IPr)AuCl and AgOTf (Figure 2.15)

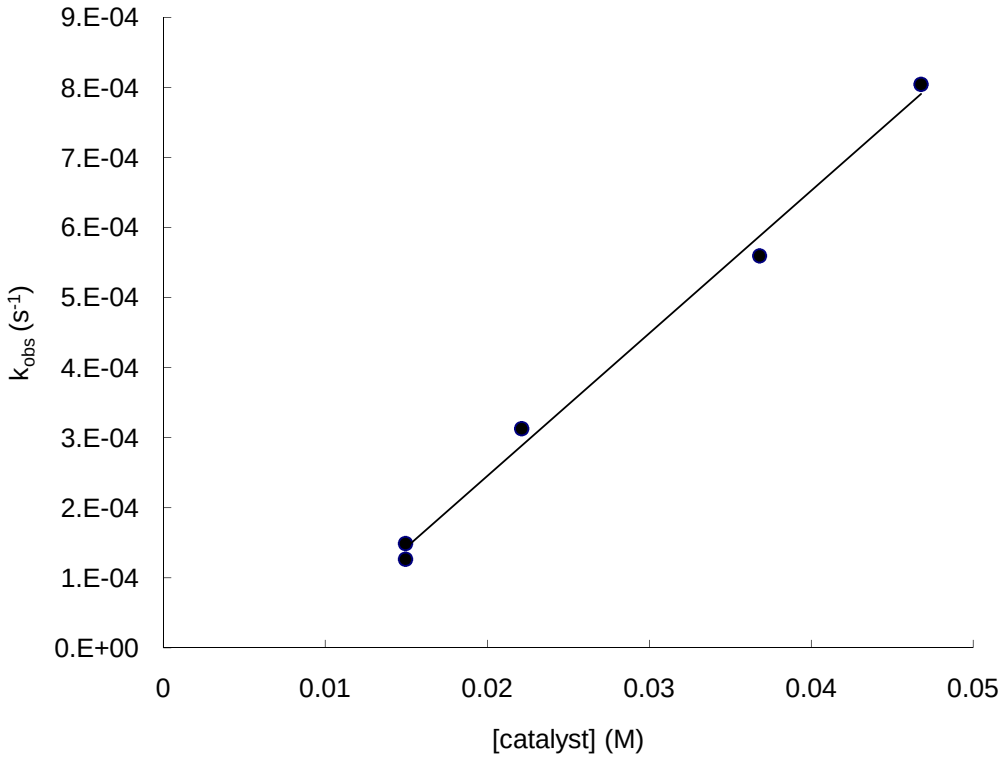

Figure 2.14. Plot of observed rate versus time for the intermolecular hydroamination of 4 (0.2 M) with 2 (2 M) using (IPr)AuCl/AgOTf (15 mM to 47 mM) as the catalyst in dioxane. The plot indicates first-order behavior with respect to catalyst.

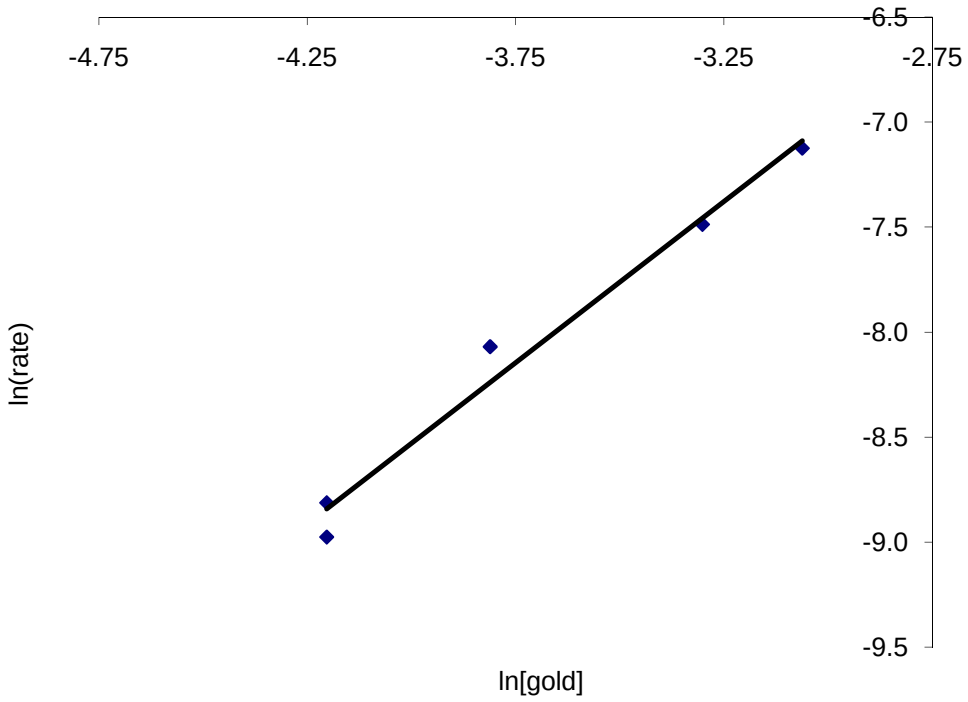

Figure 2.15. Van't Hoff plot for the intermolecular hydroamination 4 (0.2 M) with 2 (2 M) using (IPr)AuCl/AgOTf (15 mM to 47 mM) as the catalyst in dioxane. The slope of the line was found to be 1.53 ± 0.13.

2.3.3 Rate dependence on allene concentration

Having established the first-order dependence of both [**4**] and [catalyst] under pseudo first-order conditions (excess allene), we sought to determine the rate dependence of gold(I)-catalyzed hydroamination on [allene]. To this end, pseudo first-order rate constants were determined at constant [**4**] (0.2 M) and [catalyst] (19 mM) as a function of [**2**] from 0.32 M to 3.8 M in dioxane at 24 °C (Table 2.4, entry 4 - 15). Reactions in which pseudo first-order kinetic conditions were not maintained were monitored until ~ 10% conversion (Table 2.4, entry 4 – 7, 12 – 15). A plot of pseudo first-order rate constants versus [allene] revealed non-linear dependence of the rate on [allene], as was observed for hydroalkoxylation the rate increased approximately linearly with increasing [allene] at low concentrations (0-2 M) then more slowly from 2-4 M with saturation achieved at ~2.5M (Figure 2.16). Overall, the empirical rate law can be expressed as rate = k_3[**4**]^1[allene]^1[catalyst]^1 , where the third order rate constant, k_3 = 6.49 x 10^{-5} $M^{-2}s^{-1}$ at low concentrations of allene and rate = k_{sat} [**4**]^1[catalyst] ^{1}, where the pseudo second order rate constant k_{sat} = 0.0204 ± 0.0001 $M^{-1}s^{-1}$ at saturation in allene.

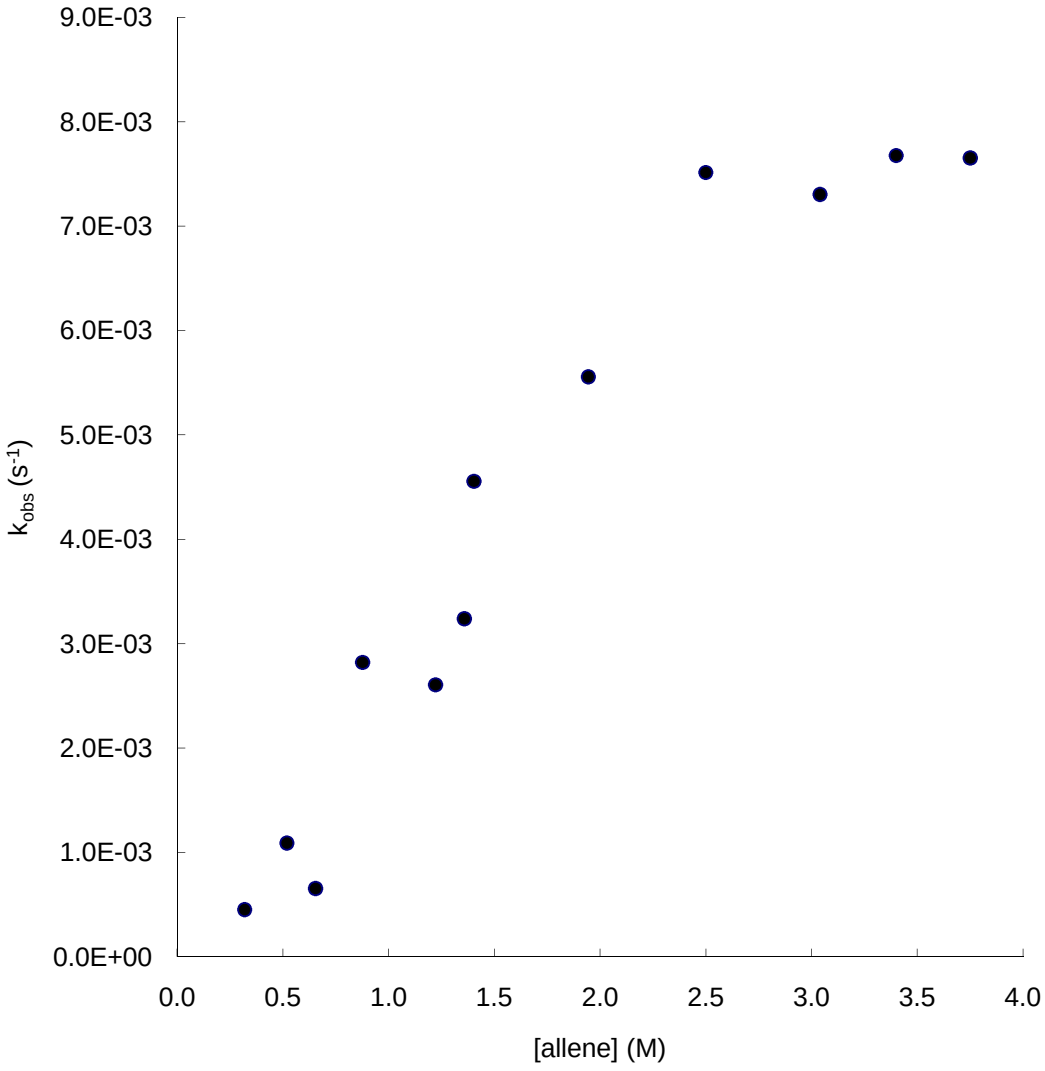

Figure 2.16. Plot of observed rate constants versus time for the intermolecular hydroamination of 4 (~ 0.21 M) with 2 catalyzed by [(IPr)AuCl/AgOTf] (19 mM) in dioxane at 24 - 25 °C.

2.3.4 Effect of excess triflate anion on the gold(I)-catalyzed hydroamination of 2 with 4

We sought to evaluate the effect of increasing the [TfO^-] on the rate of gold(I)-catalyzed hydroamination. To this end, **4** (0.36 M) was treated with **2** (2.5 M), [(IPr)AuCl/AgOTf] (15 mM), and Bu_4NOTf (0.52 M) at room temperature . The observed rate constant for the reaction with excess triflate was found to be $3.2 \pm 0.6 \times 10^{-4}$ s^{-1}. This observed rate constant was compared with the observed rate constant for the reaction of [**4**] (0.28 M), [**2**] (2.7 M) and [(IPr)AuCl/AgOTf] (15 mM) at room temperature $1.49 \pm 0.01 \times 10^{-4}$ s^{-1} (Table 2.5). As shown in Table 2.5, the presence of excess triflate slowed the reaction by approximately 47 %, which is shown graphically in Figure 2.17.

Table 2.5. Observed rate constant for the intermolecular hydroamination of carbamate with allene catalyzed by (IPr)AuCl and AgOTf in dioxane at 24 °C as a function of [allene], [carbamate], [catalyst] = 15 mM, ands [Bu_4NOTf].

Entry	[allene] (M)	[carbamate] (M)	[Bu_4NOTf] (M)	k_{obs} (s^{-1}) (10^{-4})[a]
1	2.7	0.29	0.00	1.49 ± 0.01
2	2.5	0.36	0.52	3.2 ± 0.6

[a] Error in k_{obs} values determined from the standard deviation of the slope for the plot of ln[carbamate] versus time

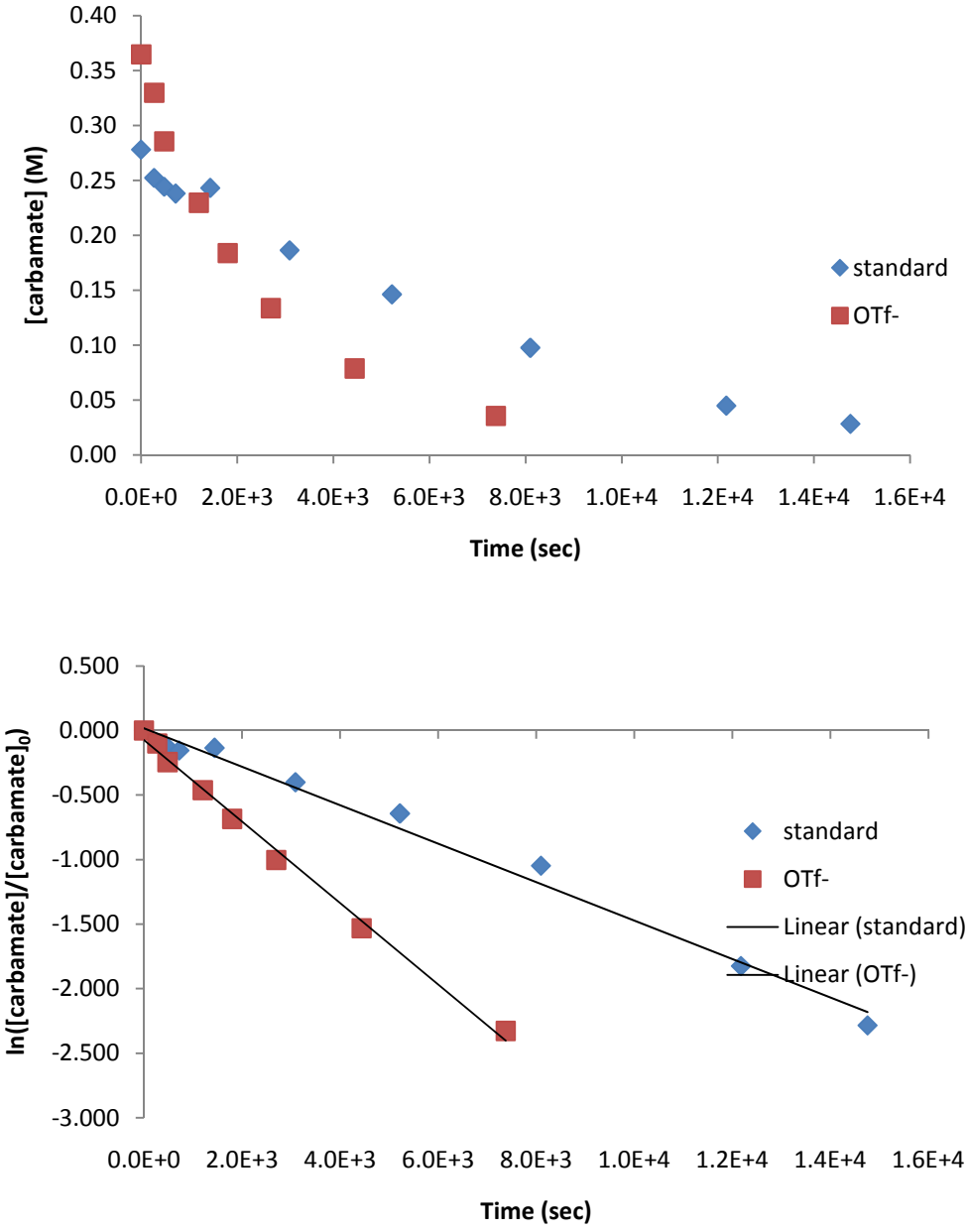

Figure 2.17. Concentration versus time (top) and pseudo first-order (bottom) plots for the reaction of 4 (0.29 M and 0.36 M) and 2 (2.7 M and 2.5 M) catalyzed by (IPr)AuCl/AgOTf (15 mM) in the absence of Bu_4NOTf and in the presence of 0.25 M Bu_4NOTf. Pseudo first-order rate constants were 1.49 ± 0.01 x 10^{-4} s^{-1} and 3.2 ± 0.6 x 10^{-4} s^{-1}, respectively, indicating a ~ 2 fold decrease in reaction rate (Table 2.5, entry 1 & 2).

2.3.5 Deuterium Labeling Studies

To further probe the mechanism of the gold(I)-catalyzed intermolecular hydroamination of **4** with **2** catalyzed by (IPr)AuCl and AgOTf, we evaluated the rate of hydroamination employing *N*-deuterated benzyl carbamate (**4-*d*$_2$**). To this end, a mixture of **2** (2.52 M), **4-*d*$_2$** (0.27 M) (≥95% d), (IPr)AuCl and AgOTf (25 mM) and *n*-tetradecane in dioxane was stirred at room temperature (eq 2.24) and the disappearance of **4-*d*$_2$** was monitored by GC analysis, which presumably formed phenyl (1,1-dimethylprop-2-en-1-yl)carbamate-d$_2$.

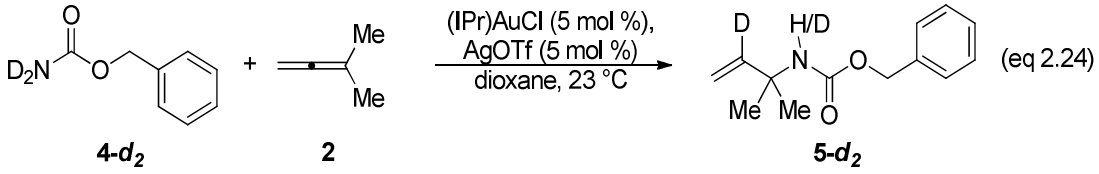

A plot ln [**4-*d*$_2$**] versus time gave a straight line with a slope of k_{obs} = 2.18 ± 0.11 x 10^{-4} s^{-1} (Figure 2.18). As a point of comparison, **2** (2.47 M) was reacted with **4** (0.25 M) catalyzed by (IPr)AuCl and AgOTf (25 mM) in dioxane at room temperature. A plot of ln [**4**] versus time gave a straight line with a slope of k_{obs} = 2.57 ± 0.05 x 10^{-4} s^{-1} (Figure 2.18), which corresponds to a KIE of k_H/k_D = 1.2 ± 0.1 (Table 2.6). It should be noted that deuterium incorporation into the product was not confirmed; however the kinetic isotope effect value was small, we can conclude that protonolysis is not involved in the rate determining step for the gold(I)-catalyzed intermolecular hydroamination of **2** with **4** catalyzed by (IPr)AuCl and AgOTf in dioxane at room temperature.[63]

Table 2.6. Observed rate constants for the intermolecular hydroamination of 3-methyl-1,2-butadiene with proteo and deutero benzy carbamate catalyzed by (IPr)AuCl and AgOTf in dioxane at 24 °C as a function of [allene] = 2.5 M, [4], and [catalyst] = 25 mM.

Entry	[**4**] (M)	k_{obs} (s^{-1}) (10^{-4})[a]
1	NH_2-0.25	2.6 ± 0.1
2	ND_2-0.27	2.2 ± 0.1

[a] Error in k_{obs} values determined from the standard deviation of the slope for the plot of ln[carbamate] versus time

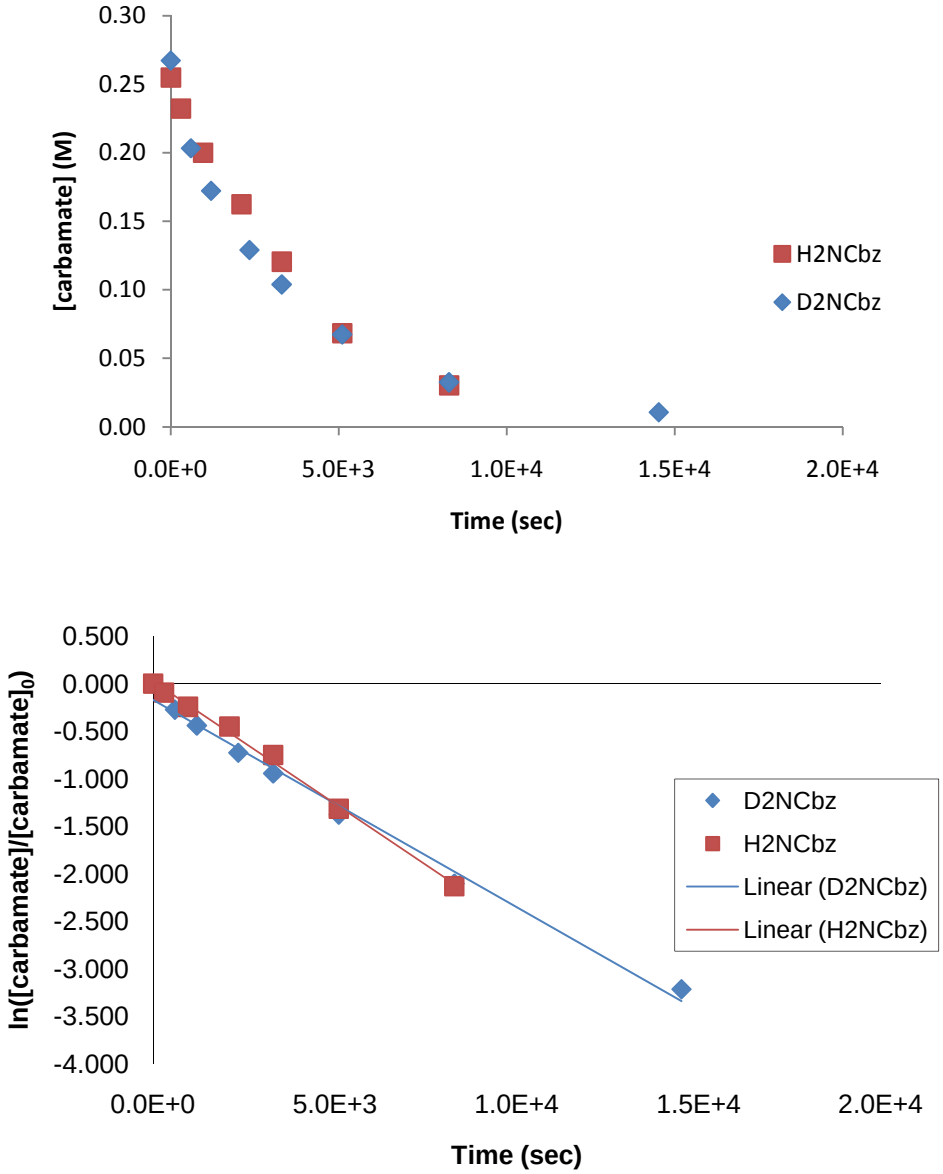

Figure 2.18. Concentration versus time (top) and pseudo first-order (bottom) plots for the reaction of 4 (0.25 M) and 4-d_2 (0.27 M) with allene (2.5 M) catalyzed by (IPr)AuCl and AgOTf (25 mM) in dioxane at 24 °C k_{obs} = 2.6 ± 0.1 x 10^{-4} s^{-1} and 2.2 ± 0.1 x 10^{-4} s^{-1}, respectively (Table 2.6, entry 1 and 2).

2.4 Competition Experiment: Hydroalkoxylation versus Hydroamination

The rate of hydroalkoxylation was greater than hydroamination under comparable conditions. For example, the rate of hydroalkoxylation of **1** and hydroamination of **4** with **2** catalyzed by a 1:1 ratio of (IPr)AuCl and AgOTf (5 mol %) in dioxane was found to be $2.8 \pm 0.1 \times 10^{-4}$ s^{-1} and $1.27 \pm 0.1 \times 10^{-4}$ s^{-1}, respectively when [**1**] = 0.34 M, [**2**] = 2.5 M, and [(IPr)AuCl/AgOTf] = 15 mM in toluene at 24 °C and when [**4**] = 0.29 M, [**2**] = 2.8 M, and [(IPr)AuCl/AgOTf] = 15 mM in dioxane at 24 °C (Table 2.1, entry 20 and Table 2.4, entry 17). We sought to determine if the rate difference was due to greater nucleophilicity of the alcohol or carbamate or if it was due to inhibitory complexation of nucleophile to gold. To distinguish between these possibilities and evaluate the inherent nucleophilicity of alcohol and carbamate in gold(I)-catalyzed hydrofunctionalizations, we performed a competition experiment employing alcohol and carbamate. To this end, **2** (2.45 M) was reacted with a mixture of **1** (0.31 M) and **4** (0.30 M) and a catalytic 1:1 mixture of (IPr)AuCl and AgOTf (14 mM) in dioxane at 23 °C (eq 2.25).

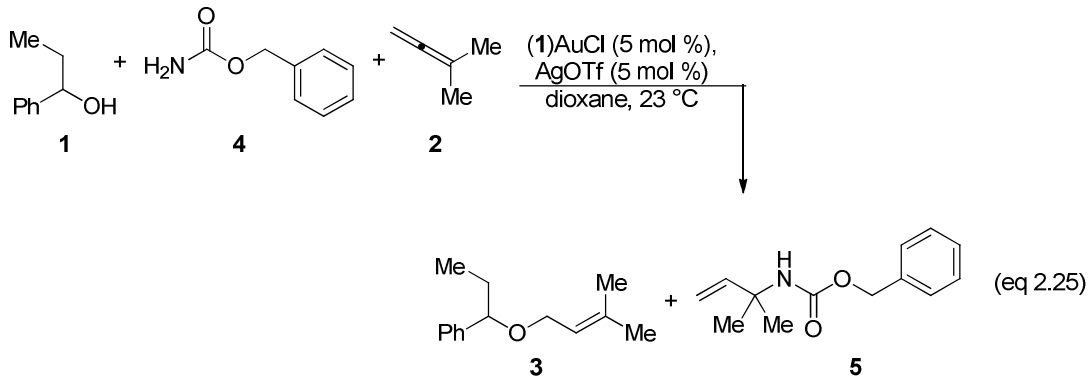

Plots of concentrations of [**1**] and [**4**] versus time showed pronounced curvature indicative of non-zero-order behavior (Figure 2.21). Plots of ln[**1**]/ [**1**]$_0$ and ln[**4**]/ [**4**]$_0$ versus time were linear, consistent with first-order dependence of the rate on both [**1**] and [**4**] and provided pseudo first-order rate constants for hydroalkoxylation k_{obs} = 6.1 ± 0.1 x 10^{-5} s^{-1} and hydroamination k_{obs} = 3.4 ± 0.1 x 10^{-4} s^{-1} (Figure 2.21). The rate of hydroalkoxylation under the competition experiment conditions slowed by approximately 4.6 times when compared to the gold(I)-catalyzed hydroalkoxylation in the absence of carbamate (Figure 2.19). The rate of hydroamination under the competition experiment conditions increased by 3.7 times when compared to the gold(I)-catalyzed hydroalkoxylation in the absence of alcohol (Figure 2.20). The ratio of the amount of **5** to **3** formed was used to create Figure 2.22. Within the first five minutes of reaction, **5** is formed 4.5 times faster than **3**. As the reaction precedes, the ratio of **5**:**3** decreases, for instance after 1 h the ratio decreases to 3:1, then decreases again after 1.75 h to 2.3:1(Figure 2.22). Since **4** is a stronger nucleophile than **1**, the increased rate for the

hydroamination reaction under competition protocols compared to standard protocols is presumably due to the increase in the rate of formation of the gold-π-allene complex.

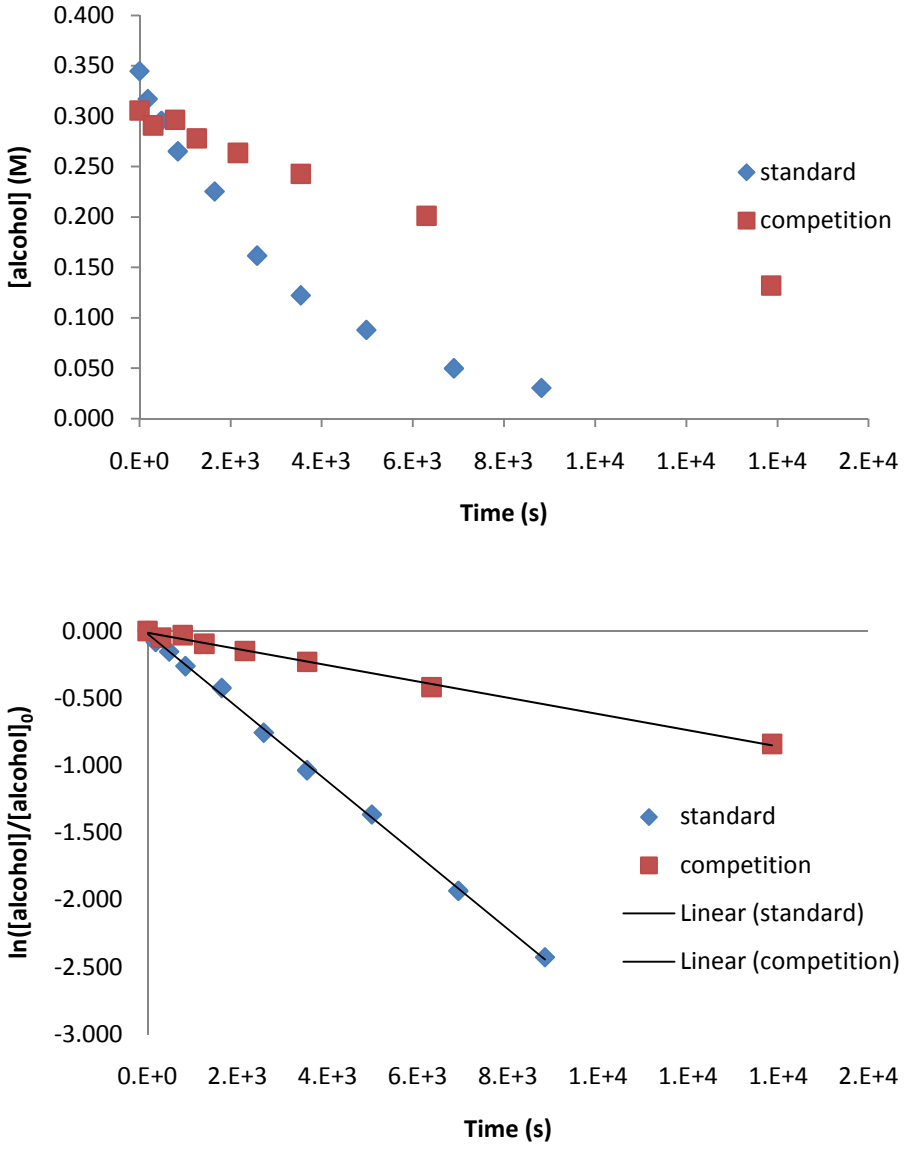

Figure 2.19. Concentration versus time (top) and pseudo first-order (bottom) plots for the gold(I)-catalyzed hydroalkoxylation of 1 with 2 catalyzed by (IPr)AuCl in the absence and presence of 4 ([1] = 0.34 M, [2] = 2.5 M, and [(IPr)AuCl/AgOTf] = 15 mM $k_{obs} = 2.8 \pm 0.1 \times 10^{-4}$ s^{-1}) ([1] = 0.31 M, [4] = 0.30 M, [2] = 2.5 M, and (IPr)AuCl/AgOTf = 14 mM $k_{obs} = 6.1 \pm 0.1 \times 10^{-5}$ s^{-1}).

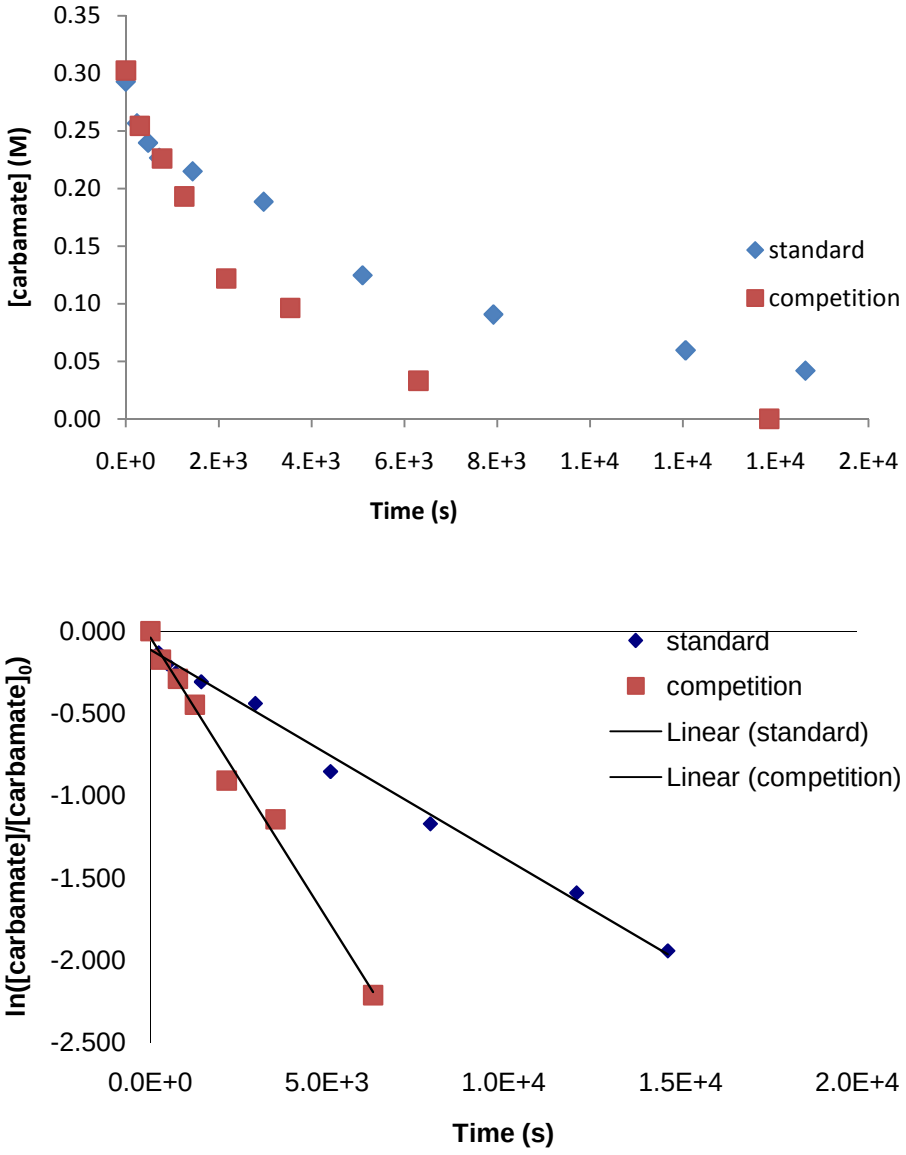

Figure 2.20. Concentration versus time (top) and pseudo first-order (bottom) plots for the gold(I)-catalyzed hydroamination of 4 with 2 catalyzed by (IPr)AuCl in the absence and presence of 1 ([4] = 0.29 M, [2] = 2.8 M, and [(IPr)AuCl/AgOTf] = 15 mM k_{obs} = 12.7 ± 0.1 x 10^{-5} s^{-1}) ([1] = 0.31 M, [4] = 0.30 M, [2] = 2.5 M, and (IPr)AuCl/AgOTf = 14 mM k_{obs} = 3.4 ± 0.1 x 10^{-4} s^{-1}).

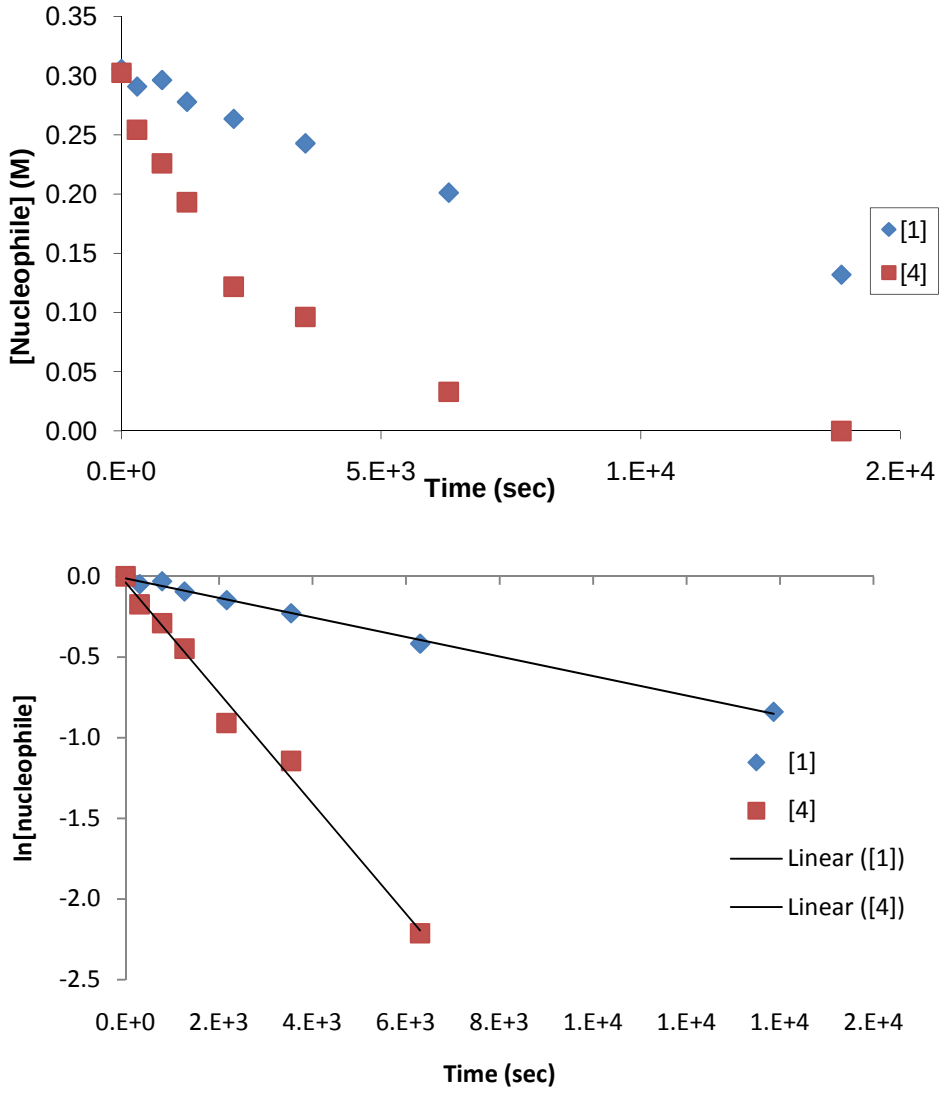

Figure 2.21. Concentration versus time (top) and pseudo first-order (bottom) plots for the disappearance of 1 and 4 in the reaction of a 1:1 mixture of [1] = 0.31 M and [4] = 0.30 M and [allene] = 2.5 M catalyzed by (IPr)AuCl and AgOTf (14 mM) in dioxane at 25 °C hydroalkoxylation (k_{obs} = 6.1 ± 0.1 x 10^{-5} s^{-1}) and hydroamination (k_{obs} = 3.4 ± 0.1 x 10^{-4} s^{-1}).

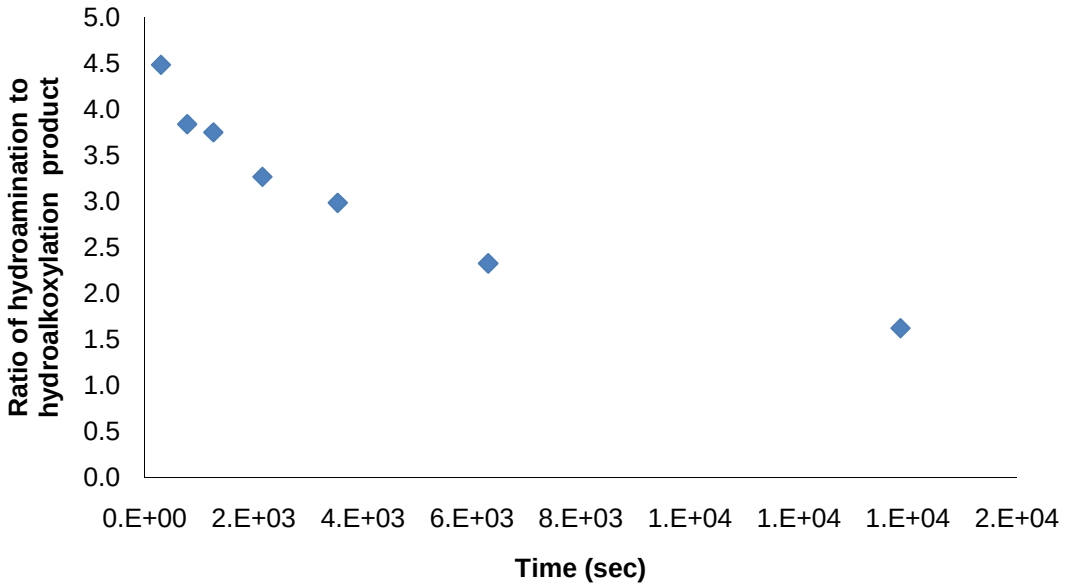

Figure 2.22. Ratio of 5 to 3 formed from the reaction of 1 and 4 with 2 catalyzed by (IPr)AuCl and AgOTf system in dioxane at room temperature.

2.5 Discussion

2.5.1 Hydrofunctionalization

The kinetics for hydrofunctionalization was interpreted in the context of the simplified mechanism depicted in Scheme 2.1 and its associated rate equations, shown in eq 2.26-2.28, which was constructed on the basis of the following assumptions: (1) the overall reaction is irreversible, which is supported by experimental observation; (2) gold-nucleophile complex, **I**, and gold π-allene complex, **II**, are in a rapid pre-equilibrium; (3) the total gold concentration equals the concentration of species **I** and **II** and substitution into the equilibrium equation for eq 2.26 gives eq 2.30. From these latter two assumptions, we derive the equation, $[Au]_{tot} = [I]+[II]$, which relates the concentration of **I** and **II** to the total gold concentration. Differential rate equations for the gold(I)-catalyzed hydrofunctionalization were derived under four scenarios: (1) rate-limiting irreversible C-Nuc ($k_{-1} = 0$) bond formation; (2) reversible rate-limiting C-Nuc bond formation followed by rapid protodeauration ($k_1 << k_{-1} + k_2$); (3) rapid and reversible C-Nuc bond formation followed by rate-limiting protodeauration ($k_2 << k_{-1} + k_1$); (4) rapid, irreversible C-Nuc formation followed by rate-limiting protodeauration.

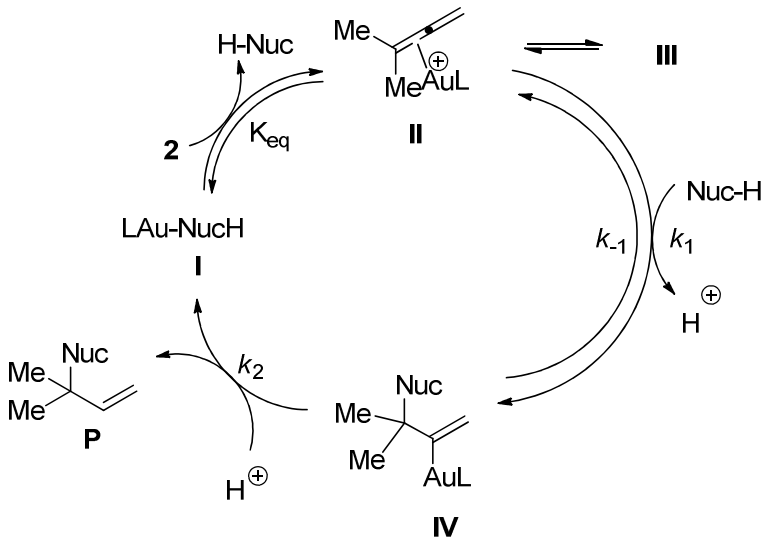

Scheme 2.1. Proposed mechanism for the gold(I)-catalyzed hydrofunctionalization of allenes with H-X (X = OR , NHCbz) catalyzed by (IPr)AuCl/AgOTf

$$\mathbf{I} + \mathbf{2} \underset{}{\overset{K_{eq}}{\rightleftharpoons}} \mathbf{II} + \text{NucH} \qquad \text{(eq 2.26)}$$

$$\mathbf{II} + \text{NucH} \underset{k_{-1}}{\overset{k_1}{\rightleftharpoons}} \mathbf{IV} + H^+ \qquad \text{(eq 2.27)}$$

$$\mathbf{IV} + H^+ \xrightarrow{k_2} \text{product} \qquad \text{(eq 2.28)}$$

In the first scenario, rate-limiting irreversible C-Nuc ($k_{-1} = 0$) bond formation the rate law can be described as the rate of formation of **IV** as shown in equation 2.29. Substitution of the relationship for [**II**] depicted in eq 2.30 gives the two-term rate law depicted in eq 2.31. Eq 2.31 simplifies to the limiting rate laws depicted in eq 2.32 and eq 2.33 depending on the position of equilibrium involving **I** and **II**. When K_{eq}[**2**] is much greater than [NucH], the rate law simplifies to eq 2.32, which predicts first order behavior in catalyst and nucleophile, but zero-order behavior in allene (**2**). Conversely,

when the concentration of nucleophile is much greater than $K_{eq}[\mathbf{2}]$, the rate law simplifies to eq 2.33, which predicts first-order behavior in catalyst and allene, but zero order behavior in nucleophile.

$$\text{Rate} = \frac{d\mathbf{IV}}{dt} = k_1[\mathbf{II}][\text{NucH}] \quad \text{(eq 2.29)}$$

$$[\mathbf{II}] = \frac{K_{eq}[\text{Au}]_{tot}[\mathbf{2}]}{K_{eq}[\mathbf{2}] + [\text{NucH}]} \text{ (eq 2.30)}$$

$$\text{Rate} = \frac{k_1 K_{eq}[\text{Au}]_{tot}[\mathbf{2}][\text{NucH}]}{K_{eq}[\mathbf{2}] + [\text{NucH}]} \quad \text{(eq 2.31)}$$

$$K_{eq}[\mathbf{2}] \gg [\text{NucH}]\text{: Rate} \approx k_1[\text{Au}]_{tot}[\text{NucH}] \quad \text{(eq 2.32)}$$

$$K_{eq}[\mathbf{2}] \ll [\text{NucH}]\text{: Rate} \approx k_1 K_{eq}[\text{Au}]_{tot}[\mathbf{2}] \quad \text{(eq 2.33)}$$

In the second scenario, reversible rate-limiting C-Nuc bond formation followed by rapid protodeauration ($k_1 << k_{-1} + k_2$), k_{-1} is not negligible and the rate is defined as the rate of formation of hydrofunctionalized product (eq 2.34). Steady state treatment of gold vinyl species, **IV** (eq 2.35), gives the relationship shown in eq 2.36. Substitution of the relationship for $[\mathbf{IV}][H^+]$ shown in eq 2.36 into rate eq 2.34 gives eq 2.37. Substitution of the relationship for **II** shown in eq 2.30 gives rate law shown in eq 2.38, it should be noted that eq 2.38 is in the same form as 2.31 as depicted in eq 2.39. The rate law depicted in eq 2.39 for the rapid and reversible C-Nuc bond formation and rate-limiting protodeauration rapid can be simplified to a two-term rate law (as noted previously) when the equilibrium concentration of **2** is much larger than the concentration of NucH

(eq 2.40) or when the concentration of NucH is much larger than the equilibrium concentration of **2** (eq 2.41).

$$\text{Rate} = \frac{d\mathbf{P}}{dt} = k_2[\mathbf{IV}][H^+] \quad \text{(eq 2.34)}$$

$$\frac{d\mathbf{IV}}{dt} = k_1[\mathbf{II}][\text{NucH}] - k_{-1}[\mathbf{IV}][H^+] - k_2[\mathbf{III}][H^+] = 0 \text{ (eq 2.35)}$$

$$\frac{k_1[\mathbf{II}][\text{NucH}]}{(k_{-1} + k_2)} = [\mathbf{IV}][H^+] \text{ (eq 2.36)}$$

$$\text{Rate} = \frac{k_1 k_2[\mathbf{II}][\text{NucH}]}{(k_{-1} + k_2)} \quad \text{(eq 2.37)}$$

$$\text{Rate} = \frac{k_1 k_2 K_{eq}[\text{NucH}][\text{Au}]_{tot}[\mathbf{2}]}{(k_{-1} + k_2)\left(K_{eq}[\mathbf{2}] + [\text{NucH}]\right)} \quad \text{(eq 2.38)}$$

$$\text{Rate} = \frac{k_1 k_2 K_{eq}[\text{NucH}][\text{Au}]_{tot}[\mathbf{2}]}{k' K_{eq}[\mathbf{2}] + k'[\text{NucH}]} \text{ where } k' = k_{-1} + k_2 \quad \text{(eq 2.39)}$$

$$K_{eq}[\mathbf{2}] \gg [\text{NucH}]\text{: Rate} \approx k_{obs}[\text{Au}]_{tot}[\text{NucH}], \text{when } k_{obs} = \frac{k_1 k_2}{k'} \quad \text{(eq 2.40)}$$

$$K_{eq}[\mathbf{2}] \ll [\text{NucH}]\text{: Rate} \approx k_{obs}[\text{Au}]_{tot}[\mathbf{2}], \text{when } k_{obs} = \frac{k_1 k_2 K_{eq}}{k'} \quad \text{(eq 2.41)}$$

In the third scenario, rapid and reversible C-Nuc bond formation followed by rate limiting protodeauration ($k_2 \ll k_{-1} + k_1$), the rate can be described as the rate of formation of product (eq 2.34) with a pre-equilibrium assumption for the formation of **IV**. The equilibrium constant for the reaction shown in eq 2.27 gives the relationship between the forward and reverse reactions shown in eq 2.42. Solving for [**IV**] (shown in eq 2.43) and substitution into eq 2.34 and simplification gives eq 2.44. Substitution of the relationship for **II** shown in eq 2.30 gives the rate law depicted in eq 2.45. Eq 2.45 is in the same form as eq 2.30 and can be distinguished from scenarios one and two (eq 2.31

and eq 2.38) because deuterium should not affect k_1/k_{-1}, thus it predicts no kinetic isotope effect.

$$\frac{k_1}{k_{-1}} = \frac{[\mathbf{IV}][H^+]}{[\mathbf{II}][NucH]} \quad \text{(eq 2.42)}$$

$$[\mathbf{IV}] = \frac{k_1[\mathbf{II}][NucH]}{k_{-1}[H^+]} \quad \text{(eq 2.43)}$$

$$\text{Rate} = \frac{k_2 k_1[\mathbf{II}][NucH]}{k_{-1}} \quad \text{(eq 2.44)}$$

$$\text{Rate} = \frac{k_2 k_1 K_{eq}[Au]_{tot}[\mathbf{2}][NucH]}{k_{-1}(K_{eq}[\mathbf{2}] + [NucH])} \quad \text{(eq 2.45)}$$

In the fourth scenario (rapid, irreversible C-Nuc formation followed by rate-limiting protodeauration) the [**IV**] is equal to the total gold concentration (eq 2.46), so the rate would be zero-order in both [**2**] and [NucH] and first-order in catalyst.

$$[Au]_{tot} = [\mathbf{IV}] \quad \text{(eq 2.46)}$$

Experimentally, we derived the rate law for gold(I)-catalyzed hydroamination of allenes with carbamates. It was found that the rate law varied at low and high concentrations of allene. At low [allene] the empirical rate law can be expressed as rate = $k_3[\mathbf{4}]^1[\text{allene}]^1[\text{catalyst}]^1$, where the third order rate constant, $k_3 = 6.49 \times 10^{-5}\ M^{-2}s^{-1}$; at high concentrations of allene saturation behavior was observed, the rate law can be expressed as rate = $k_{sat}[\mathbf{4}]^1[\text{catalyst}]^1$, where the pseudo second order rate constant $k_{sat} = 0.0204 \pm 0.0001\ M^{-1}s^{-1}$. Of the four differential rate equations derived for gold(I)-catalyzed hydrofunctionalization the fourth scenario, rapid, irreversible C-Nuc formation followed by rate-limiting protodeauration scenario can be discounted because it predicts zero-

order dependence of the rate on [**2**] and [NucH] and first-order dependence of the rate on [**2**] and [carbamate] was observed experimentally. Also, the second scenario involving reversible rate-limiting C-Nuc bond formation followed by rapid protodeauration can be discounted because it predicts a kinetic isotope effect, but experimentally the KIE value was low ($k_H/k_D = 1.2 \pm 0.1$). Experimental observations support scenario one (rate-limiting irreversible C-Nuc bond formation) and scenario three (rapid and reversible C-Nuc bond formation followed by rate-limiting protodeauration).

We therefore propose the mechanism for gold(I)-catalyzed hydroamination of allenes with carbamates catalyzed by (IPr)AuCl and AgOTf depicted in Scheme 2.2. The active gold catalyst, **I**, is complexed with allene forming a gold-π-allene complex, **II**. **II** then undergoes outer-sphere attack by carbamate and deprotonation to form a gold-σ-alkenyl complex, **IV**, or **II** could racemize into its cationic form **III** followed by outer-sphere attack of carbamate. Racemization of **II** to **III** is explained by the loss of enantiomeric enrichment in the gold(I)-catalyzed intramolecular hydroamination of carbamates with allenes (eq 2.18) and intermolecular hydroalkoxylation of alcohols with allenes (eq 2.19). Protonolysis of **IV** releases the hydroamination product and regenerates the active catalyst. C-N bond formation was determined to be rate limiting because of the lack of kinetic isotope effect, while all previous steps were determined to be reversible. The addition of excess soluble triflate caused a two-fold decrease in the rate; mechanistically this can be observed as **I** complexes allene to become **II** because

triflate is a potentially coordinating ligand for gold, and in this reaction, triflate competes with allene to bind with gold.

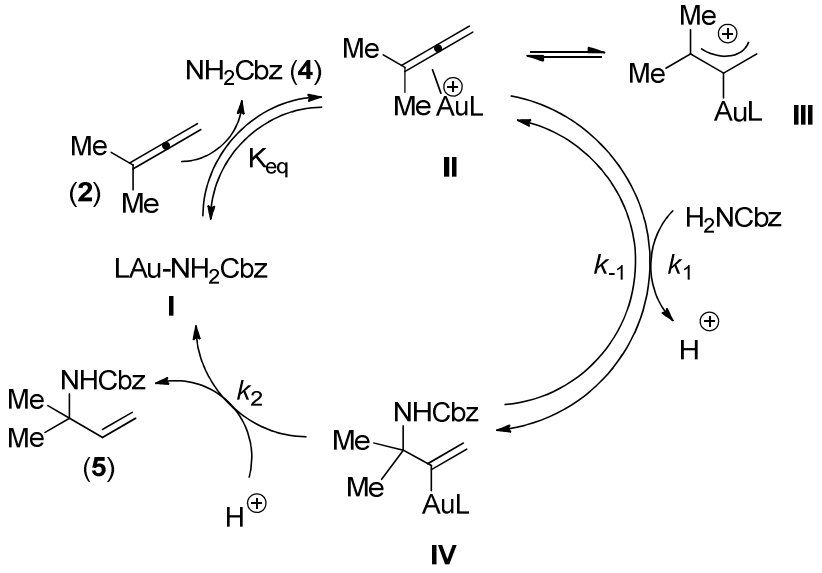

Scheme 2.2. Proposed mechanism for the gold(I)-catalyzed hydroamination of allenes with carbamates catalyzed by (IPr)AuCl/AgOTf

Experimentally, we derived the rate law for gold(I)-catalyzed hydroamination of allenes with alcohol. It was found that the rate law varied at low and high concentrations of allene. At low [allene] the empirical rate law can be expressed as rate = k_3[**1**]^1[allene]^1[catalyst]^1, with a third order rate of k_3 = 0.0244 ± 0.004 M^{-2} s^{-1}; at high concentrations of allene saturation behavior was observed and the rate can be expressed as: rate = k_{sat} [**1**]^1[catalyst] ^{1} with a second-order rate of k_{sat} = 0.018 ± 0.004 $M^{-1}s^{-1}$. Analysis of the four differential rate equations presented for gold(I)-catalyzed hydrofunctionalization with respect to the first-order dependence of [**1**], [allene], and [catalyst] at low concentrations of allene and first-order dependence of [**1**] and [catalyst]

and zero-order dependence at high [allene] and KIE value of $k_H/k_D = 1.8 \pm 0.2$ supports scenario one and three. The proposed mechanism for gold(I)-catalyzed hydroalkoxylation of **1** with **2** must differ from gold(I)-catalyzed hydroamination because of the reversal of stereochemistry observed. It was determined that tertiary alkyl ether product does not isomerize to the secondary alkyl ether product under catalytic conditions, so the regiochemical difference arises when alcohol attacks the gold-π-allenyl complex. Thus, alcohol can attack the unsubstituted allene terminus kinetically. If C-O bond formation is reversible then the kinetic selectivity of C-O bond formation is irrelevant, only the relative rates of protonolysis matters. So, in the scenario where alcohol attacks both termini of the allene reversibility, the more stable tri-substituted gold vinyl complex is protonated preferentially. If C-O bond formation is rate limiting and irreversible (scenario one) we would expect to see both the tertiary alkyl ether and secondary alkyl ether formed experimentally; however only one regioisomer is observed experimentally. We there propose an outer-sphere mechanism for the gold(I)-catalyzed hydroalkoxylation of allenes with alcohol that is similar to the proposed mechanism for the gold(I)-catalyzed hydroamination of allenes with carbamates except for an additional isomerization between the gold-π-allenyl complexes **II** and **V** to account for the regiochemistry differences between the hydrofunctionalized products (Scheme 2.3).

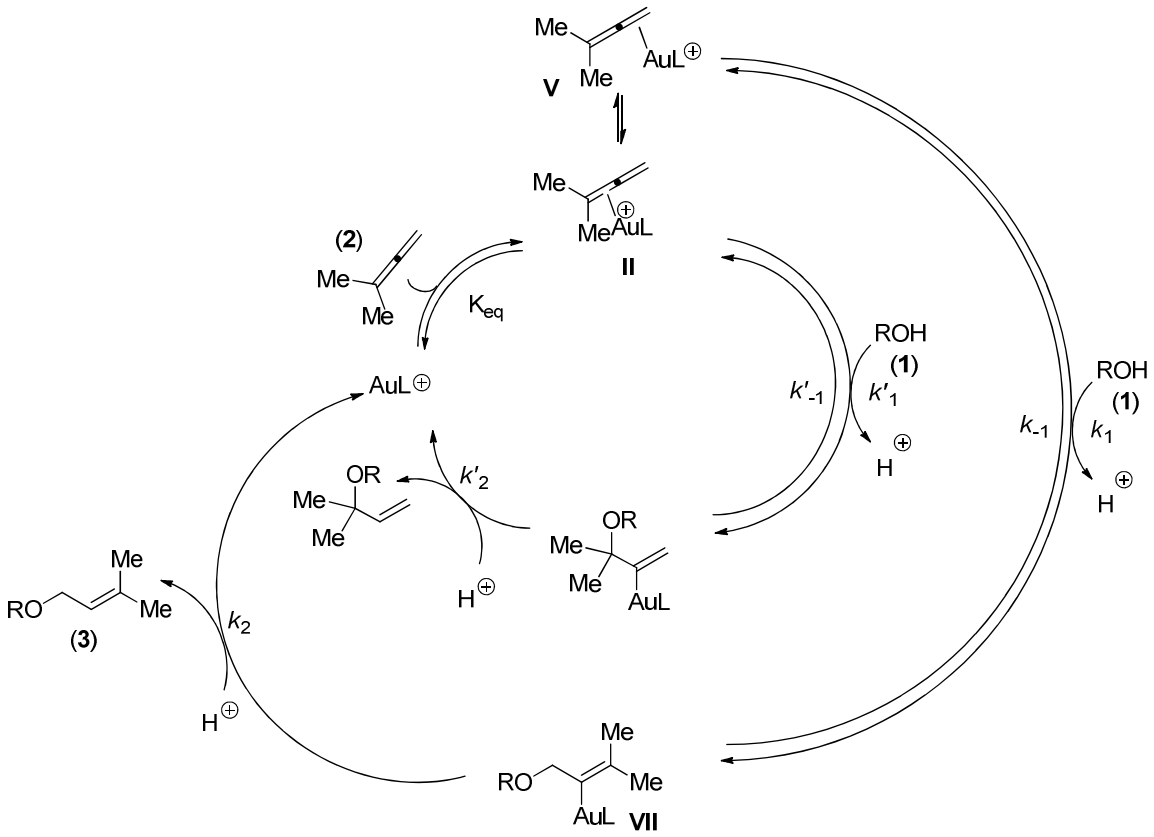

Scheme 2.3. Proposed mechanism for the gold(I)-catalyzed hydroalkoxylation of allenes with alcohol catalyzed by (IPr)AuCl/AgOTf that accounts for the observed kinetic selectivity.

2.6 Summary

In summary, we conclude that the mechanism for the gold(I)-catalyzed hydroamination of allenes with carbamates is similar to that of the gold(I)-catalyzed hydroalkoxylation of allenes with alcohols. This assumption is made because experimental rate laws were the similar with respect to allene, nucleophile, and catalyst. Also, the KIE was low for both reactions and the excess soluble triflate slowed both reactions. We propose an outer-sphere mechanism with turnover limiting protonolysis

for gold(I)-catalyzed hydroamination and hydroalkoxylation in Scheme 2.1 and Scheme 2.3. This result is supported by stereochemical analysis of the reaction of (*S*)-penta-2,3-dien-1-yl benzoate with benzyl alcohol catalyzed by (IPr)AuCl/AgOTf (5 mol %) in toluene at room temperature for 20 min led to the isolation of (*R,E*)-4-[1-(benzyloxy)ethoxy]but-2-en-1-yl benzoate in 83 % yield and 79 % ee (eq 3.17), which is consistent with outer-sphere attack by alcohol. [36] Also, the stereo-specific conversion of (S)- benzyl nona-4,5-dien-1-ylcarbamate to (*R*)- benzyl 2-(pent-1-en-1-yl)pyrrolidine-1-carboxylate catalyzed the Au[P(*t*-Bu)$_2$(*o*-biphenyl)]Cl and AgOTf (5 mol %) in dioxane at room temperature implies a mechanism involving nucleophilic anti-attack of the carbamate nitrogen. [32] The nucleophilicity of **1** and **4** was evaluated in a competition experiment because the rate of hydroamination was much slower than hydroalkoxylation. The enhanced nucleophilicity of carbamate was demonstrated in the ratio of **3**:**5** of 4.5:1. We presume that the differences in the rate of hydroalkoxylation versus hydroamination are due to increased affinity for alcohol to complex gold and not the nucleophilicity of the alcohol or carbamate.

2.7 Experimental Methods

Reactions were performed under a nitrogen atmosphere employing standard Schlenk and glove box techniques unless specified otherwise. Catalytic reactions were performed under an atmosphere of dry nitrogen. NMR spectra were obtained on a Varian spectrometer operating at 400 MHz for ^{1}H NMR and 101 MHz for ^{13}C NMR in

$CDCl_3$ at 25 °C unless noted otherwise. Gas chromatography was performed on a Hewlett-Packard 5890 gas chromatography equipped with a 15 m or 25 m polydimethylsiloxane capillary column and FID detector.

AgOTf (Aldrich), benzyl carbamate (Aldrich), 1-phenyl-1-propanol (Aldrich), 3-methyl-1,2-butadiene (Aldrich), deuterium oxide (Aldrich), were used as received. Dioxane (Aldrich) and toluene (Aldrich) were dried using the PureSolv™ solvent purification system. (IPr)AuCl [IPr = 1,3-bis(2,6-diisopropylphenyl)imidazol-2-ylidine] [127] and 3-Methoxy-3-methyl-1-butene[128] was synthesized using published procedures.

2.7.1 Deuterium labeled compounds

Deutero 1-phenyl-1-propanol. ≥95% d incorporation was determined by integrating the –OH peak on ^{1}H NMR. Deutero 1-phenyl-1-propanol was synthesized employing a published procedure.[129] ^{1}H NMR: δ 7.34-7.33 (m, 5 H), 4.50 (t, *J* = 7.2 Hz, 1 H), 1.78-1.60 (m, 2 H), (t, *J* = 7.6 Hz, 3 H) ^{13}C {H} NMR: δ 144.56, 128.38, 127.48, 125.95, 75.98, 31.85, 10.11

Deutero benzyl carbamate. ≥95% d incorporation was determined by integrating the –NH_2 peak on ^{1}H NMR. Deutero benzyl carbamate was synthesized employing a published procedure. [129] ^{1}H NMR: δ 7.35-7.34 (m, 5 H), 5.09(s, 2 H), ^{13}C {H} NMR: δ 157.34, 136.48, 77.66, 77.35, 77.03, 67.07, 1.27

2.7.2 Derivation of Differential Equations

The kinetics for hydrofunctionalization was interpreted in the context of the three simplified equations (eq 2.26-2.28), these were constructed on the basis of the following assumptions: (1) the overall reaction is irreversible, which is supported by experimental observation; (2) gold-nucleophile complex, **I**, and gold π-allene complex, **II**, are in a rapid pre-equilibrium; (3) the total gold concentration equals the concentration of species **I** and **II** and substitution into the equilibrium equation for eq 2.26 gives eq 2.30. From these latter two assumptions, we derive the equation, $[Au]_{tot} = [I]+[II]$, which relates the concentration of **I** and **II** to the total gold concentration. Differential rate equations for the gold(I)-catalyzed hydrofunctionalization were derived under four scenarios: (1) rate-limiting irreversible C-Nuc ($k_{-1} = 0$) bond formation; (2) reversible rate-limiting C-Nuc bond formation followed by rapid protodeauration ($k_1 << k_{-1} + k_2$); (3) rapid and reversible C-Nuc bond formation followed by rate-limiting protodeauration ($k_2 << k_{-1} + k_1$); (4) rapid, irreversible C-Nuc formation followed by rate-limiting protodeauration.

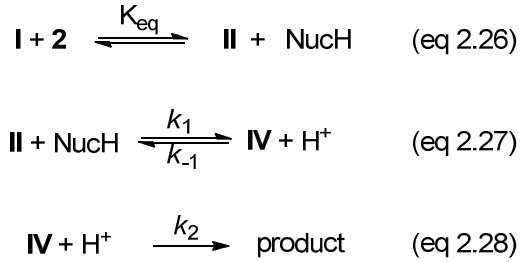

2.7.2.1 Scenario 1: Rate-limiting irreversible C-Nuc ($k_{-1} = 0$) bond formation

In the first scenario, rate-limiting irreversible C-Nuc ($k_{-1} = 0$) bond formation the rate law can be described as the rate of formation of **IV** as shown in equation 2.29. Applying the pre-equilibrium assumptions to the formation of **II** gives the equilibrium constant expression shown in eq 2.47, applying the $[\text{Au}]_{\text{tot}} = [\mathbf{I}] + [\mathbf{II}]$ assumption and solving for [**I**] gives eq 2.48. Simplification of eq 2.48 and solving for [**II**] gives eq 2.30. Substitution of the relationship for [**II**] depicted in eq 2.30 into eq 2.29 gives the two-term rate law depicted in eq 2.31. Eq 2.31 simplifies to the limiting rate laws depicted in eq 2.32 and eq 2.33 depending on the position of equilibrium involving **I** and **II**. When $K_{eq}[\mathbf{2}]$ is much greater than [NucH], the rate law simplifies to eq 2.32. Conversely, when the concentration of nucleophile is much greater than $K_{eq}[\mathbf{2}]$, the rate law simplifies to eq 2.33.

$$\text{Rate} = \frac{\text{d}\mathbf{IV}}{\text{dt}} = k_1[\mathbf{II}][\text{NucH}] \quad \text{(eq 2.29)}$$

$$K_{eq} = \frac{[\mathbf{II}][\text{NucH}]}{[\mathbf{I}][\mathbf{2}]} \quad \text{(eq 2.47)}$$

$$K_{eq} = \frac{[\mathbf{II}][\text{NucH}]}{([[\text{Au}]_{\text{tot}} - [\mathbf{II}])[\mathbf{2}]} \quad \text{(eq 2.48)}$$

$$K_{eq} = \frac{[\mathbf{II}][\text{NucH}]}{[\text{Au}]_{\text{tot}}[\mathbf{2}] - [\mathbf{II}][\mathbf{2}]} \quad \text{(eq 2.49)}$$

$$K_{eq}([\text{Au}]_{\text{tot}}[\mathbf{2}] - [\mathbf{II}][\mathbf{2}]) = [\mathbf{II}][\text{NucH}] \quad \text{(eq 2.50)}$$

$$K_{eq}\big[\text{Au}\big]_{\text{tot}}[\mathbf{2}] - K_{eq}[\mathbf{II}][\mathbf{2}] = [\mathbf{II}][\text{NucH}] \quad \text{(eq 2.51)}$$

$$K_{eq}[\mathrm{Au}]_{\mathrm{tot}}[\mathbf{2}] = [\mathbf{II}](K_{eq}[\mathbf{2}] + [\mathrm{NucH}]) \quad \text{(eq 2.52)}$$

$$[\mathbf{II}] = \frac{K_{eq}[\mathrm{Au}]_{\mathrm{tot}}[\mathbf{2}]}{K_{eq}[\mathbf{2}] + [\mathrm{NucH}]} \quad \text{(eq 2.30)}$$

$$\mathrm{Rate} = k_1[\mathrm{NucH}]x\frac{K_{eq}[\mathrm{Au}]_{\mathrm{tot}}[\mathbf{2}]}{K_{eq}[\mathbf{2}] + [\mathrm{NucH}]} \quad \text{(eq 2.53)}$$

$$\mathrm{Rate} = \frac{k_1 K_{eq}[\mathrm{Au}]_{\mathrm{tot}}[\mathbf{2}][\mathrm{NucH}]}{K_{eq}[\mathbf{2}] + [\mathrm{NucH}]} \quad \text{(eq 2.31)}$$

This rate law sets up two limiting kinetic scenarios

- if $K_{eq}[\mathbf{2}] \gg [\mathrm{NucH}]$ (such as high allene concentration):

$$\mathrm{Rate} \approx \frac{k_1 K_{eq}[\mathbf{2}][\mathrm{Au}]_{\mathrm{tot}}[\mathrm{NucH}]}{K_{eq}[\mathbf{2}]} \quad \text{(eq 2.54)}$$

$$\mathrm{Rate} \approx k_1[\mathrm{Au}]_{\mathrm{tot}}[\mathrm{NucH}] \quad \text{(eq 2.32)}$$

- if $K_{eq}[\mathbf{2}] \ll [\mathrm{NucH}]$ (such as high carbamate concentration):

$$\mathrm{Rate} \approx \frac{k_1 K_{eq}[\mathrm{Au}]_{\mathrm{tot}}[\mathbf{2}][\mathrm{NucH}]}{[\mathrm{NucH}]} \quad \text{(eq 2.55)}$$

$$\mathrm{Rate} \approx k_1 K_{eq}[\mathrm{Au}]_{\mathrm{tot}}[\mathbf{2}] \quad \text{(eq 2.33)}$$

2.7.2.2 Scenario 2: Reversible rate-limiting C-Nuc bond formation followed by rapid protodeauration ($k_1 \ll k_{-1} + k_2$).

In the second scenario, reversible rate-limiting C-Nuc bond formation followed by rapid protodeauration ($k_1 \ll k_{-1} + k_2$), k_{-1} is not negligible and the rate is defined as the rate of formation of hydrofunctionalized product (eq 2.34). Steady state approximation to the formation of **IV** gives eq 2.35. Simplification of this equation gives the relationship shown in eq 2.36 for [**IV**][H^+]. Substitution of the relationship for [**IV**][H^+] into rate eq

2.34 gives eq 2.58 and simplifies to eq 2.37. Further substitution of the relationship for **II** shown in eq 2.30 into eq 2.37 gives the rate law shown in eq 2.59 and further simplification gives eq 2.38. The rate law depicted in eq 2.39 for the rapid and reversible C-Nuc bond formation and rate-limiting protodeauration rapid can be simplified to a two-term rate law when the equilibrium concentration of **2** is much larger than the concentration of NucH (eq 2.40) or when the concentration of NucH is much larger than the equilibrium concentration of **2** (eq 2.41).

$$\text{Rate} = \frac{\text{d}[\mathbf{P}]}{\text{dt}} = k_2[\mathbf{IV}][\text{H}^+] \quad \text{(eq 2.34)}$$

$$\frac{\text{d}\mathbf{IV}}{\text{dt}} = k_1[\mathbf{II}][\text{NucH}] - k_{-1}[\mathbf{IV}][\text{H}^+] - k_2[\mathbf{III}][\text{H}^+] = 0 \quad \text{(eq 2.35)}$$

$$k_1[\mathbf{II}][\text{NucH}] = k_{-1}[\mathbf{IV}][\text{H}^+] + k_2[\mathbf{IV}][\text{H}^+] \quad \text{(eq 2.56)}$$

$$k_1[\mathbf{II}][\text{NucH}] = [\mathbf{IV}][\text{H}^+](k_{-1} + k_2) \quad \text{(eq 2.57)}$$

$$\frac{k_1[\mathbf{II}][\text{NucH}]}{(k_{-1} + k_2)} = [\mathbf{IV}][\text{H}^+] \quad \text{(eq 2.36)}$$

$$\text{Rate} = \frac{\text{d}\mathbf{5}}{\text{dt}} = k_2[\mathbf{IV}][\text{H}^+] = k_2\frac{k_1[\mathbf{II}][\text{NucH}]}{(k_{-1} + k_2)} \quad \text{(eq 2.58)}$$

$$\text{Rate} = \frac{k_1k_2[\mathbf{II}][\text{NucH}]}{(k_{-1} + k_2)} \quad \text{(eq 2.37)}$$

$$\text{Rate} = \frac{k_1k_2[\text{NucH}]}{(k_{-1} + k_2)}x\frac{K_{eq}[\text{Au}]_{\text{tot}}[\mathbf{2}]}{K_{eq}[\mathbf{2}] + [\text{NucH}]} \quad \text{(eq 2.59)}$$

$$\text{Rate} = \frac{k_1k_2K_{eq}[\text{NucH}][\text{Au}]_{\text{tot}}[\mathbf{2}]}{(k_{-1} + k_2)(K_{eq}[\mathbf{2}] + [\text{NucH}])} \quad \text{(eq 2.38)}$$

If $k' = k_{-1} + k_2$

$$\text{Rate} = \frac{k_1k_2K_{eq}[\text{NucH}][\text{Au}]_{\text{tot}}[\mathbf{2}]}{k'K_{eq}[\mathbf{2}] + k'[\text{NucH}]} \quad \text{(eq 2.39)}$$

The rate law for scenario 2 is in the same form as the derived rate law in scenario 1.

- if K_{eq}[**2**] ≫ [NucH] (such as high allene concentration):

$$\text{Rate} \approx k_{obs}[\text{Au}]_{\text{tot}}[\text{NucH}] \quad \text{(eq 2.40)}$$

$$\text{when } k_{obs} = \frac{k_1 k_2}{k'}$$

- if K_{eq}[**2**] ≪ [NucH] (such as high nucleophile concentration):

$$\text{Rate} \approx k_{obs}[\text{Au}]_{\text{tot}}[\mathbf{2}] \quad \text{(eq 2.41)}$$

$$\text{when } k_{obs} = \frac{k_1 k_2 K_{eq}}{k'}$$

2.7.2.3 Scenario 3: Rapid and reversible C-Nuc bond formation followed by rate-limiting protodeauration ($k_2 << k_{-1} + k_1$)

In the third scenario, rapid and reversible C-Nuc bond formation followed by rate limiting protodeauration ($k_2 << k_{-1} + k_1$), the rate can be described as the rate of formation of product (eq 2.34). A pre-equilibrium assumption was applied for the formation of **IV**. The equilibrium constant for the reaction shown in eq 2.27 gives the equilibrium expression shown in eq 2.42. Solving for [**IV**] (shown in eq 2.43) and substitution into eq 2.34 gives eq 2.60. Simplification of eq 2.60 gives eq 2.44. Substitution of the relationship for **II** shown in eq 2.30 gives the rate law depicted in eq 2.45.

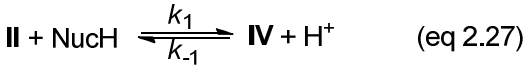

(eq 2.27)

$$\frac{k_1}{k_{-1}} = \frac{[\mathbf{IV}][\text{H}^+]}{[\mathbf{II}][\text{NucH}]} \quad \text{(eq 2.42)}$$

$$[\mathbf{IV}] = \frac{k_1[\mathbf{II}][\mathrm{NucH}]}{k_{-1}[\mathrm{H^+}]} \quad \text{(eq 2.43)}$$

$$\text{Rate} = \frac{\mathrm{d}\mathbf{P}}{\mathrm{dt}} = k_2[\mathbf{IV}][\mathrm{H^+}] \quad \text{(eq 2.34)}$$

$$\text{Rate} = \frac{k_2 k_1[\mathbf{II}][\mathrm{NucH}][\mathrm{H^+}]}{k_{-1}[\mathrm{H^+}]} \quad \text{(eq 2.60)}$$

$$\text{Rate} = \frac{k_2 k_1[\mathbf{II}][\mathrm{NucH}]}{k_{-1}} \quad \text{(eq 2.44)}$$

$$[\mathbf{II}] = \frac{K_{eq}[\mathrm{Au}]_{\mathrm{tot}}[\mathbf{2}]}{K_{eq}[\mathbf{2}] + [\mathrm{NucH}]} \quad \text{(eq 2.30)}$$

$$\text{Rate} = \frac{k_2 k_1 K_{eq}[\mathrm{Au}]_{\mathrm{tot}}[\mathbf{2}][\mathrm{NucH}]}{k_{-1}(K_{eq}[\mathbf{2}] + [\mathrm{NucH}])} \quad \text{(eq 2.45)}$$

2.7.2.4 Scenario 4: Rapid, irreversible C-Nuc formation followed by rate-limiting protodeauration.

In the fourth scenario (rapid, irreversible C-Nuc formation followed by rate-limiting protodeauration) the [**IV**] is equal to the total gold concentration (eq 2.46), so the rate would be zero-order in both [**2**] and [NucH] and first-order in catalyst.

$$[\mathrm{Au}]_{tot} = [\mathbf{IV}] \quad \text{(eq 2.46)}$$

2.7.3 General Procedure for Kinetic Study of Au(I)-catalyzed Intermolecular Hydroalkoxylation of Allenes with Alcohols

(1-(3-Methyl-2-butenyloxy)propyl)benzene. A mixture of (IPr)AuCl (6.2 mg, 0.010 mmol) and AgOTf (2.6 mg, 0.010 mmol) in toluene (0.5 mL) was stirred at room temperature for 5 min, treated with 3-methyl-1,2-butadiene (13.6 mg, 0.20 mmol), 1-phenyl-1-propanol (30.0 mg, 0.22 mmol), and *n*-tetradecane (6.7 mg, 0.034 mmol) as the internal standard. The resulting suspension was stirred at room temperature for 4 h. The

disappearance of 1-phenyl-1-propanol (2.6 min) was monitored by analyzing 10 μL aliquots purified through a cotton plug pipet filled with silica gel with EtOAc via gas chromatography compared to the internal standard *n*-tetradecane (4.1 min). The concentration of **1** was determined from the integration of the GC peak of **1** relative to that of n-tetradecane, internal standard.

- Pseudo first-order rate constants were determined for the gold(I)-catalyzed hydroalkoxylation of allenes with alcohols as a function of [alcohol] at [alcohol] = 0.14 to 0.48 M in Figure 2.23 to Figure 2.25.
- Pseudo first-order rate constants were determined for the gold(I)-catalyzed hydroalkoxylation of allenes with alcohols as a function of [catalyst] at [catalyst] = 5 to 57 mM in Figure 2.37 to Figure 2.42.
- Pseudo first-order rate constants were determined for the gold(I)-catalyzed hydroalkoxylation of allenes with alcohols as a function of [allene] at [allene] = 0.32 to 3.7 M in Figure 2.26 to Figure 2.36

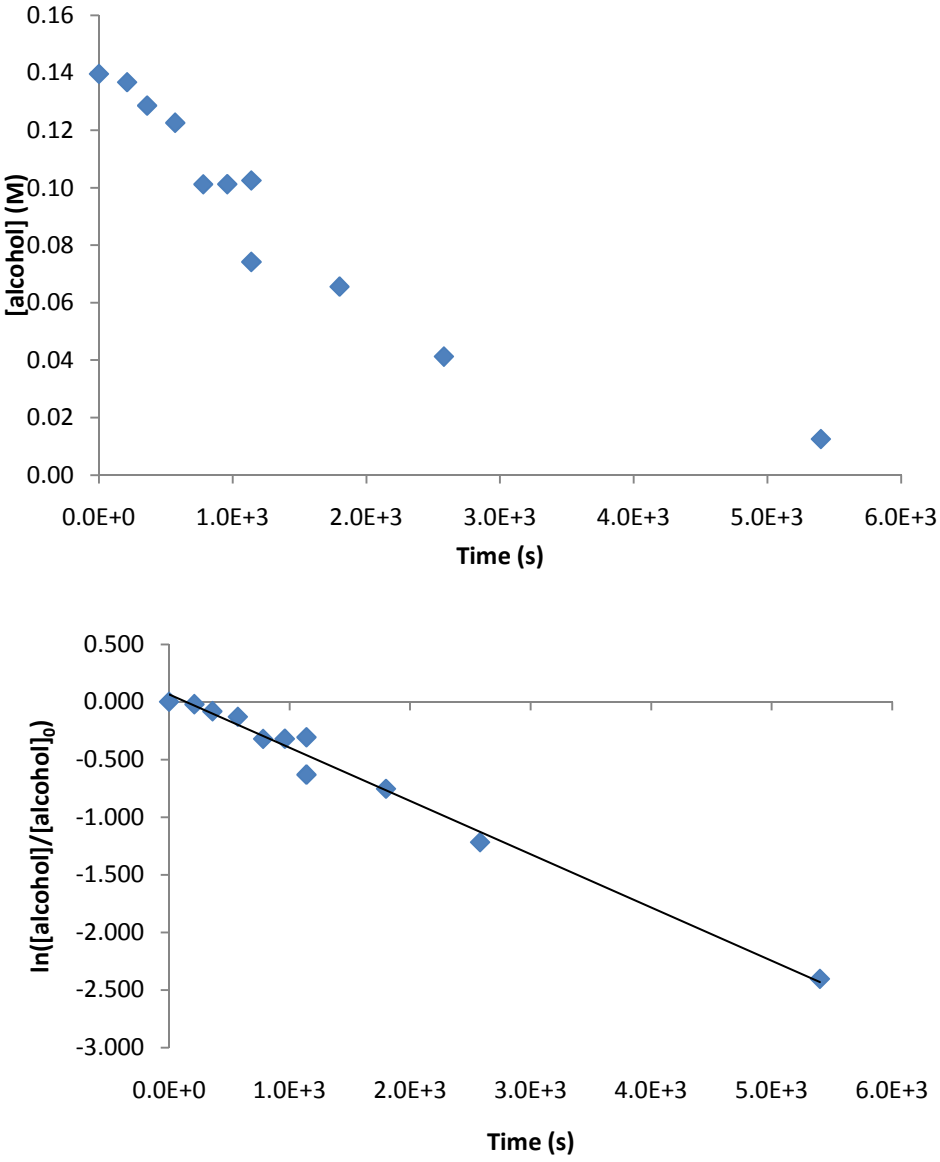

Figure 2.23. Concentration versus time plot for the gold(I)-catalyzed intermolecular hydroalkoxylation of 1-phenylpropanol with 3-methyl-1,2-butadiene in toluene at room temperature. [2] = 1.7 M, [1] = 0.14 M, [(IPr)AuCl/AgOTf] = 15 mM k_{obs} = 4.6 ± 0.1 x 10^{-4} s^{-1} (Table 2.1, entry 1)

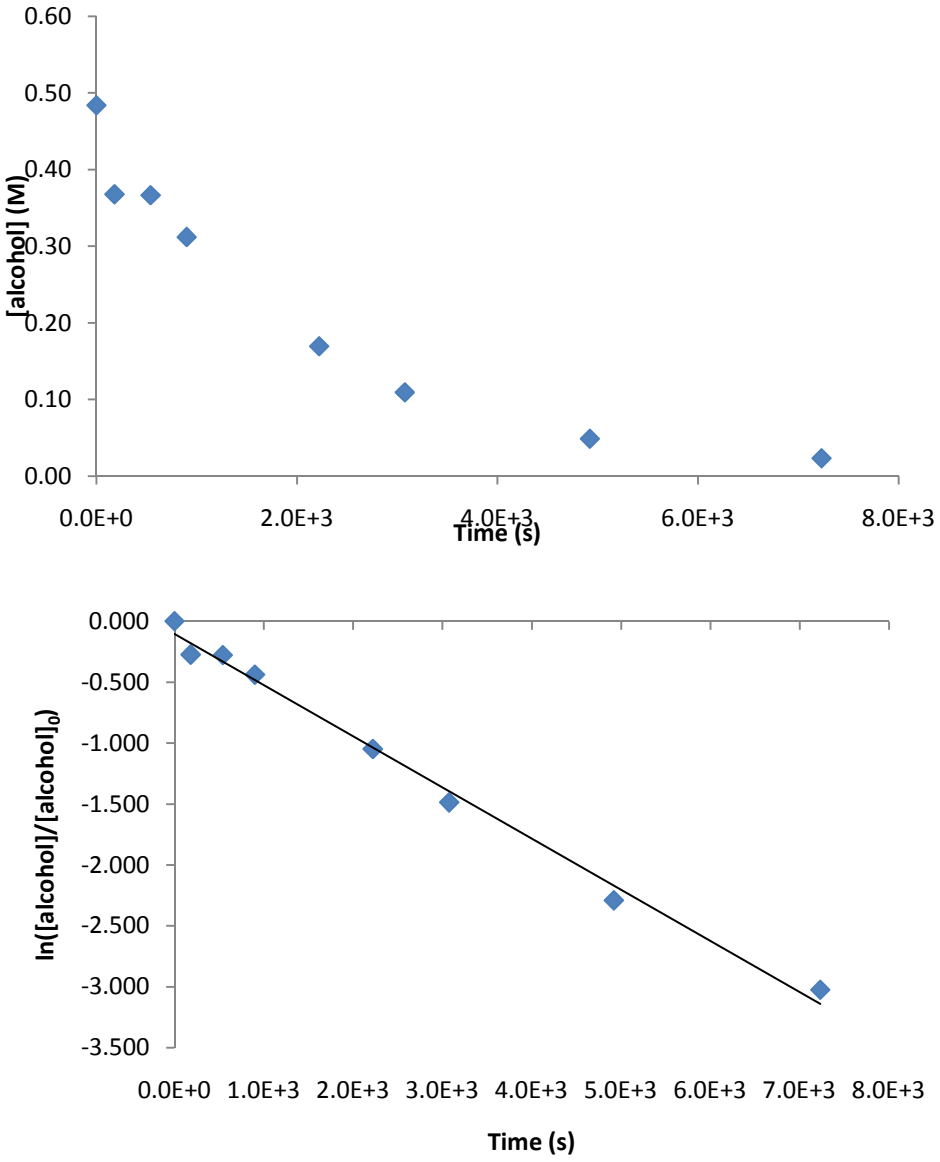

Figure 2.24. Pseudo first-order plot for the gold(I)-catalyzed intermolecular hydroalkoxylation of 1-phenylpropanol with 3-methyl-1,2-butadiene in toluene at room temperature. [2] = 5.2 M, [1] = 0.48 M, [(IPr)AuCl/AgOTf] = 15 mM k_{obs} = 4.2 ± 0.1 x 10^{-4} s^{-1} (Table 2.1, entry 2)

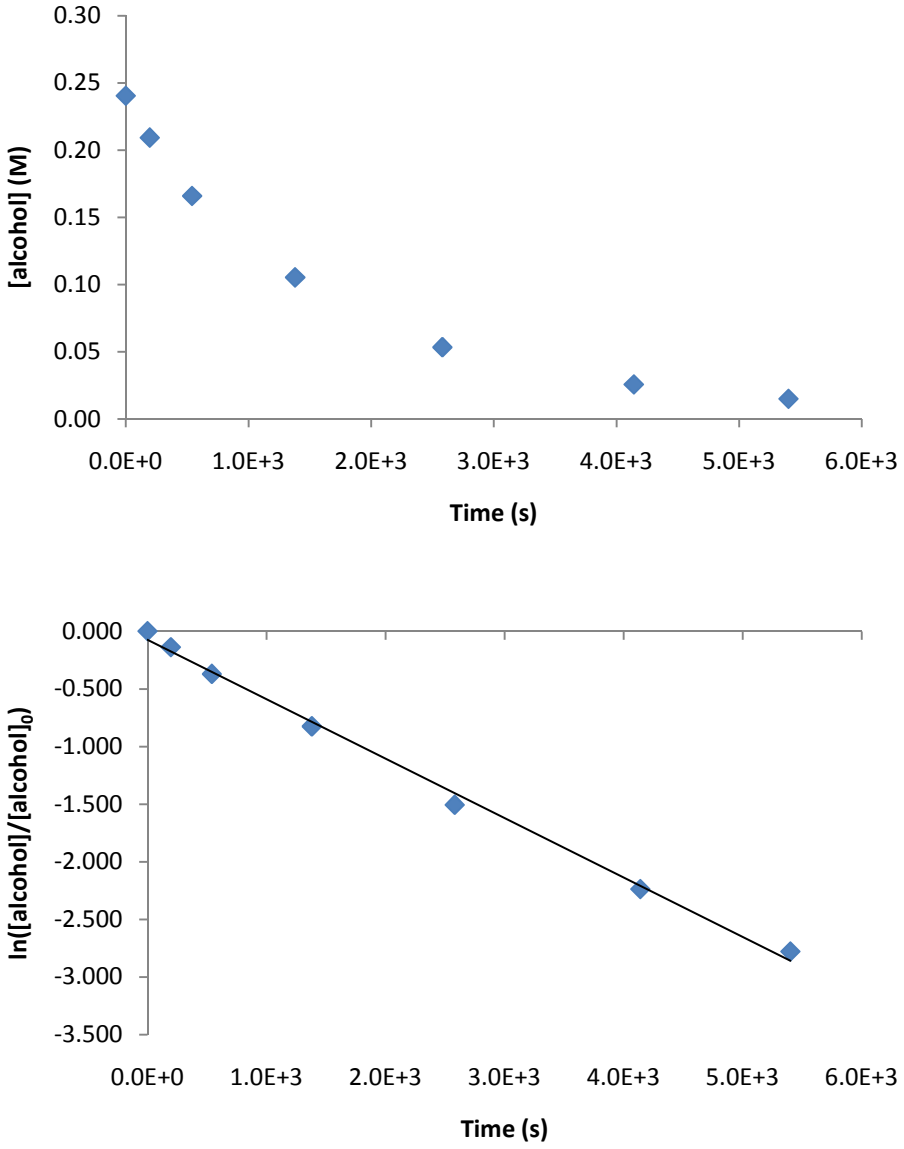

Figure 2.25. Concentration versus time plot for the gold(I)-catalyzed intermolecular hydroalkoxylation of 1-phenylpropanol with 3-methyl-1,2-butadiene in toluene at room temperature. [2] = 3.0 M, [1] = 0.24 M, [(IPr)AuCl/AgOTf] = 15 mM k_{obs} = 5.1 ± 0.1 x 10^{-4} s^{-1} (Table 2.1, entry 3)

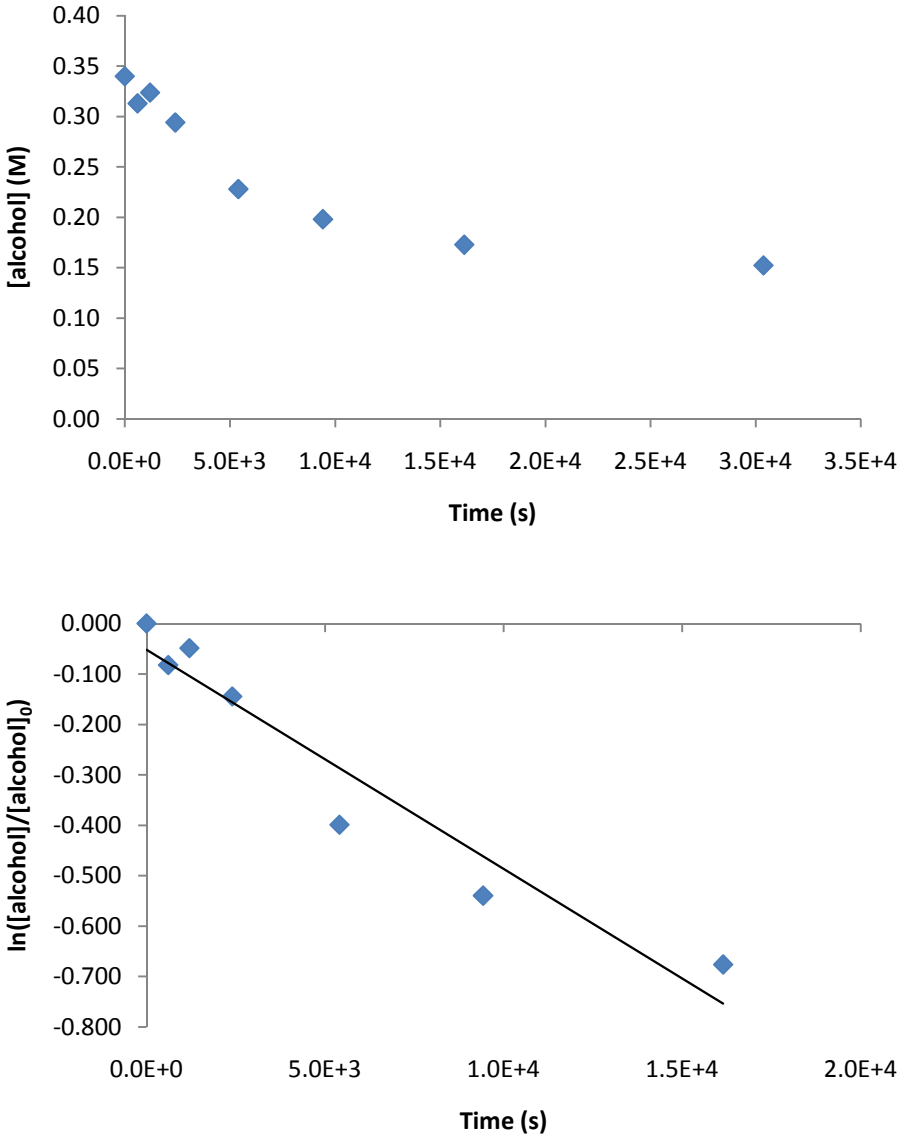

Figure 2.26. Concentration versus time plot for the gold(I)-catalyzed intermolecular hydroalkoxylation of 1-phenylpropanol with 3-methyl-1,2-butadiene in toluene at room temperature. [2] = 0.32 M, [1] = 0.34 M, [(IPr)AuCl/AgOTf] = 15 mM k_{obs} = 0.5 ± 0.1 x 10^{-4} s^{-1} (Table 2.1, entry 4)

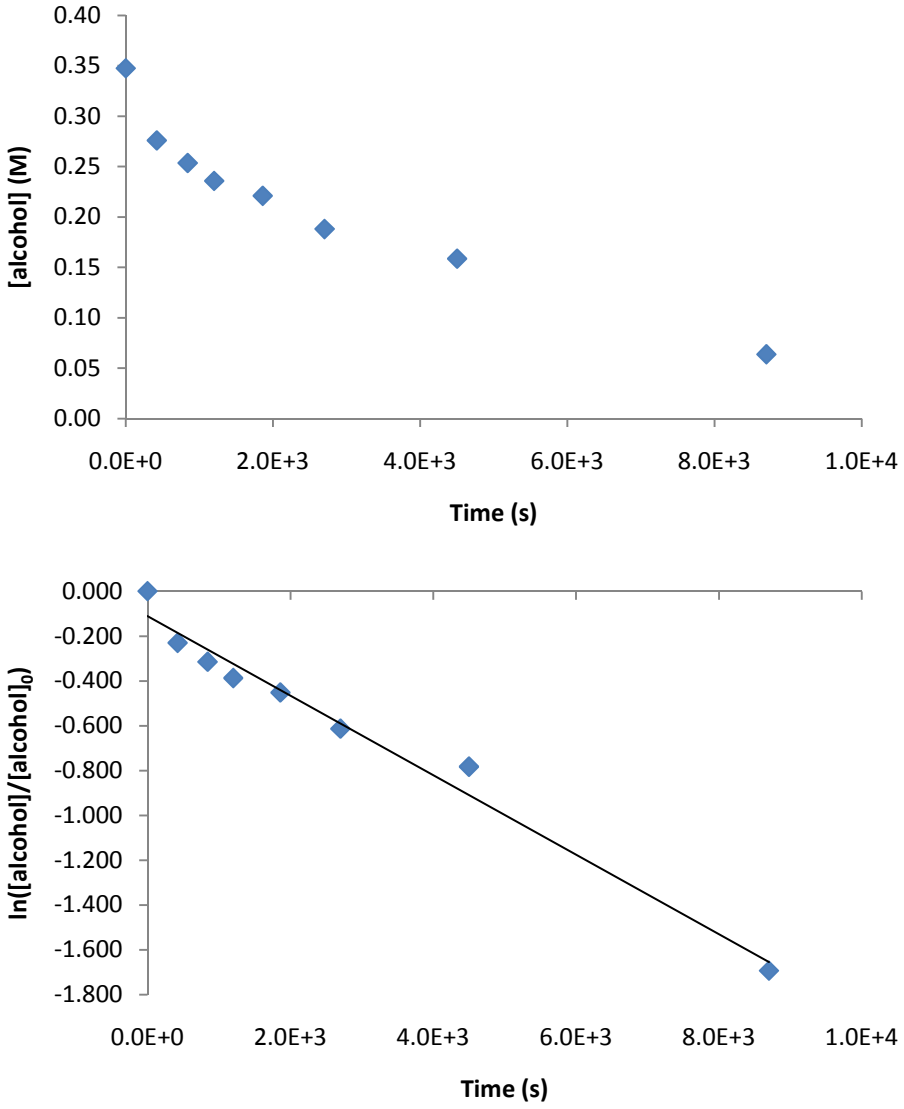

Figure 2.27. Concentration versus plot for the gold(I)-catalyzed intermolecular hydroalkoxylation of 1-phenylpropanol with 3-methyl-1,2-butadiene in toluene at room temperature. [2] = 0.65 M, [1] = 0.35 M, [(IPr)AuCl/AgOTf] = 15 mM k_{obs} = 1.8 ± 0.1 x 10^{-4} s^{-1} (Table 2.1, entry 5)

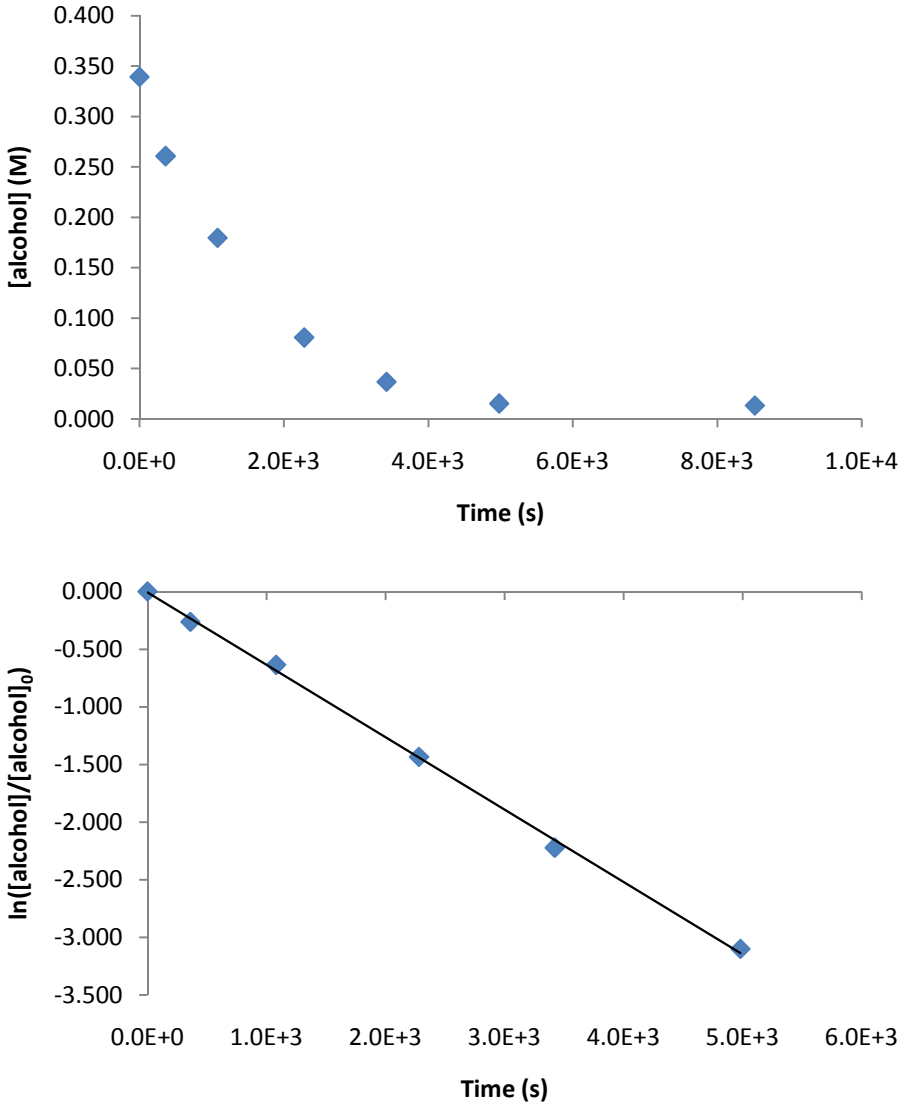

Figure 2.28. Concentrationversus time plot for the gold(I)-catalyzed intermolecular hydroalkoxylation of 1-phenylpropanol with 3-methyl-1,2-butadiene in toluene at room temperature. [2] = 1.9 M, [1] = 0.34 M, [(IPr)AuCl/AgOTf] = 15 mM k_{obs} = 4.1 ± 0.1 x 10^{-4} s^{-1} (Table 2.1, entry 6)

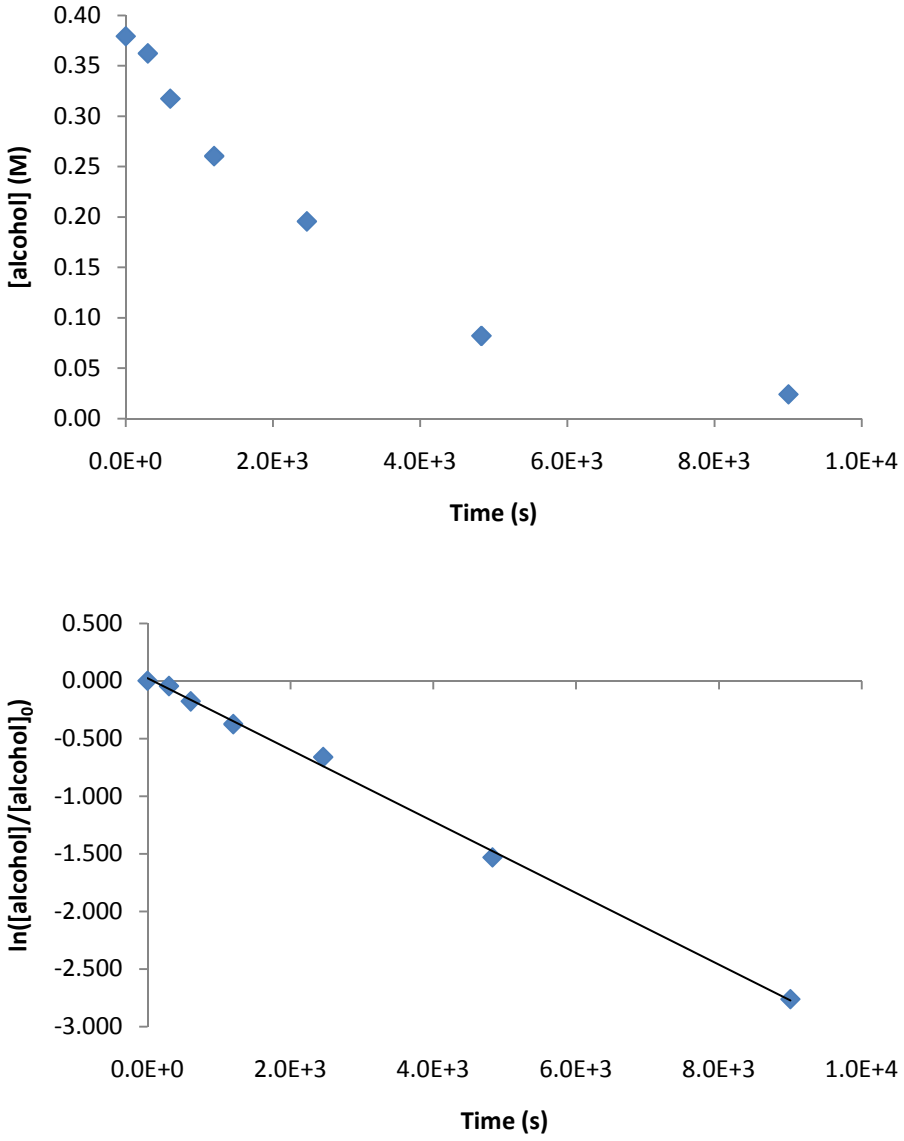

Figure 2.29. Pseudo first-order plot for the gold(I)-catalyzed intermolecular hydroalkoxylation of 3-methyl-1,2-butadiene with 1-phenylpropanol in toluene at room temperature. [2] = 1.0 M, [1] = 0.38 M, [(IPr)AuCl/AgOTf] = 14 mM k_{obs} = 3.11 ± 0.05 x 10^{-4} s^{-1} (Table 2.1, entry 7)

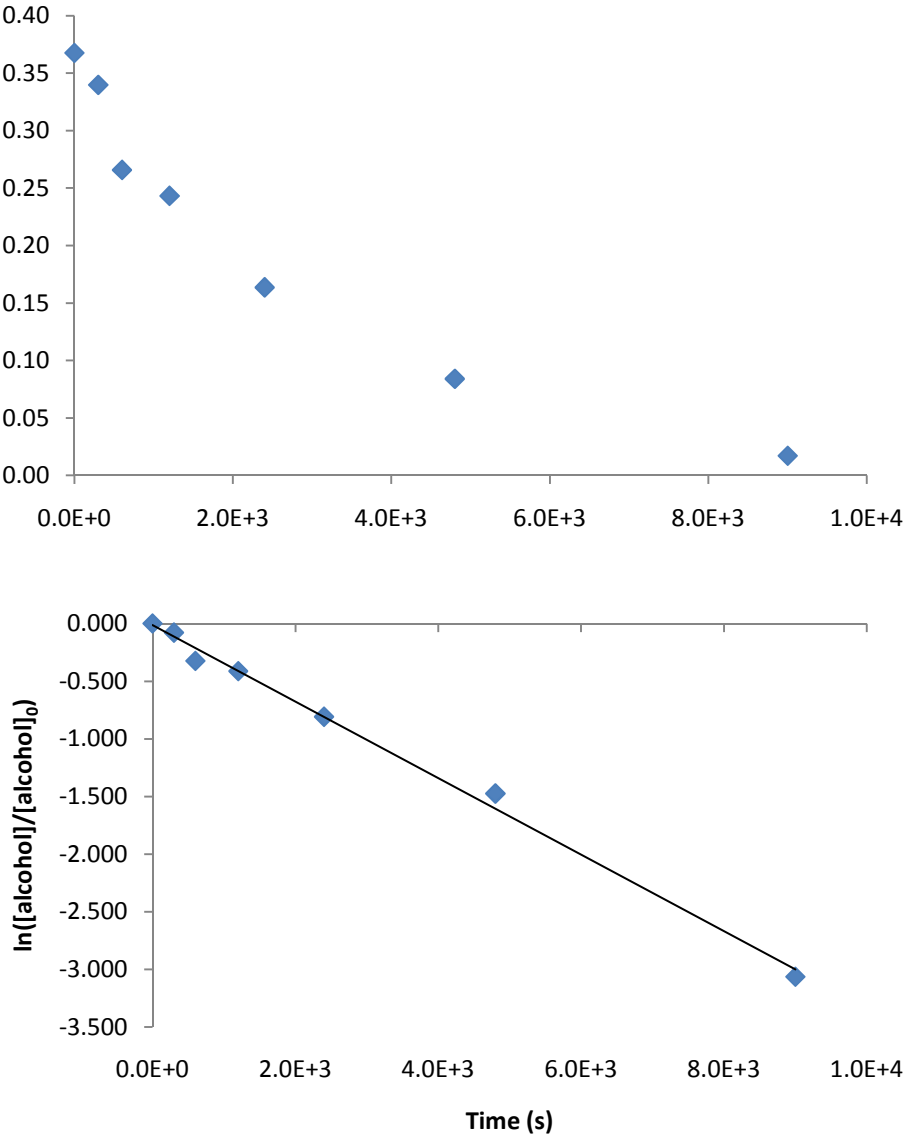

Figure 2.30. Concentration versus time plot for the gold(I)-catalyzed intermolecular hydroalkoxylation of 1-phenylpropanol with 3-methyl-1,2-butadiene in toluene at room temperature. [2] = 1.4 M, [1] = 0.37 M, [(IPr)AuCl/AgOTf] = 14 mM k_{obs} = 3.3 ± 0.1 x 10^{-4} s^{-1} (Table 2.1, entry 8)

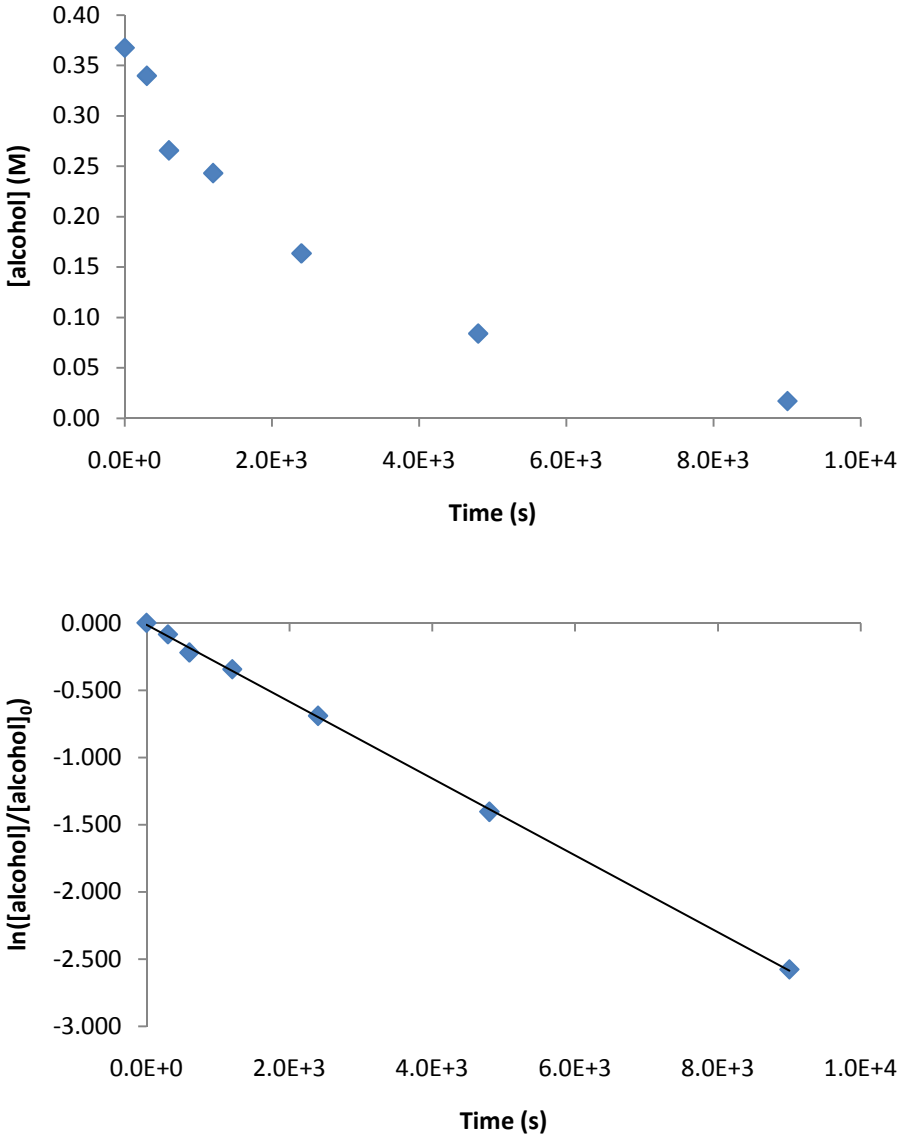

Figure 2.31. Concentration versus time plot for the gold(I)-catalyzed intermolecular hydroalkoxylation of 1-phenylpropanol with 3-methyl-1,2-butadiene in toluene at room temperature. [2] = 0.87 M, [1] = 0.35 M, [(IPr)AuCl/AgOTf] = 14 mM k_{obs} = 2.86 ± 0.02 x 10-4 s-1 (Table 2.1, entry 9)

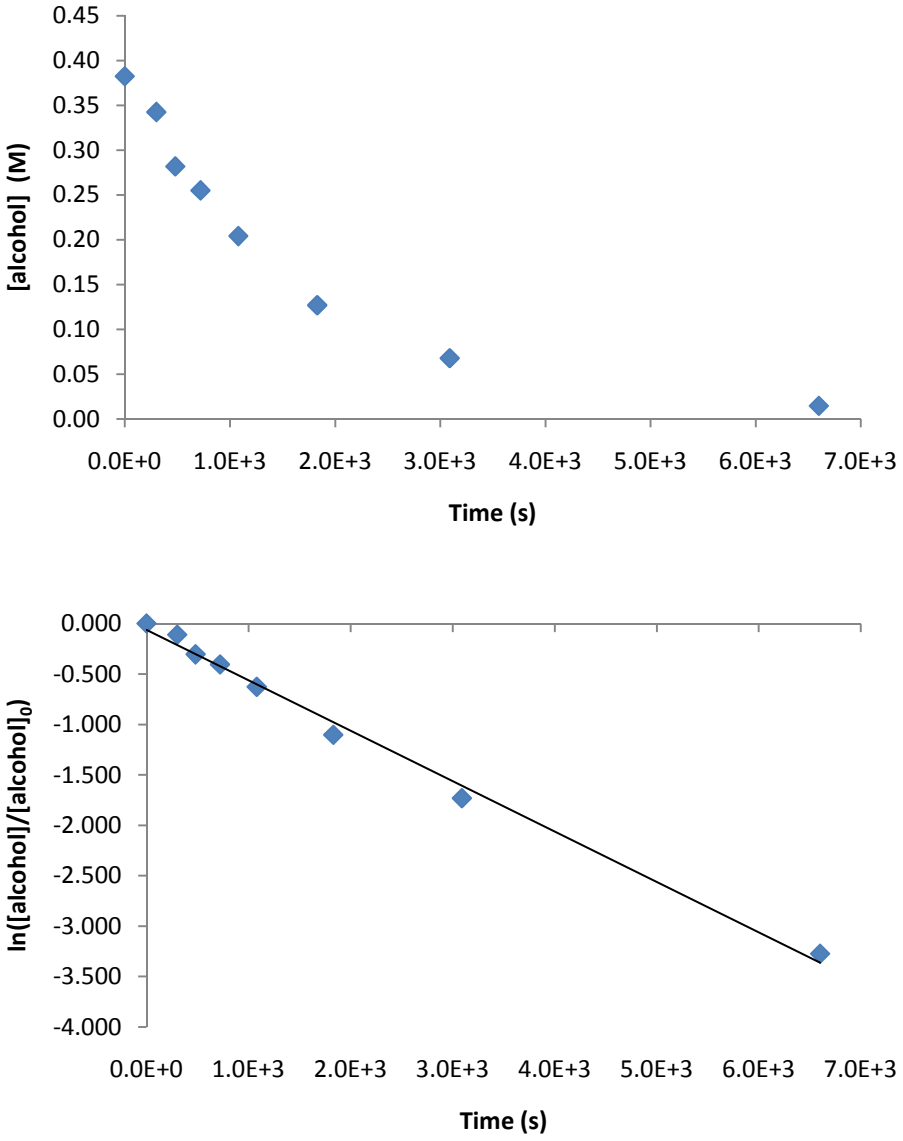

Figure 2.32. Concentration versus time plot for the gold(I)-catalyzed intermolecular hydroalkoxylation of 1-phenylpropanol with 3-methyl-1,2-butadiene in toluene at room temperature. [2] = 2.4 M, [1] = 0.38 M, [(IPr)AuCl/AgOTf] = 15 mM k_{obs} = 5.0 ± 0.1 x 10^{-4} s^{-1} (Table 2.1, entry 10)

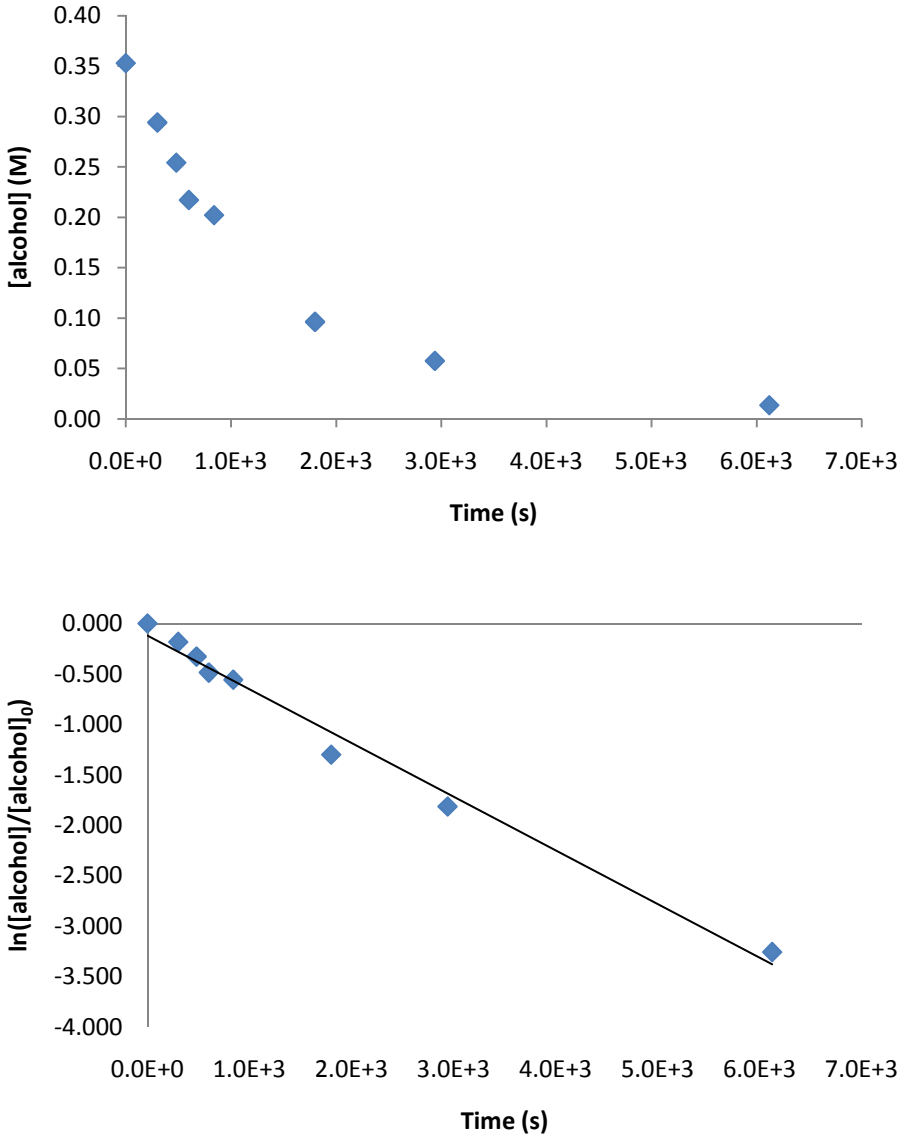

Figure 2.33. Concentration versus time plot for the gold(I)-catalyzed intermolecular hydroalkoxylation of 1-phenylpropanol with 3-methyl-1,2-butadiene in toluene at room temperature. [2] = 3.4 M, [1] = 0.35 M, [(IPr)AuCl/AgOTf] = 14 mM k_{obs} = 5.3 ± 0.1 x 10^{-4} s^{-1} (Table 2.1, entry 11)

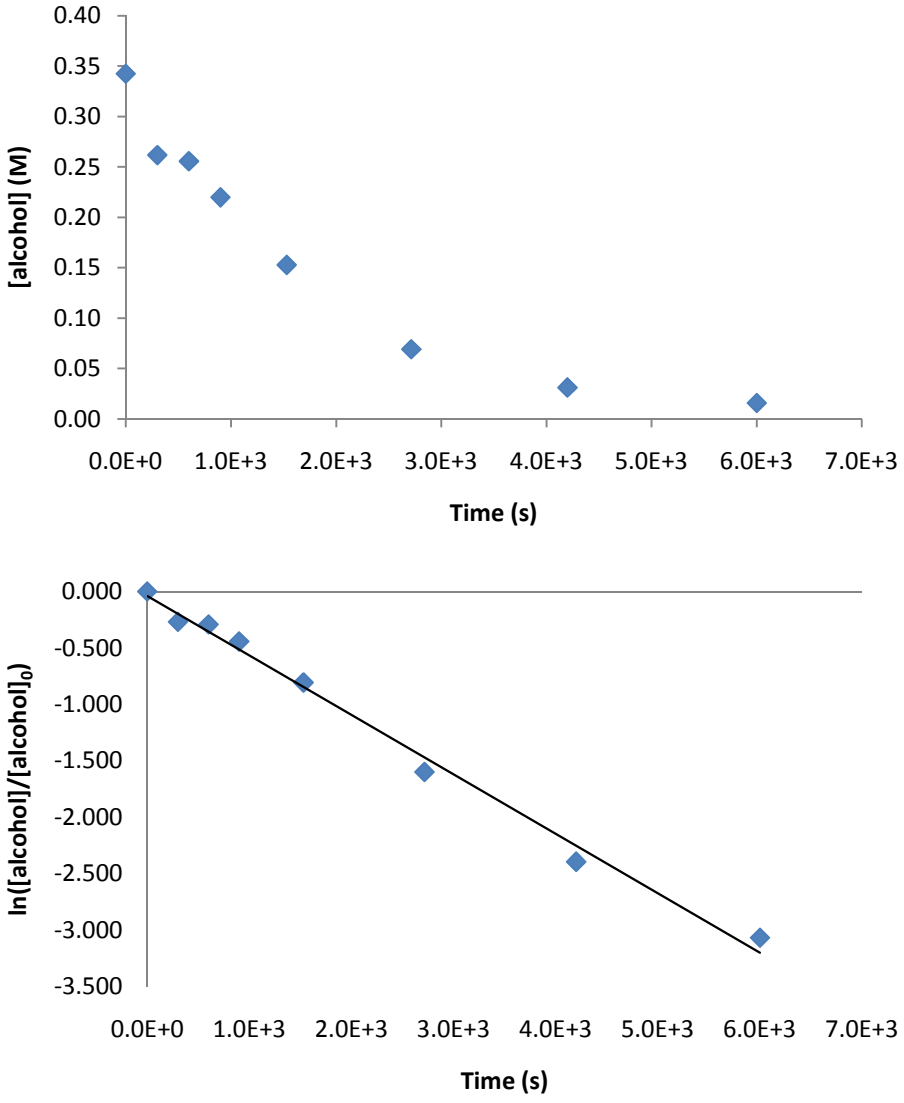

Figure 2.34. Concentration versus time plot for the gold(I)-catalyzed intermolecular hydroalkoxylation of 1-phenylpropanol with 3-methyl-1,2-butadiene in toluene at room temperature. [2] = 2.7 M, [1] = 0.34 M, [(IPr)AuCl/AgOTf] = 15 mM k_{obs} = 5.3 ± 0.1 x 10^{-4} s^{-1} (Table 2.1, entry 12)

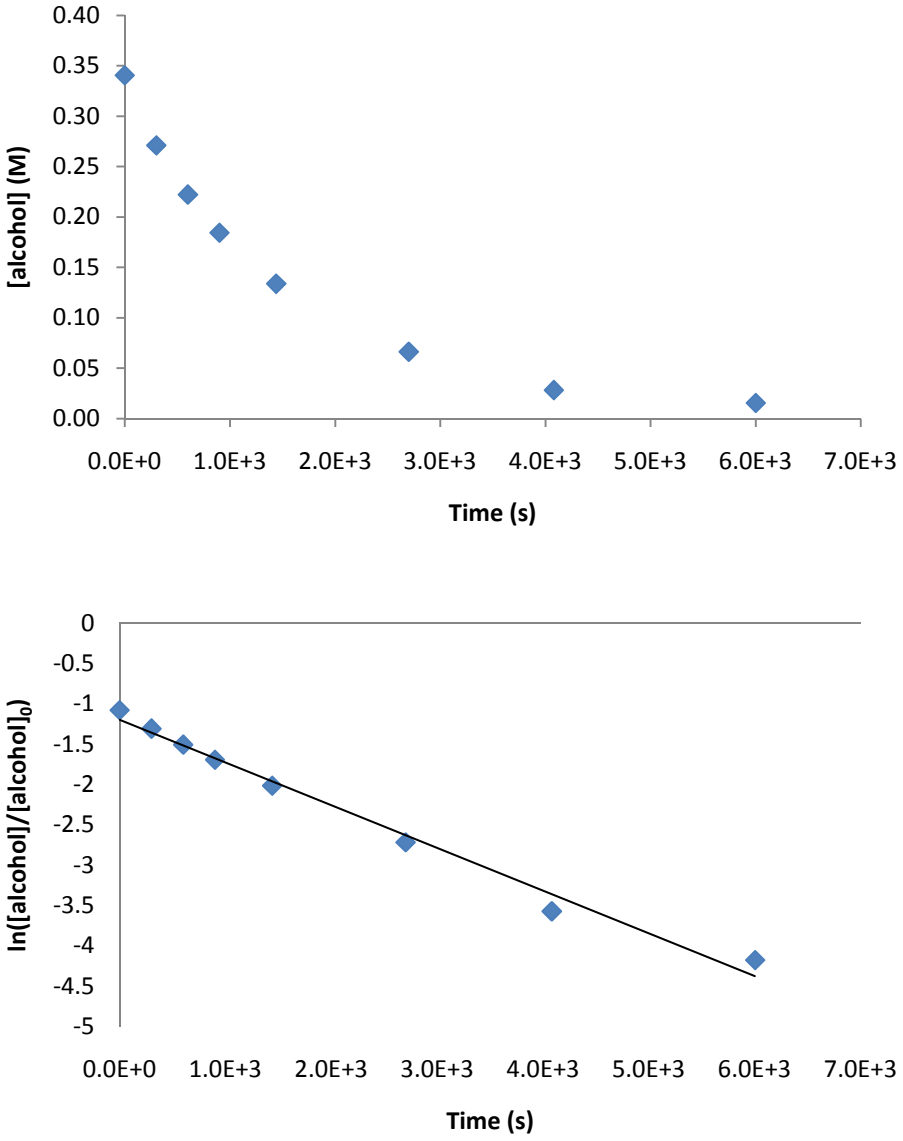

Figure 2.35. Concentration versus time plot for the gold(I)-catalyzed intermolecular hydroalkoxylation of 1-phenylpropanol with 3-methyl-1,2-butadiene in toluene at room temperature. [2] = 3.7 M, [1] = 0.34 M, [(IPr)AuCl/AgOTf] = 15 mM k_{obs} = 5.3 ± 0.1 x 10^{-4} s^{-1} (Table 2.1, entry 13)

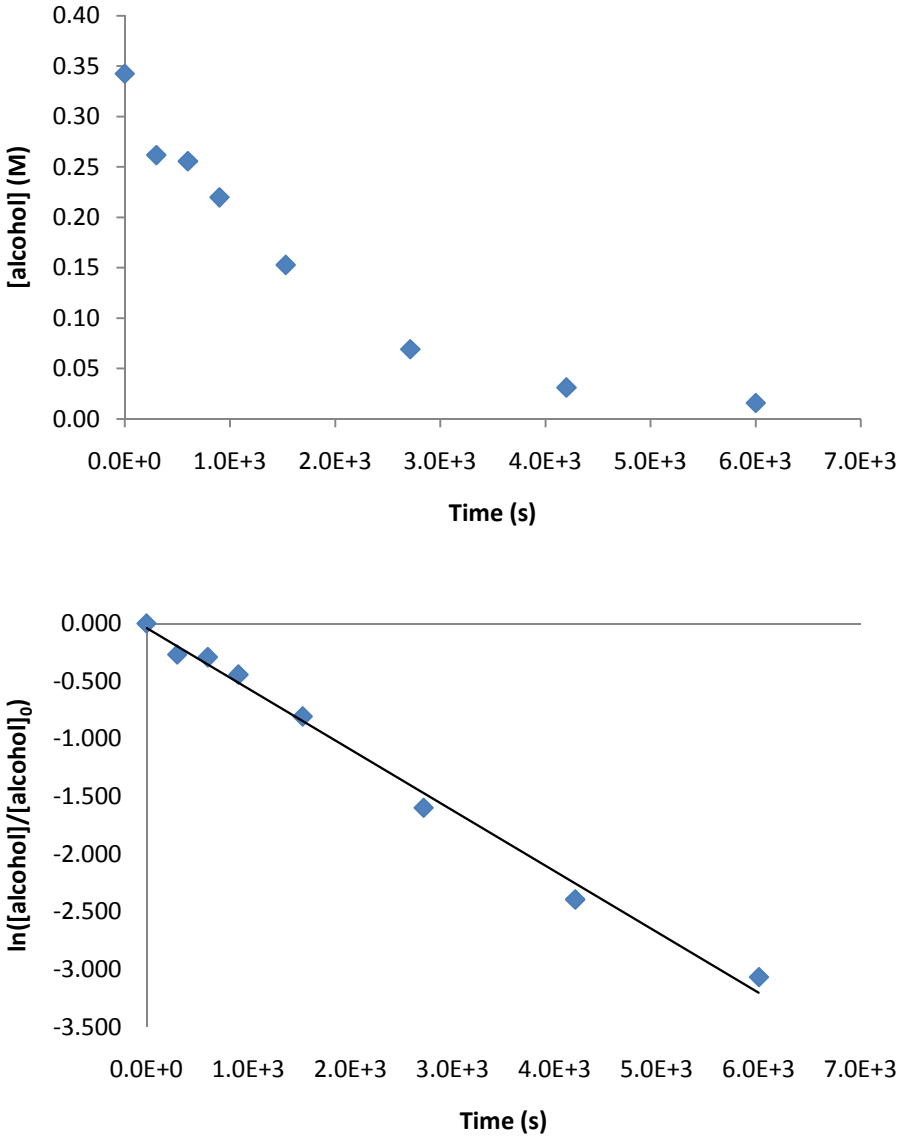

Figure 2.36. Concentration versus time plot for the gold(I)-catalyzed intermolecular hydroalkoxylation of 1-phenylpropanol with 3-methyl-1,2-butadiene in toluene at room temperature. [2] = 2.7 M, [1] = 0.34 M, [(IPr)AuCl/AgOTf] = 15 mM k_{obs} = 5.3 ± 0.1 x 10^{-4} s^{-1} (Table 2.1, entry 14)

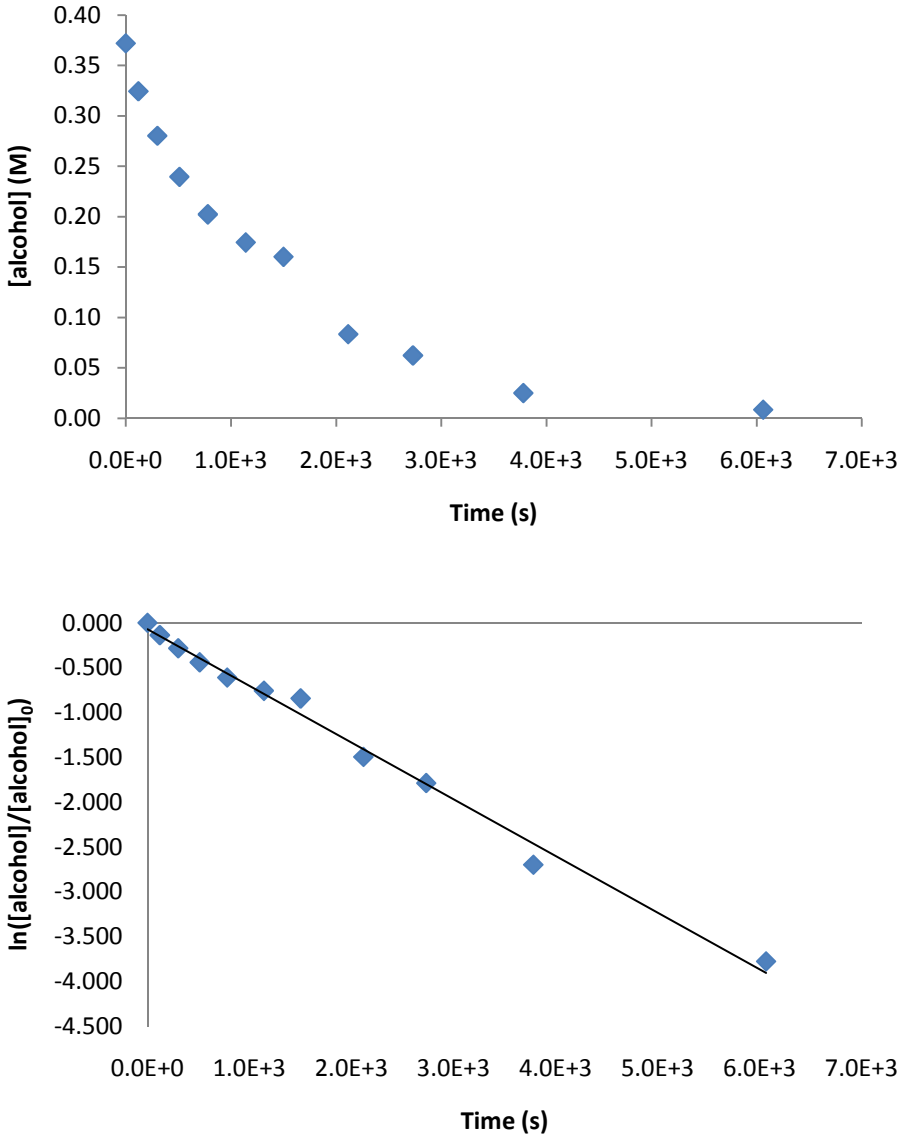

Figure 2.37. Concentration versus time plot for the gold(I)-catalyzed intermolecular hydroalkoxylation of 1-phenylpropanol with 3-methyl-1,2-butadiene in toluene at room temperature. [2] = 2.5 M, [1] = 0.37 M, [(IPr)AuCl/AgOTf] = 28 mM k_{obs} = 6.3 ± 0.1 x 10^{-4} s^{-1} (Table 2.1, entry 15)

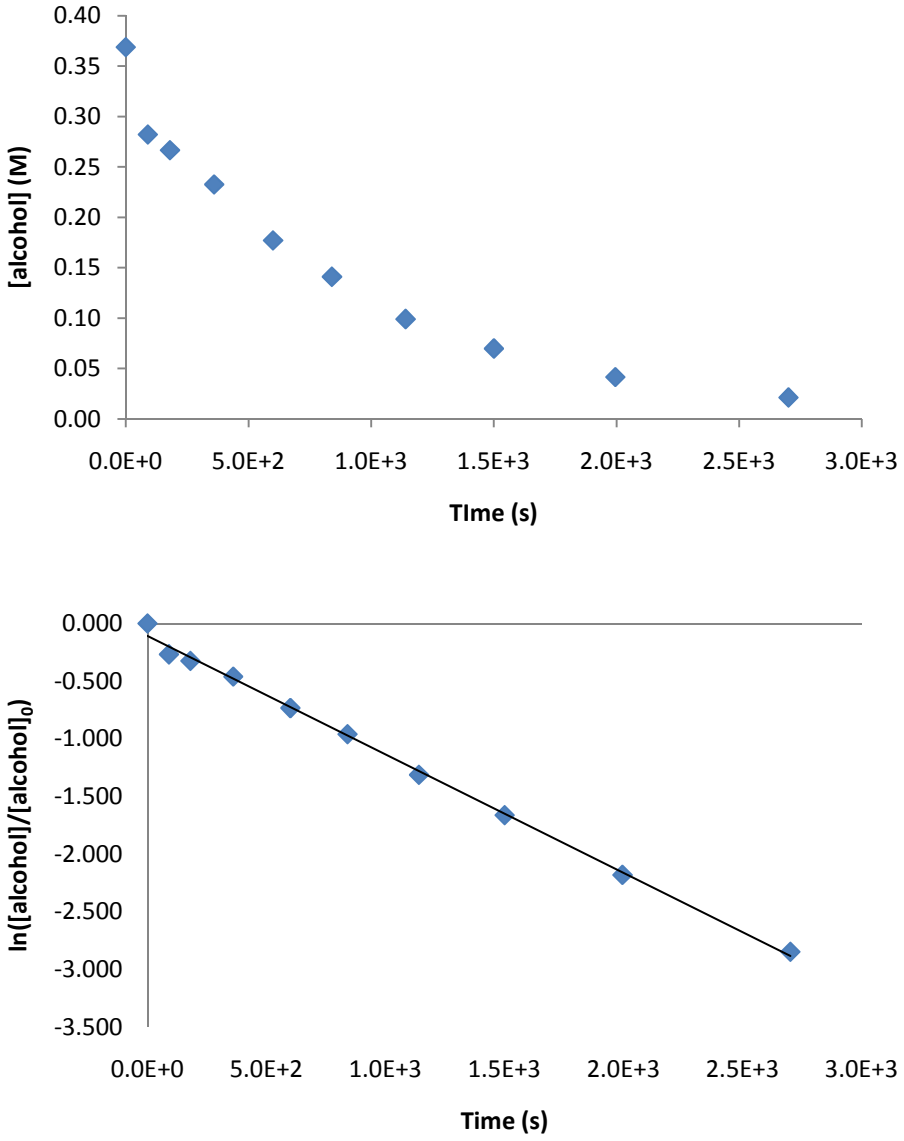

Figure 2.38. Concentration versus time plot for the gold(I)-catalyzed intermolecular hydroalkoxylation of 1-phenylpropanol with 3-methyl-1,2-butadiene in toluene at room temperature. [2] = 2.5 M, [1] = 0.37 M, [(IPr)AuCl/AgOTf] = 57 mM k_{obs} = 10.3 ± 0.5 x 10^{-4} s^{-1} (Table 2.1, entry 16)

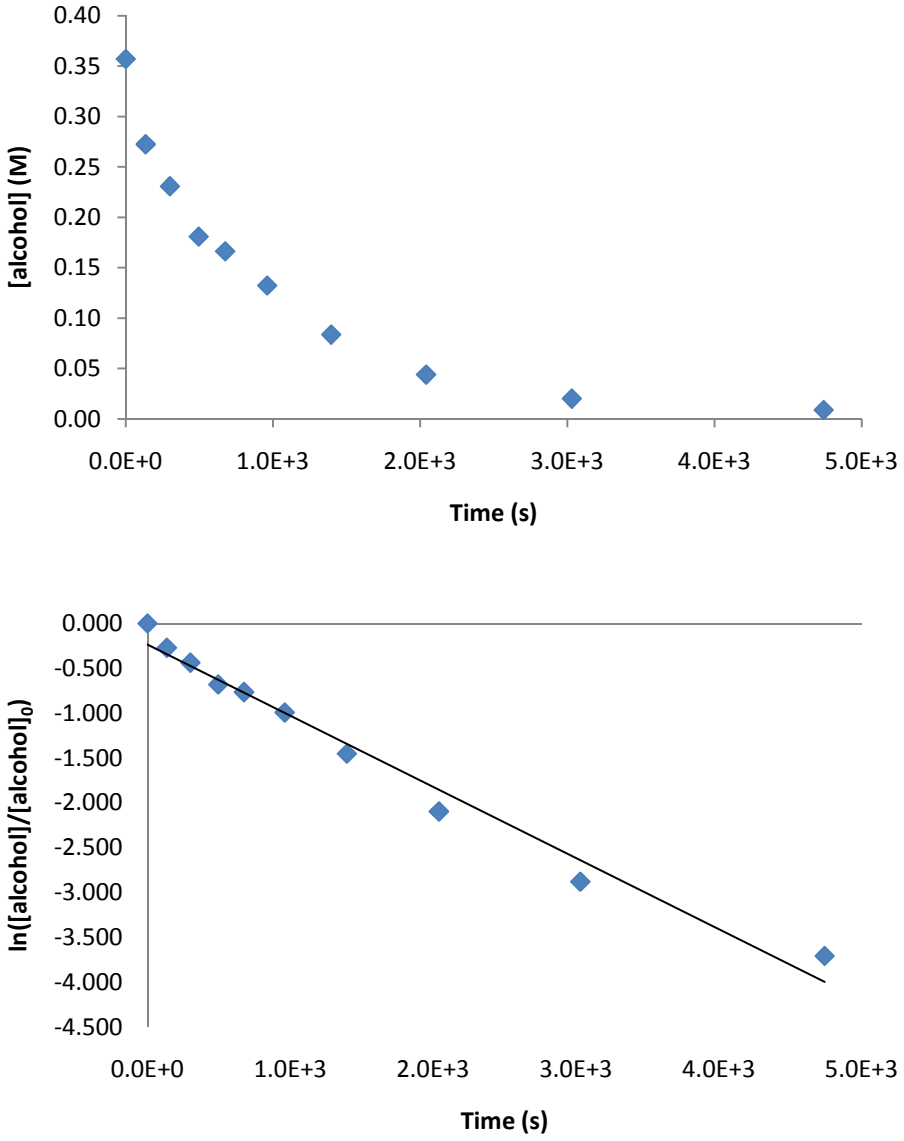

Figure 2.39. Concentration versus time plot for the gold(I)-catalyzed intermolecular hydroalkoxylation of 1-phenylpropanol with 3-methyl-1,2-butadiene in toluene at room temperature. [2] = 2.6 M, [1] = 0.36 M, [(IPr)AuCl/AgOTf] = 43 mM k_{obs} = 7.9 ± 0.2 x 10^{-4} s^{-1} (Table 2.1, entry 17)

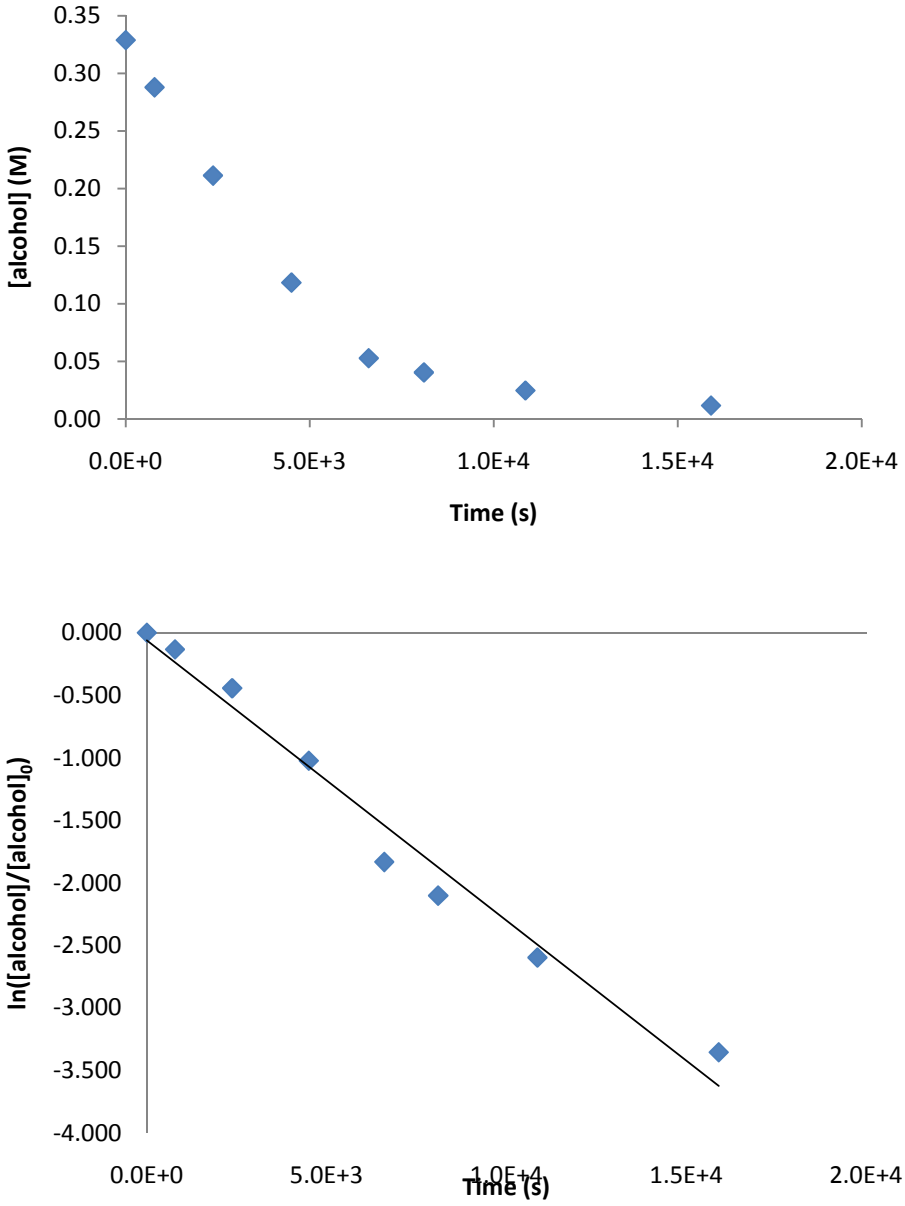

Figure 2.40. Concentration versus time plot for the gold(I)-catalyzed intermolecular hydroalkoxylation of 1-phenylpropanol with 3-methyl-1,2-butadiene in toluene at room temperature. [2] = 2.5 M, [1] = 0.33 M, [(IPr)AuCl/AgOTf] = 10 mM k_{obs} = 2.2 ± 0.2 x 10^{-4} s^{-1} (Table 2.1, entry 18)

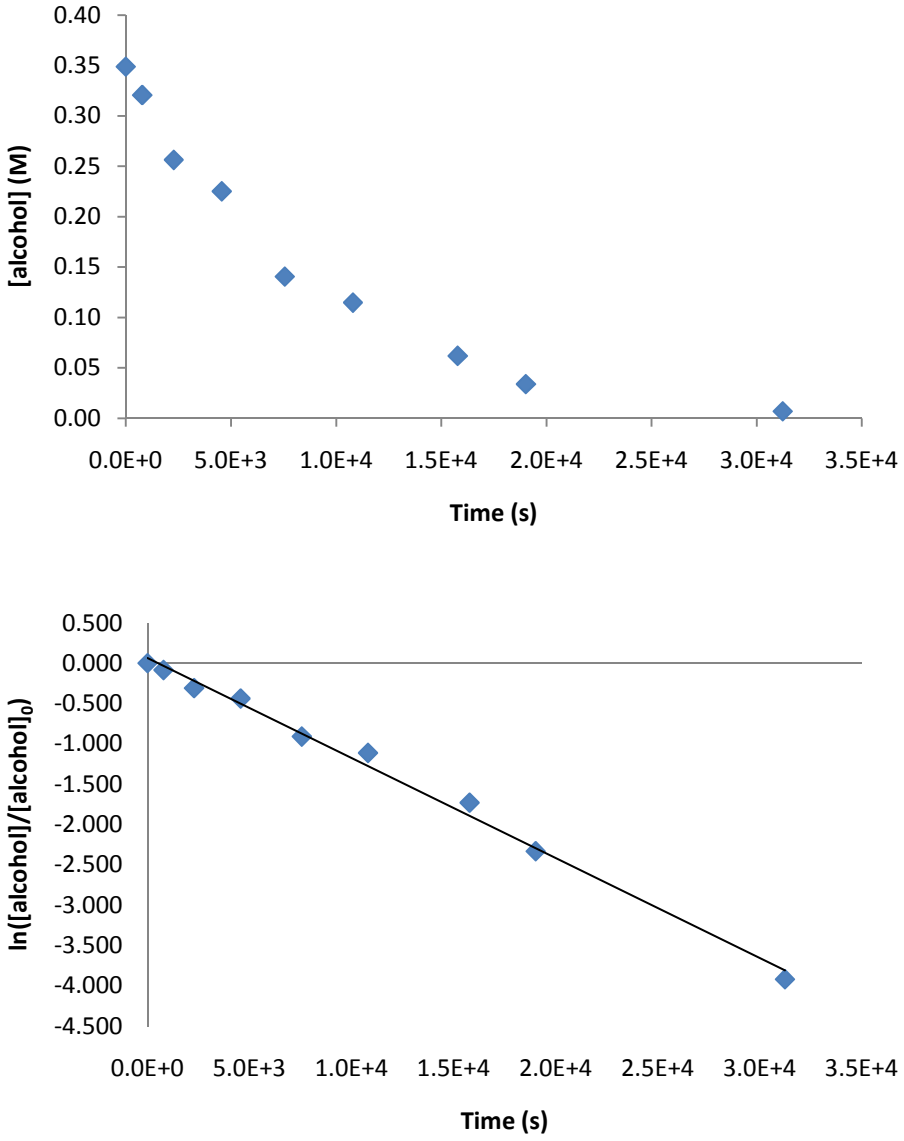

Figure 2.41. Concentration versus time plot for the gold(I)-catalyzed intermolecular hydroalkoxylation of 1-phenylpropanol with 3-methyl-1,2-butadiene in toluene at room temperature. [2] = 2.6 M, [1] = 0.35 M, [(IPr)AuCl/AgOTf] = 5 mM k_{obs} = 1.2 ± 0.1 x 10^{-4} s^{-1} (Table 2.1, entry 19)

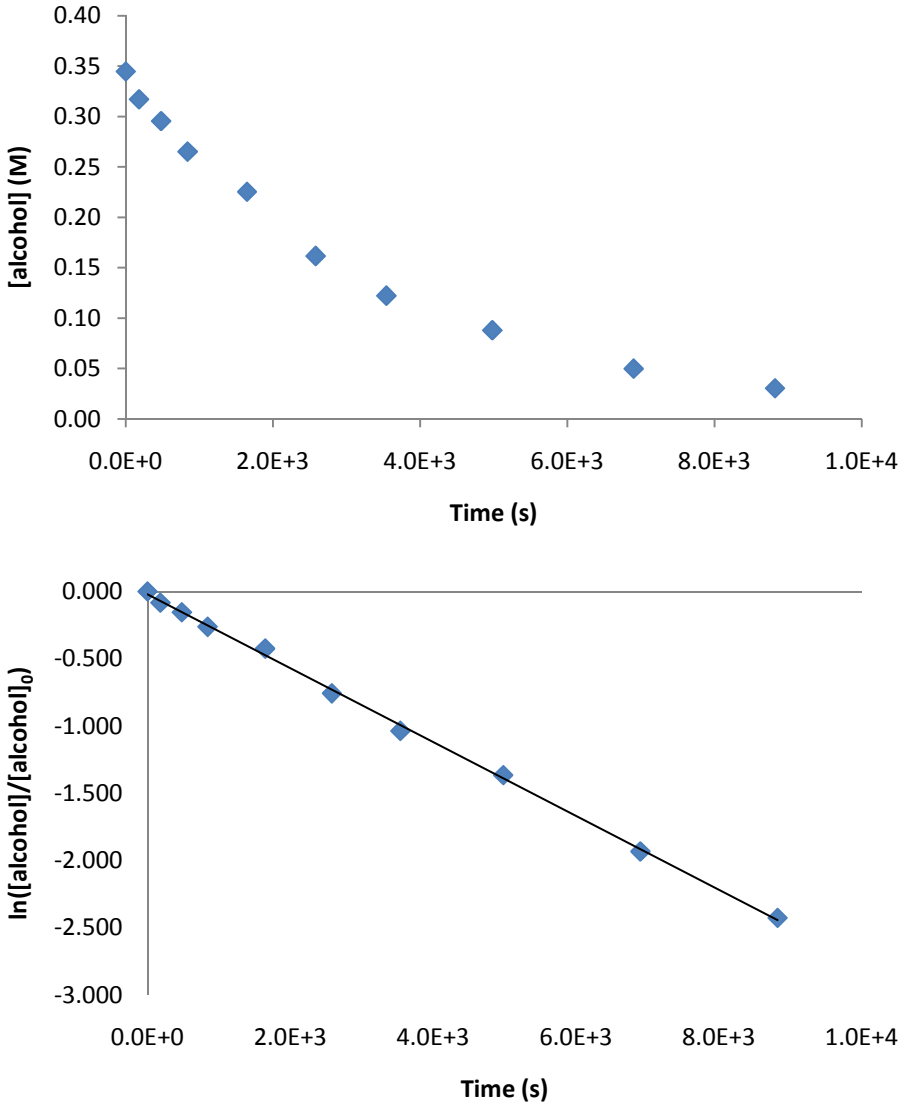

Figure 2.42. Concentration versus time (top) and pseudo first-order (bottom) plots for the gold(I)-catalyzed intermolecular hydroalkoxylation of 1-phenylpropanol with 3-methyl-1,2-butadiene in toluene at room temperature. [2] = 2.5 M, [1] = 0.34 M, [(IPr)AuCl/AgOTf] = 15 mM k_{obs} = 2.8 ± 0.0 x 10^{-4} s^{-1} (Table 2.1, entry 20 and Table 2.2, entry 1)

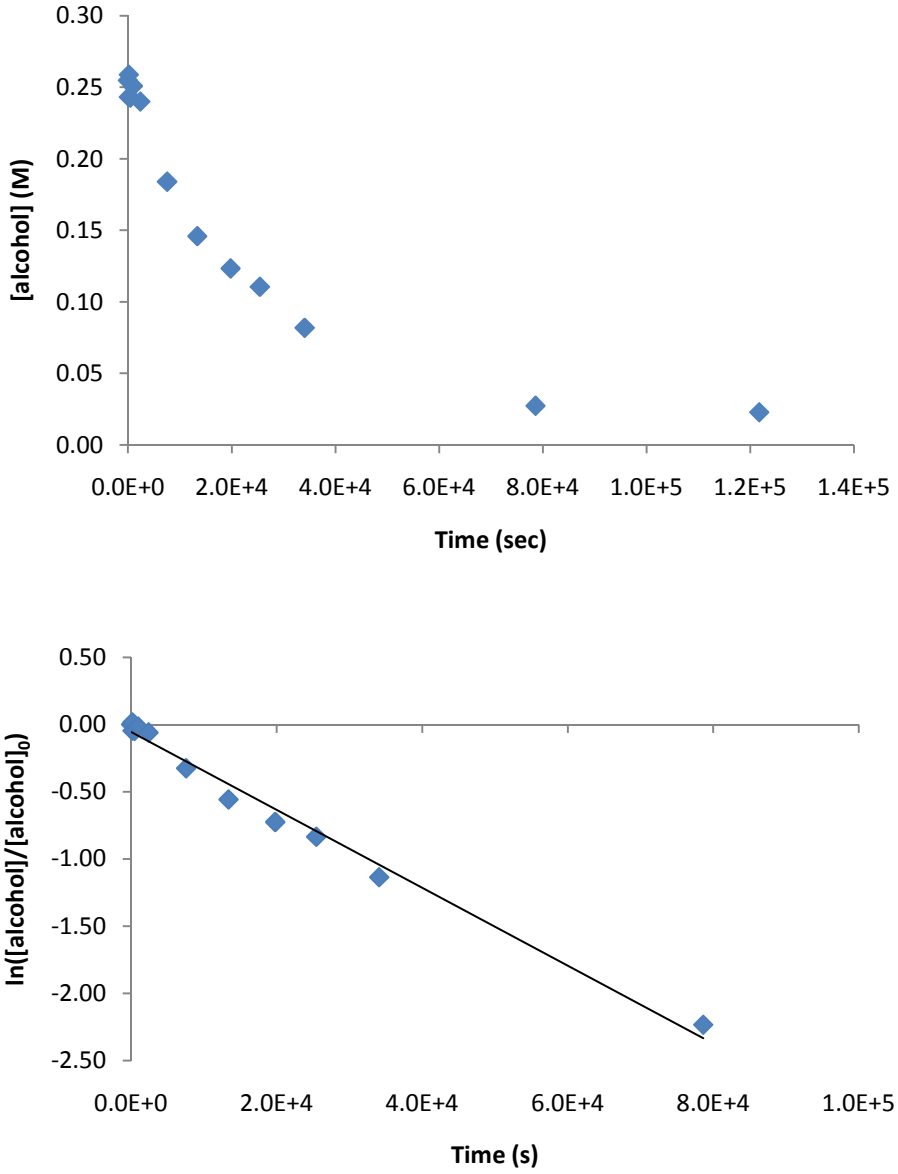

Figure 2.43. Concentration versus time (top) and pseudo first-order (bottom) plots for the gold(I)-catalyzed intermolecular hydroalkoxylation of 1-phenylpropanol with 3-methyl-1,2-butadiene in toluene at room temperature. [2] = 2.0 M, [1] = 0.25 M, [(IPr)AuCl/AgOTf] = 11 mM k_{obs} = 0.22 ± 0.03 x 10^{-4} s^{-1} (Table 2.2, entry 2)

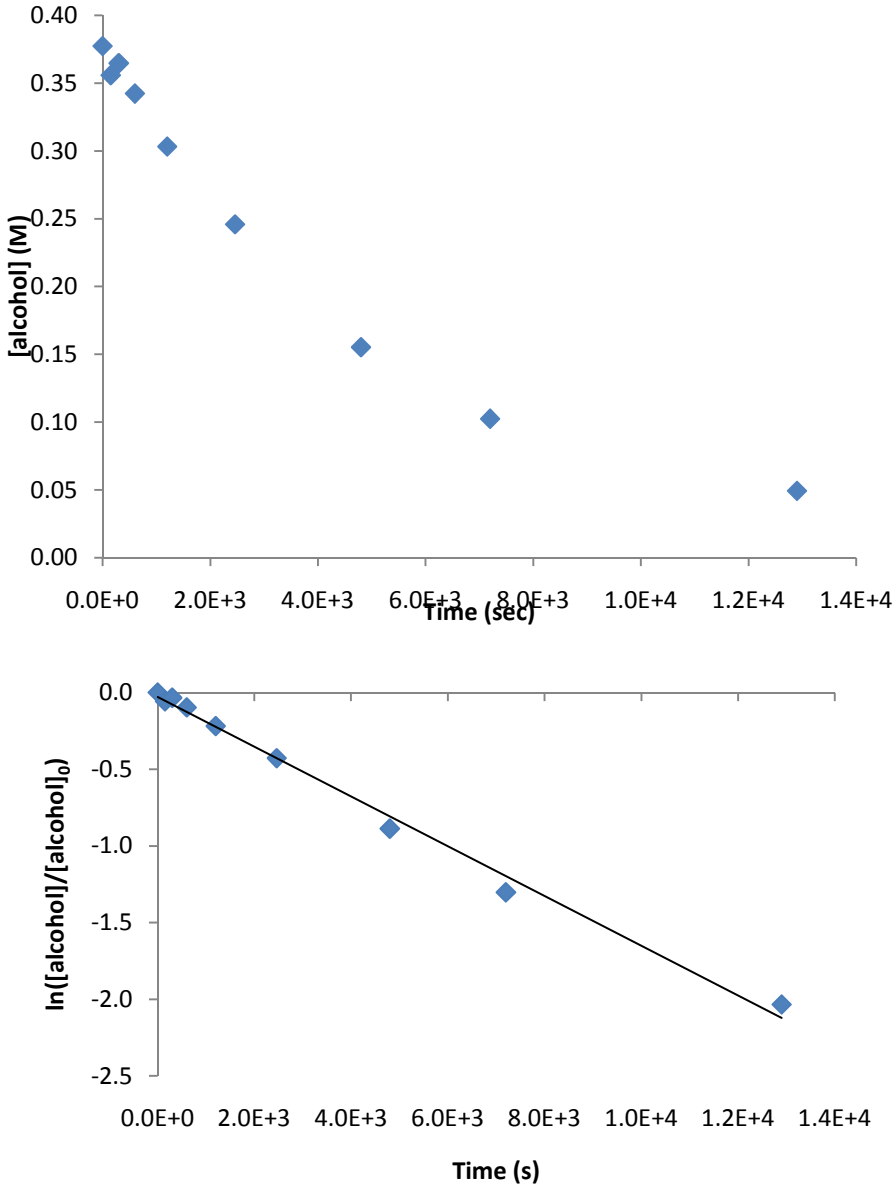

Figure 2.44. Concentration versus time (top) and pseudo first-order (bottom) plots for the reaction of 1-d_1 (0.37 M) with 2 (1.4 M) catalyzed by (IPr)AuCl and AgOTf (15 mM) in toluene at 24 ° C k_{obs} = 1.6 ± 0.1 x 10^{-4} s^{-1} (Table 2.3, entry 2).

2.7.4 General Procedure for Kinetic Study of Au(I)-catalyzed Intermolecular Hydroamination of Allenes with Carbamates

Benzyl (1,1-dimethylallyl)carbamate. A suspension of 3-methyl-1,2-butadiene (24.5 mg, 0.36 mmol), benzyl carbamate (54.5 mg, 0.36 mmol), (**2**)(IPr)AuCl (10.0 mg, 0.016 mmol), AgOTf (4.1 mg, 0.016 mmol), and *n*-tetradecane (8.0 mg, 0.040 mmol) in dioxane (0.5 mL) was stirred at room temperature for 24 h. The disappearance of benzyl carbamate was monitored by analyzing 10 μL aliquots purified through a cotton plug pipet filled with silica gel with DCM via gas chromatography compared to the internal standard, *n*-tetradecane. The disappearance of benzyl carbamate (3.9 min) was monitored by analyzing 10 μL aliquots purified through a cotton plug pipet filled with silica gel with EtOAc via gas chromatography compared to the internal standard *n*-tetradecane (4.1 min). The concentration of **4** was determined from the integration of the GC peak of **1** relative to that of n-tetradecane, internal standard.

- Pseudo first-order rate constants were determined for the gold(I)-catalyzed hydroamination of allenes with carbamates as a function of [carbamate] at [carbamate] = 0.10 to 0.42 M in Figure 2.45 to Figure 2.47.
- Pseudo first-order rate constants were determined for the gold(I)-catalyzed hydroamination of allenes with carbamate as a function of [catalyst] at [catalyst] = 15 to 47 mM in Figure 2.60 to Figure 2.64

- Pseudo first-order rate constants were determined for the gold(I)-catalyzed hydroamination of allenes with carbamate as a function of [allene] at [allene] = 0.32 to 3.8 M in Figure 2.48 to Figure 2.59.

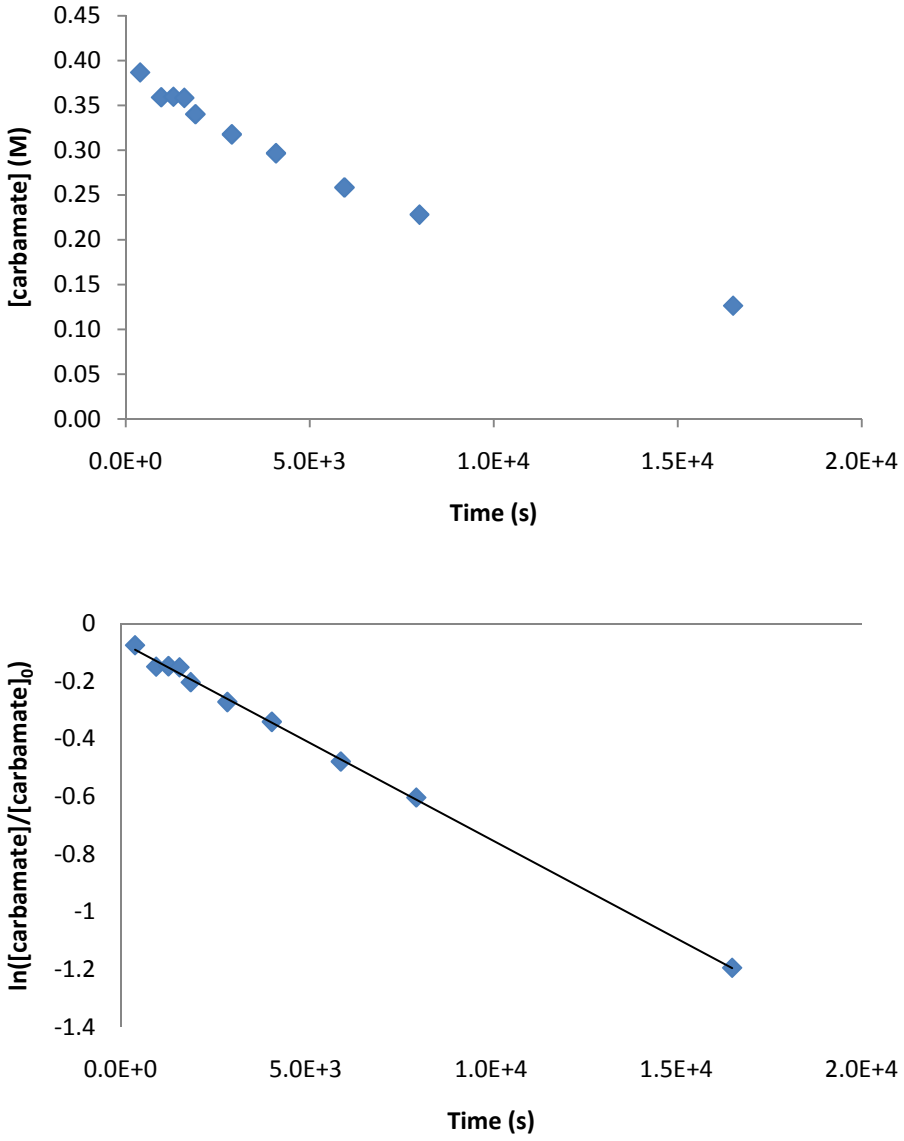

Figure 2.45. Concentration versus time plot for the gold(I)-catalyzed intermolecular hydroamination of benzyl carbamate with 3-methyl-1,2-butadiene in dioxane at room temperature. [2] = 4.2 M, [4] = 0.42 M, [(IPr)AuCl/AgOTf] = 19 mM k_{obs} = 6.85 ± 0.01 x 10^{-5} s^{-1} (Table 2.4, entry 1)

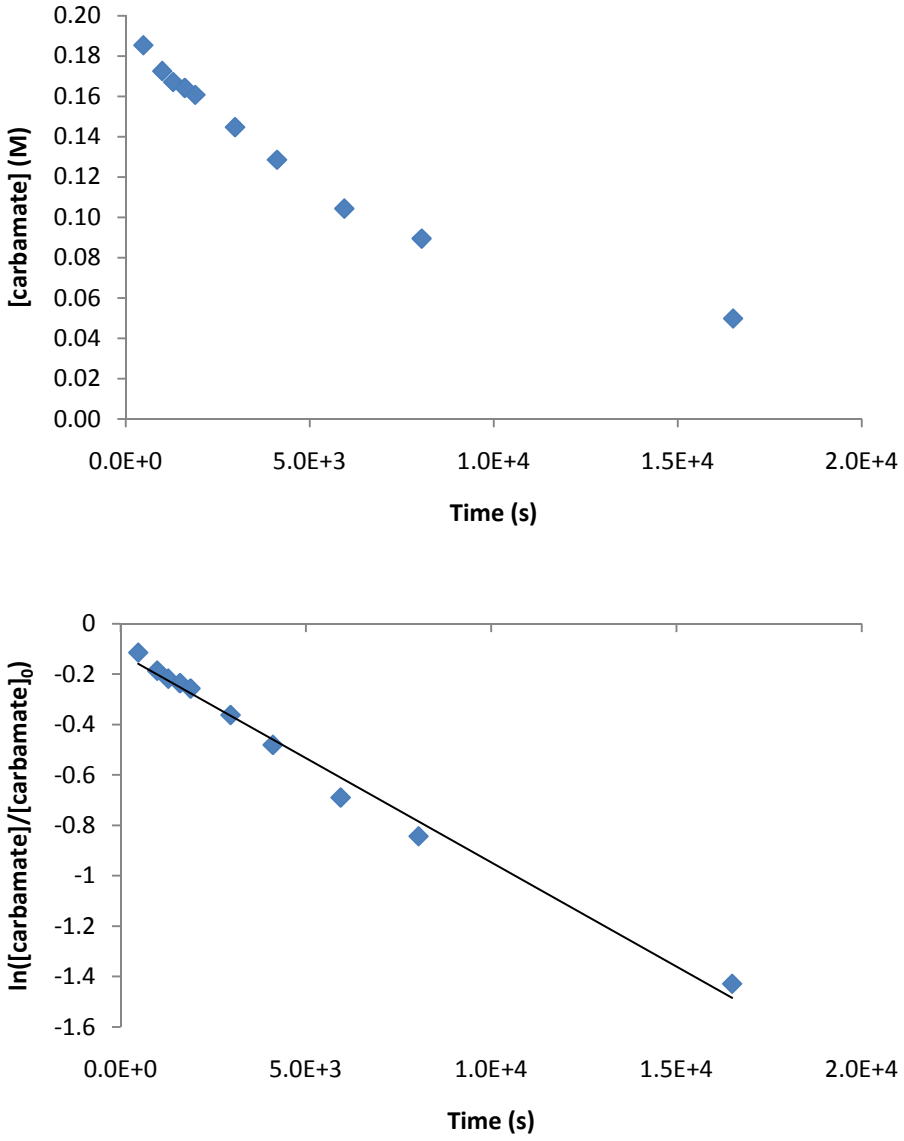

Figure 2.46. Concentration versus time plot for the gold(I)-catalyzed intermolecular hydroamination of benzyl carbamate with 3-methyl-1,2-butadiene in dioxane at room temperature. [2] = 4.2 M, [4] = 0.21 M, [(IPr)AuCl/AgOTf] = 19 mM k_{obs} = 8.27 ± 0.05 x 10^{-5} s^{-1} (Table 2.4, entry 2)

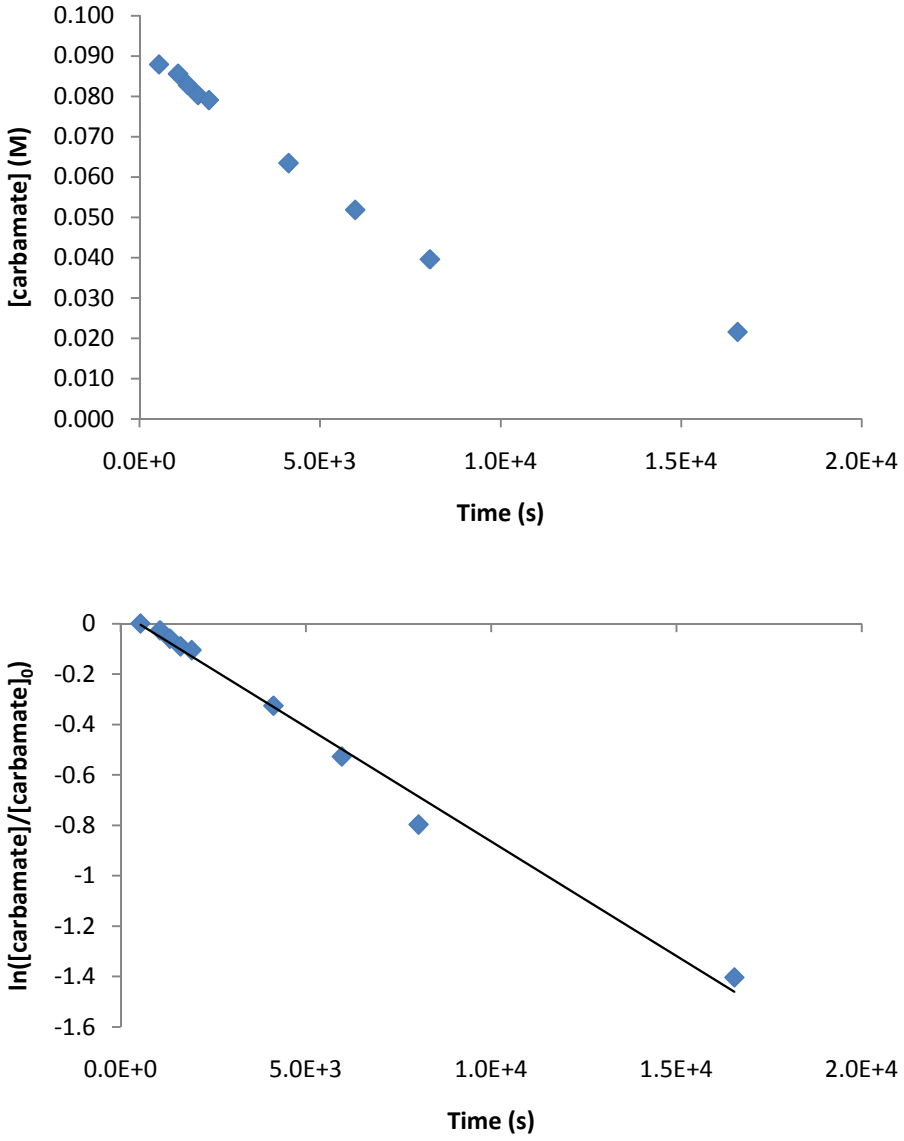

Figure 2.47. Concentration versus time plot for the gold(I)-catalyzed intermolecular hydroamination of benzyl carbamate with 3-methyl-1,2-butadiene in dioxane at room temperature. [2] = 4.2 M, [4] = 0.10 M, [(IPr)AuCl/AgOTf] = 19 mM k_{obs} = 9.10 ± 0.05 x 10^{-5} s^{-1} (Table 2.4, entry 3)

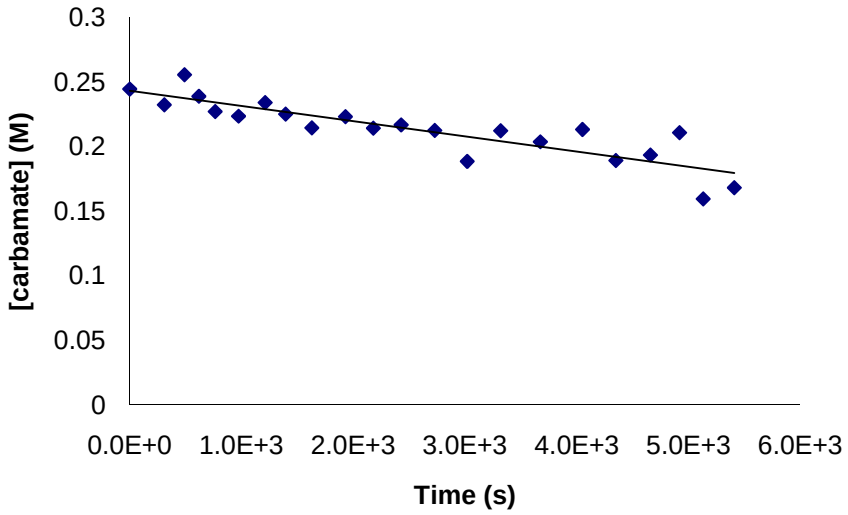

Figure 2.48. Concentration versus time plot for the gold(I)-catalyzed intermolecular hydroamination of benzyl carbamate with 3-methyl-1,2-butadiene in dioxane at room temperature. [2] = 0.88 M, [4] = 0.24 M, [(IPr)AuCl/AgOTf] = 20 mM k_{obs} = 5.7 ± 0.1 x 10^{-5} Ms^{-1} (Table 2.4, entry 4)

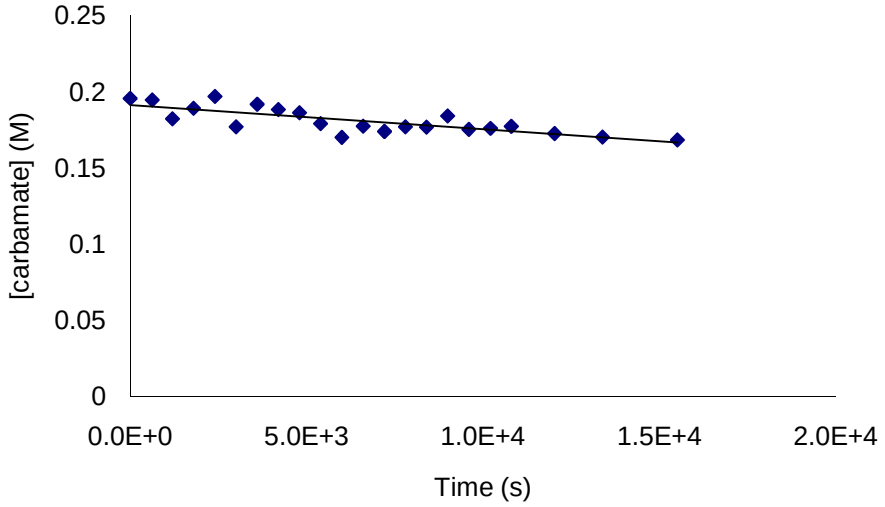

Figure 2.49. Concentration versus time plot for the gold(I)-catalyzed intermolecular hydroamination of benzyl carbamate with 3-methyl-1,2-butadiene in dioxane at room temperature. [2] = 0.32 M, [4] = 0.20 M, [(IPr)AuCl/AgOTf] = 19 mM k_{obs} = 0.87 ± 0.02 x 10^{-5} Ms^{-1} (Table 2.4, entry 5)

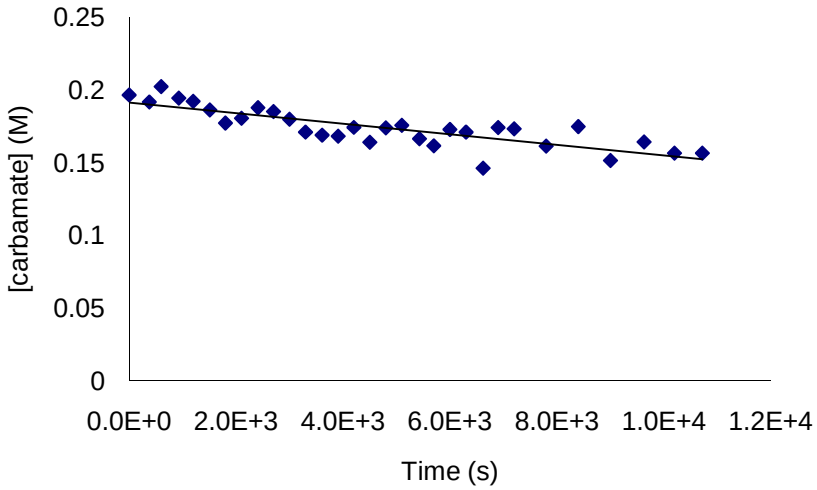

Figure 2.50. Concentration versus time plot for the gold(I)-catalyzed intermolecular hydroamination of benzyl carbamate with 3-methyl-1,2-butadiene in dioxane at room temperature. [2] = 0.52 M, [4] = 0.20 M, [(IPr)AuCl/AgOTf] = 19 mM k_{obs} = 2.08 ± 0.05 x 10^{-5} Ms^{-1} (Table 2.4, entry 6)

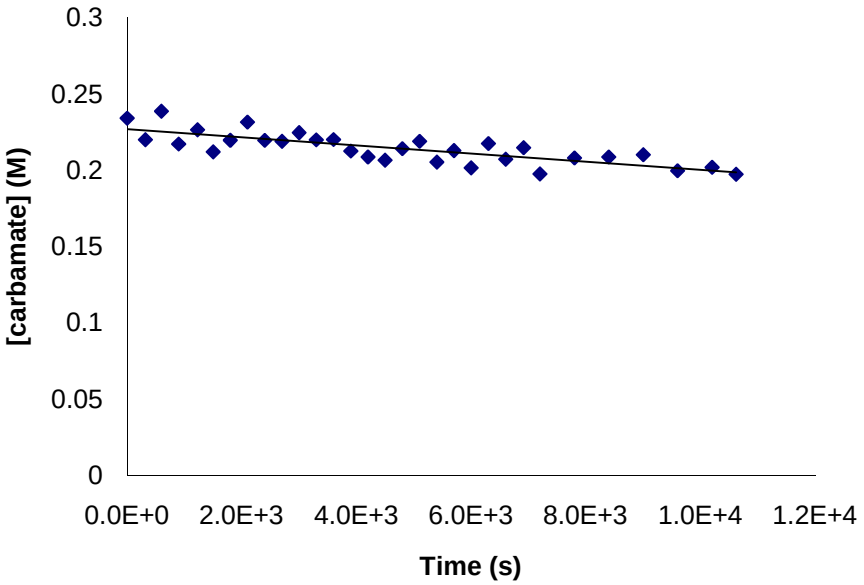

Figure 2.51. Concentration versus time plot for the gold(I)-catalyzed intermolecular hydroamination of 3-methyl-1,2-butadiene with benzyl carbamate in dioxane at room temperature. [2] = 0.65 M, [4] = 0.23 M, [(IPr)AuCl/AgOTf] = 19 mM k_{obs} = 1.25 ± 0.05 x 10^{-5} Ms^{-1} (Table 2.4, entry 7)

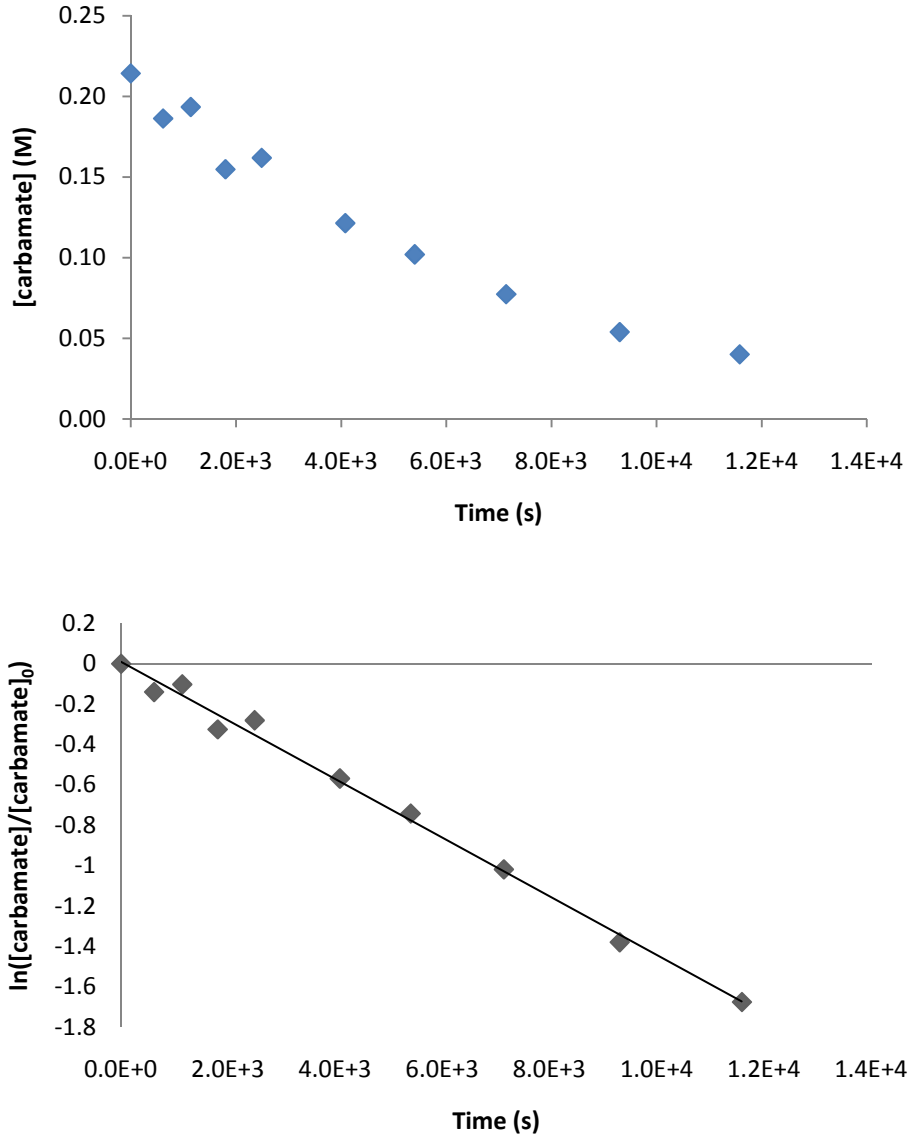

Figure 2.52. Concentration versus time plot for the gold(I)-catalyzed intermolecular hydroamination of benzyl carbamate with 3-methyl-1,2-butadiene in dioxane at room temperature. [2] = 3.8 M, [4] = 0.21 M, [(IPr)AuCl/AgOTf] = 19 mM k_{obs} = 14.5 ± 0.5 x 10^{-5} s^{-1} (Table 2.4, entry 8)

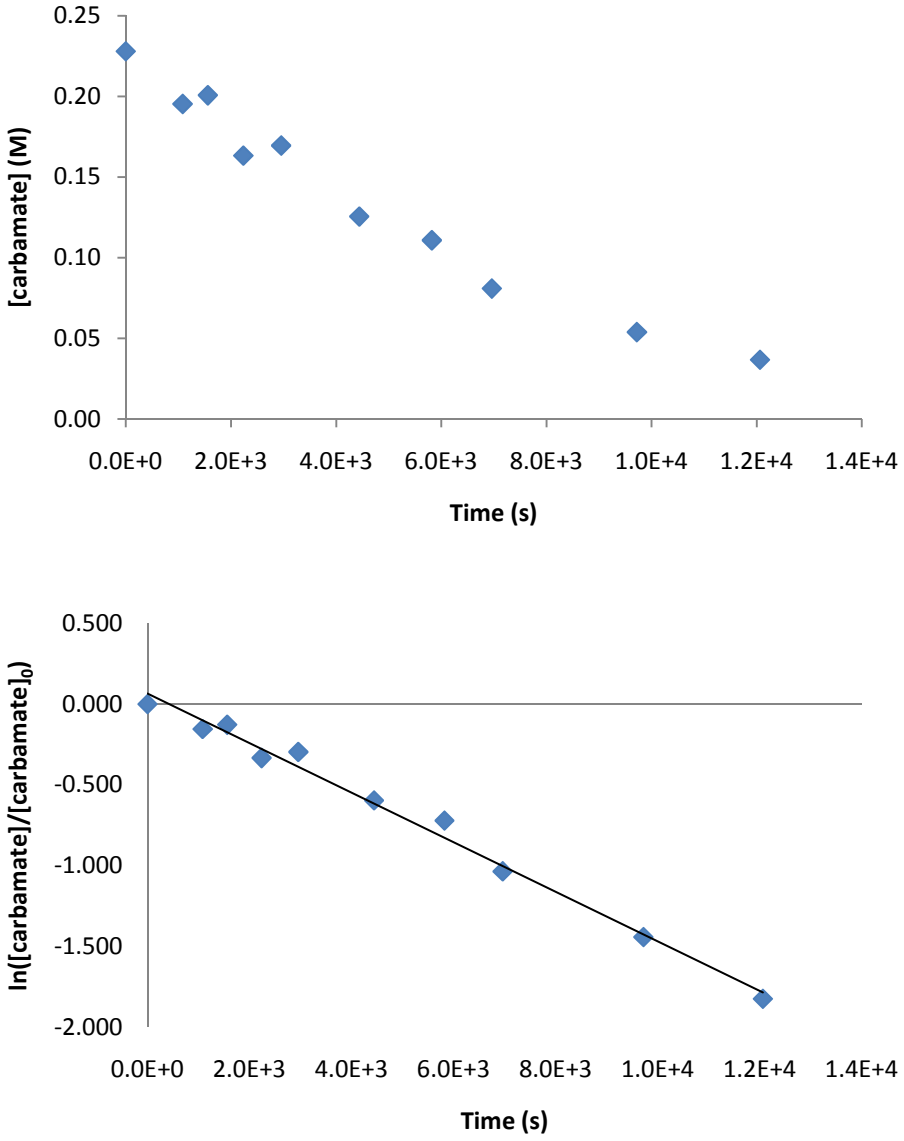

Figure 2.53. Concentration versus time plot for the gold(I)-catalyzed intermolecular hydroamination of benzyl carbamate with 3-methyl-1,2-butadiene in dioxane at room temperature. [2] = 3.4 M, [4] = 0.23 M, [(IPr)AuCl/AgOTf] = 20 mM k_{obs} = 15.3 ± 0.7 x 10^{-5} s^{-1} (Table 2.4, entry 9)

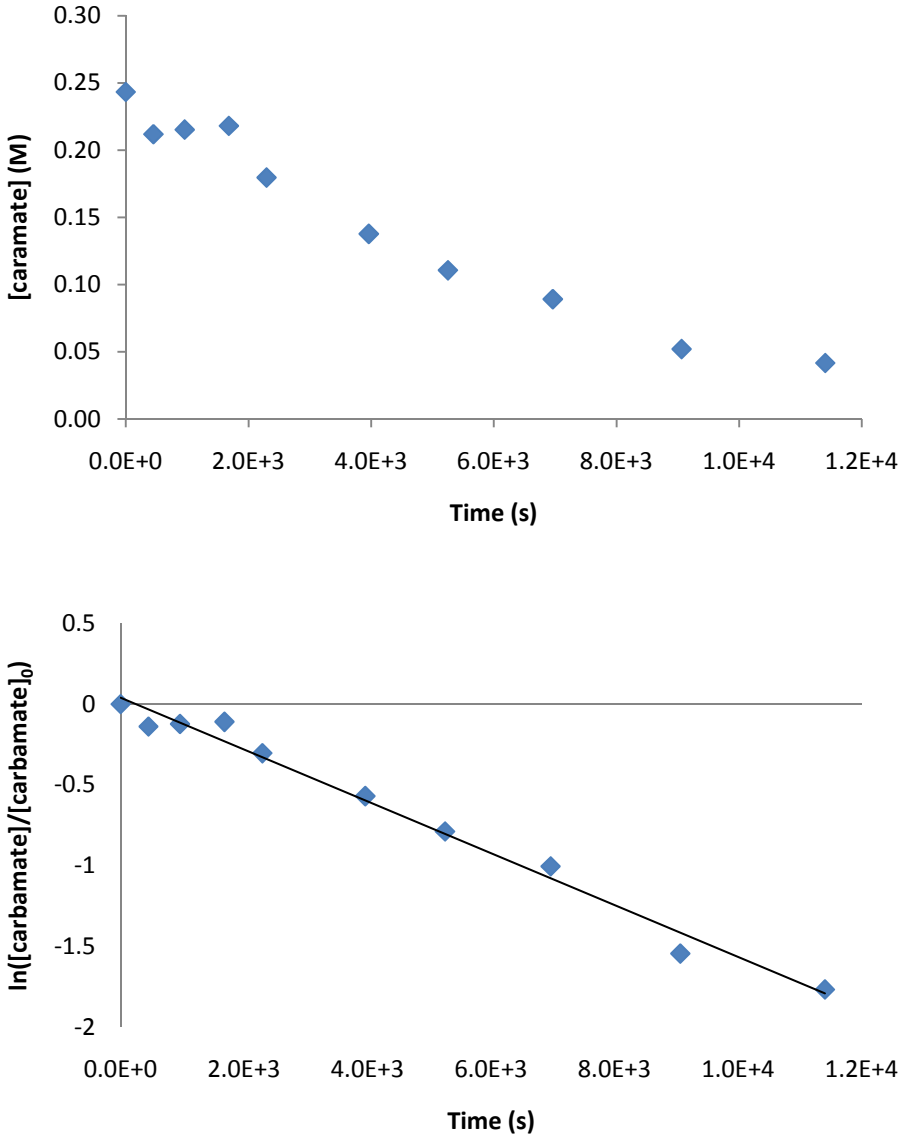

Figure 2.54. Concentration versus time plot for the gold(I)-catalyzed intermolecular hydroamination of benzyl carbamate with 3-methyl-1,2-butadiene in dioxane at room temperature. [2] = 3.0 M, [4] = 0.24 M, [(IPr)AuCl/AgOTf] = 22 mM k_{obs} = 16.1 ± 0.8 x 10^{-5} s^{-1} (Table 2.4, entry 10)

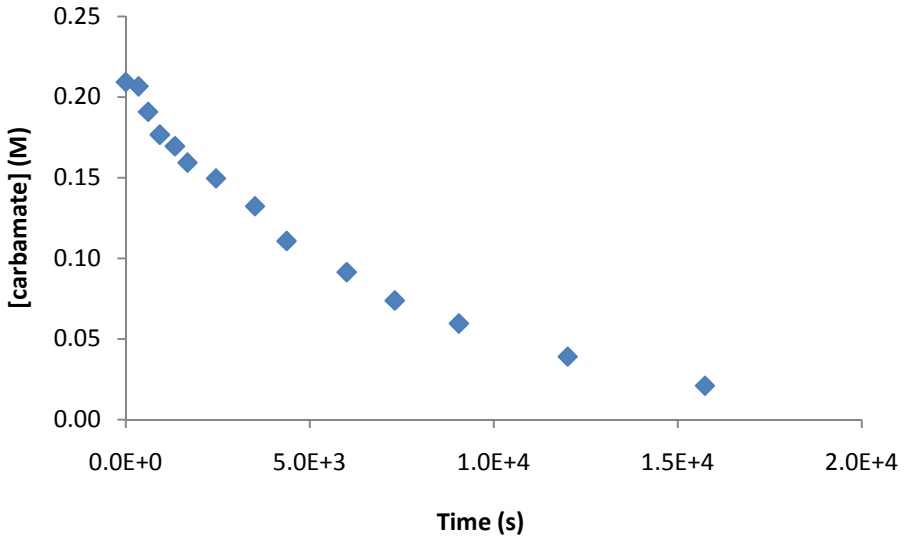

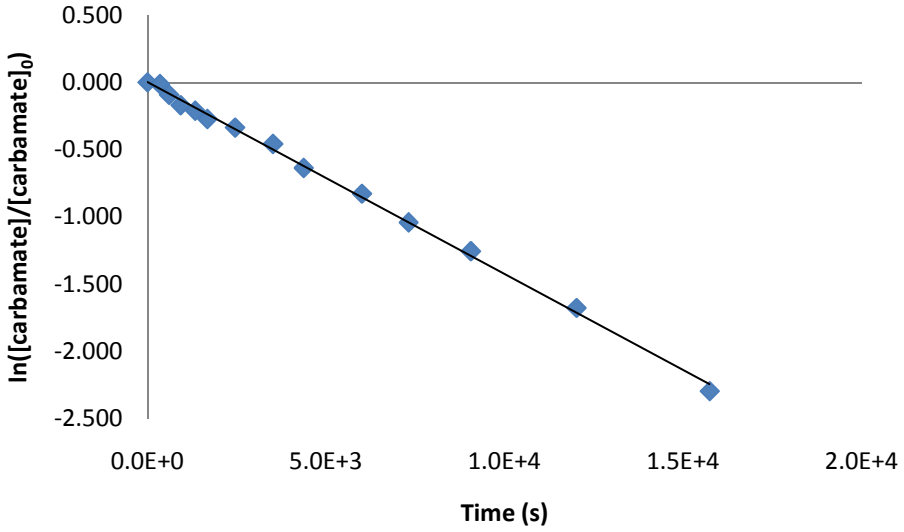

Figure 2.55. Concentration versus time plot for the gold(I)-catalyzed intermolecular hydroamination of benzyl carbamate with 3-methyl-1,2-butadiene in dioxane at room temperature. [2] = 2.5 M, [4] = 0.21 M, [(IPr)AuCl/AgOTf] = 19 mM k_{obs} = 14.2 ± 0.3 x 10^{-5} s^{-1} (Table 2.4, entry 11)

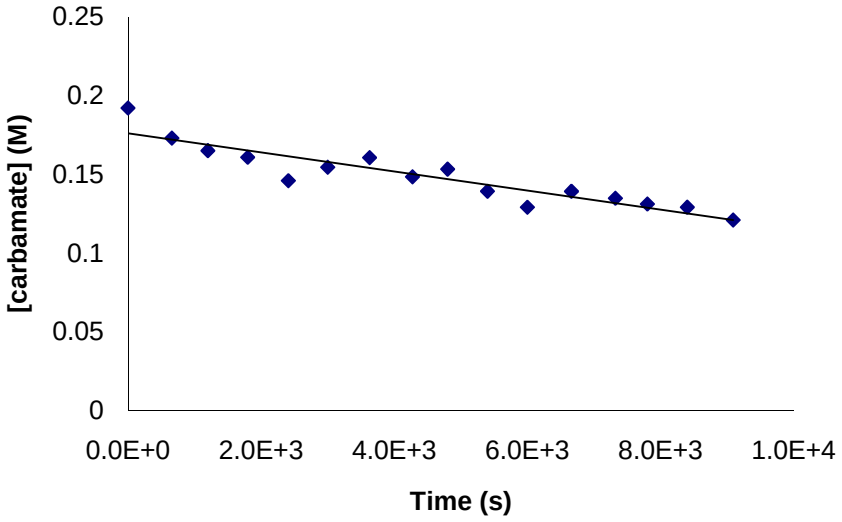

Figure 2.56. Concentration versus time plot for the gold(I)-catalyzed intermolecular hydroamination of benzyl carbamate with 3-methyl-1,2-butadiene in dioxane at room temperature. [2] = 1.2 M, [4] = 0.19 M, [(IPr)AuCl/AgOTf] = 18 mM k_{obs} = 4.76 ± 0.05 x 10^{-5} Ms^{-1} (Table 2.4, entry 12)

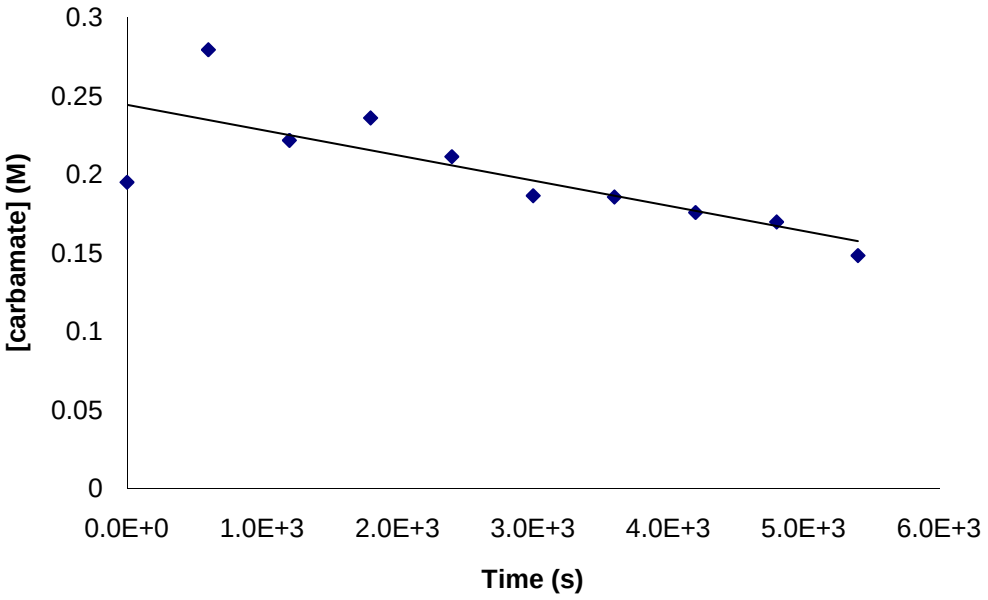

Figure 2.57. Concentration versus time plot for the gold(I)-catalyzed intermolecular hydroamination of benzyl carbamate with 3-methyl-1,2-butadiene in dioxane at room temperature. [2] = 1.4 M, [4] = 0.19 M, [(IPr)AuCl/AgOTf] = 18 mM k_{obs} = 8.0 ± 0.1 x 10^{-5} Ms^{-1} (Table 2.4, entry 13)

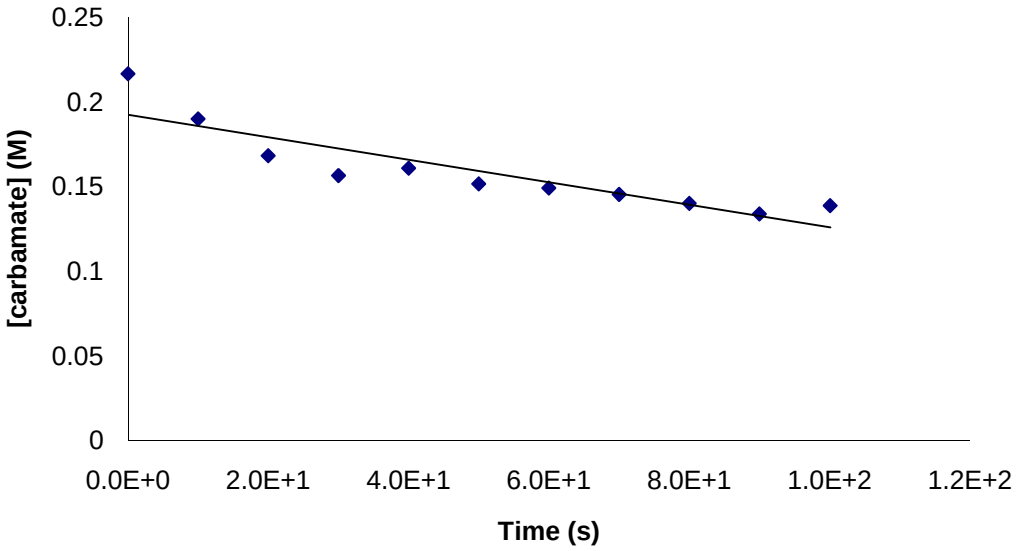

Figure 2.58. Concentration versus time plot for the gold(I)-catalyzed intermolecular hydroamination of benzyl carbamate with 3-methyl-1,2-butadiene in dioxane at room temperature. [2] = 1.4 M, [4] = 0.19 M, [(IPr)AuCl/AgOTf] = 21 mM k_{obs} = 6.7 ± 0.1 x 10^{-5} Ms^{-1} (Table 2.4, entry 14)

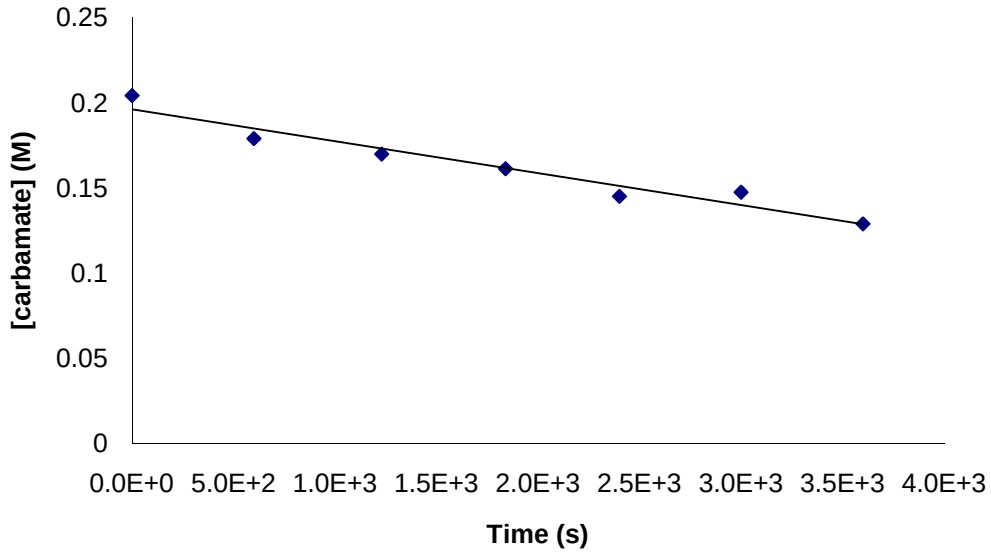

Figure 2.59. Concentration versus time plot for the gold(I)-catalyzed intermolecular hydroamination of benzyl carbamate with 3-methyl-1,2-butadiene in dioxane at room temperature. [2] = 1.9 M, [4] = 0.20 M, [(IPr)AuCl/AgOTf] = 21 mM k_{obs} = 11.2 ± 0.1 x 10^{-5} Ms^{-1} (Table 2.4, entry 15)

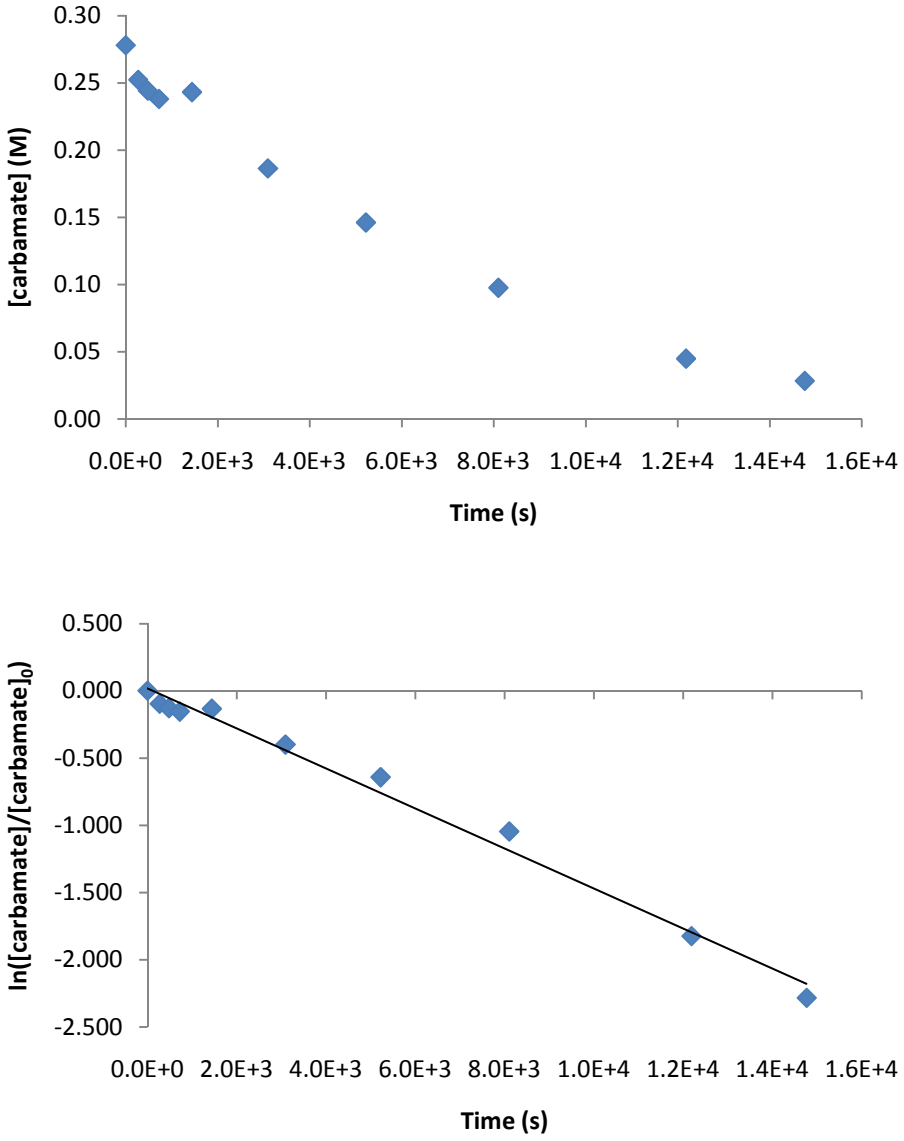

Figure 2.60. Concentration versus time plot for the gold(I)-catalyzed intermolecular hydroamination of benzyl carbamate with 3-methyl-1,2-butadiene in dioxane at room temperature. [2] = 2.7 M, [4] = 0.28 M, [(IPr)AuCl/AgOTf] = 15 mM k_{obs} = 14.9 ± 0.1 x 10^{-5} s^{-1} (Table 2.4, entry 16)

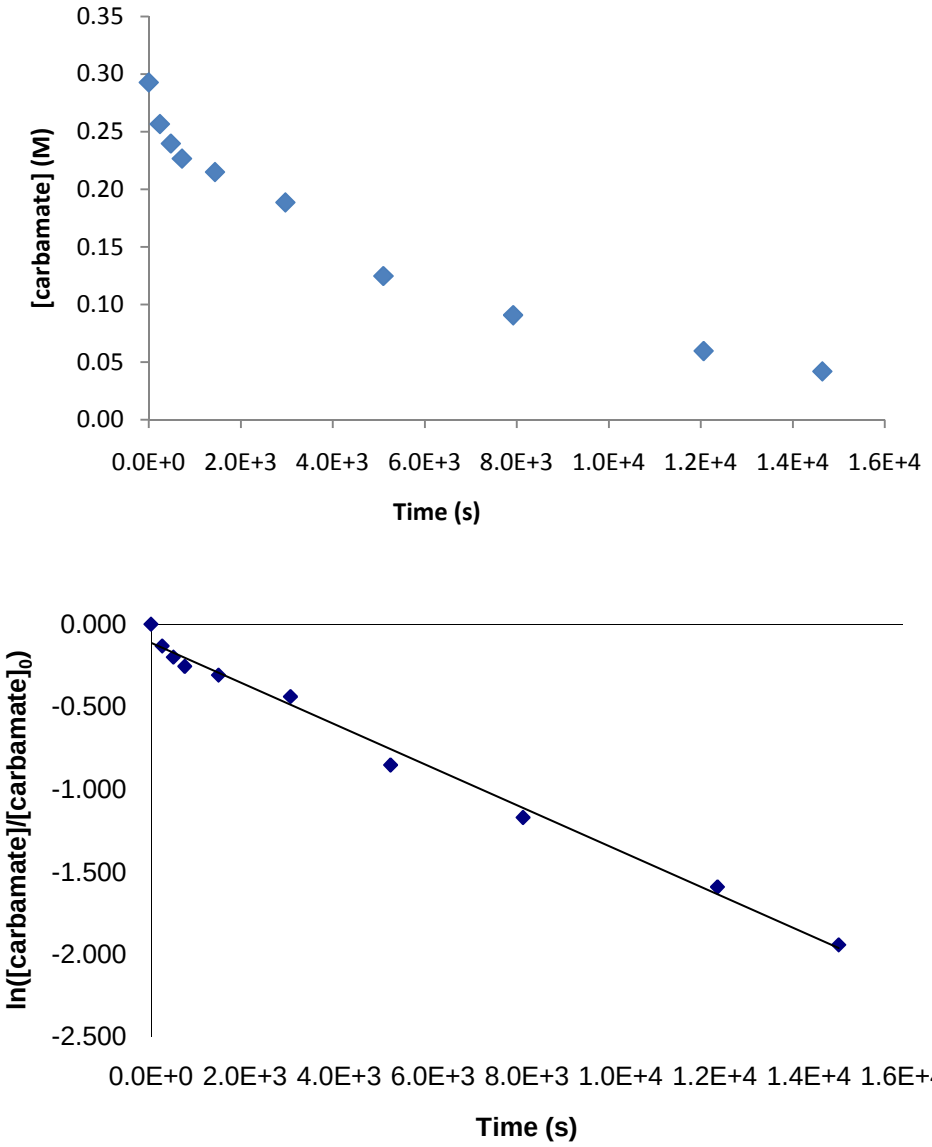

Figure 2.61. Concentration versus time plot for the gold(I)-catalyzed intermolecular hydroamination of benzyl carbamate with 3-methyl-1,2-butadiene in dioxane at room temperature. [2] = 2.8 M, [4] = 0.29 M, [(IPr)AuCl/AgOTf] = 15 mM k_{obs} = 12.7 ± 0.1 x 10^{-5} s^{-1} (Table 2.4, entry 17)

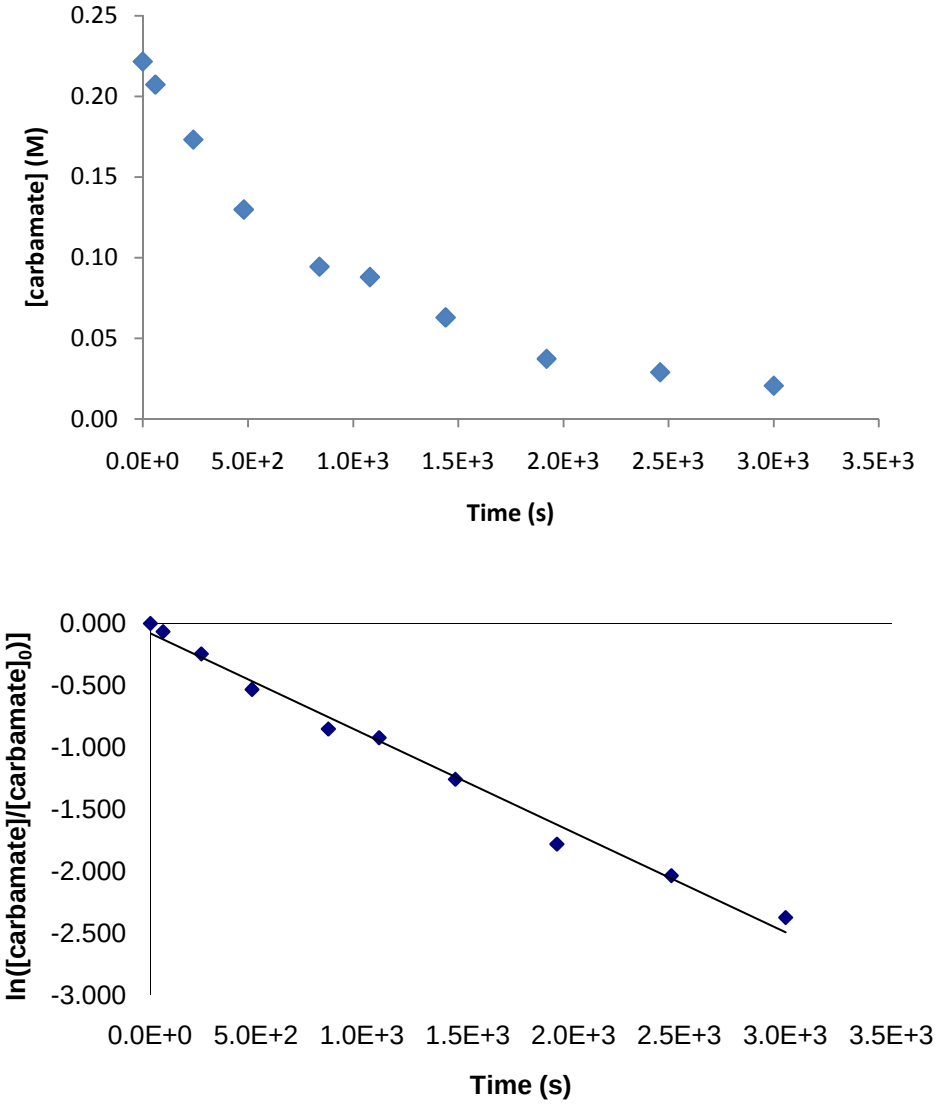

Figure 2.62. Concentration versus time plot for the gold(I)-catalyzed intermolecular hydroamination of benzyl carbamate with 3-methyl-1,2-butadiene in dioxane at room temperature. [2] = 2.2 M, [4] = 0.22 M, [(IPr)AuCl/AgOTf] = 47 mM k_{obs} = 80.5 ± 0.9 x 10^{-5} s^{-1} (Table 2.4, entry 18)

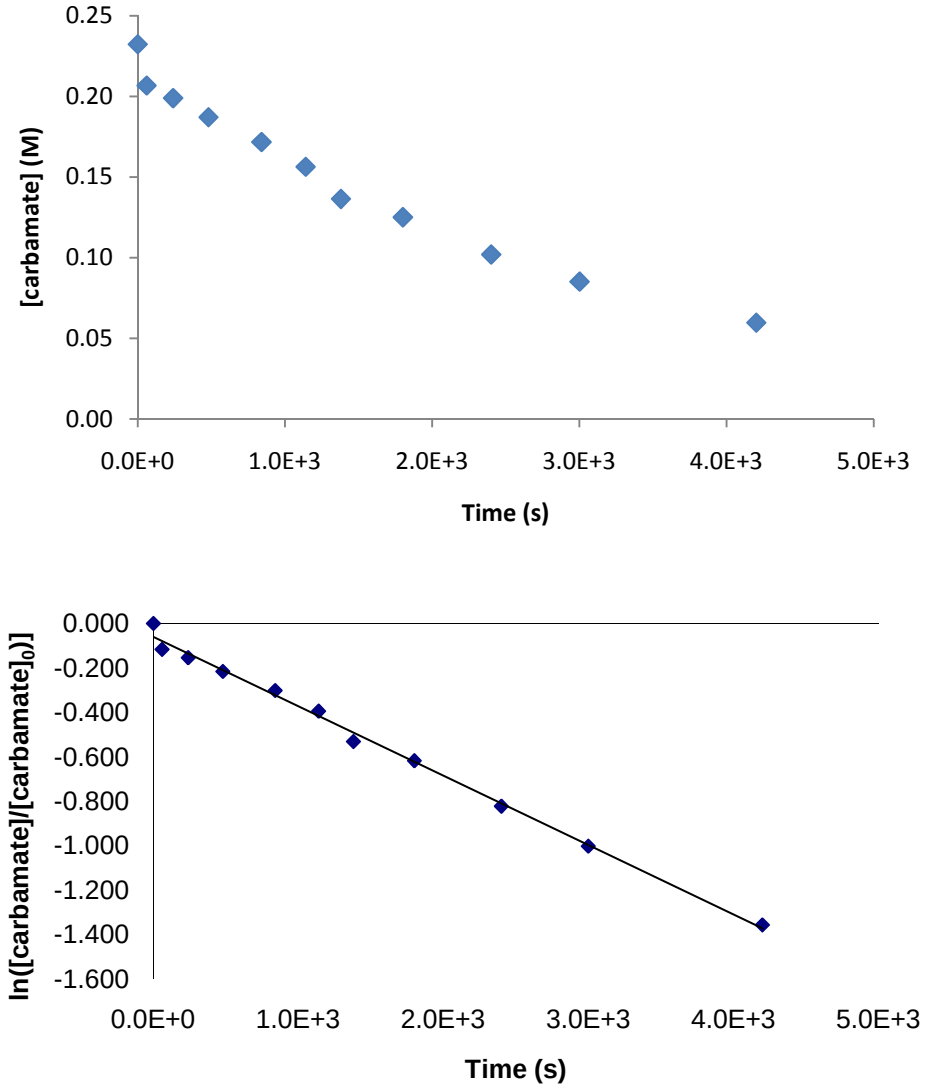

Figure 2.63. Concentration versus time plot for the gold(I)-catalyzed intermolecular hydroamination of benzyl carbamate with 3-methyl-1,2-butadiene in dioxane at room temperature. [2] = 2.2 M, [4] = 0.23 M, [(IPr)AuCl/AgOTf] = 22 mM k_{obs} = 31.3 ± 0.3 x 10^{-5} s^{-1} (Table 2.4, entry 19)

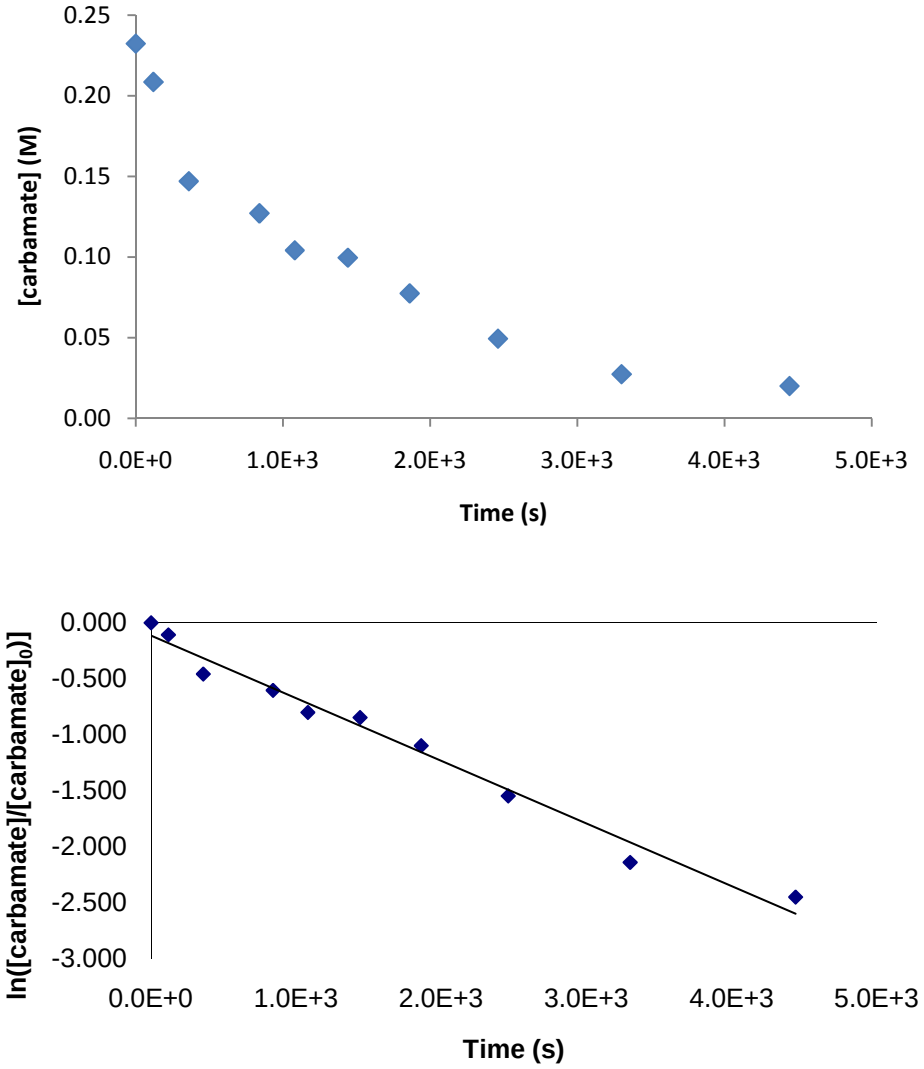

Figure 2.64. Concentration versus time plot for the gold(I)-catalyzed intermolecular hydroamination of benzyl carbamate with 3-methyl-1,2-butadiene in dioxane at room temperature. [2] = 2.3 M, [4] = 0.23 M, [(IPr)AuCl/AgOTf] = 37 mM k_{obs} = 56.0 ± 1.2 x 10^{-5} s^{-1} (Table 2.4, entry 20)

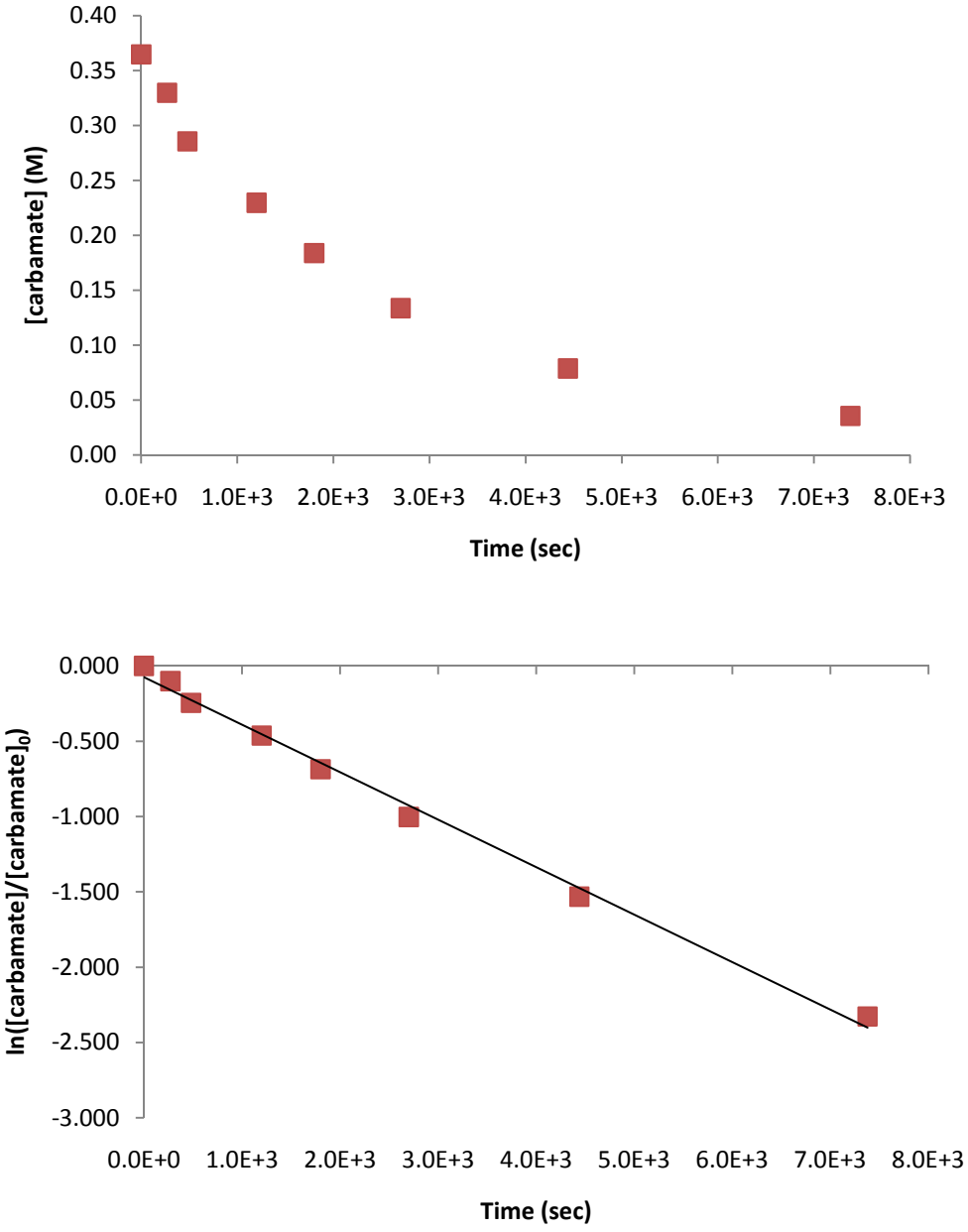

Figure 2.65. Concentration versus time (top) and pseudo first-order (bottom) plots for the reaction of 4 (0.36 M) and 2 (2.5 M) catalyzed by (IPr)AuCl/AgOTf (15 mM) in the presence of 0.25 M Bu_4NOTf (k_{obs} = 3.2 ± 0.6 x 10^{-4} s^{-1}) (Table 2.5, entry 2).

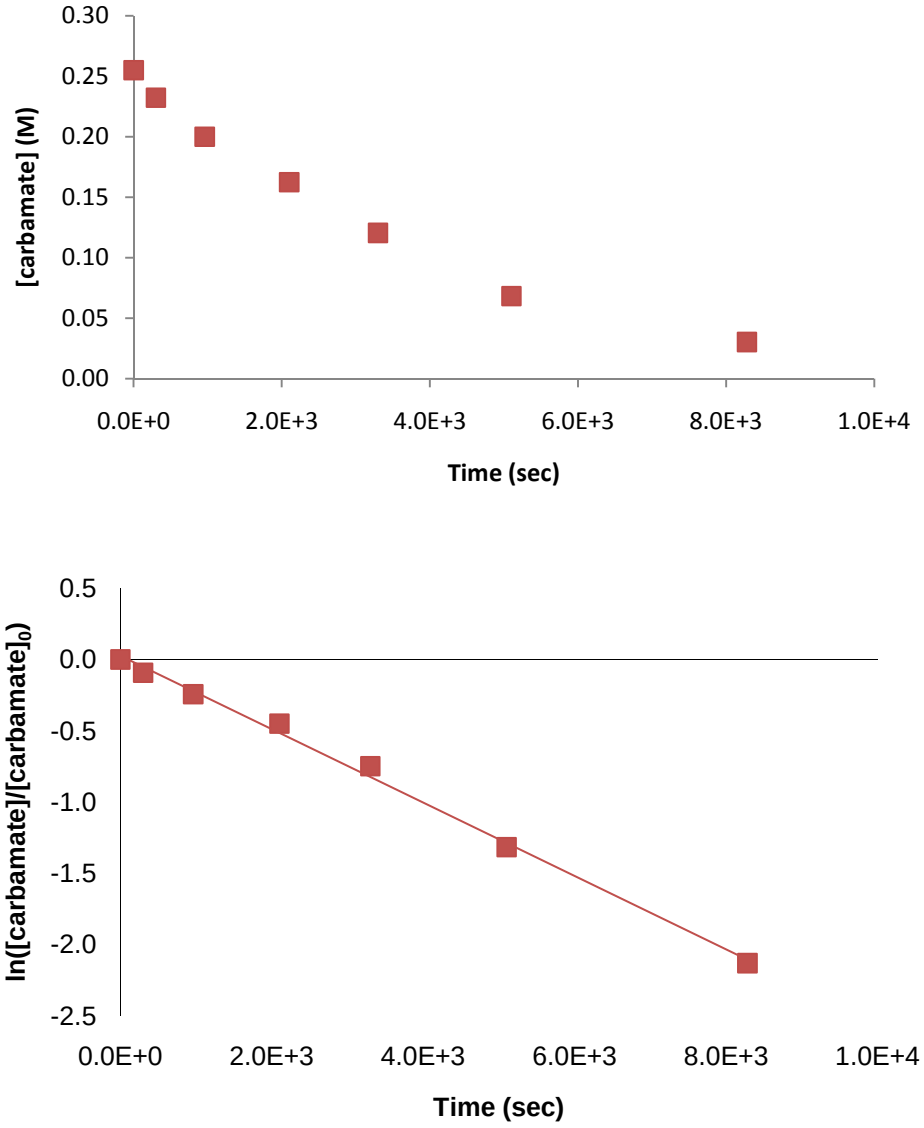

Figure 2.66. Concentration versus time (top) and pseudo first-order (bottom) plots for the reaction of 4 (0.25 M) with allene (2.5 M) catalyzed by (IPr)AuCl and AgOTf (25 mM) in dioxane at 24 °C k_{obs} = 2.6 ± 0.1 x 10^{-4} s^{-} (Table 2.6, entry 1).

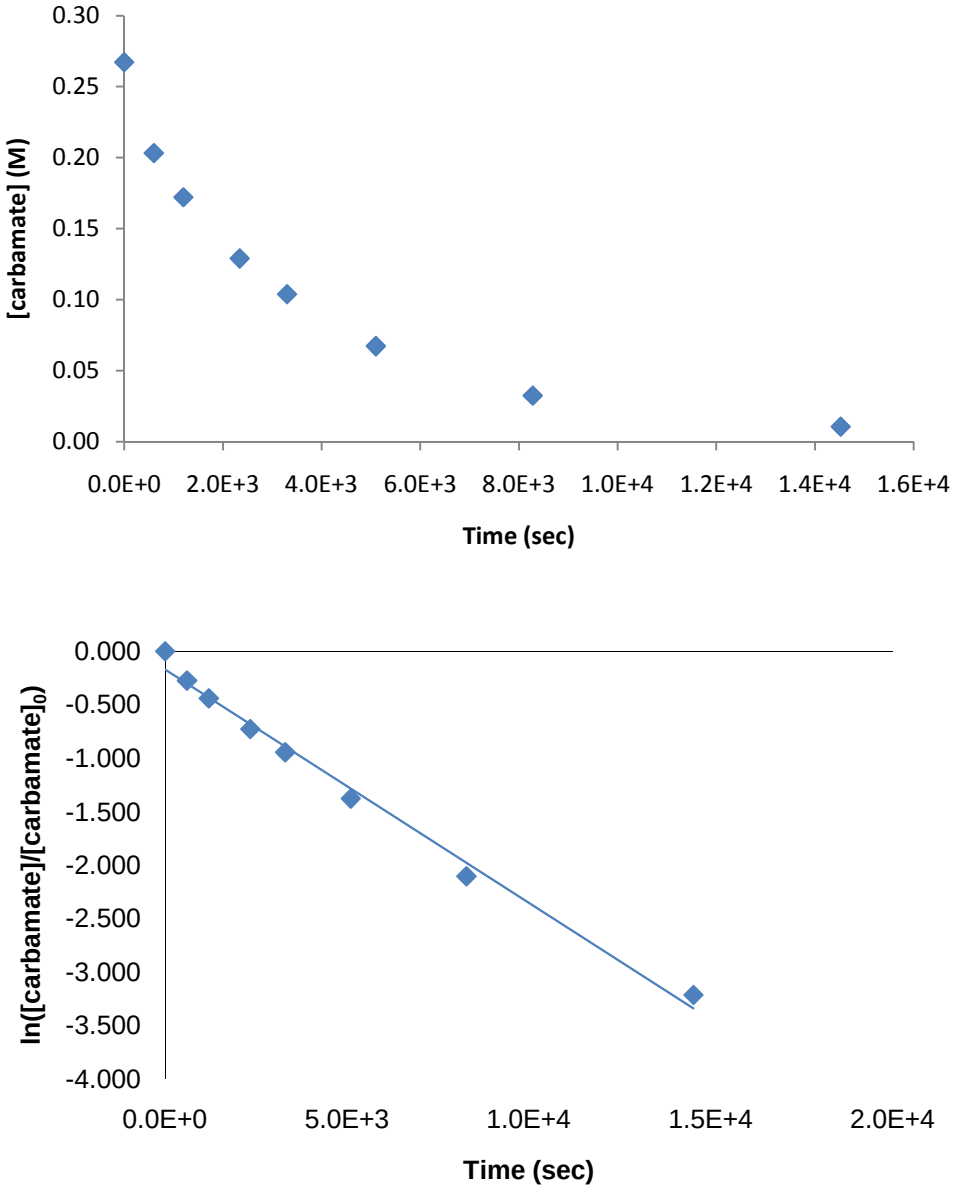

Figure 2.67. Concentration versus time (top) and pseudo first-order (bottom) plots for the reaction of 4-d_2 (0.27 M) with allene (2.5 M) catalyzed by (IPr)AuCl and AgOTf (25 mM) in dioxane at 24 °C k_{obs} = 2.2 ± 0.1 x 10^{-4} s^{-1} (Table 2.6, entry 2).

3 Mechanistic Studies of the Gold(I)-Catalyzed Intermolecular Hydroamination of Allenes with Arylamines

3.1 Introduction

The catalytic hydroamination of alkenes, alkynes, and allenes has attracted considerable interest from the synthetic community as an atom economical approach for the formation of C-N bonds. [24, 30, 130-133] Various transition metals have been used to catalyze hydroamination reactions. [9, 22, 131, 134-148] Transition metal-catalyzed reactions with allenes face increasing selectivity problems relative to alkenes and alkynes. Additions to unsymmetrical alkenes can form two possible constitutionally isomeric products (Markovnikov versus anti-Markovnikov regioselectivity, with associated stereochemistry). Additions to alkynes can be regioselective, stereoselective (*cis* or *trans* addition leading to stereoisomers), and chemoselective (single or double addition leading to different products). Additions to allenes face the selectivity problems of alkenes and alkynes (regioselectivity, stereoselectivity, and chemoselectivity) and positional selectivity (single addition at different double bonds leading to constitutional isomers). [10-13, 149-161]

The mechanisms for gold(I)-catalyzed hydroalkoxylation, [32, 108, 116, 162, 163] hydroarylation, [32, 164] and hydroamination [32, 108, 116, 118, 165] of C-C multiple bonds have been proposed. However, the majority of these proposed mechanisms are not based on experimental observations such as kinetic studies or stereochemical analysis that can distinguish between inner-sphere and outer-sphere pathways. [22, 108, 116, 166, 167] Proposed mechanisms for hydrofunctionalization of allenes by gold(I)-

catalysts fall into two categories: outer-sphere and inner-sphere mechanisms. An inner-sphere mechanism for the hydrofunctionalization of allenes with a gold(I)-catalyst involving a *trans*-gold allene complex is depicted in Scheme 3.1 to demonstrate the stereochemical outcome of the transformation. A tri-coordinate gold(I) species is formed by complexation of both the allene and nucleophile to the active gold catalyst. β-Migratory insertion occurs from this tri-coordinate species followed by protonolysis the cationic gold-σ-alkenyl complex to release the hydrofunctionalized product. [22, 168] In the outer-sphere mechanism, attack of the nucleophile on the two-coordinate gold-π-allene complex (*cis*-allene gold complex) forms a cationic gold-σ-alkenyl complex (Scheme 3.2). Protodemetalation of this species releases the hydrofunctionalized product and regenerates the catalyst. [32, 169]

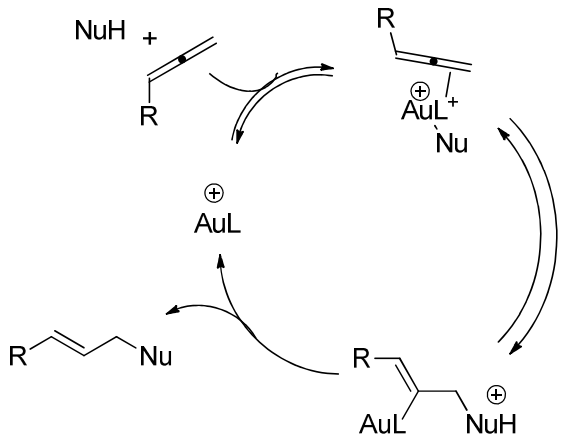

Scheme 3.1. Proposed inner-sphere mechanism for the hydrofunctionalization of allenes with gold(I) catalysts

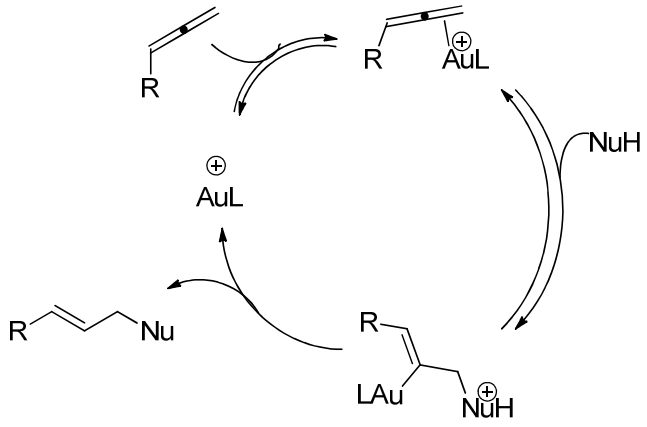

Scheme 3.2. Proposed outer-sphere mechanism for the hydrofunctionalization of allenes with gold(I) catalysts

Based on the stereoselective formation of *N*-[(1S,2E)-1-methyl-3-phenylprop-2-en-1-yl]aniline from the gold(III)-catalyzed reaction of aniline with (*R*)-1-methyl-3-phenylallene, Yamamoto proposed an inner-sphere mechanism for the gold(III)-

catalyzed intermolecular hydroamination of allenes with aniline (eq 3.1). [23] Yamamoto proposed that gold(III)-catalyzed hydroamination of allenes with aniline was initiated by formation of the aniline-gold complex. The mechanism accounts for stereochemistry of the product by involving an isomerization between the E and Z forms of the vinyl gold species (Scheme 3.3). [23, 170] Widenhoefer and coworkers proposed an outer-sphere mechanism that accounts for the stereospecific conversion of (*R*)-1-methyl-3-phenylallene *to N*-[(1S,2E)-1-methyl-3-phenylprop-2-en-1-yl]aniline without needing to invoke an isomerization of the vinyl gold complex (Scheme 3.4). [169]

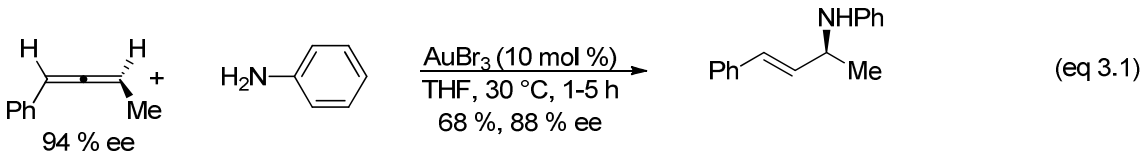

(eq 3.1)

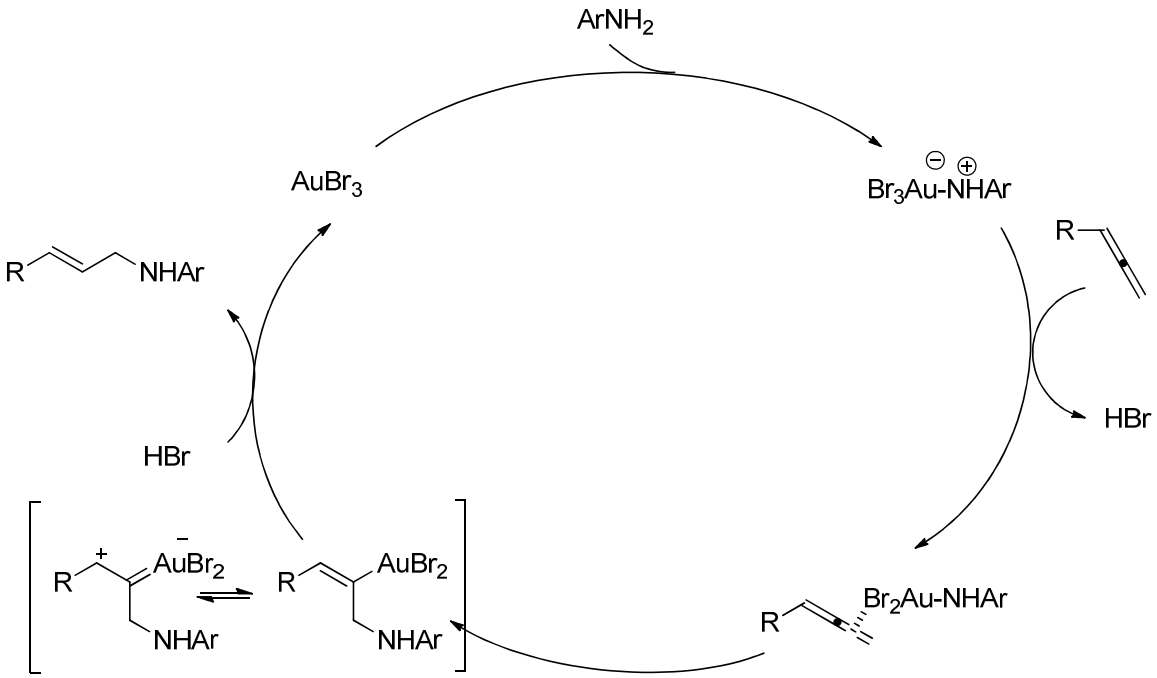

Scheme 3.3. Proposed inner-sphere mechanism for the gold(III)-catalyzed intermolecular hydroamination of allenese with arylamines.

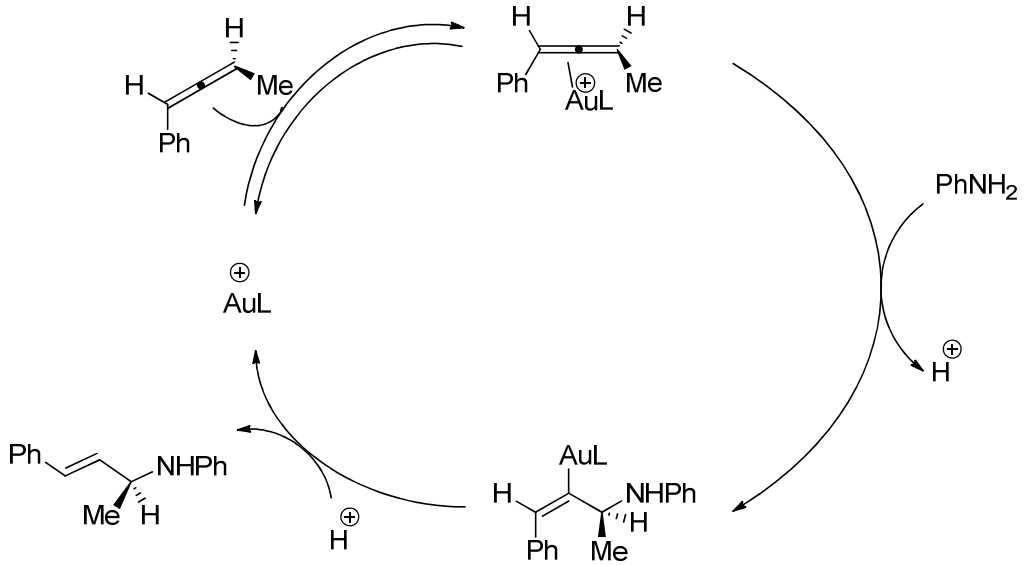

Scheme 3.4. Proposed outer-sphere mechanism for the gold(III)-catalyzed intermolecular hydroamination of allenese with arylamines.

Bertrand and coworkers gained insight into the mechanism of gold(I)-catalyzed hydroamination of allenes with alkyl amines by evaluating the complexation of 3-methyl-1,2-butadiene and diethylamine to a cationic gold(I) complex supported by a cyclic(alkyl)(amino)carbene (**Cat2**) (Scheme 3.5). [22] In one experiment, excess allene was added to **Cat2** in deuterated benzene at room temperature and the solution was heated at 50 °C; however, the desired allene gold complex was not formed. In another experiment, diethylamine is treated with **Cat2** in deuterated benzene at room temperature to form amine gold complex, **I**. This complex was then treated with excess allene in C_6D_6 at 70 °C for 16 h to form 3-methyl-2-butenyl amine complex, **II**. They concluded that complexation only occurred between amine and gold and not between allene and gold; these observations suggest an inner-sphere mechanism with transient formation of a tricoordinated gold complex. [22]

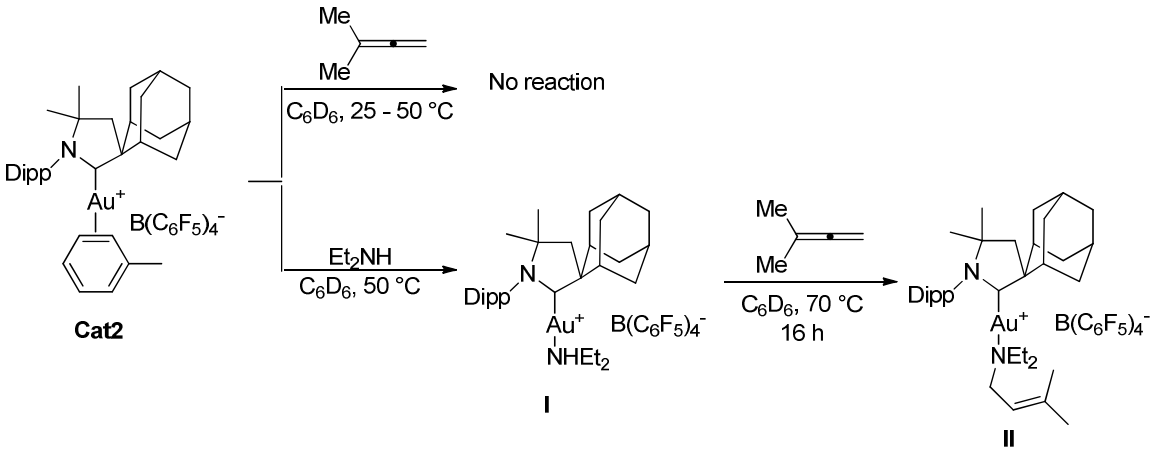

Scheme 3.5. Experiments to probe the mechanism of the gold(I) catalyzed intermolecular hydroamination of allenes with secondary amines

Widenhoefer and coworkers proposed an outer-sphere mechanism for the gold(I)-catalyzed the intramolecular *exo*-hydroamination of *N*-allenylcarbamates based on the stereoselective conversion of (*S*)-benzyl nona-4,5-dien-1-ylcarbamate to (*R,E*)-benzyl 2-(pent-1-en-1-yl)pyrrolidine-1-carboxylate (eq 3.2). The mechanism is initiated by rapid and reversible formation of the (allene)gold complex, followed by outer-sphere attack of the carbamate nitrogen atom on the allene moiety. Protodeauration gives the hydroamination product with retention of stereochemistry.

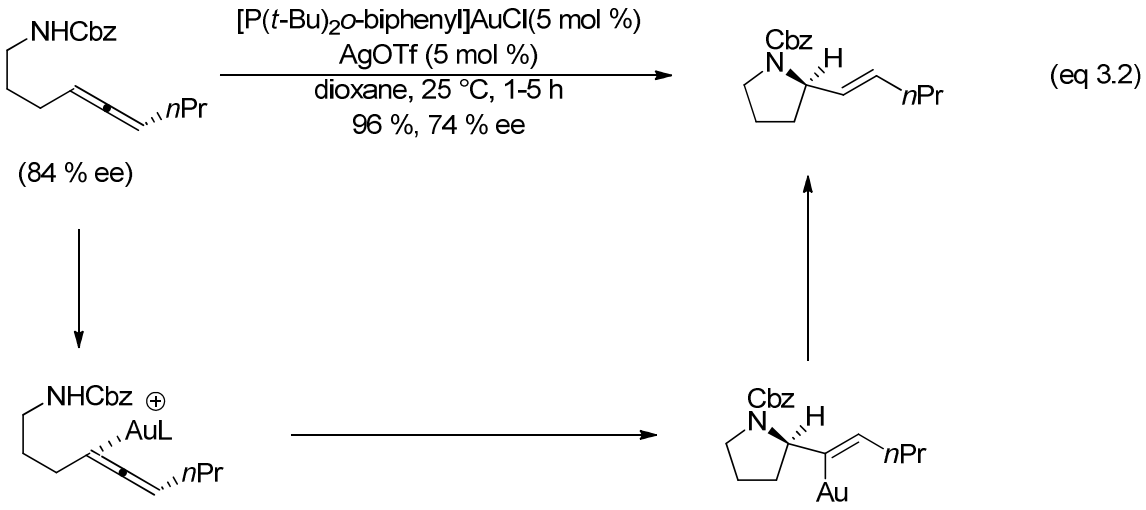

(eq 3.2)

We previously showed that a mixture of (**1**)AuCl [(**1**) = (1,1'-biphenyl-2-yl)di-*tert*-butylphosphine] and AgOTf catalyzed the hydroamination of arylamines with a variety of mono, di, and tri-substituted allenes. [118] Here we report kinetic and deuterium-labeling studies that provide insight into the mechanism of the C-N bond formation and the proton transfer in the conversion of 3-methyl-1,2-butadiene (**2**) with aniline catalyzed by (**1**)AuCl and AgOTf to form *N*-prenylaniline (**3**) and *N, N*-diprenylaniline

in a 4.1:1 ratio (eq 3.3). Also, we report and analyze the stereochemistry of the gold(I)-catalyzed hydroamination of an axially chiral 1,3-disubstituted allene.

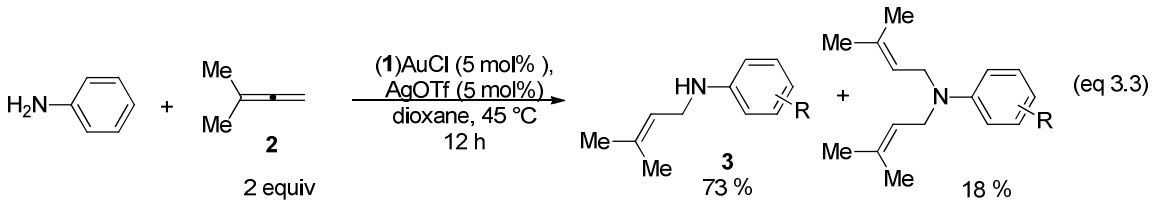

3.1.1 Proposed Mechanism

Inner-sphere [22, 133] and outer-sphere [24, 32] mechanism have been established for the gold catalyzed hydroamination of allenes with nitrogen nucleophiles. We therefore considered both pathways for the gold(I)-catalyzed hydroamination of allenes with arylamines. In the outer-sphere pathway, endoergonic displacement of aniline from gold-aniline complex, **III**, via the 16-electron, three-coordinate intermediate **IV** would form the gold(I) π-allene complex **V**. Outer-sphere attack of the aniline on **V** would then form the gold σ-alkenyl ammonium complex **VI**. Deprotonation of complex **VI** by free aniline would generate **VII**. Protonolysis of the Au-C bond of **VII** would release the *N*-prenylaniline with regeneration of the gold-aniline complex, **III**. Alternatively, β-migratory insertion of the coordinated allene into the Au-N bond of **IV** would likewise generate **VI** via an inner-sphere pathway, which would proceed to product in a like manner.

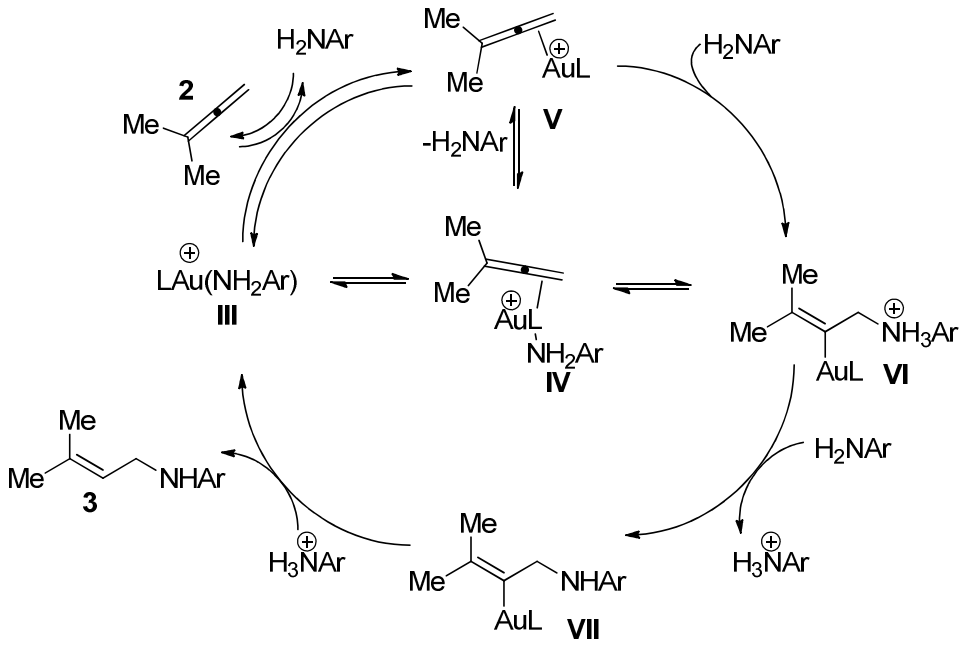

Scheme 3.6. Proposed outer-sphere and inner-sphere mechanism for the gold(I)-catalyzed hydroamination of allenes with arylamines

3.2 Results

3.2.1 Stereochemical Analysis of Hydroamination

To distinguish between inner and outer-sphere pathways for the gold(I)-catalyzed hydroamination of allenes with aniline, we sought to determine the stereochemistry of the gold(I)-catalyzed hydroamination of allenes with arylamines. We have previously shown that the reaction of 1-phenyl-1,2-butadiene (**4**) (two equivalents) with 3-bromoaniline and a catalytic amount of (**1**)AuCl (5 mol %) and AgOTf (5 mol %) in dioxane at 45 °C for 24 h formed exclusively (3-bromophenyl)-(1-methyl-3-phenyl-

allyl)-amine in 86 % isolated yield (eq 3.4). Since aniline attacks the C3 position of **4**, the gold(I)-catalyzed hydroamination reaction between enantiomerically enriched (*R*)-1-phenyl-1,2-butadiene [(*R*)-**4**] and aniline could produce two of four possible stereoisomers resulting from attack of aniline at the allenyl C3 carbon atom. To distinguish between inner and outer sphere pathways enantiomerically enriched (*R*)-**4** was synthesized so the stereochemistry of gold(I)-catalyzed hydroamination could be evaluated. Enantiomerically enriched allene, (*R*)-**4**, was synthesized in 89 % ee from the reaction of (*R*)-4-phenylbut-3-yn-2-ol with Ph_3P (1.5 equiv) in THF and was subsequently treated with *o*-nitrobenzenesulfonyl chloride (1.5 equiv). [35]

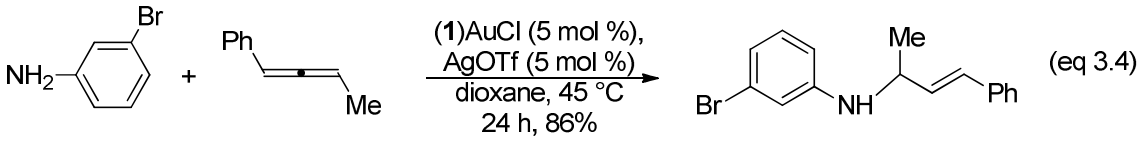

(eq 3.4)

To this end, we targeted the reaction of aniline with enantiomerically enriched **4**. An outer-sphere mechanism for the reaction of enantiomerically enriched (*R*)-**4** with aniline produces (*R,Z*)-**5** and *(S,E)*-**5** resulting from addition to the *cis* or *trans*-gold allene complex (Scheme 3.7). An inner-sphere mechanism produces (*R,E*)-**5** and (*S,Z*)-**5** resulting from β-migratory insertion of the tri-coordinate gold complex (Scheme 3.7). Of the four possible stereoisomers, we only consider the formation of (*R,E*)-**5** and (*S,E*)-**5** (pathways **B** and **C**), because experimentally the hydroamination of racemic allenes with aniline forms solely the *E*-hydroamination product, thus (*R,Z*)-**5** and (*S,Z*)-**5** (pathways **A** and **D**) can be excluded as possible stereoisomers for the reaction. [118] Therefore, we

sought to distinguish between the inner and outer-sphere pathways by determining the configuration at the chiral carbon of the hydroamination product (Scheme 3.7).

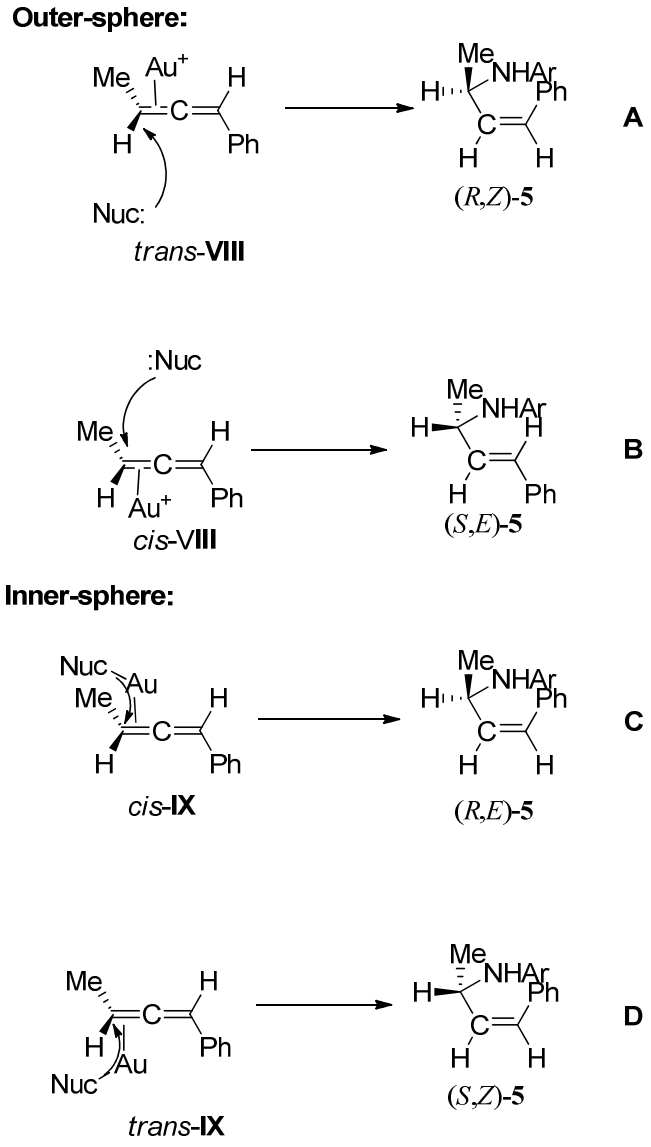

Scheme 3.7. Origin of the four potential stereoisomers from gold(I)-catalyzed hydroamination of aniline with (*R*)-4

Enantiomerically enriched (*R*)-**4** (89 % ee) was treated with 1.1 equivalents of aniline and a catalytic 1:1 mixture of (**1**)AuCl (5 mol %) and AgOTf (5 mol %) in dioxane at 45 °C for 36 h to form *N*-[(*E*)-1-methyl-3-phenylprop-2-en-1-yl]aniline, (*S,E*)-**5**, with 51% ee in 76% yield (eq 3.5). The relative configuration of **5** was established as *E* by the $^{3}J_{HH}$ coupling constant of 16.1 Hz for the alkenyl protons. The enantiomeric purity of (*E*)-**5** was established by HPLC, equipped with a Chiralpak AD-H column (Figure 3.1).

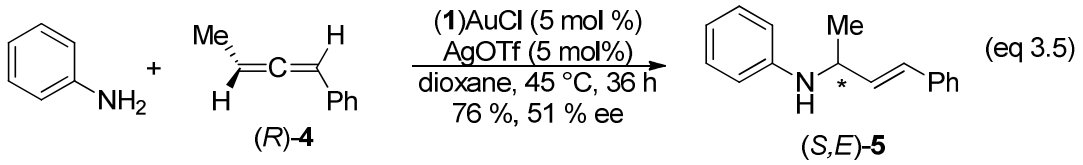

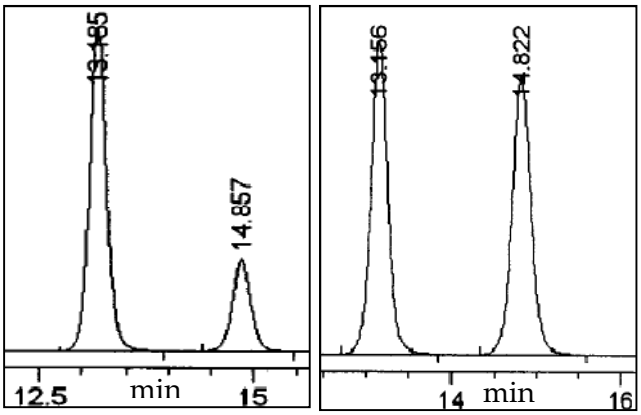

Figure 3.1. HPLC trace of enantiomerically enriched (*E*)-5 (left) from the reaction of (*R*)-4 and aniline catalyzed by (1)AuCl (5 mol %) and AgOTf (5 mol %) in dioxane at 45 °C and racemic trace (right) from the reaction of 4 and aniline catalyzed by (1)AuCl (5 mol %) and AgOTf (5 mol %) in dioxane at 45 °C

To determine the absolute configuration of (*E*)-**5** formed in the gold(I)-catalyzed intermolecular hydroamination of (*R*)-**4** with aniline, we independently synthesized enantiomerically enriched *N*-[(*S,E*)-1-methyl-3-phenylprop-2-en-1-yl] [(*S,E*)-**5**] (Scheme 3.8). To this end, *trans*-4-phenyl-3-buten-2-one [(*E*)-**6**] was treated with titanium

isopropoxide to form (3*E*)-4-phenylbut-3-en-2-amine [(*E*)-**7**], in 34 % yield. [171] Compound (*E*)-**7** and L-(+)-tartaric acid were dissolved in ethanol and the resting solution was allowed to sit for 4 h until crystals formed. The crystals were recrystallized in a solution of ethanol and hexanes. The precipitate was collected and treated with aqueous sodium hydroxide to give the enantiomerically enriched amine, (2*S*,3*E*)-4-phenylbut-3-en-2-amine [(*S*,*E*)-**7**], in 22 % yield. [172] The optical rotation of (*S*,*E*)-**7** at 1.01 g/ 100 mL (0.069 M) in chloroform at 25.6 °C was determined to be $[\alpha]_D^{20} - 13.2^{\circ}$, this value was compared to the literature value of $[\alpha]_D^{20} + 25.8^{\circ}$ for (*R*,*E*)-**7** (100 % ee) at 1.16 g/ 100 mL (0.079 M) in chloroform at 22 °C. As such, the absolute configuration of (*S*,*E*)-7 was determine to be S on the basis of this comparison. [173] Compound (*S*,*E*)-**7** was subjected to Buchwald-Hartwig amination; [174] bromobenzene was treated with (*S*,*E*)-**7** **(**1.1 eq) , $Pd(OAc)_2$, (3 mol %), BINAP (6 mol %) and 1.4 equivalents of sodium *tert*-butoxide in toluene at 80 °C for 72 h to give (*S*,*E*)-**5** 36 % yield and 18% ee . Compound (*S*,*E*)-**5** was analyzed by HPLC equipped with a Chiralpak AD-H column and this trace was compared to the HPLC trace of (*E*)-**5** formed from the gold-catalyzed intermolecular hydroamination of (*R*)-**4** and aniline (Figure 3.2). From this comparison, we determined that (*S*,*E*)-**5** formed from the gold(I)-catalyzed hydroamination of (*R*)-**4** and aniline had an *S* configuration (eq 3.5), The stereochemistry for this reaction established the anti-addition of the N-H bond of the aniline across the C=C bond of the allene, which suggests the mechanism is likely to occur through an outer-sphere pathway. The partial

loss of enantiopurity as the gold(I)-catalyzed hydroamination of aniline with (*R*)-**4** (89 % ee) to form (*S,E*)-**5** (51 % ee) is not surprising as gold(I) complexes are known to racemize allenes. [36, 175]

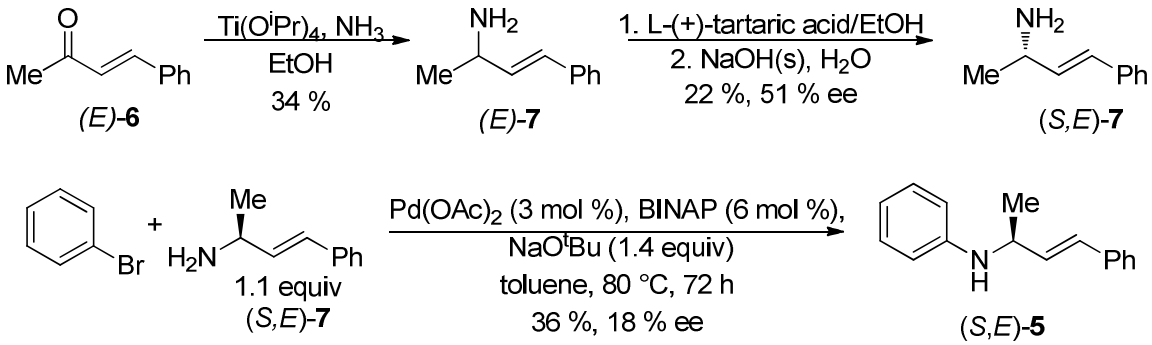

Scheme 3.8. Synthesis of enantiomerically enriched (*S,E*)-5 from (*E*)-6

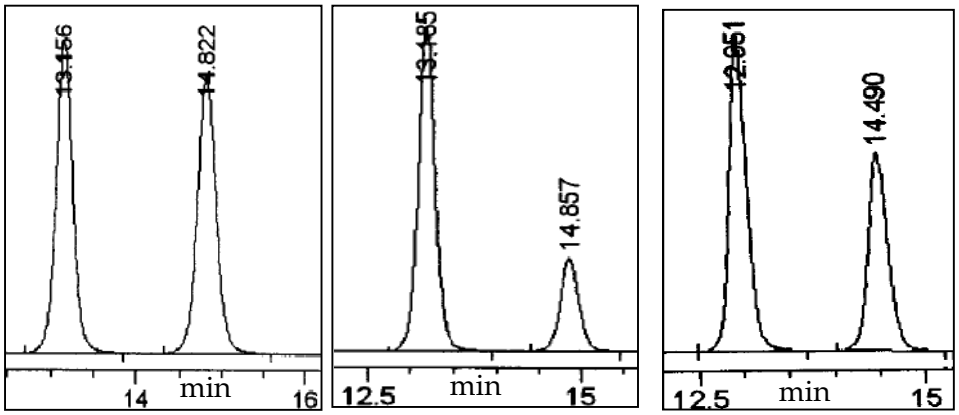

Figure 3.2. HPLC trace of racemic (*E*)-5 (left trace), (*S,E*)-5, synthesized from the gold(I)-catalyzed hydroamination with allene (middle trace), and (*S,E*)-5 from the independently synthesized from (*E*)-6 (right trace)

3.3 Kinetics of intermolecular Hydroamination

3.3.1 Rate dependence on aniline concentration

We sought to establish the rate behavior of the gold(I)-catalyzed hydroamination of aniline with 3-methyl-1,2-butadiene (**2**) catalyzed by (**1**)AuCl and AgOTf under conditions that approximated the relative and absolute concentrations of arylamine, allene, and catalyst used in preparatory scale reactions.[118] Aniline was employed in subsequent kinetic studies because it is the simplest arylamine and **2** was employed because it has been extensively used in gold(I)-catalyzed hydroamination protocols. [22, 118] Kinetic studies of the hydroamination of aniline and **2** catalyzed by (**1**)AuCl and AgOTf were carried out at various concentrations of aniline, **2**, and (**1**)AuCl/AgOTf in dioxane at 45 °C (eq 3.6). The reaction mixtures were monitored periodically by removing aliquots (10 μL) at regular intervals, which were analyzed by gas chromatography (GC). The decrease in peak percentage of aniline compared to the internal standard, *n*-tetradecane, was monitored by GC and was then used to calculate the concentration change in aniline.

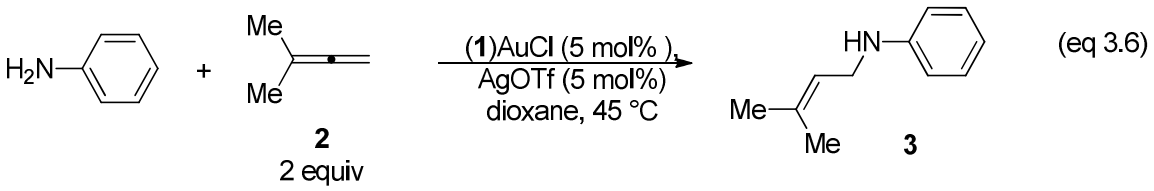

(eq 3.6)

The reaction order in aniline was likewise determined by monitoring the disappearance of aniline (0.29 M) under pseudo first-order conditions of excess allene (2.8 M) catalyzed by (**1**)AuCl and AgOTf (18 mM) (Table 3.1, entry 2 and Figure 3.3).

Aniline concentration was monitored to > 90% conversion. A plot of $[aniline]_t$ versus time showed pronounced curvature, consistent with non zero-order dependence of the rate of conversion of aniline to **3**. Conversely, a plot of $ln[aniline]_t/ln[aniline]_0$ versus time was linear (Figure 3.3), consistent with a first-order-dependence of the rate on [aniline] from 0.029-0.29 M.

The rate dependence on [aniline] was determined as a function of $[aniline]_0$ at concentrations ranging from 0.06 to 0.28 M employing **2** (≥10 eq) and (**1**)AuCl (19 mM) (Table 3.1, entry 2, 5, and 7; Figure 3.3 - Figure 3.5). First-order-dependence of the rate on [aniline] to **3** was observed over the concentration range of 0.06 to 0.28 M.

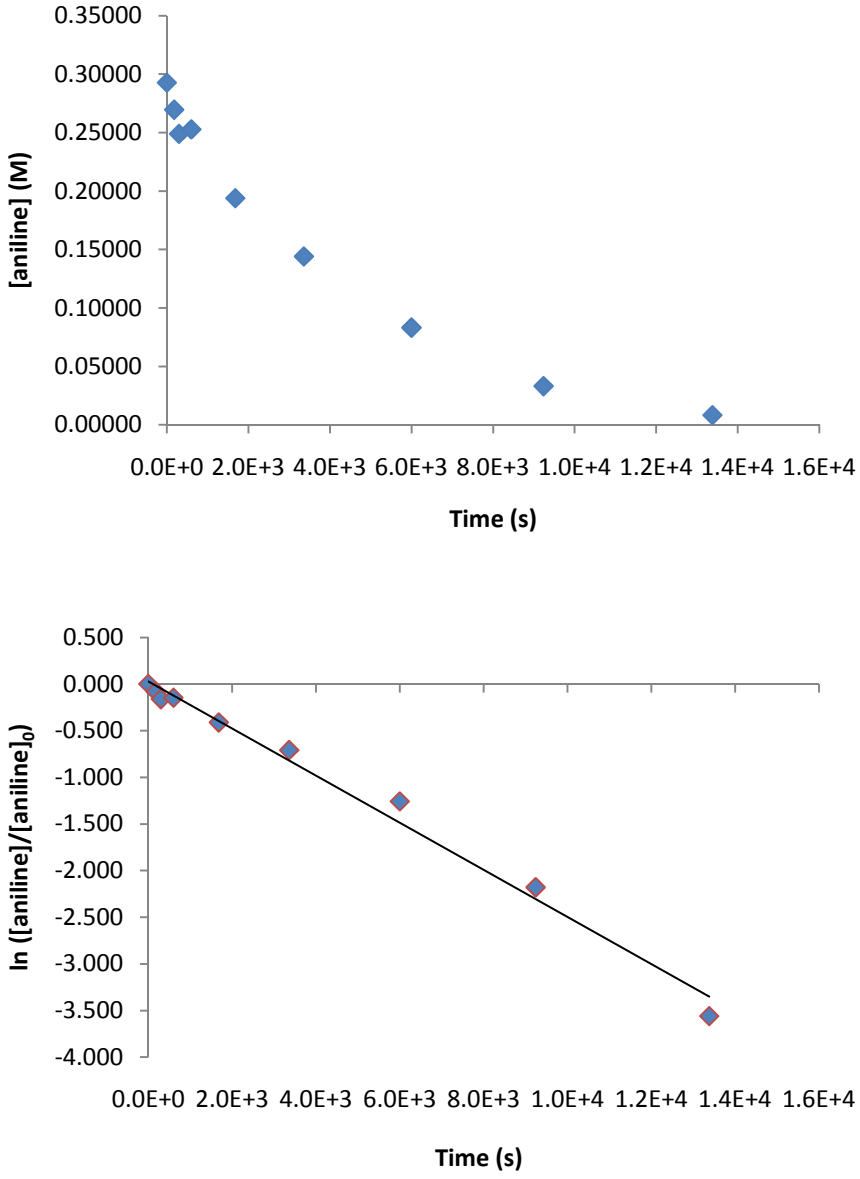

Figure 3.3. Concentration versus time plot for the gold(I)-catalyzed intermolecular hydroamination of 3-methyl-1,2-butadiene with aniline catalyzed by (1)AuCl/AgOTf in dioxane at 45 °C. [Aniline] = 0.29 M, [2] = 2.8 M, [(1)AuCl] = 18 mM k_{obs} = 2.5 ± 0.1 x 10^{-4} s^{-1} (Table 3.1, entry 2).

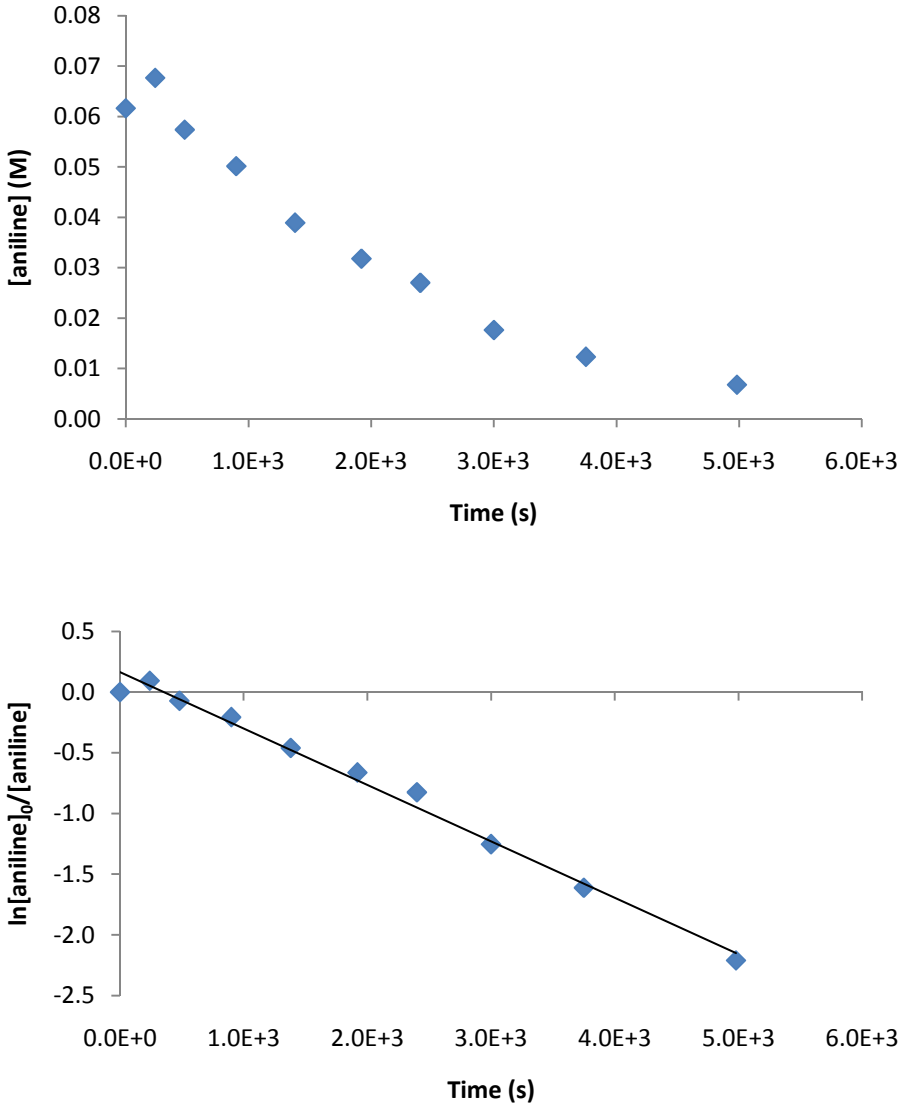

Figure 3.4. Concentration versus time (top) and pseudo first-order (bottom) plots for the gold(I)-catalyzed intermolecular hydroamination of 3-methyl-1,2-butadiene with aniline catalyzed by (1)AuCl/AgOTf in dioxane at 45 °C. [Aniline] = 0.06 M, [2] = 0.73 M, [(1)AuCl] = 18 mM k_{obs} = 4.6 ± 0.1 x 10^{-4} s^{-1} (Table 3.1, entry 5).

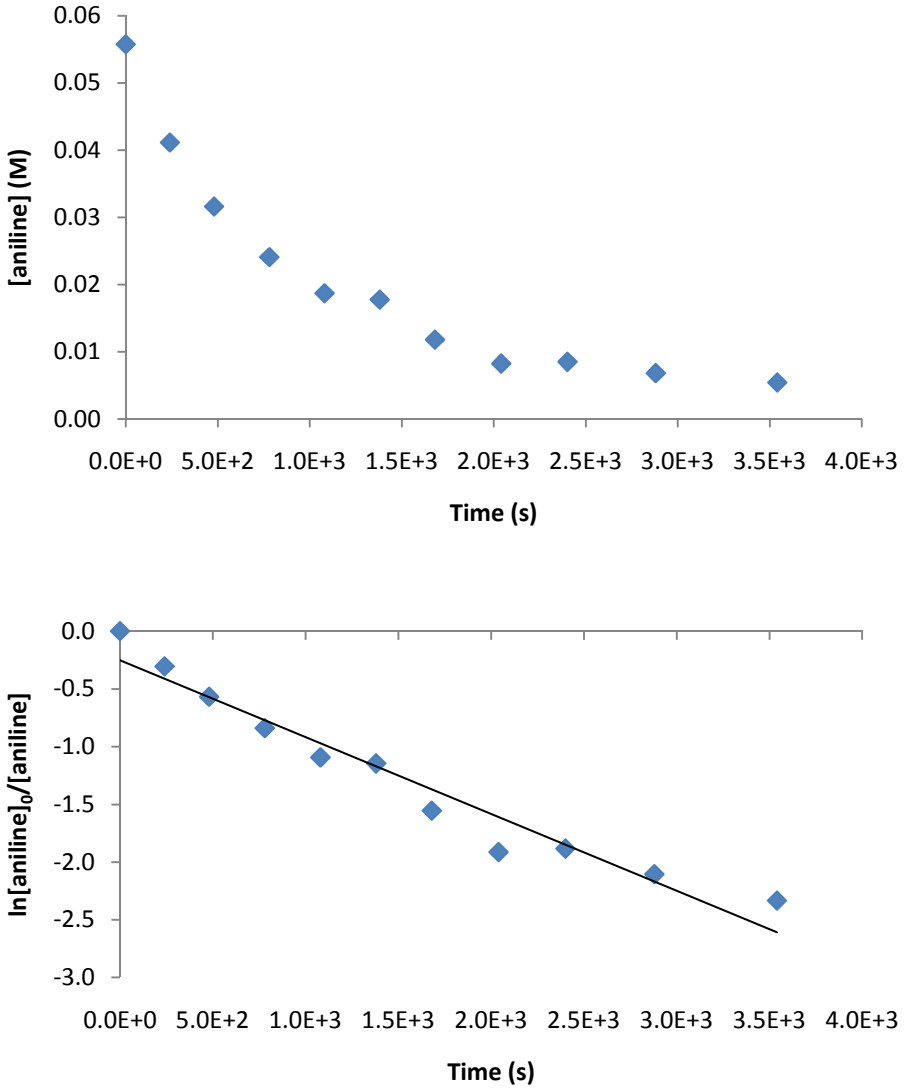

Figure 3.5. Concentration versus time (top) and pseudo first-order (bottom) plots for the gold(I)-catalyzed intermolecular hydroamination of 3-methyl-1,2-butadiene with aniline catalyzed by (1)AuCl/AgOTf in dioxane at 45 °C. [Aniline] = 0.06 M, [2] = 1.4 M, [(1)AuCl] = 18 mM k_{obs} = 6.6 ± 0.4 x 10^{-4} s^{-1} (Table 3.1, entry 7).

Table 3.1. Pseudo first-order rate constants for the intermolecular hydroamination of aniline with allene catalyzed by (1)AuCl in dioxane at 45 °C as a function of [allene], [aniline], and [Au] (Figure 3.11 to Figure 3.24).

Entry	[allene](M)	[aniline] (M)	[Au] (mM)	k_{obs} (s^{-1}) (10^{-4})[a]
1	1.4	0.45	19	0.75 ± 0.09
2	2.8	0.29	18	2.5 ± 0.1
3	1.4	0.11	20	2.2 ± 0.2
4	1.7	0.10	19	-
5	0.73	0.06	18	4.6 ± 0.1
6	0.38	0.06	19	2.3 ± 0.2
7	1.4	0.06	18	6.6 ± 0.4
8	0.25	0.06	18	0.60 ± 0.12
9	0.13	0.06	19	0.18 ± 0.08
10	2.4	0.07	19	11.4 ± 0.3
11	0.80	0.07	36	4.6 ± 0.1
12	0.83	0.06	54	6.5 ± 0.1
13	0.88	0.06	18	2.17 ± 0.04
14	0.90	0.46	20	0.54 ± 0.08

[a] Error in k_{obs} values determined from the standard deviation of the slope for the plot of ln[aniline] versus time

3.3.2 Rate dependence on gold concentration

To further probe the mechanism of the gold(I)-catalyzed intermolecular hydroamination of allenes with aniline, we sought to determine the rate dependence on [catalyst]. To this end, pseudo first-order rate constants were determined for the reaction of aniline (0.1 M) with **2** (0.8 M) at 45 °C as a function of [(**1**)AuCl/AgOTf] over the concentration range 18 – 54 mM (Table 3.1, entry 12 - 14). In each case, plots of ln[aniline] versus time were linear consistent with first-order decay. (Figure 3.21 to Figure 3.23). A plot of k_{obs} versus [(**1**)AuCl/AgOTf] was linear with a pseudo second-order rate constant of $k_2 = 1.2 \times 10^{-2}\ M^{-1}s^{-1}$, consistent with first-order dependence of the rate on [(**1**)AuCl] (Figure 3.6). To confirm the apparent first-order dependence of the rate on [catalyst] a van't Hoff plot was created. Specifically, a plot of ln[k_{obs}] versus ln[catalyst] was linear with a slope of 1, supporting the apparent first-order dependence of the rate on [catalyst] (Figure 3.7).

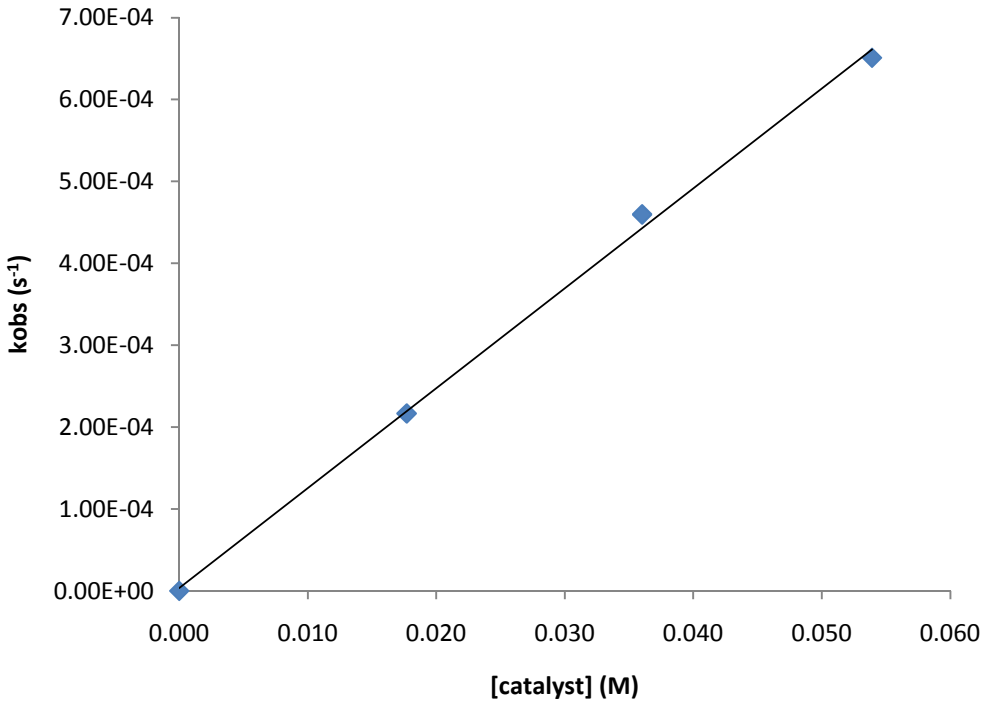

Figure 3.6. Plot of k_{obs} versus [catalyst] for the gold(I)-catalyzed intermolecular hydroamination reaction of aniline with 3-methyl-1,2-butadiene catalyzed by (1)AuCl/AgOTf in dioxane at 45 °C.

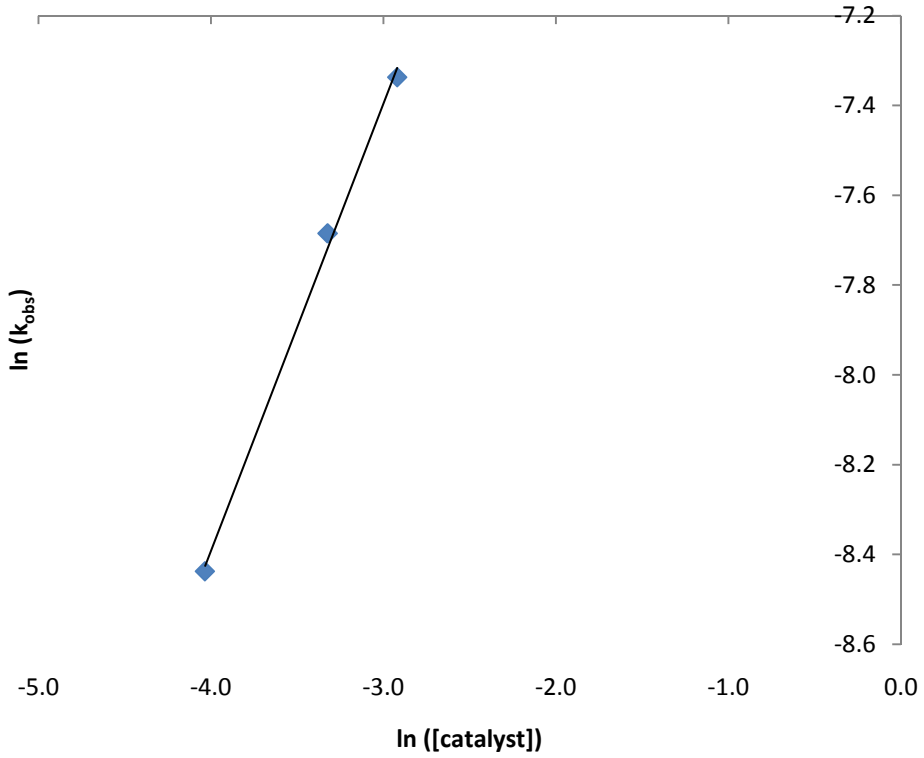

Figure 3.7. Natural logarithm of k_{obs} versus the natural logarithm of [catalyst] for the gold(I)-catalyzed intermolecular hydroamination reaction of aniline with 3-methyl-1,2-butadiene catalyzed by (1)AuCl in dioxane at 45 °C. The slope of the line was found to be 1.0 indicative of the first-order behavior with respect to catalyst

3.3.3 Rate dependence on allene concentration

We sought to establish the rate dependence of allene on the rate of gold(I)-catalyzed hydroamination of aniline with **2** catalyzed by (**1**)AuCl and AgOTf. To this end, we determined the pseudo-first-order rate constants for the disappearance of aniline (0.06 M) as a function of [**2**] over the concentration range 0.13 M to 2.4 M catalyzed by (**1**)AuCl/AgOTf (18 mM) (Table 3.1, entry 5-10, and 13; Figure 3.15 - Figure 3.20; and Figure 3.23). Relatively low concentrations of aniline (0.06 M) were employed for these studies to maintain pseudo first-order conditions over the allene concentration range and because the concentrations were more aligned with published catalytic conditions for the gold(I)-catalyzed hydroamination of allenes with arylamines. [118] A plot of pseudo first-order rate constants versus allene concentration was linear, indicative of apparent first-order behavior with respect to allene over the concentration range 0.13 – 2.4 M (Figure 3.8). It can be concluded that the gold(I)-catalyzed intermolecular hydroamination of aniline and **2** with (**1**)AuCl and AgOTf to form **3** is first-order in **2** and does not display saturation over the observed concentrations of **2** (0.13 M to 2.4 M). Overall, the empirical rate law can be expressed as rate = k_3 [aniline][**2**][(**1**)AuCl/AgOTf], where the third order rate constant, $k_3 = 2.6 \times 10^{-2}$ $M^{-2}s^{-1}$ over the concentration range [**2**] = 0.13 – 2.4 M.

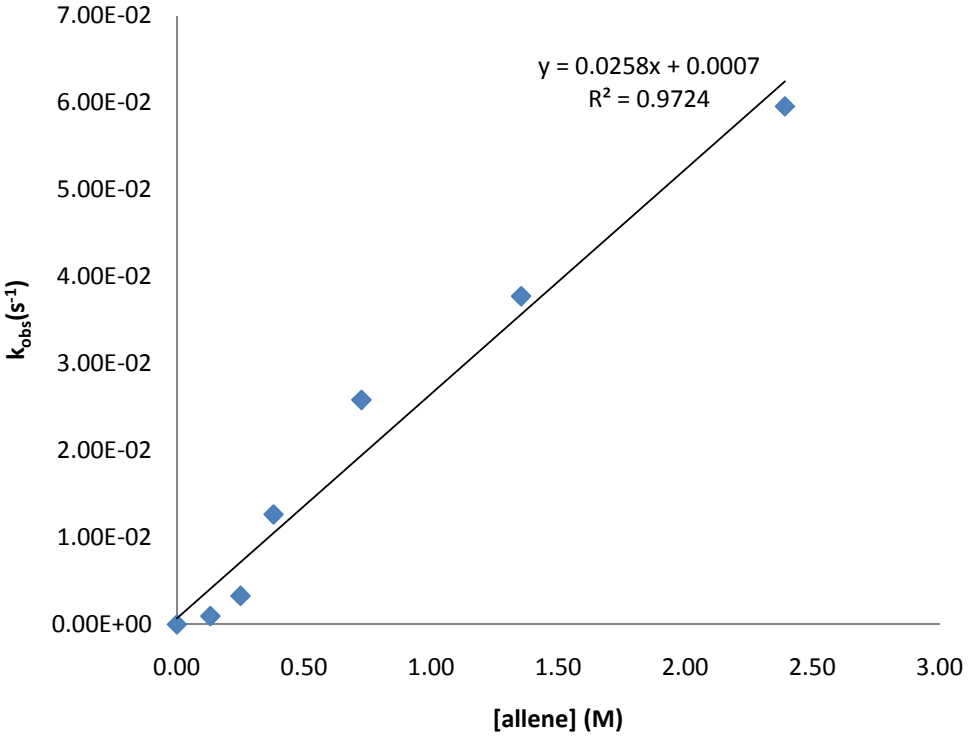

Figure 3.8. Plot of k_{obs} versus [2] for the intermolecular gold(I)-catalyzed hydroamination of 2 with aniline catalyzed by (1)AuCl/AgOTf in dioxane at 45 °C ([2] = 0.13 M, 0.25 M, 0.38 M, 0.73 M, 0.88 M, 1.4 M, and 2.4 M)

3.3.4 Effect of excess triflate on the rate of gold(I)-catalyzed intermolecular hydroamination of 2 with aniline

AgOTf is required in the gold(I)-catalyzed hydroamination of allenes with arylamines to abstract the chloride ligand from the gold to generate the active gold cationic catalyst, (**1**)Au-OTf. However, triflates can potentially affect the ratio of hydroamination. For example, the presence of excess triflate anion in the platinum(II)-catalyzed enantioselective hydroformylation of styrene decreased both the rate and enantioselectivity. [176] Since triflate is a potential coordinating ligand for gold, we sought to evaluate the effect of [TfO^-] on the rate of gold(I)-catalyzed hydroamination. To this end, we determined the pseudo first-order rate constants for the reaction of aniline ([aniline] = 0.1 and 0.4 M) with a tenfold excess of **2** catalyzed by a 1:1 mixture of (**1**)AuCl and AgOTf in dioxane at 45 °C as a function of [OTf^-], employing Bu_4NOTf as a source of soluble triflate anion. In one experiment, reaction of [aniline] (0.06 M), [**2**] (0.72 M), [(**1**)AuCl] (18 mM), and Bu_4NOTf (0.06 M) in dioxane at 45 °C was monitored periodically by GC analysis (Table 3.2, entry 2). A plot of ln[aniline] versus time was linear with a pseudo first-order constant of $k_{obs} = 3.5 \pm 0.1 \times 10^{-4}\ s^{-1}$ (Figure 3.25). When this observed rate value was compared to the observed rate for the reaction of [aniline] (0.06 M), [**2**] (0.73 M) and [(**1**)AuCl] (18 mM)in dioxane at 45 °C ($k_{obs} = 4.6 \pm 0.1 \times 10^{-4}\ s^{-1}$) (Table 3.2, entry 1 and Figure 3.15) the presence of excess triflate anion (0.06 M) slowed the reaction by approximately 24 %.

Table 3.2. Pseudo first-order rate constants for the intermolecular hydroamination of aniline with allene catalyzed by (1)AuCl in dioxane at 45 °C as a function of [allene], [aniline], [(1)AuCl] and [Bu_4NOTf] at low concentrations of aniline.

Entry	[allene] (M)	[aniline] (M)	[Au] (mM)	[Bu_4NOTf] (M)	k_{obs} (s^{-1}) (10^{-4})
1	0.73	0.06	18	0.00	4.6 ± 0.1
2	0.72	0.06	18	0.06	3.5 ± 0.1

[a] Error in k_{obs} values determined from the standard deviation of the slope for the plot of ln[aniline] versus time

3.3.5 Deuterium Labeling Studies

The mechanism of the gold(I)-catalyzed intermolecular hydroamination of **2** with aniline catalyzed by (**1**)AuCl and AgOTf was studied through two deuterium labeling experiments. In the first experiment, aniline-d_2 (62% d) was treated with 0.75 equivalents of **2** and 5 mol % (**1**)AuCl/AgOTf in dioxane at 45 °C for 12 h. The reaction mixture was purified through a cotton plug pipet filled with silica gel and eluted with $CDCl_3$, and a ^{1}H NMR spectrum of the crude reaction mixture was obtained (eq 3.7). The peak area for the methyl protons of *N*-(3-methyl-2-butyl)aniline (δ 1.73 and 1.69) were compared to the peak area for the internal alkene protons (δ 5.36) and the difference between expected and observed values indicated ~25 % deuterium incorporation at the internal alkene position. **3**-d_1 could not be isolated without H/D exchange, but we presume based on the integration of the alkenyl protons compared to the methyl protons that deuterium was incorporated at the internal alkene.

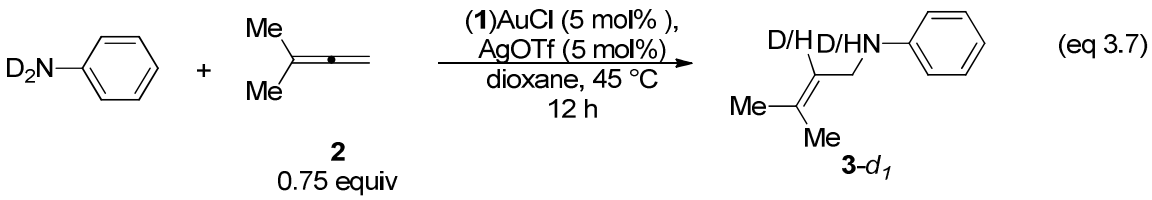

(eq 3.7)

In a second experiment, we determined the pseudo first-order rate constant for the gold(I)-catalyzed hydroamination of **2** with aniline-d_2. To this end, a mixture of **2** (1.3 M), aniline-d_2 (0.45 M), (**1**)AuCl and AgOTf (20 mM) and *n*-tetradecane in dioxane was stirred at 45 °C (eq 3.8). A plot of the ln[aniline -d_2] versus time was linear with a slope of $0.42 \pm 0.12 \times 10^{-4}$ s^{-1} (Figure 3.9) (Table 3.3, entry 2). We determined the pseudo first-order rate constant for the reaction of aniline and **2** under identical conditions ([**2**] = 1.3 M [aniline] = 0.45 M, (**1**)AuCl and AgOTf = 20 mM) in dioxane at 45 °C). A plot of the ln[aniline] versus time was linear with an observed rate constant of $k_{obs} = 0.79 \pm 0.04 \times 10^{-4}$ s^{-1} , which corresponds to a primary KIE of $k_H/k_D = 1.8 \pm 0.1$ (Figure 3.9) (Table 3.3, entry 1). Since deuterium incorporation into the internal alkene position of **3** was low (~25%), this observed k_H/k_D suggests the true KIE is much higher.

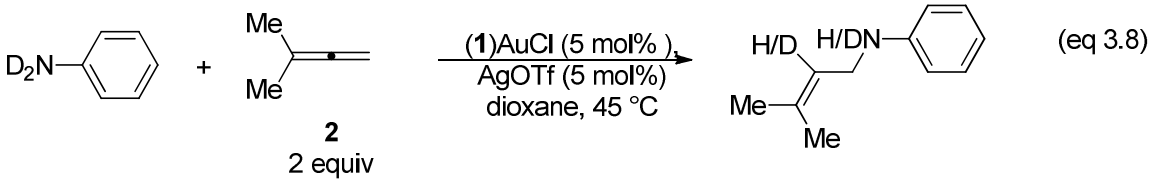

(eq 3.8)

Table 3.3. Observed rate constant for the intermolecular hydroamination of aniline and aniline-d_2 with allene catalyzed by (1)AuCl in dioxane at 45 °C as a function of [allene], [aniline], and [Au].

Entry	[allene](M)	[aniline] (M)	[Au] (mM)	k_{obs} (s^{-1}) (10^{-4})
1	1.3	0.46	20	0.79 ± 0.04
2	1.3	0.45	20	0.42 ± 0.12

[a] Error in k_{obs} values determined from the standard deviation of the slope for the plot of ln[aniline] versus time

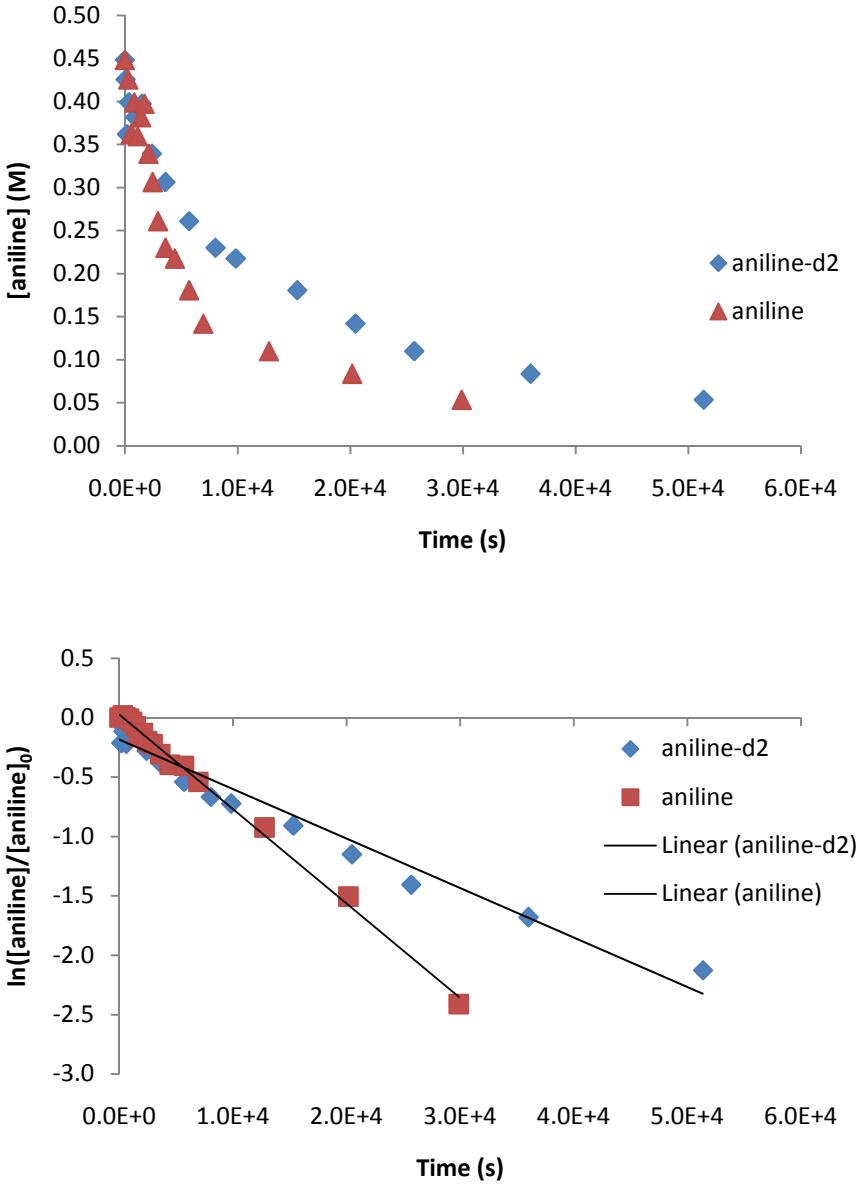

Figure 3.9. Concentration versus time (top) and pseudo first-order (bottom) plots for the gold(I)-catalyzed intermolecular hydroamination of 2 with aniline catalyzed by (1)AuCl/AgOTf in dioxane at 45 °C. [Aniline] = 0.46 M, [2] = 1.3 M, [(1)AuCl] = 20 mM k_{obs} = 0.79 ± 0.04 x 10^{-4} s^{-1} (Table 3.3, entry 1) and [aniline-d_2] = 0.45 M, [2] = 1.3 M, [(1)AuCl] = 20 mM k_{obs} = 0.42 ± 0.12 x 10^{-4} s^{-1} (Table 3.3, entry 1 and 2)

3.4 Discussion

3.4.1 Mechanism of gold(I)-catalyzed hydroamination of aniline with 2

The kinetics of the catalytic hydroamination were interpreted in the context with Scheme 3.9 and associated equations (eq 3.9-3.11), which was constructed on the basis of the following assumptions: (1) rapid ligand exchange to form the active catalyst, (2) pre-equilibrium assumption to the formation of **V**, (3) steady state treatment approximation to the formation of **VII**, (4) the total catalyst concentration is equal to the formation of **III** and **V** ($[Au]_{tot} = [\mathbf{III}] + [\mathbf{V}]$), and (5) aniline is the base.

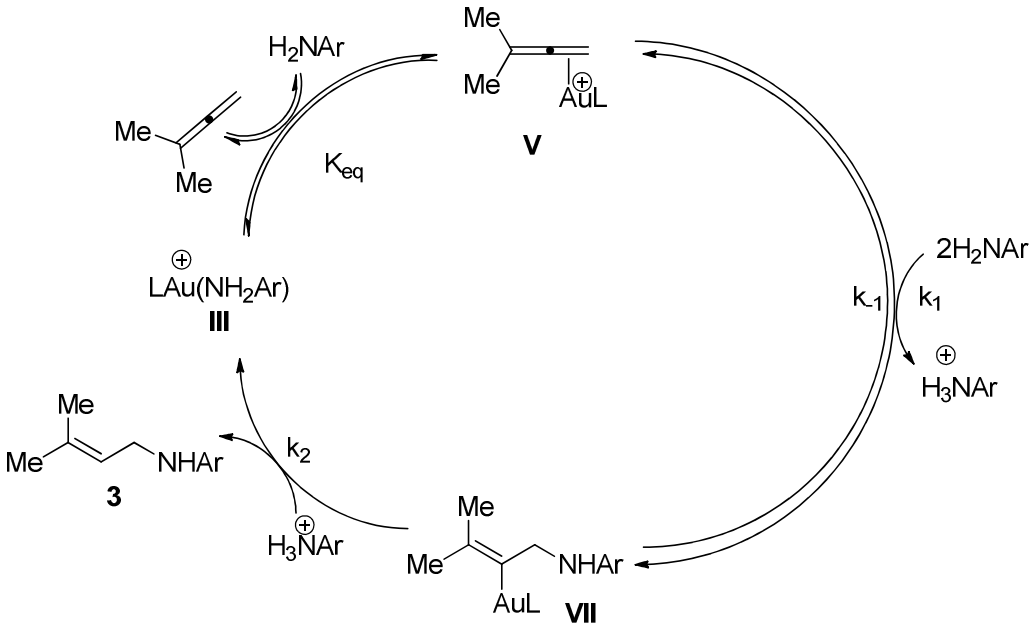

Scheme 3.9. Proposed Mechanism for the Intermolecular Hydroamination of Allenes with Arylamines

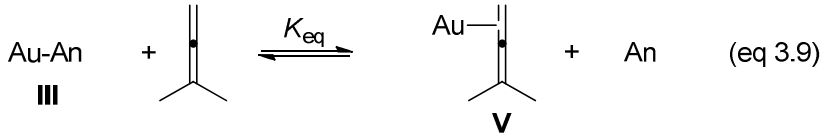

(eq 3.9)

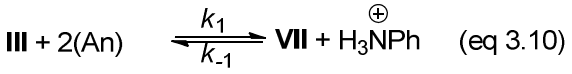

(eq 3.10)

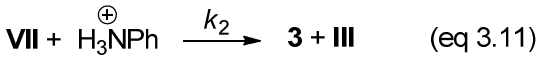

(eq 3.11)

From these assumptions, we derive the rate law for the formation of **3**, which relates the concentration of **VII** to the concentration of benzenaminium (eq 3.12). Steady state approximation for the formation **VII**, shown in eq 3.13 can be simplified to eq 3.14. Substitution of the relationship established for [**VII**][H_3N^+Ph] in eq 3.14 into eq 3.12, produced the two term rate law depicted in eq 3.15. Eq 3.15 can be further simplified by the assumption that the total catalyst concentration is equal to **III** and **V** (eq 3.16), solving for [**III**] (eq 3.17), and applying a pre-equilibrium assumption for the formation of **V** (eq 3.18). Substituting eq 3.17 into eq 3.18 and solving for [**V**] gives eq 3.19. Substituting the relationship for [**V**] shown in eq 3.19 into eq 3.15 gives the three term rate law shown in eq 3.20. When the equilibrium favors aniline complex, the three term rate law is simplified to eq 3.21.

$$\text{rate} = \frac{\mathrm{d}[\mathbf{3}]}{\mathrm{dt}} = k_2[\mathbf{VII}][\mathrm{H_3N^+Ph}] \text{(eq 3.12)}$$

$$\frac{\mathrm{d}[\mathbf{VII}]}{\mathrm{dt}} = 0 = k_1[\mathbf{V}][\text{aniline}]^2 - k_{-1}[\mathbf{VII}][\mathrm{H_3N^+Ph}] - k_2[\mathbf{VII}][\mathrm{H_3N^+Ph}] \text{(eq 3.13)}$$

$$[\mathbf{VII}][\mathrm{H_3N^+Ph}] = \frac{k_1k_2[\mathbf{V}][\text{aniline}]^2}{(k_{-1}+k_2)} \text{ (eq 3.14)}$$

$$\text{rate} = \frac{k_1 k_2 [\mathbf{V}][\text{aniline}]^2}{(k_{-1} + k_2)} \quad \text{(eq 3.15)}$$

$$[\text{Au}]_{\text{tot}} = [\mathbf{III}] + [\mathbf{V}] \quad \text{(eq 3.16)}$$

$$[\mathbf{III}] = [\text{Au}]_{\text{tot}} - [\mathbf{V}] \quad \text{(eq 3.17)}$$

$$K_{eq} = \frac{[\mathbf{V}][\text{aniline}]}{[\mathbf{III}][\mathbf{2}]} \quad \text{(eq 3.18)}$$

$$[\boldsymbol{V}] = \frac{K_{eq}[\text{Au}]_{\text{tot}}[\mathbf{2}]}{K_{eq}[\mathbf{2}] + [\text{aniline}]} \quad \text{(eq 3.19)}$$

$$\text{rate} = \frac{k_1 k_2 K_{eq}[\text{Au}]_{\text{tot}}[\mathbf{2}][\text{aniline}]^2}{(k_{-1} + k_2) K_{eq}[\mathbf{2}] + (k_{-1} + k_2)[\text{aniline}]} \quad \text{(eq 3.20)}$$

$$K_{eq}[\mathbf{2}] << [\text{aniline}]: \text{rate} \approx k_{obs}[\text{Au}]_{\text{tot}}[\mathbf{2}][\text{aniline}] \quad \text{(eq 3.21)}$$

Experimentally we derived the rate law: rate = k_3 [aniline][**2**][(**1**)AuCl/AgOTf], where k_3 = 2.6 x 10^{-2} $M^{-2}s^{-1}$ when [**2**] was varied and [aniline]and [(**1**)AuCl/AgOTf] were held constant. The derived rate law for rate-limiting protodeauration which occurs from **VII** to **III** supports the experimental results because the experimental rate law is of the same form as eq 3.16. The KIE for gold(I)-catalyzed hydroamination of **2** with aniline was determined to be of k_H/k_D = 1.8 ± 0.1; however the true KIE value is much higher since only ~25% deuterium was incorporated into the hydroamination product. This suggests that either deprotonation or protonation is the turnover limiting step. The results from the stereochemical analysis of hydroamination establish an anti-attack by aniline consistent with an outer-sphere mechanism. Our observations regarding the

gold(I)-catalyzed intermolecular hydroamination of allenes with arylamines are in accord with the outer-sphere mechanism depicted in Scheme 3.9.

The overall reaction mechanism for the gold(I)-catalyzed hydroamination of aniline with (*R*)-**4** is depicted in Scheme 3.10, the outer-sphere pathway accounts for the observed stereochemistry of the hydroamination product. The active gold catalyst, **III**, undergoes reversible ligand exchange with aniline and is replaced with allene forming a gold-π-allene complex, **X**. **X** then undergoes reversible outer-sphere attack by aniline to form a gold-σ-alkenyl ammonium complex, (*S*)-**XII**, or **X** could racemize into its cationic form **XI** followed by outer-sphere attack of aniline. The racemization of **X** to **XI** accounts for the loss of enantiomeric enrichment that occurred in eq 3.5. Deprotonation of (*S*)-**XII** by free aniline forms the neutral gold-σ-alkenyl complex (*S*)-**XIII**. Protonolysis of (*S*)-**XIII** releases the hydroamination product, (*S*,*E*)-**5**, and regenerates the active catalyst.

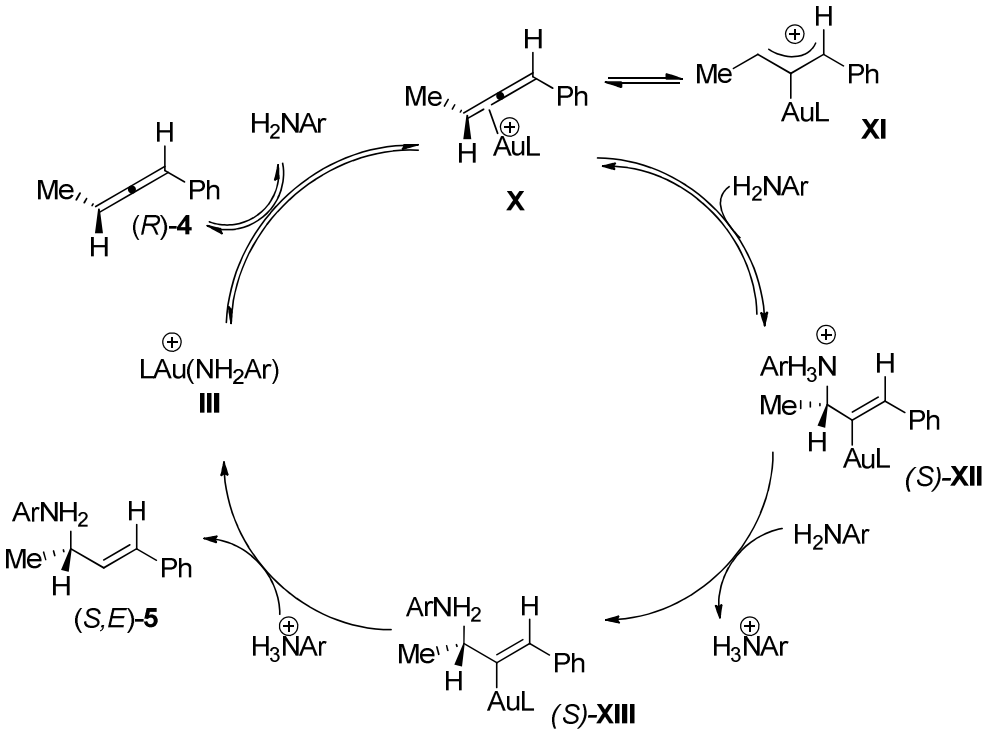

Scheme 3.10. Proposed Mechanism for the Intermolecular Hydroamination of Allenes with Arylamines

Experiments to determine the effect of excess triflate anion on the gold(I)-catalyzed hydroamination of aniline with **2**, indicate additional triflate anion (1 equivalent relative to aniline), slows the reaction on average by 69 %. The presence of the triflate anion in the reaction assists in the development of the active gold catalyst, **III**, and stabilizes the gold-σ-alkenyl ammonium complex, **X**. Excess triflate presumably clogs the reactive intermediate, **X** and slows deprotonation of the gold-σ-alkenyl ammonium complex by free aniline. Additionally, deuterium labeling experiments shows that the proton transfer is the rate limiting step and because proton transfers

more readily than deuterium and that the presence of deuterium slows the reaction. This observation is realized as **XIII** undergoes protonolysis to release the product.

3.5 Summary

In summary, we have concluded that the mechanism for the gold(I)-catalyzed intermolecular hydroamination of allenes with arylamines involves outer-sphere attack of aniline on the gold-π-allene complex based on stereochemical analysis of the hydroamination product. Experimentally we derived the rate law: rate = k_3 [aniline][**2**][(**1**)AuCl/AgOTf], where $k_3 = 2.6 \times 10^{-2}$ $M^{-2}s^{-1}$, which is supported by the derived differential rate law for rate limiting protodeauration. The reaction was found to be first-order in aniline, **2** and (**1**)AuCl/AgOTf. The presence of excess triflate slowed the gold(I)-catalyzed hydroamination of aniline with **2**. Experiments to establish the KIE suggested that either deprotonation or protonation is the turnover limiting step because of the low percentage of deuterium incorporation into the hydroamination product.

3.6 Experimental Methods

3.6.1 General Methods

Catalytic reactions were performed in sealed glass tubes under an atmosphere of dry nitrogen unless noted otherwise. NMR spectra were obtained on a Varian spectrometer operating at 500 MHz for ^1H NMR and 125 MHz for ^{13}C NMR in $CDCl_3$

unless noted otherwise. IR spectra were obtained on a Bomen MB-100 FT IR spectrometer. Gas chromatography was performed on a Hewlett-Packard 5890 gas chromatograph equipped with a 25 m polydimethylsiloxane capillary column employing FID detection. Chiral HPLC was performed on a Hewlett-Packard chromatograph equipped with a 0.46 cm x 25 cm Chiralpak AD-H column. Column chromatography was performed employing 200-400 mesh silica gel (EM). Thin layer chromatography (TLC) was performed on silica gel 60 F254. Elemental analyses were performed by Complete Analysis Laboratories (Parsippany, NJ).

Aniline, 3-methyl-1,2-butadiene (**2**), *trans*-4-phenyl-3-buten-2-one (*E*)-**6**, titanium(IV) isopropoxide, sodium borohydride, ammonia (2.0 M solution in ethanol), ethanol, [P(t-Bu)$_2$o-biphenyl]AuCl [(**1**)AuCl], and silver trifluoromethanesulfonate were purchased from major chemical suppliers and were used as received. Dioxane (Aldrich) was dried using the PureSolv™ solvent purification system. 1-Phenyl-1,2-butadiene (**4**), [35] (*R*)-1-Phenyl-1,2-butadiene [(*R*)-**4**], [35] aniline-d$_2$, [149] and (2*S*, 3*E*)-4-phenylbut-3-en-2-amine [(S,*E*)-**7**] [171-173] were synthesized employing published procedures.

3.6.2 Hydroamination of Allenes with Arylamines

***N*-[(2*E*)-1-methyl-3-phenylprop-2-en-1-yl]aniline [(*E*)-5]**. Dioxane (0.50 mL) was added to a mixture of aniline (61.4 mg, 0.66 mmol), (**1**)AuCl (15.2 mg, 2.9×10^{-2} mmol), and AgOTf (2.8 mg, 4.1×10^{-2} mmol) and the resulting solution was stirred for 10 minutes at room temperature. 1-Phenyl-1,2-butadiene (**4**) (85 mg, 0.65 mmol) was added

via syringe and the resulting mixture was stirred at 45 °C for 36 h. Column chromatography of the reaction mixture (hexanes–EtOAc = 15:1) gave *N*-[(2*E*)-1-methyl-3-phenylprop-2-en-1-yl]aniline [(*E*)-**5**] (115 mg, 79% yield) as a pale yellow oil. TLC (ether–hexanes = 1:2): R_f = 0.76 ^{1}H NMR: δ 7.34 (d, *J* = 7.0 Hz, 2H), 7.28 (t, *J* = 7.0 Hz, 2H), 7.20 (tt, *J* = 1.0, 7.5 Hz, 1H), 7.15 (t, *J* = 8.0 Hz, 2H), 6.68 (tt, *J* = 1.0, 7.5 Hz, 1H), 6.64 (dd, *J* = 1.5, 6.5 Hz, 2H), 6.56 (dd, *J* = 1.0, 15.0 Hz, 1H), 6.21 (dd, *J* = 6.0, 16.0 Hz, 1H), 4.13 (quintet, *J* = 6.5 Hz, 1H), 3.69 (br s, 1H), 1.39 (d, *J* = 6.5 Hz, 3H) ^{13}C{^{1}H} NMR: δ 147.4, 137.0, 133.3, 133.2, 129.3, 129.2, 128.5, 127.4, 126.4, 117.4, 113.4, 50.9, 22.1 IR (neat, cm^{-1}): 3670, 2975, 2906, 1601, 1495, 1395, 1245, 1061, 883, 746, 690. HRMS calcd (found) for $C_{16}H_{17}N$ (M^+): 223.3128 (223.1366). Anal. calcd (found) for $C_{16}H_{17}N$: C, 86.05 (85.93); H, 7.67 (7.74);

(*S*,*E*)-**5** was synthesized using an analogous method to the procedure above. Enantiomeric purity was established by HPLC equipped with a Chiralpak AD-H column, and determined to be 51 % ee the HPLC trace is right trace shown in Figure 3.10.

3.6.3 Independent synthesis of *N*-[(1*S*,2*E*)-1-methyl-3-phenylprop-2-en-1-yl]aniline [(*S*,*E*)-5][174]

Toluene (1.0 mL) was added to a reaction vial that contained (±)-BINAP (12.3 mg, 0.020 mmol) and heated until the BINAP dissolved (approximately 1 min at 80 °C). The reaction mixture was cooled to room temperature and $Pd(OAc)_2$ (3.6 mg, 0.016 mmol) was added. The walls of the vial were rinsed with one additional portion of toluene (1.0

mL) and the resulting solution was stirred for 2 min at room temperature. Bromobenzene (51.8 mg, 0.33 mmol) and (2*S*, 3*E*)-4-phenylbut-3-en-2-amine [(*S*,*E*)-**7**] (57.1 mg, 0.39 mmol) [(*S*,*E*-**7**) was synthesized via published procedures and its enantiomeric purity (51 % ee) and absolute configuration was established via optical rotation] [171-173] were added via syringe and the reaction mixture was stirred for an additional 2 min. Sodium *tert*-butoxide was added under nitrogen, the reaction was then heated at 80 °C for 72 h. Column chromatography of the reaction mixture (hexanes–EtOAc = 15:1) gave *N*-[(1*S*,2*E*)-1-methyl-3-phenylprop-2-en-1-yl]aniline [(*S*,*E*)-**5**] (26.4 mg, 36% yield) as a pale yellow oil. Enantiomeric purity of (*S*,*E*)- **5** was established by HPLC equipped with a Chiralpak AD-H column, and determined to be 18 % ee the HPLC trace is right trace shown in Figure 3.10.

3.6.4 HPLC traces

Chiral HPLC traces of racemic (left trace) and enantiomerically enriched (middle trace, 51% ee) and S-enriched (right trace, 18% ee) of *N*-[(2*E*)-1-methyl-3-phenylprop-2-en-1-yl]aniline (**5**). The racemic trace is from the reaction of **4** with aniline catalyzed by (**1**)AuCl (5 mol %) and AgOTf (5 mol %) in dioxane at 45 °C for 24 h to form (*E*)-5 in 86 % yield and 0 % ee. The enantiomerically enriched trace is from the reaction of (*R*)-**4** with aniline catalyzed by (**1**)AuCl (5 mol %) and AgOTf (5 mol %) in dioxane at 45 °C for 36 h to form (*S*,*E*)-**5** in 76 % yield and 51 % ee. The *S*-enriched trace is from the synthesis

of enantiomerically enriched (*S*,*E*)-**5** *from* (*E*)-**6** described in the preceding paragraph in 36 % yield and 18 % ee.

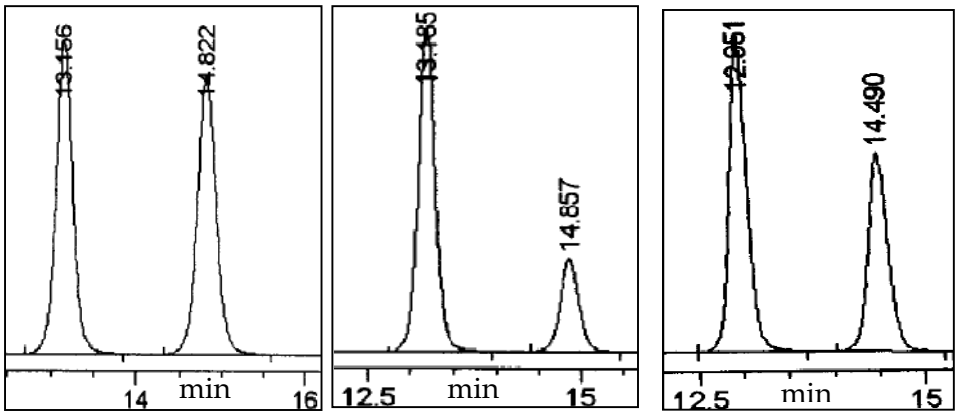

Figure 3.10. HPLC traces of racemic (left trace) and enantiomerically enriched (middle trace, 51% ee) and *S*-enriched (right trace, 18% ee) of (*S*,*E*)- 5

3.6.5 Differential Rate Equation

The kinetics of the catalytic hydroamination were interpreted in the context with Scheme 3.9 (reproduced below), which was constructed on the basis of the following assumptions: (1) rapid ligand exchange to form the active catalyst, (2) pre-equilibrium exists prior to the formation of **V**, (3) steady state treatment approximation to the formation of **VII**, (4) the total catalyst concentration is equal to the formation of **III** and **V**, and (5) aniline is the base. From these assumptions, we derive the rate law for the formation of **3**, which relates the concentration of **VII** to the concentration of benzenaminium(eq 3.9).

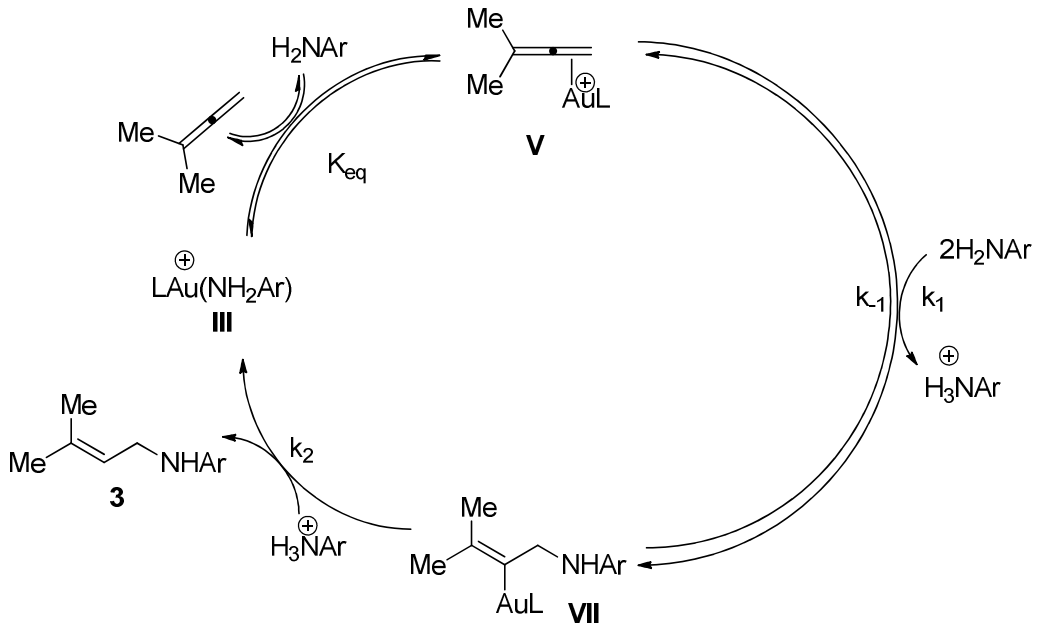

$$\text{rate} = \frac{\text{d}[\mathbf{3}]}{\text{dt}} = k_2[\mathbf{VII}][\text{H}_3\text{N}^+\text{Ph}] \text{(eq 3.12)}$$

$$\frac{\text{d}[\mathbf{VII}]}{\text{dt}} = 0 = k_1[\mathbf{V}][\text{aniline}]^2 - k_{-1}[\mathbf{VII}][\text{H}_3\text{N}^+\text{Ph}] - k_2[\mathbf{VII}][\text{H}_3\text{N}^+\text{Ph}] \text{(eq 3.13)}$$

$$k_1[\mathbf{V}][\text{aniline}]^2 = k_{-1}[\mathbf{VII}][\text{H}_3\text{N}^+\text{Ph}] + k_2[\mathbf{VII}][\text{H}_3\text{N}^+\text{Ph}] \text{ (eq 3.22)}$$

$$k_1[\mathbf{V}][\text{aniline}]^2 = [\mathbf{VII}][\text{H}_3\text{N}^+\text{Ph}](k_{-1} + k_2) \quad \text{(eq 3.23)}$$

$$[\mathbf{VII}][\text{H}_3\text{N}^+\text{Ph}] = \frac{k_1 k_2[\mathbf{V}][\text{aniline}]^2}{(k_{-1} + k_2)} \text{ (eq 3.14)}$$

$$\text{rate} = \frac{k_1 k_2[\mathbf{V}][\text{aniline}]^2}{(k_{-1} + k_2)} \text{ (eq 3.15)}$$

Using the pre-equilibrium for the formation of **V** and the assumption that the total catalyst concentration is equal to **III** and **V** and solving for **V** and substitution into

eq 3.7 produces the three term rate law shown in eq 3.8. When the equilibrium favors aniline complex, the three term rate law depicted in eq 3.8 is simplified to eq 3.9

$$[\mathrm{Au}]_{\mathrm{tot}} = [\mathbf{III}] + [\mathbf{V}] \text{(eq 3.16)}$$

$$[\mathbf{III}] = [\mathrm{Au}]_{\mathrm{tot}} - [\mathbf{V}] \text{(eq 3.17)}$$

$$K_{eq} = \frac{[\mathbf{V}][\mathrm{aniline}]}{[\mathbf{III}][\mathbf{2}]} \text{ (eq 3.18)}$$

$$K_{eq} = \frac{[\mathbf{V}][\mathrm{aniline}]}{([\mathrm{Au}]_{\mathrm{tot}} - [\mathbf{V}])[\mathbf{2}]} \text{ (eq 3.24)}$$

$$K_{eq} = \frac{[\mathbf{V}][\mathrm{aniline}]}{[\mathrm{Au}]_{\mathrm{tot}}[\mathbf{2}] - [\mathbf{V}][\mathbf{2}]} \text{ (eq 3.25)}$$

$$K_{eq}[\mathrm{Au}]_{\mathrm{tot}}[\mathbf{2}] - K_{eq}[\mathbf{V}][\mathbf{2}] = [\mathbf{V}][\mathrm{aniline}] \text{(eq 3.26)}$$

$$K_{eq}[\mathrm{Au}]_{\mathrm{tot}}[\mathbf{2}] = [\mathbf{V}][\mathrm{aniline}] + K_{eq}[\mathbf{V}][\mathbf{2}] \text{(eq 3.27)}$$

$$K_{eq}[\mathrm{Au}]_{\mathrm{tot}}[\mathbf{2}] = [\mathbf{V}]\big([\mathrm{aniline}] + K_{eq}[\mathbf{2}]\big) \text{(eq 3.28)}$$

$$[\mathbf{V}] = \frac{K_{eq}[\mathrm{Au}]_{\mathrm{tot}}[\mathbf{2}]}{K_{eq}[\mathbf{2}] + [\mathrm{aniline}]} \text{ (eq 3.19)}$$

$$\mathrm{Rate} = \frac{k_1 k_2 K_{eq}[\mathrm{Au}]_{\mathrm{tot}}[\mathbf{2}][\mathrm{aniline}]^2}{(k_{-1} + k_2)K_{eq}[\mathbf{2}] + (k_{-1} + k_2)[\mathrm{aniline}]} \text{ (eq 3.20)}$$

If $K_{eq}[\mathbf{2}] \ll [\mathrm{aniline}]$ indicating that equilibrium favors aniline complex then,

$$\mathrm{Rate} \approx \frac{k_1 k_2 K_{eq}[\mathrm{Au}]_{\mathrm{tot}}[\mathbf{2}][\mathrm{aniline}]^2}{(k_{-1} + k_2)[\mathrm{aniline}]} \text{ (eq 3.29)}$$

$$\mathrm{Rate} \approx \frac{k_1 k_2 K_{eq}[\mathrm{Au}]_{\mathrm{tot}}[\mathbf{2}][\mathrm{aniline}]}{(k_{-1} + k_2)} \text{ (eq 3.30)}$$

$$\mathrm{Rate} \approx k_{obs}[\mathrm{Au}]_{\mathrm{tot}}[\mathbf{2}][\mathrm{aniline}] \text{(eq 3.21)}$$

$$\text{Where,} \qquad k_{obs} = \frac{k_1 k_2 K_{eq}}{k_{-1} + k_2} \text{ (eq 3.31)}$$

3.6.6 General Procedure for Kinetic Study of Au(I)-catalyzed Intermolecular Hydroamination of Allenes with Arylamines

Kinetic reactions were performed under standard Schlenk techniques under an atmosphere of dry nitrogen in oven-dried reaction vials at 45 °C. Dioxane was added to a mixture of aniline, (**1**)AuCl, AgOTf, and tetradecane (internal standard) and stirred for 10 minutes at room temperature. 3-methyl-1,2-butadiene was then added via syringe. The disappearance of aniline was monitored by analyzing 10 μL aliquots purified through a cotton plug pipet filled with silica gel with EtOAc via gas chromatography compared to the internal standard tetradecane. Relative concentrations of aniline were determined by integrating the peak of aniline at the start of the reaction relative to the peak of the internal standard at the indicated time with the GC spectrum.

- In a series of experiments the reaction order with respect to aniline for the gold(I)-catalyzed hydroamination of aniline with **2** catalyzed by (**1**)AuCl (5 mol %) and AgOTf (5 mol %) in dioxane at 45 °C was determined by analyzing aniline concentration from 0.06 M to 0.40 M as shown in Figure 3.12 to Figure 3.15, and Figure 3.17.
- In a series of experiments the reaction order with respect to gold catalyst for the gold(I)-catalyzed hydroamination of aniline with **2** catalyzed by (**1**)AuCl (5 mol %) and AgOTf (5 mol %) in dioxane at 45 °C was determined by analyzing catalyst concentration from 18 mM to 54 mM as shown in Figure 3.21 to Figure 3.23.

- In a series of experiments the reaction order with respect to **2** for the gold(I)-catalyzed hydroamination of aniline with **2** catalyzed by (**1**)AuCl (5 mol %) and AgOTf (5 mol %) in dioxane at 45 °C was determined by analyzing catalyst concentration from 18 mM to 54 mM as shown in Figure 3.15 to Figure 3.17, Figure 3.18 to Figure 3.20, and Figure 3.23.

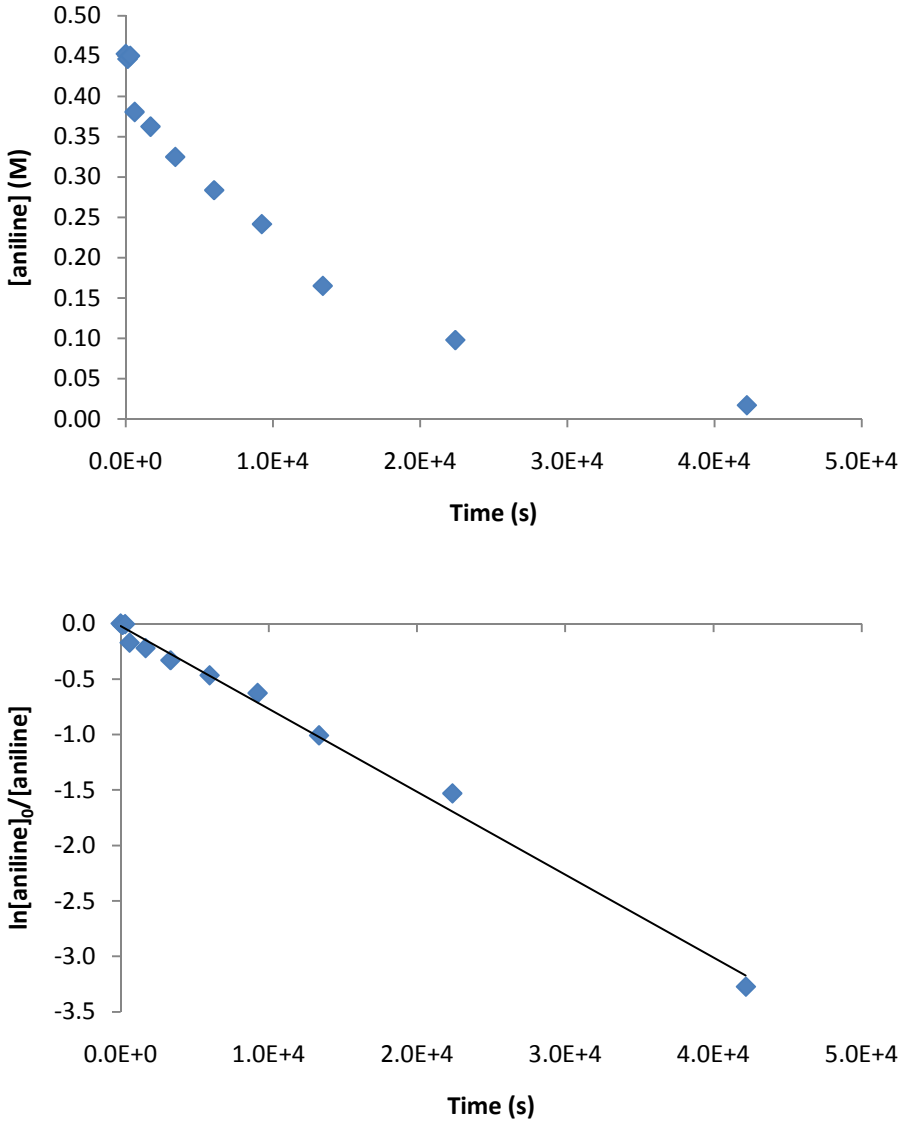

Figure 3.11. Concentration versus time (top) and pseudo first-order (bottom) plots for the gold(I)-catalyzed intermolecular hydroamination of 3-methyl-1,2-butadiene with aniline catalyzed by (1)AuCl/AgOTf in dioxane at 45 °C. [Aniline] = 0.45 M, [2] = 1.4 M, [(1)AuCl] = 19 mM k_{obs} = 0.75 ± 0.09 x 10^{-4} s^{-1} (Table 3.1, entry 1).

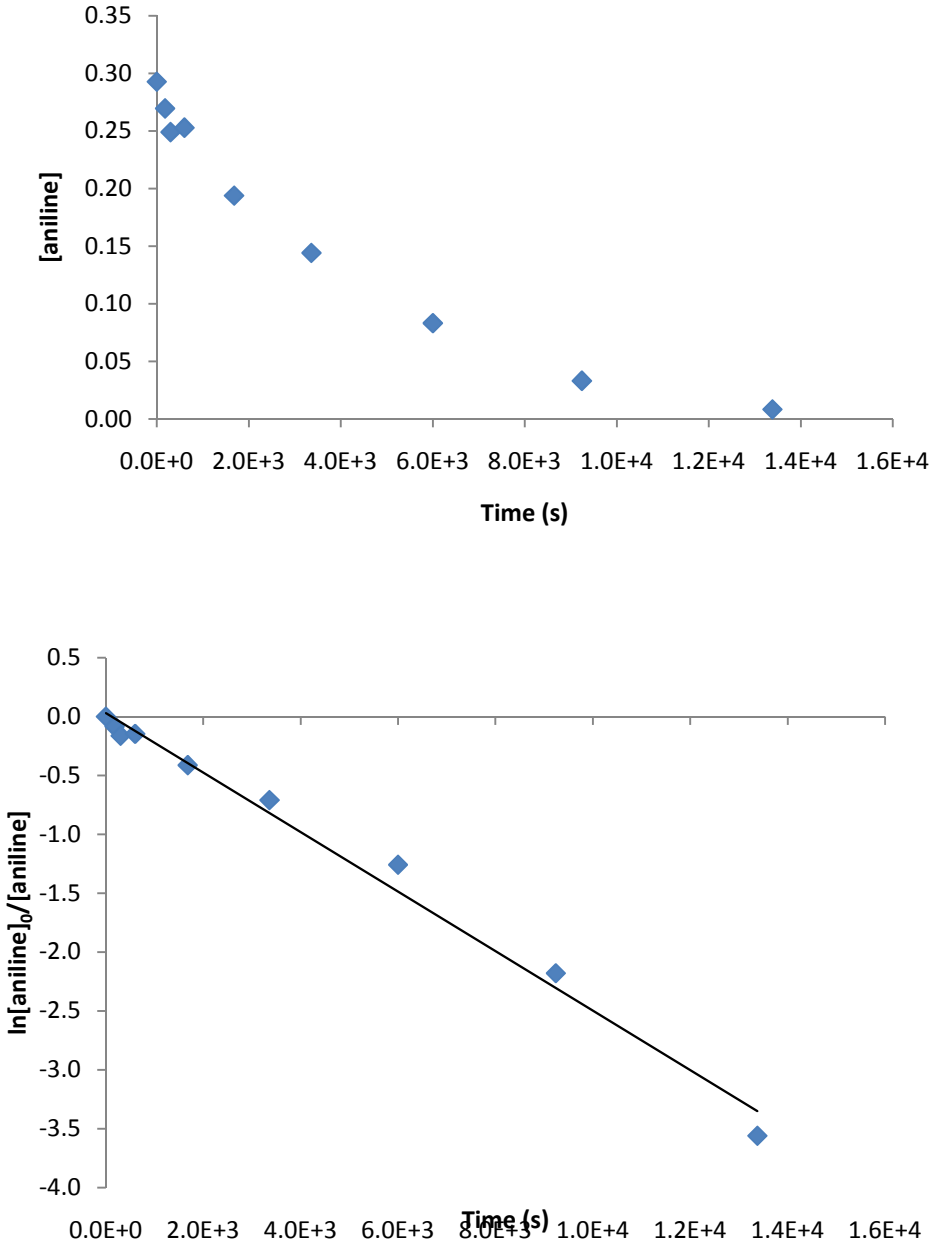

Figure 3.12. Concentration versus time (top) and pseudo first-order (bottom) plots for the gold(I)-catalyzed intermolecular hydroamination of 3-methyl-1,2-butadiene with aniline catalyzed by (1)AuCl/AgOTf in dioxane at 45 °C. [Aniline] = 0.29 M, [2] = 2.8 M, [(1)AuCl] = 18 mM k_{obs} = 2.5 ± 0.1 x 10^{-4} s^{-1} (Table 3.1, entry 2)

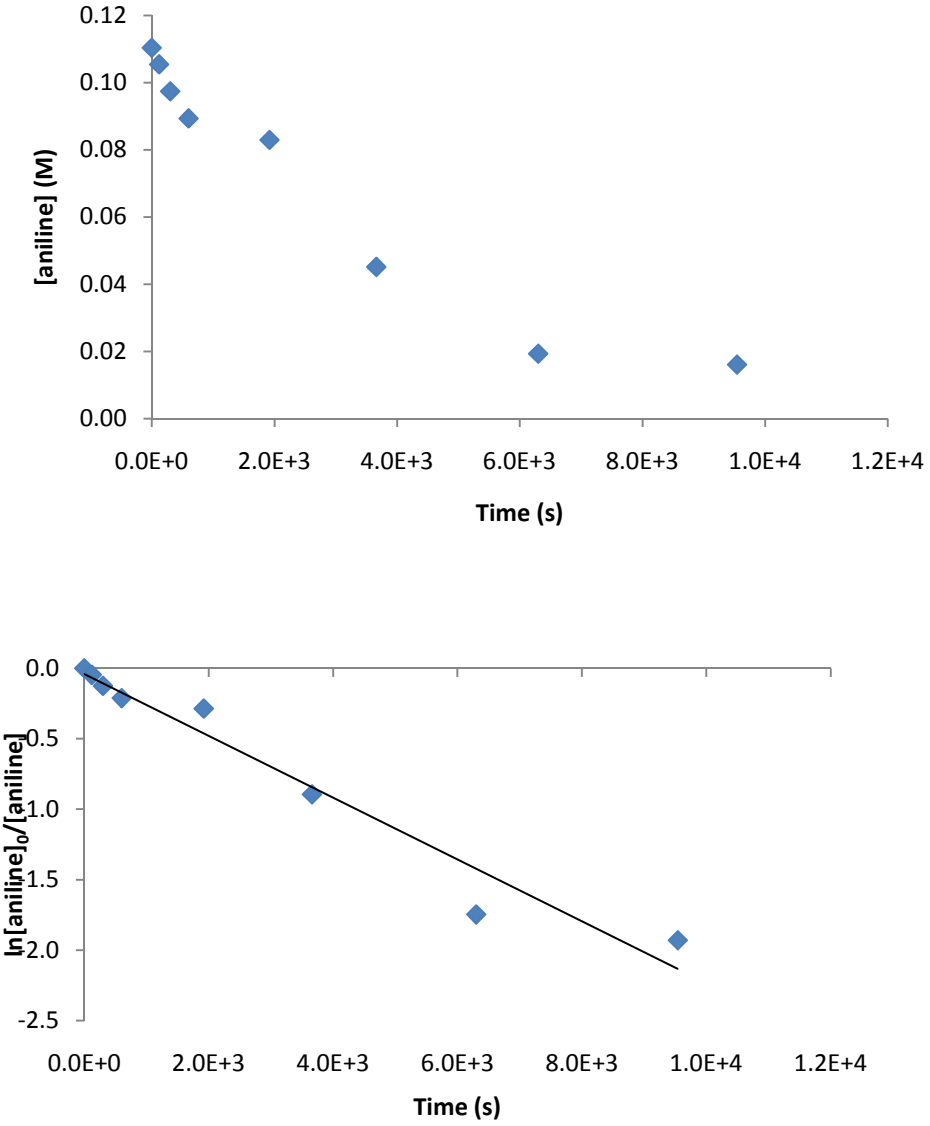

Figure 3.13. Concentration versus time (top) and pseudo first-order (bottom) plots for the gold(I)-catalyzed intermolecular hydroamination of 3-methyl-1,2-butadiene with aniline catalyzed by (1)AuCl/AgOTf in dioxane at 45 °C. [Aniline] = 0.11 M, [2] = 1.4 M, [(1)AuCl] = 20 mM k_{obs} = 2.2 ± 0.2 x 10^{-4} s^{-1} (Table 3.1, entry 3)

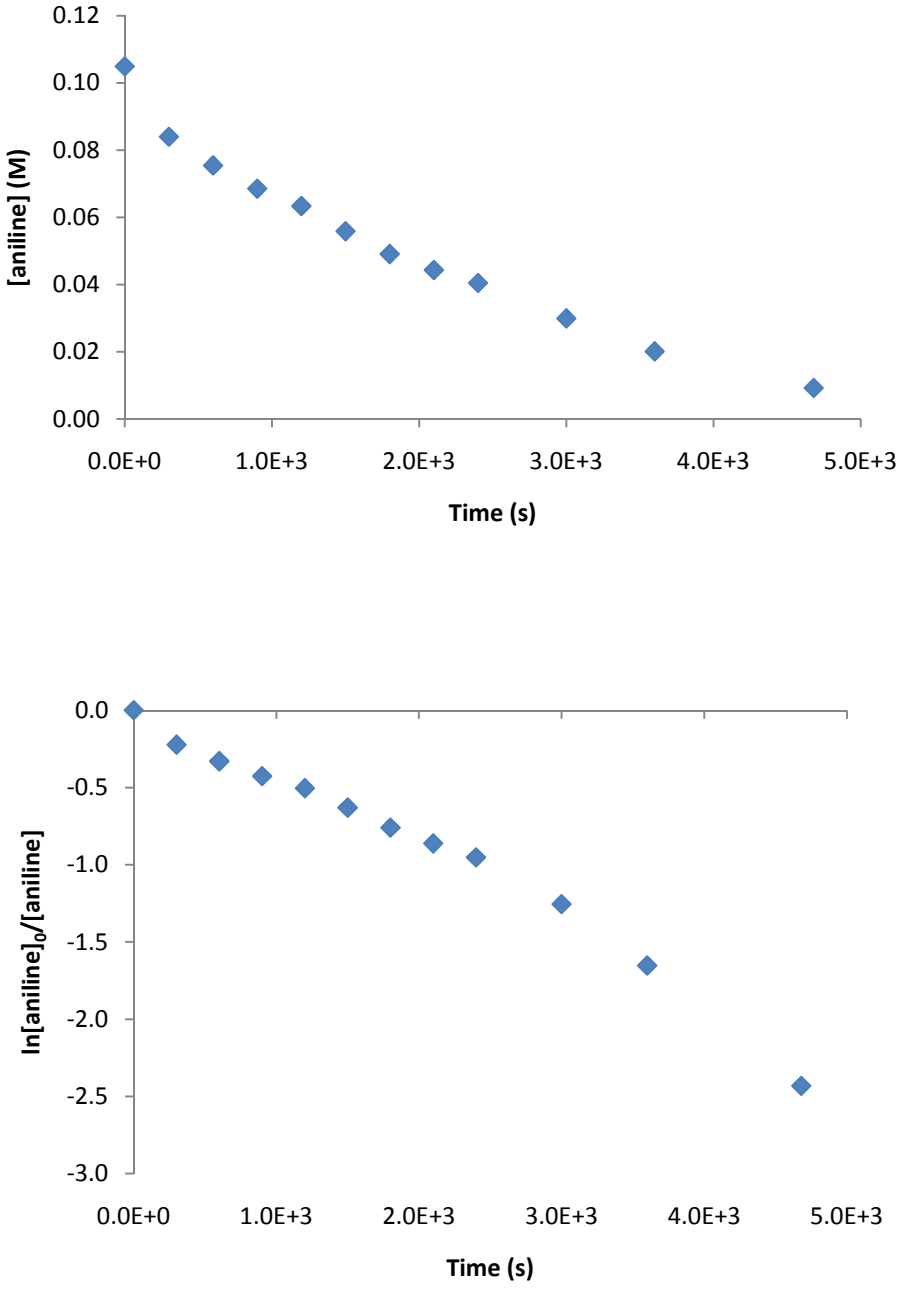

Figure 3.14. Concentration versus time (top) and pseudo first-order (bottom) plots for the gold(I)-catalyzed intermolecular hydroamination of 3-methyl-1,2-butadiene with aniline catalyzed by (1)AuCl/AgOTf in dioxane at 45 °C. [Aniline] = 0.10 M, [2] = 1.7 M, [(1)AuCl] = 19 mM (Table 3.1, entry 4)

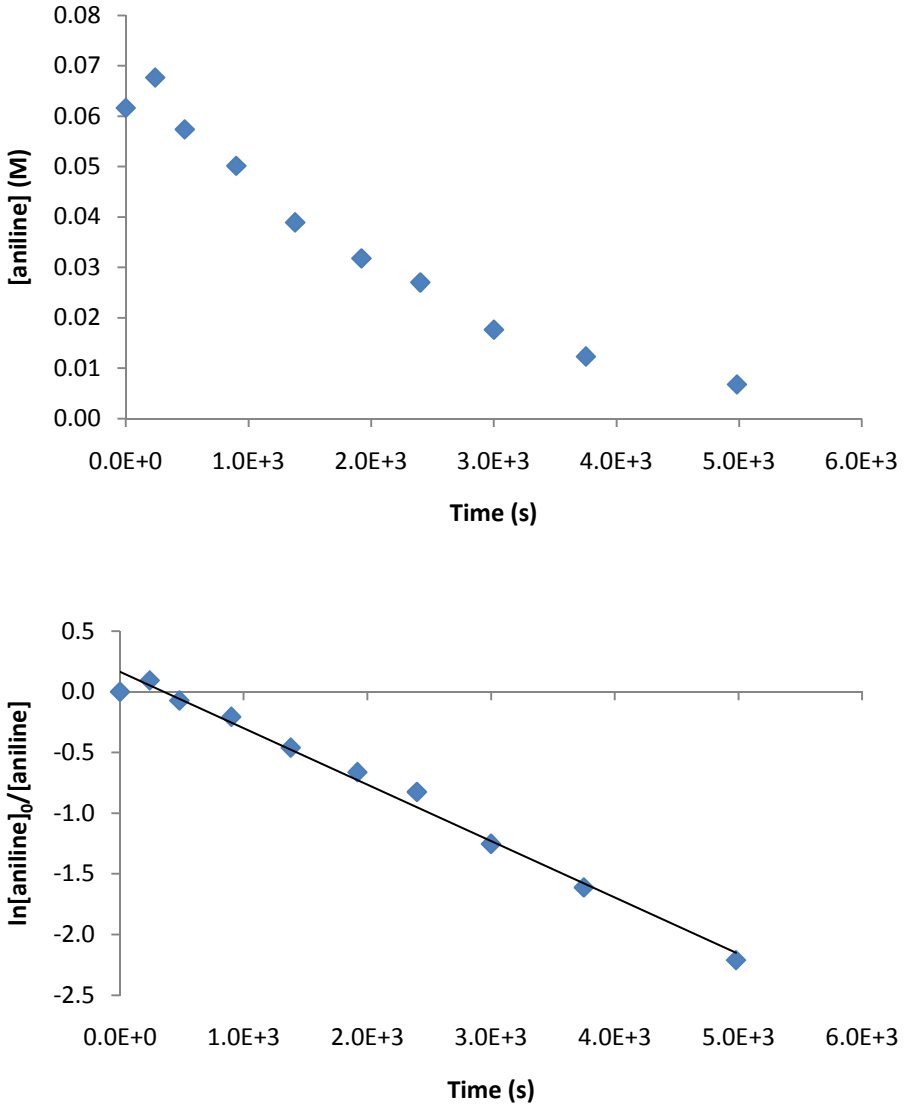

Figure 3.15. Concentration versus time (top) and pseudo first-order (bottom) plots for the gold(I)-catalyzed intermolecular hydroamination of 3-methyl-1,2-butadiene with aniline catalyzed by (1)AuCl/AgOTf in dioxane at 45 °C. [Aniline] = 0.06 M, [2] = 0.73 M, [(1)AuCl] = 18 mM k_{obs} = 4.6 ± 0.1 x 10^{-4} s^{-1} (Table 3.1, entry 5).

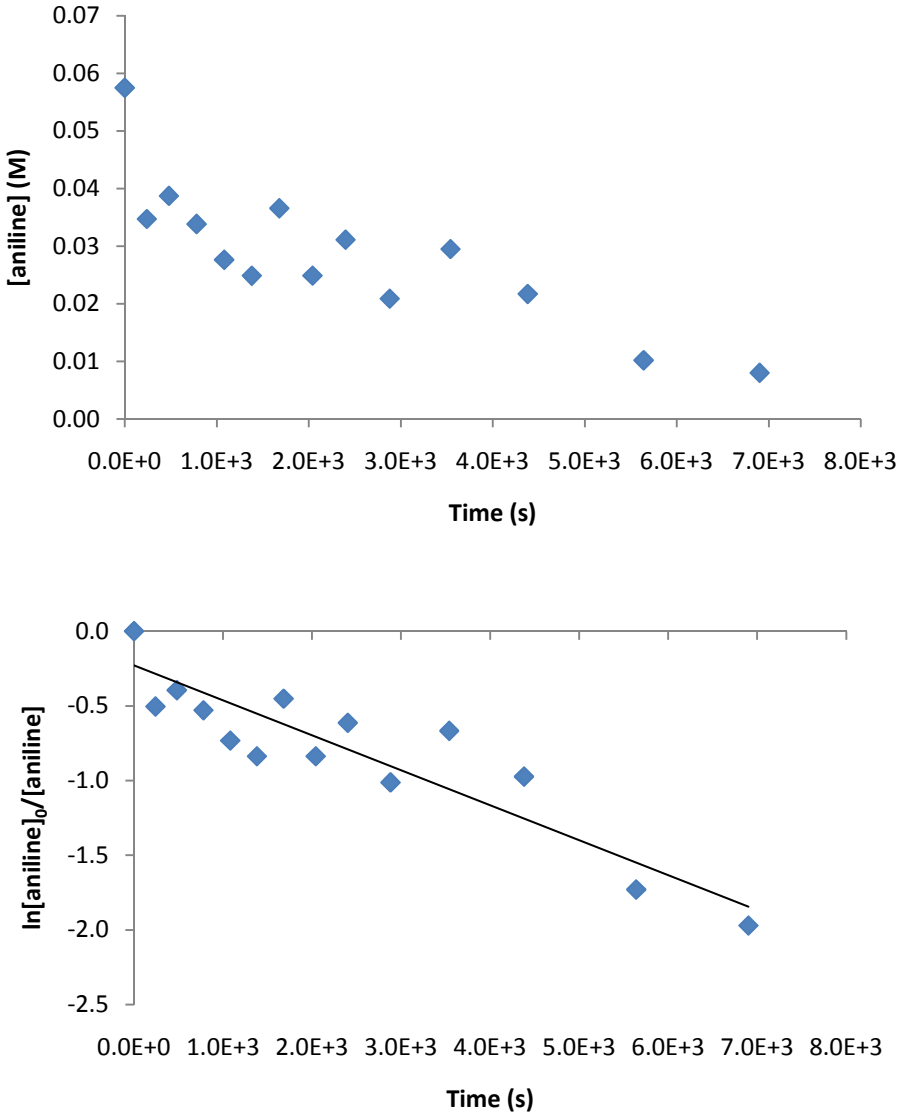

Figure 3.16. Concentration versus time (top) and pseudo first-order (bottom) plots for the gold(I)-catalyzed intermolecular hydroamination of 3-methyl-1,2-butadiene with aniline catalyzed by (1)AuCl/AgOTf in dioxane at 45 °C. [Aniline] = 0.06 M, [2] = 0.38 M, [(1)AuCl] = 19 mM k_{obs} = 2.3 ± 0.2 x 10^{-4} s^{-1} (Table 3.1, entry 6)

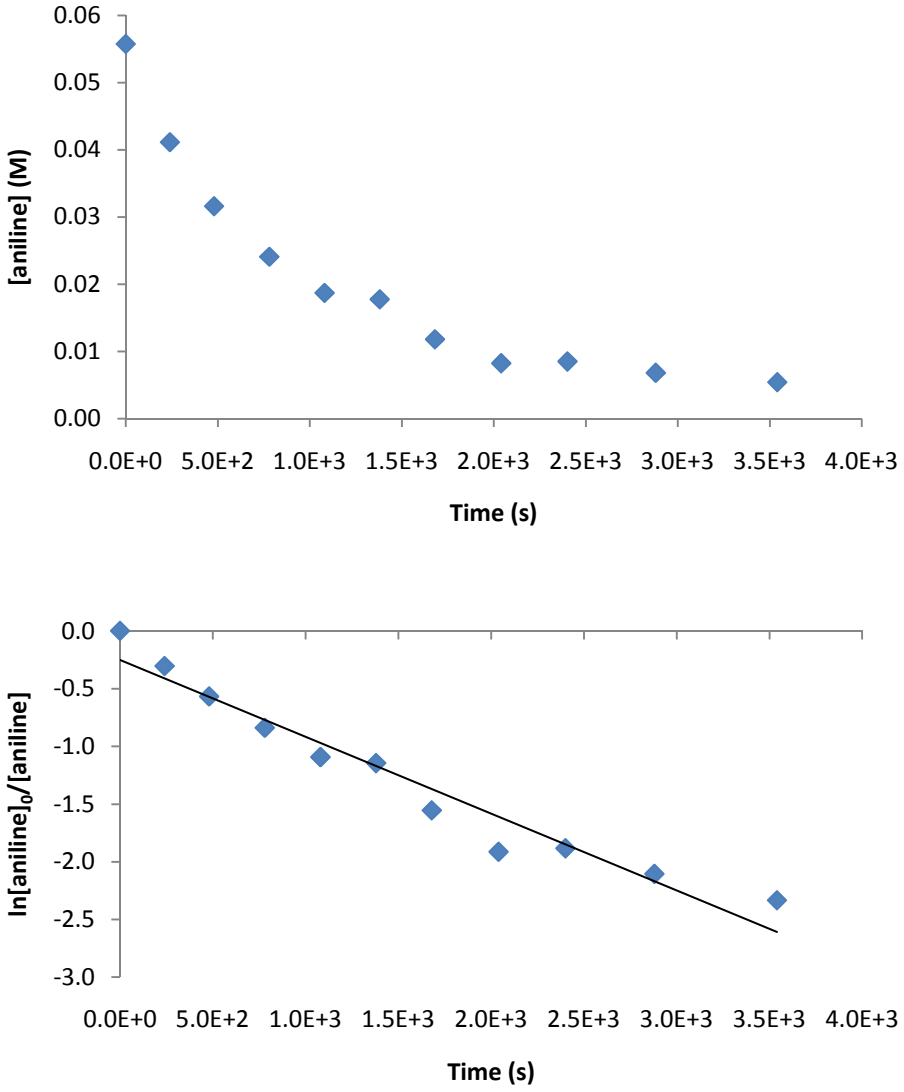

Figure 3.17. Concentration versus time (top) and pseudo first-order (bottom) plots for the gold(I)-catalyzed intermolecular hydroamination of 3-methyl-1,2-butadiene with aniline catalyzed by (1)AuCl/AgOTf in dioxane at 45 °C. [Aniline] = 0.06 M, [2] = 1.4 M, [(1)AuCl] = 18 mM k_{obs} = 6.6 ± 0.4 x 10^{-4} s^{-1} (Table 3.1, entry 7).

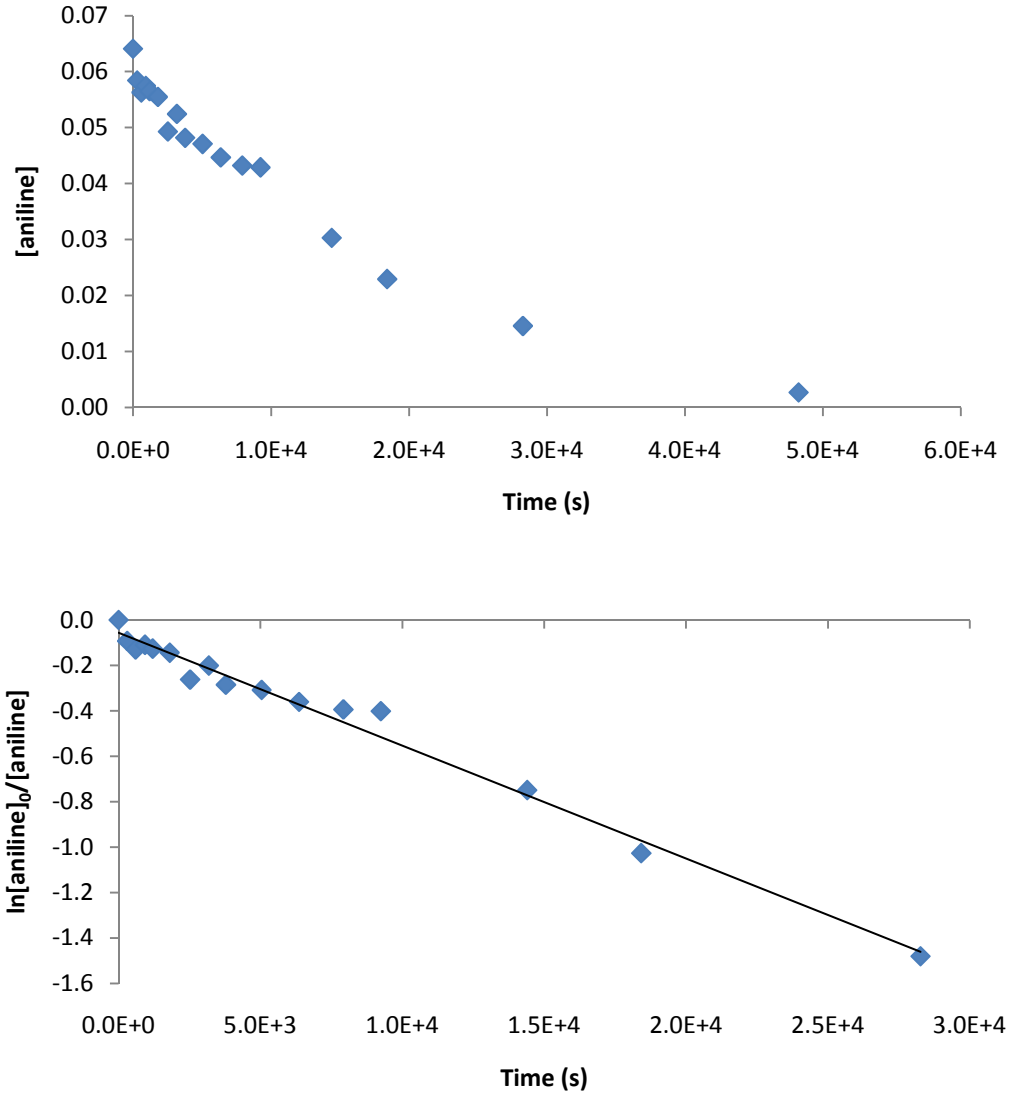

Figure 3.18. Concentration versus time (top) and pseudo first-order (bottom) plots for the gold(I)-catalyzed intermolecular hydroamination of 3-methyl-1,2-butadiene with aniline catalyzed by (1)AuCl/AgOTf in dioxane at 45 °C. [Aniline] = 0.06 M, [2] = 0.25 M, [(1)AuCl] = 18 mM k_{obs} = 0.60 ± 0.12 x 10^{-4} s^{-1} (Table 3.1, entry 8).

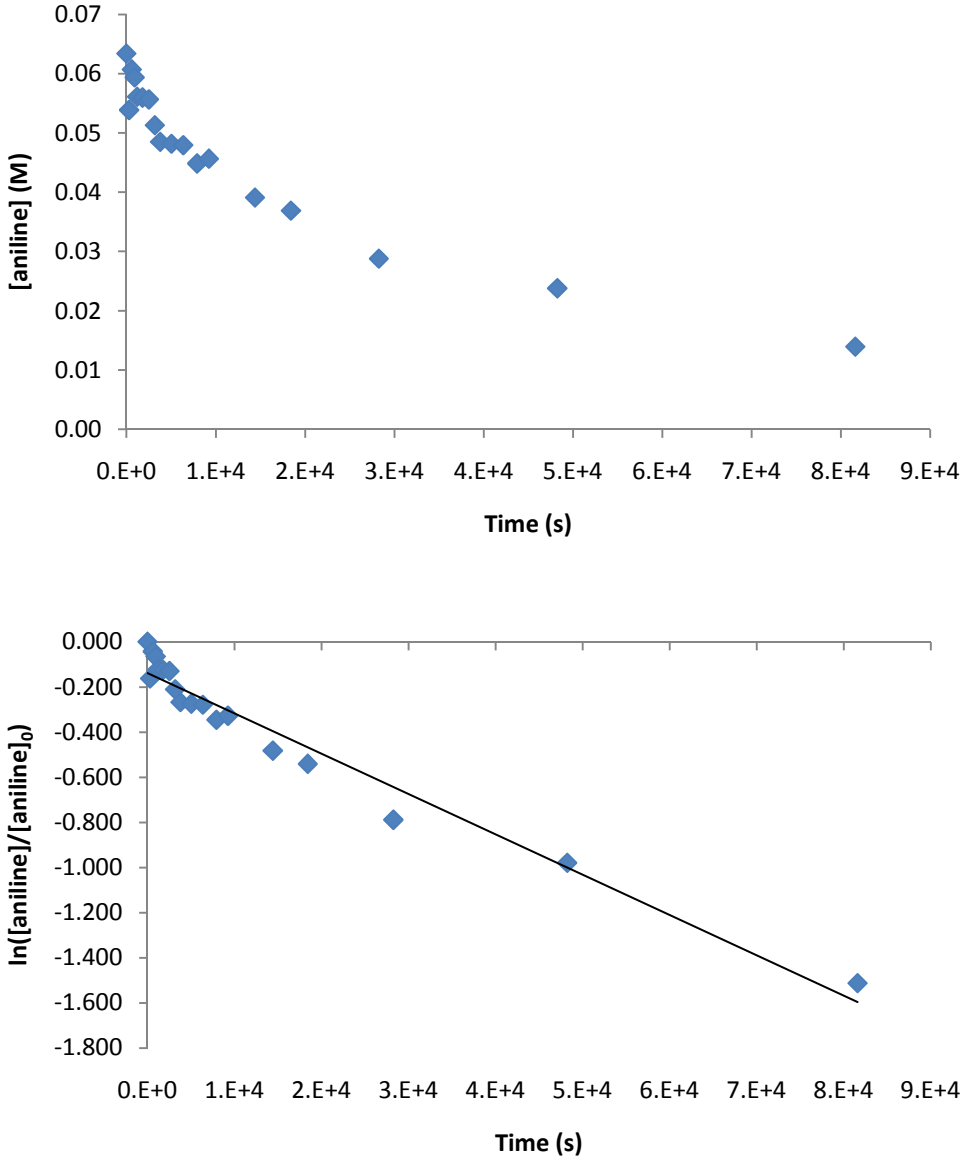

Figure 3.19. Concentration versus time (top) and pseudo first-order (bottom) plots for the gold(I)-catalyzed intermolecular hydroamination of 3-methyl-1,2-butadiene with aniline catalyzed by (1)AuCl/AgOTf in dioxane at 45 °C. [Aniline] = 0.06 M, [2] = 0.13 M, [(1)AuCl] = 19 mM k_{obs} = 0.18 ± 0.08 x 10^{-4} s^{-1} (Table 3.1, entry 9).

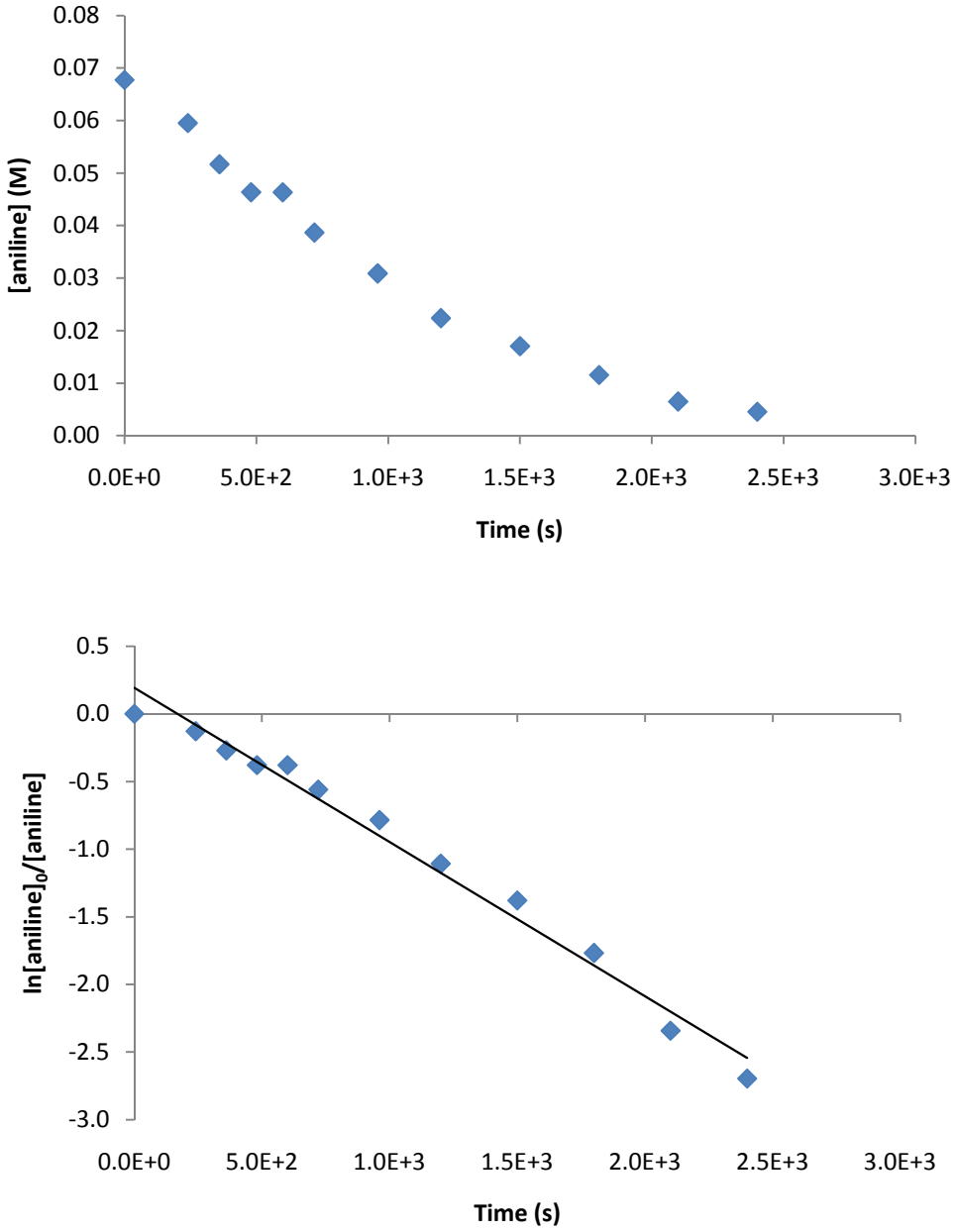

Figure 3.20. Concentration versus time (top) and pseudo first-order (bottom) plots for the gold(I)-catalyzed intermolecular hydroamination of 3-methyl-1,2-butadiene with aniline catalyzed by (1)AuCl/AgOTf in dioxane at 45 °C. [Aniline] = 0.07 M, [2] = 2.4 M, [(1)AuCl] = 19 mM k_{obs} = 11.4 ± 0.3 x 10^{-4} s^{-1} (Table 3.1, entry 10).

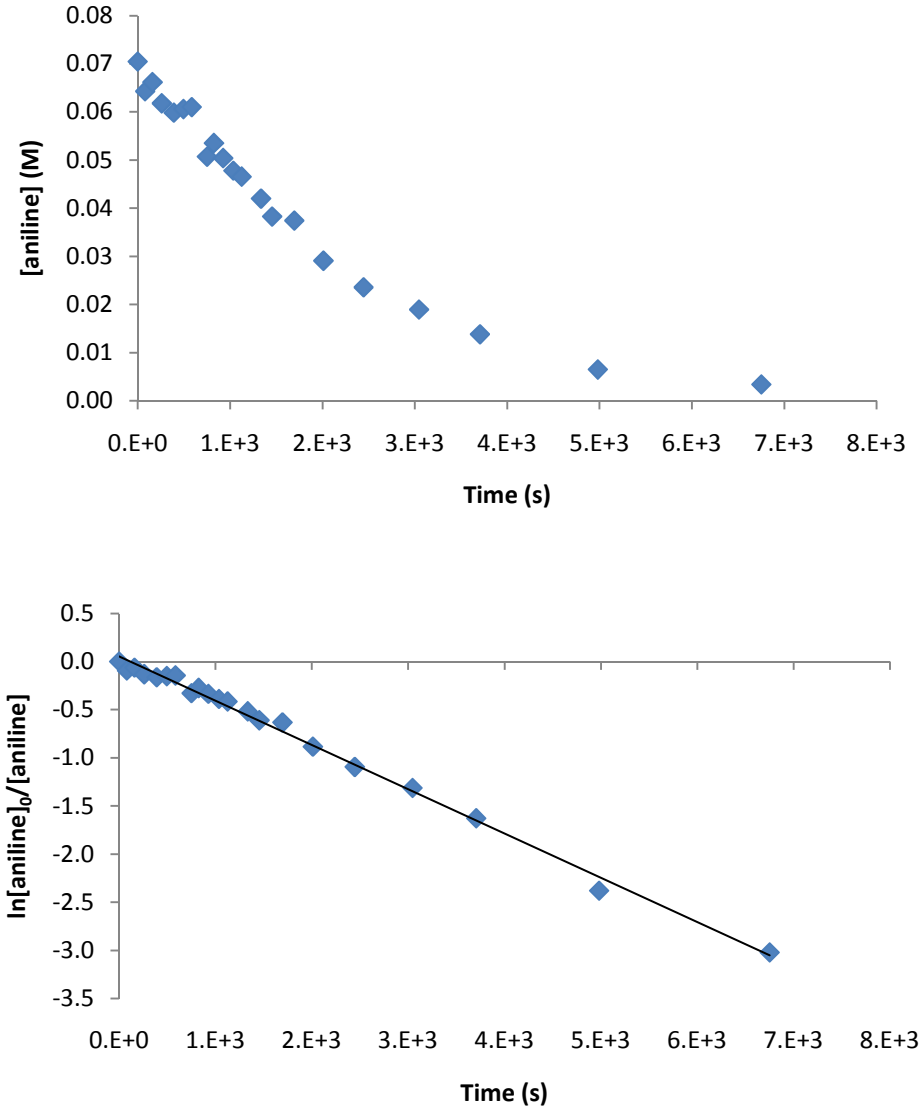

Figure 3.21. Concentration versus time (top) and pseudo first-order (bottom) plots for the gold(I)-catalyzed intermolecular hydroamination of 3-methyl-1,2-butadiene with aniline catalyzed by (1)AuCl/AgOTf in dioxane at 45 °C. [Aniline] = 0.07 M, [2] = 0.80 M, [(1)AuCl] = 36 mM k_{obs} = 4.6 ± 0.1 x 10^{-4} s^{-1} (Table 3.1, entry 11).

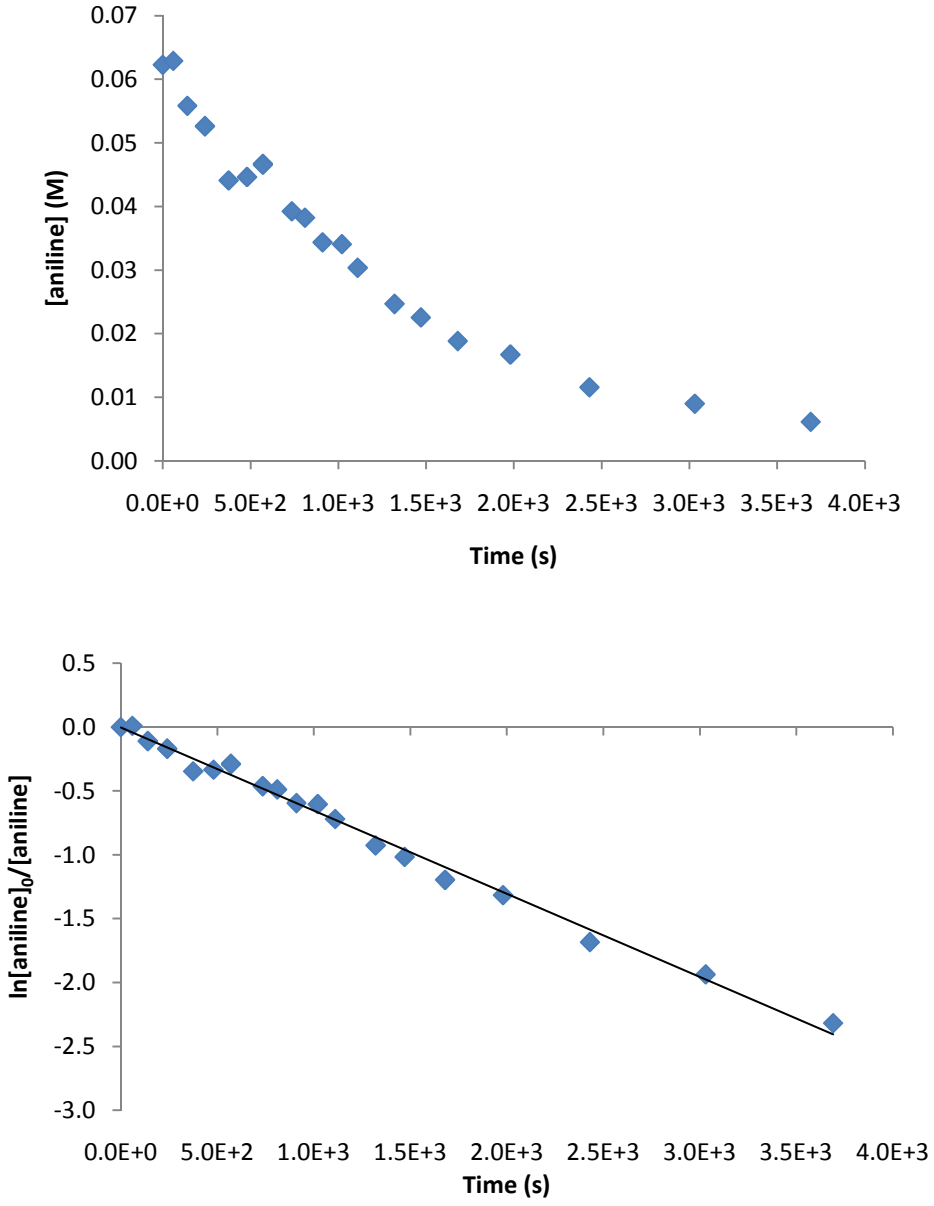

Figure 3.22. Concentration versus time (top) and pseudo first-order (bottom) plots for the gold(I)-catalyzed intermolecular hydroamination of 3-methyl-1,2-butadiene with aniline catalyzed by (1)AuCl/AgOTf in dioxane at 45 °C. [Aniline] = 0.06 M, [2] = 0.83 M, [(1)AuCl] = 54 mM k_{obs} = 6.5 ± 0.1 x 10^{-4} s^{-1} (Table 3.1, entry 12).

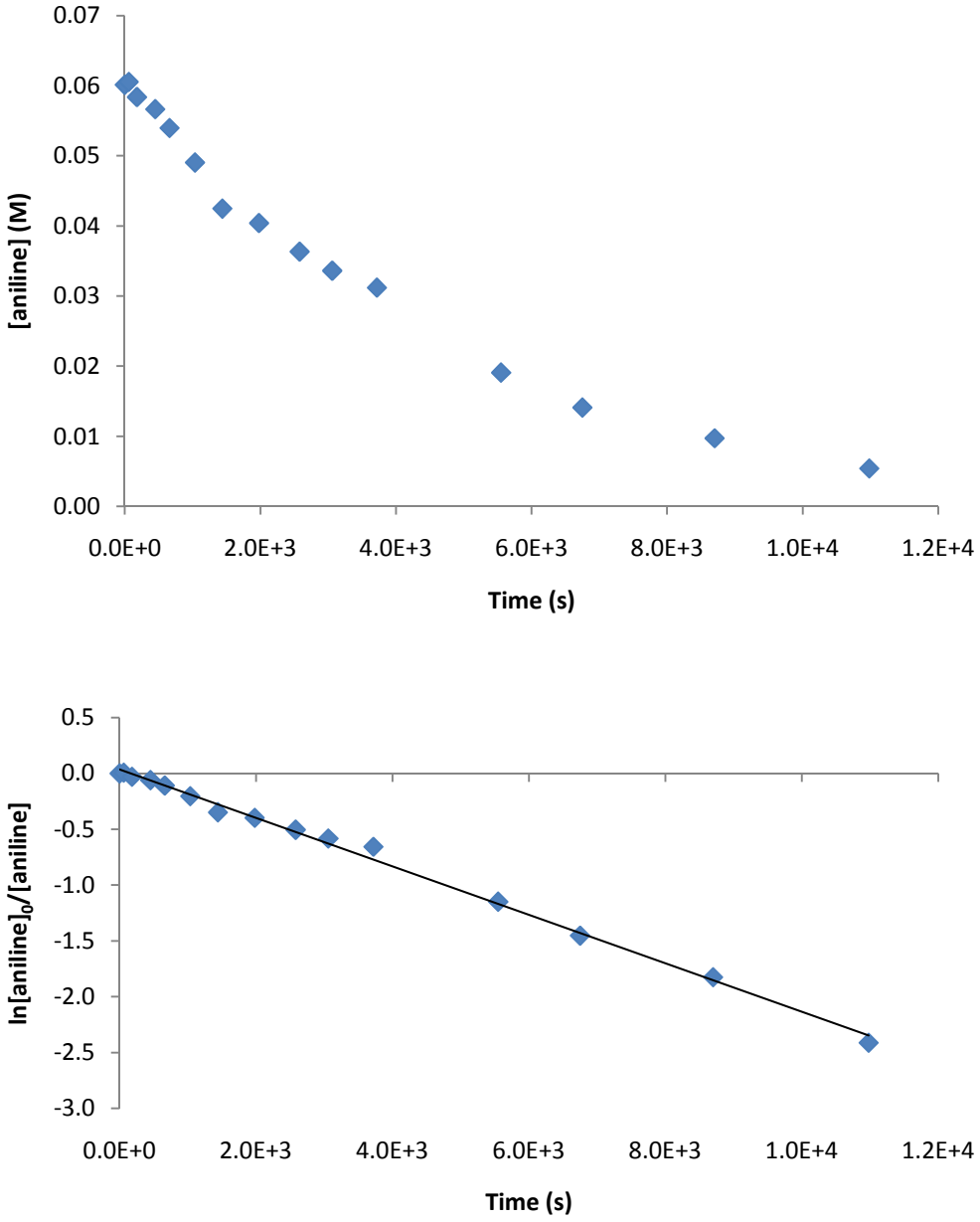

Figure 3.23. Concentration versus time (top) and pseudo first-order (bottom) plots for the gold(I)-catalyzed intermolecular hydroamination of 3-methyl-1,2-butadiene with aniline catalyzed by (1)AuCl/AgOTf in dioxane at 45 °C. [Aniline] = 0.06 M, [2] = 0.88 M, [(1)AuCl] = 18 mM k_{obs} = 2.17 ± 0.04 x 10^{-4} s^{-1} (Table 3.1, entry 13).

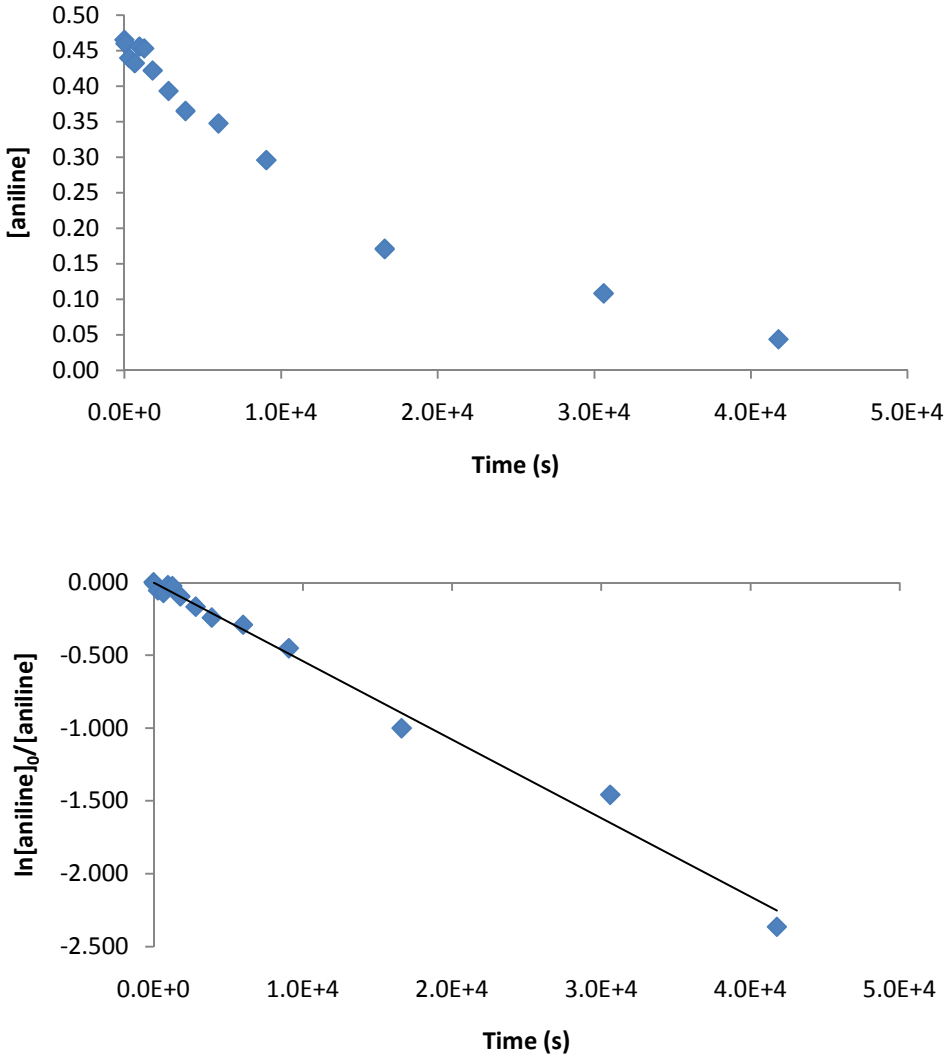

Figure 3.24. Concentration versus time (top) and pseudo first-order (bottom) plots for the gold(I)-catalyzed intermolecular hydroamination of 3-methyl-1,2-butadiene with aniline catalyzed by (1)AuCl/AgOTf in dioxane at 45 °C. [Aniline] = 0.46 M, [2] = 0.90 M, [(1)AuCl] = 20 mM k_{obs} = 0.54 ± 0.08 x 10^{-4} s^{-1} (Table 3.1, entry 14).

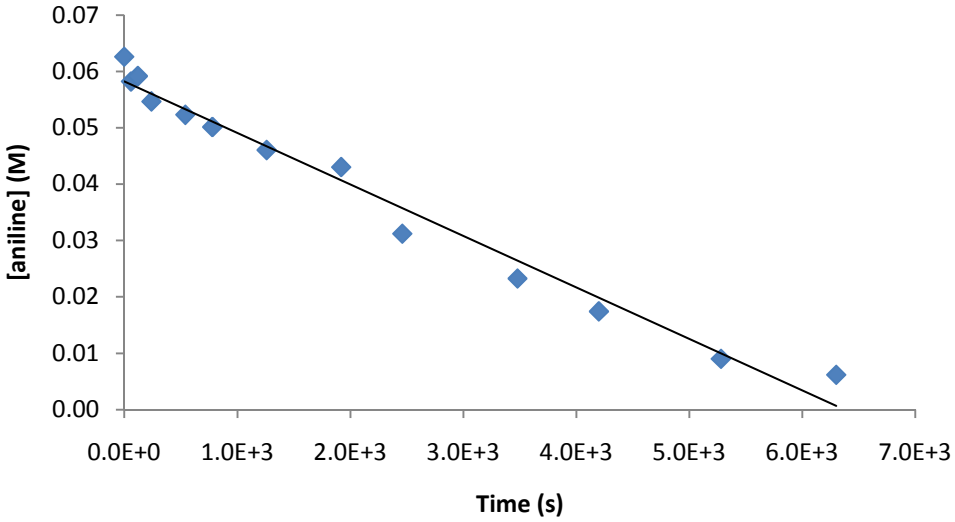

Figure 3.25. Concentration versus time (top) and pseudo first-order (bottom) plots for the gold(I)-catalyzed intermolecular hydroamination of 3-methyl-1,2-butadiene with aniline catalyzed by (1)AuCl/AgOTf in dioxane at 45 °C. [Aniline] = 0.06 M, [2] = 0.72 M, [(1)AuCl] = 18 mM, and [Bu_4NOTf] = 0.06 M k_{obs} = 3.5 x 10^{-5} Ms^{-1} (Table 3.2, entry 2)

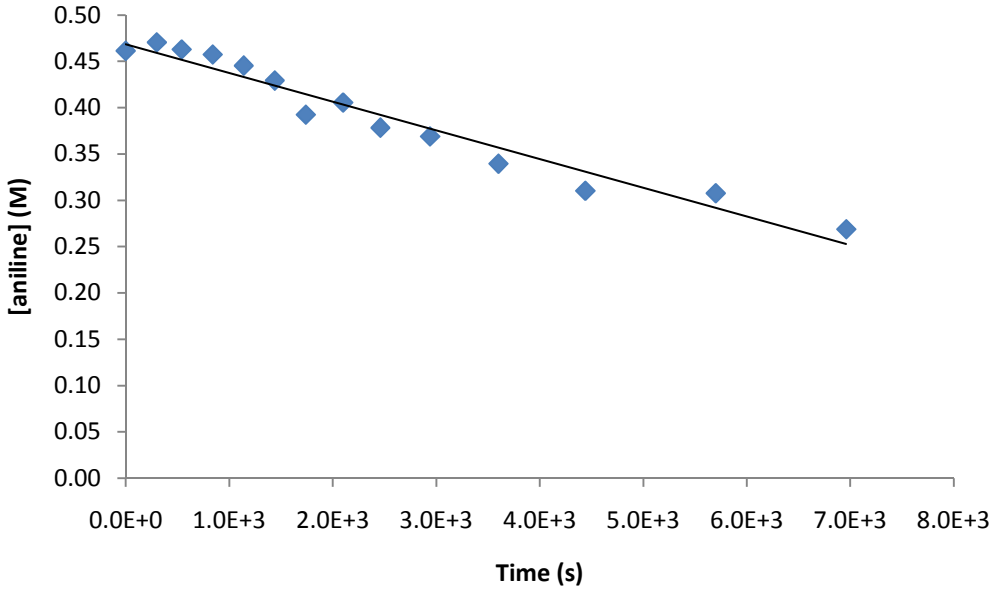

Figure 3.26. Concentration versus time plot for the gold(I)-catalyzed intermolecular hydroamination of 3-methyl-1,2-butadiene with aniline catalyzed by (1)AuCl/AgOTf in dioxane at 45 °C. [Aniline] = 0.46 M, [2] = 1.3 M, [(1)AuCl] = 20 mM k_{obs} = 0.31 ± 0.02 x 10^{-5} Ms^{-1} (Table 3.3, entry 1).

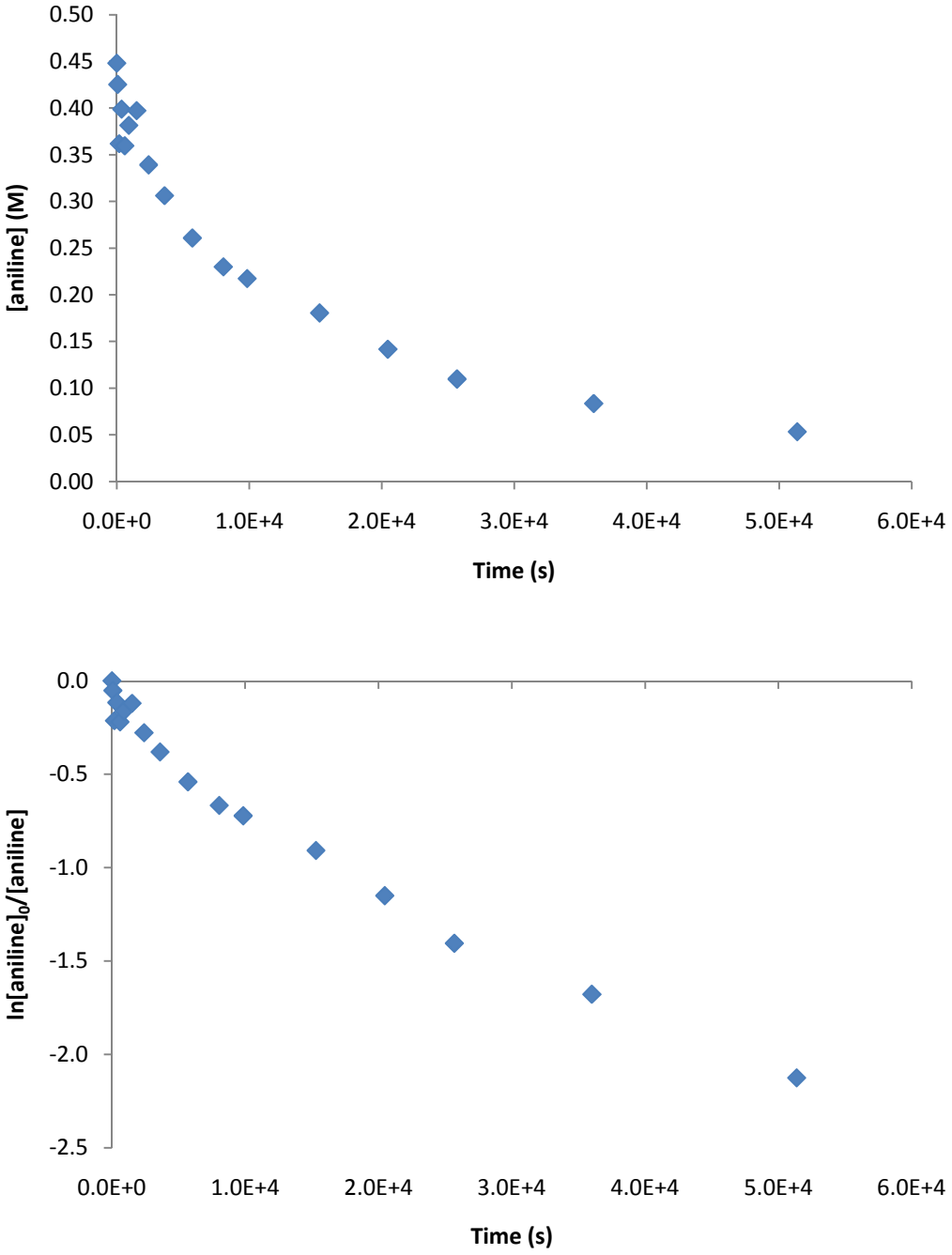

Figure 3.27. Concentration versus time (top) and pseudo first-order (bottom) plots for the gold(I)-catalyzed intermolecular hydroamination of 3-methyl-1,2-butadiene with aniline ([3-methyl-1,2-butadiene]$_0$ = 1.3 M [aniline-d$_2$]$_0$ = 0.5 M, [(1)AuCl = 20.1 mM) in dioxane at 45 °C (Table 3.3, entry 2).

References

(1) King, A. G.; Meinwald, J. *Chem. Rev.* **1996**, *96*, 1105.

(2) O'Hagan, D. *Nat. Prod. Rep.* **2000**, *17*, 435.

(3) Mitchinson, A.; Nadin, A. *Perkin 1* **2000**, 2862.

(4) Katritzky, A. R.; Jug, K.; Oniciu, D. C. *Chem. Rev.* **2001**, *101*, 1421.

(5) Doye, S. *Sci. Synth.* **2009**, *40a*, 241.

(6) Muller, T. E.; Hultzsch, K. C.; Yus, M.; Foubelo, F.; Tada, M. *Chem. Rev.* **2008**, *108*, 3795.

(7) Coulson, D. R. *J. Org. Chem.* **1973**, *38*, 1483.

(8) Besson, L.; Gore, J.; Cazes, B. *Tetrahedron Lett.* **1995**, *36*, 3857.

(9) Al-Masum, M.; Meguro, M.; Yamamoto, Y. *Tetrahedron Lett.* **1997**, *38*, 6071.

(10) Walsh, P. J.; Baranger, A. M.; Bergman, R. G. *J. Am. Chem. Soc.* **1992**, *114*, 1708.

(11) Johnson, J. S.; Bergman, R. G. *J. Am. Chem. Soc.* **2001**, *123*, 2923.

(12) Straub, B. F.; Bergman, R. G. *Angew. Chem., Int. Ed.* **2001**, *40*, 4632.

(13) Pohlki, F.; Doye, S. *Angew. Chem., Int. Ed.* **2001**, *40*, 2305.

(14) Zhang, Z.; Schafer, L. L. *Org. Lett.* **2003**, *5*, 4733.

(15) Ayinla, R. O.; Schafer, L. L. *Inorg. Chim. Acta* **2006**, *359*, 3097.

(16) Haak, E.; Bytschkov, I.; Doye, S. *Angew. Chem., Int. Ed.* **1999**, *38*, 3389.

(17) Haak, E.; Siebeneicher, H.; Doye, S. *Org. Lett.* **2000**, *2*, 1935.

(18) Shi, Y.; Ciszewski, J. T.; Odom, A. L. *Organometallics* **2001**, *20*, 3967.

(19) Cao, C.; Ciszewski, J. T.; Odom, A. L. *Organometallics* **2001**, *20*, 5011.

(20) Anderson, L. L.; Arnold, J.; Bergman, R. G. *Org. Lett.* **2004**, *6*, 2519.

(21) Naoko, N.; Yoshinori, Y. *Angew. Chem., Int. Ed.* **2006**, *45*, 3314.

(22) Zeng, X.; Soleilhavoup, M.; Bertrand, G. *Org. Lett.* **2009**, *11*, 3166.

(23) Nishina, N.; Yamamoto, Y. *Synlett* **2007**, 1767.

(24) Kinder, R. E.; Zhang, Z.; Widenhoefer, R. A. *Org. Lett.* **2008**, *10*, 3157.

(25) Hall, H. K. *J. Am. Chem. Soc.* **1957**, *79*, 5441.

(26) Wang, Z. J.; Benitez, D.; Tkatchouk, E.; Goddard, W. A., III; Toste, F. D. *J. Am. Chem. Soc.* **2010**, *132*, 13064.

(27) Toups, K. L.; Widenhoefer, R. A. *Chem. Commun. (Cambridge, U. K.)*, *46*, 1712.

(28) Chehade, K. A. H.; Andres, D. A.; Morimoto, H.; Spielmann, H. P. *J. Org. Chem.* **2000**, *65*, 3027.

(29) Minutolo, F.; Bertini, S.; Betti, L.; Di Bussolo, V.; Giannaccini, G.; Placanica, G.; Rapposelli, S.; Spielmann, H. P.; Macchia, M. *Il Farmaco* **2003**, *58*, 1277.

(30) Zhang, Z.; Lee, S. D.; Widenhoefer, R. A. *J. Am. Chem. Soc.* **2009**, *131*, 5372.

(31) Kinder, R. E.; Zhang, Z.; Widenhoefer, R. A. *Org. Lett.* **2008**, *10*, 3157.

(32) Zhang, Z.; Liu, C.; Kinder, R. E.; Han, X.; Qian, H.; Widenhoefer, R. A. *J. Am. Chem. Soc.* **2006**, *128*, 9066.

(33) Zhang, Z.; Widenhoefer, R. A. *Org. Lett.* **2008**, *10*, 2079.

(34) Alexakis, A.; Marek, I.; Mangeney, P.; Normant, J. F. *J. Am. Chem. Soc.* **1990**, *112*, 8042.

(35) Myers, A. G.; Zheng, B. *J. Am. Chem. Soc.* **1996**, *118*, 4492.

(36) Zhang, Z.; Widenhoefer, R. A. *Org. Lett.* **2008**, *10*, 2079.

(37) Yang, S.-C.; Hsu, Y.-C.; Gan, K.-H. *Tetrahedron* **2006**, *62*, 3949.

(38) Matsushima, R.; Hiramatsu, K.; Shimamoto, K. *Bull. Chem. Soc. Jpn.* **1994**, *67*, 1479.

(39) Mustafin, A. G.; Gimadieva, A. R.; Khalilov, I. N.; Spirikhin, L. V.; Fatykhov, A. A.; Nurushev, R. A.; Abdrakhmanov, I. B.; Tolstikov, G. A. *Russ. Chem. Bull.* **1998**, *47*, 188.

(40) Yuusaku, Y.; Noriko, T.; Hidemasa, H.; Satoru, K.; Natsume, T.; Hiroaki, O. *Adv. Synth. Catal.* **2007**, *349*, 662.

(41) Lee, O.-Y.; Law, K.-L.; Ho, C.-Y.; Yang, D. *J. Org. Chem.* **2008**, *73*, 8829.

(42) Fuerstner, A.; Davies, P.W. *J. Am. Chem. Soc.* **2005,** 127, 15024.

(43) Inada, S.; Kurata, R. *Bull. Chem. Soc. Jpn.* **1981**, *54*, 1581.

(44) Gagn, M. R.; Brard, L.; Conticello, V. P.; Giardello, M. A.; Stern, C. L.; Marks, T. J. *Organometallics* **1992**, *11*, 2003.

(45) Fadini, L.; Togni, A. *Chem. Commun.* **2003**, 30.

(46) Hartung, C. G.; Breindl, C.; Tillack, A.; Beller, M. *Tetrahedron* **2000**, *56*, 5157.

(47) Hong, S.; Marks, T. J. *Acc. Chem. Res.* **2004**, *37*, 673.

(48) Hong, S.; Marks, T. J. *J. Am. Chem. Soc.* **2002**, *124*, 7886.

(49) Kim, Y. K.; Livinghouse, T.; Bercaw, J. E. *Tetrahedron Lett.* **2001**, *42*, 2933.

(50) Molander, G. A.; Dowdy, E. D. *J. Org. Chem.* **1999**, *64*, 6515.

(51) Molander, G. A.; Dowdy, E. D. *J. Org. Chem.* **1998**, *63*, 8983.

(52) Molander, G. A.; Dowdy, E. D.; Pack, S. K. *J. Org. Chem.* **2001**, *66*, 4344.

(53) Motta, A.; Fragala, I. L.; Marks, T. J. *Organometallics* **2006**, *25*, 5533.

(54) O'Shaughnessy, P. N.; Knight, P. D.; Morton, C.; Gillespie, K. M.; Scott, P. *Chem. Commun.* **2003**, 1770.

(55) Pawlas, J.; Nakao, Y.; Kawatsura, M.; Hartwig, J. F. *J. Am. Chem. Soc.* **2002**, *124*, 3669.

(56) Ryu, J. S.; Li, G. Y.; Marks, T. J. *J. Am. Chem. Soc.* **2003**, *125*, 12584.

(57) Ryu, J. S.; Marks, T. J.; McDonald, F. E. *J. Org. Chem.* **2004**, *69*, 1038.

(58) Ryu, J. S.; Marks, T. J.; McDonald, F. E. *Org. Lett.* **2001**, *3*, 3091.

(59) Shimada, T.; Yamamoto, Y. *J. Am. Chem. Soc.* **2002**, *124*, 12670.

(60) Straub, T.; Haskel, A.; Neyroud, T. G.; Kapon, M.; Botoshansky, M.; Eisen, M. S. *Organometallics* **2001**, *20*, 5017.

(61) Utsunomiya, M.; Kuwano, R.; Kawatsura, M.; Hartwig, J. F. *J. Am. Chem. Soc.* **2003**, *125*, 5608.

(62) Cui, D.-M.; Zheng, Z.-L.; Zhang, C. *J. Org. Chem.* **2009**, *74*, 1426.

(63) Seo, S.; Yu, X.; Marks, T. J. *J. Am. Chem. Soc.* **2009**, *131*, 263.

(64) Dzudza, A.; Marks, T. J. *Org. Lett.* **2009**, *11*, 1523.

(65) Li, X.; Chianese, A. R.; Vogel, T.; Crabtree, R. H. *Org. Lett.* **2005**, *7*, 5437.

(66) Miller, K. J.; Kitagawa, T. T.; Abu-Omar, M. M. *Organometallics* **2001**, *20*, 4403.

(67) Yu, X.; Seo, S.; Marks, T. J. *J. Am. Chem. Soc.* **2007**, *129*, 7244.

(68) Cacchi, S.; Fabrizi, G.; Goggiamani, A.; Persiani, D. *Org. Lett.* **2008**, *10*, 1597.

(69) Hayashi, T.; Inoue, K.; Taniguchi, N.; Ogasawara, M. *J. Am. Chem. Soc.* **2001**, *123*, 9918.

(70) Kozhushkov, S. I.; Yufit, D. S.; Ackermann, L. *Org. Lett.* **2008**, *10*, 3409.

(71) Liu, C.; Widenhoefer, R. A. *Org. Lett.* **2007**, *9*, 1935.

(72) McKeown, B. A.; Foley, N. A.; Lee, J. P.; Gunnoe, T. B. *Organometallics* **2008**, *27*, 4031.

(73) Viciu, M. S.; Stevens, E. D.; Petersen, J. L.; Nolan, S. P. *Organometallics* **2004**, *23*, 3752.

(74) Watanabe, T.; Oishi, S.; Fujii, N.; Ohno, H. *Org. Lett.* **2007**, *9*, 4821.

(75) Youn, S. W.; Pastine, S. J.; Sames, D. *Org. Lett.* **2004**, *6*, 581.

(76) Yin, B.-L.; Chen, L.; Xu, H.-H.; Hu, T.-S.; Wu, Y.-L. *Chin. J. Chem.* **2006**, *24*, 240.

(77) Beller, M.; Seayad, J.; Tillack, A.; Jiao, H. *Angew. Chem., Int. Ed.* **2004**, *43*, 3368.

(78) Seijas, J. A.; Vazquez-Tato, M. P.; Martinez, M. M. *Synlett* **2001**, 875.

(79) Lee, H.-Y.; Jung, Y.; Moon, H. *Bull. Korean Chem. Soc.* **2009**, *30*, 771.

(80) Fananas, F. J.; Fernandez, A.; Cevic, D.; Rodriguez, F. *J. Org. Chem.* **2009**, *74*, 932.

(81) Faltin, C.; Fleming, E. M.; Connon, S. J. *J. Org. Chem.* **2004**, *69*, 6496.

(82) Tzalis, D.; Koradin, C.; Knochel, P. *Tetrahedron Lett.* **1999**, *40*, 6193.

(83) Stewart, I. C.; Bergman, R. G.; Toste, F. D. *J. Am. Chem. Soc.* **2003**, *125*, 8696.

(84) Wang, X.; Li, S.; Jiang, Y. *J. Phys. Chem. A* **2005**, *109*, 10770.

(85) Kelly, B. D.; Allen, J. M.; Tundel, R. E.; Lambert, T. H. *Org. Lett.* **2009**, *11*, 1381.

(86) Munro-Leighton, C.; Delp, S. A.; Blue, E. D.; Gunnoe, T. B. *Organometallics* **2007**, *26*, 1483.

(87) Stewart, I. C.; Bergman, R. G.; Toste, F. D. *J. Am. Chem. Soc.* **2003**, *125*, 8696.

(88) Coulombel, L.; Rajzmann, M.; Pons, J.-M.; Olivero, S.; Dunach, E. *Eur. J. Chem.* **2006**, *12*, 6356.

(89) Kamiya, I.; Tsunoyama, H.; Tsukuda, T.; Sakurai, H. *Chem. Lett.* **2007**, *36*, 646.

(90) Hirai, T.; Hamasaki, A.; Nakamura, A.; Tokunaga, M. *Org. Lett.* **2009**, *11*, 5510.

(91) Yadav, J. S.; Subba, R. B. V.; Narasimhulu, G.; Purnima, K. V. *Tetrahedron Lett.* **2009**, *50*, 5783.

(92) Komeyama, K.; Morimoto, T.; Nakayama, Y.; Takaki, K. *Tetrahedron Lett.* **2007**, *48*, 3259.

(93) Patil, N. T.; Lutete, L. M.; Wu, H.; Pahadi, N. K.; Gridnev, I. D.; Yamamoto, Y. *J. Org. Chem.* **2006**, *71*, 4270.

(94) Bhuvaneswari, S.; Jeganmohan, M.; Cheng, C.-H. *Eur. J. Chem.* **2007**, *13*, 8285.

(95) Bhunia, S.; Wang, K.-C.; Liu, R.-S. *Angew. Chem., Int. Ed.* **2008**, *47*, 5063.

(96) Corma, A.; Ruiz, V. R.; Leyva-Perez, A.; Sabater, M. J. *Adv. Synth. Catal.* **2010**, *352*, 1701.

(97) Chen, L.; Li, Y.; Xu, M.-H. *Org. Biomol. Chem.* **2010**, *8*, 3073.

(98) Barluenga, J.; Fernandez, A.; Dieguez, A.; Rodriguez, F.; Fananas, F. J. *Eur. J. Chem.* **2009**, *15*, 11660.

(99) Patil, N. T.; Raut, V. S.; Kavthe, R. D.; Reddy, V. V. N.; Raju, P. V. K. *Tetrahedron Lett.* **2009**, *50*, 6576.

(100) Marion, N.; Lemiere, G.; Correa, A.; Costabile, C.; Ramon, R. S.; Moreau, X.; de, F. P.; Dahmane, R.; Hours, A.; Lesage, D.; Tabet, J.-C.; Goddard, J.-P.; Gandon, V.; Cavallo, L.; Fensterbank, L.; Malacria, M.; Nolan, S. P. *Eur. J. Chem.* **2009**, *15*, 3243.

(101) Zhang, Y.; Xue, J.; Xin, Z.; Xie, Z.; Li, Y. *Synlett* **2008**, 940.

(102) Messerle, B. A.; Vuong, K. Q. *Organometallics* **2007**, *26*, 3031.

(103) Liu, B.; De, B. J. K. *Org. Lett.* **2006**, *8*, 4907.

(104) Li, X.; Chianese, A. R.; Vogel, T.; Crabtree, R. H. *Org. Lett.* **2005**, *7*, 5437.

(105) Fuerstner, A.; Davies, P. W. *J. Am. Chem. Soc.* **2005**, *127*, 15024.

(106) Camacho, D. H.; Saito, S.; Yamamoto, Y. *Tetrahedron Lett.* **2002**, *43*, 1085.

(107) Zhang, Z.; Widenhoefer, R. A. *Angew. Chem., Int. Ed.* **2007**, *46*, 283.

(108) Nishina, N.; Yamamoto, Y. *Tetrahedron* **2009**, *65*, 1799.

(109) Hadfield, M. S.; Lee, A.-L. *Org. Lett.* **2010**, *12*, 484.

(110) Cui, D.-M.; Yu, K.-R.; Zhang, C. *Synlett* **2009**, 1103.

(111) Cui, D.-M.; Zheng, Z.-L.; Zhang, C. *J. Org. Chem.* **2009**, *74*, 1426.

(112) Camacho, D. H.; Nakamura, I.; Saito, S.; Yamamoto, Y. *Angew. Chem., Int. Ed.* **1999**, *38*, 3365.

(113) Tan, J.; Zhang, Z.; Wang, Z. *Org. Biomol. Chem.* **2008**, *6*, 1344.

(114) Oe, Y.; Ohta, T.; Ito, Y. *Synlett* **2005**, *2005*, 179.

(115) Kadota, I.; Lutete, L. M.; Shibuya, A.; Yamamoto, Y. *Tetrahedron Lett.* **2001**, *42*, 6207.

(116) Nishina, N.; Yamamoto, Y. *Tetrahedron Lett.* **2008**, *49*, 4908.

(117) Zhang, Z.; Widenhoefer, R. A. *Org. Lett.* **2008**, *10*, 2079.

(118) Duncan, A. N.; Widenhoefer, R. A. *Synlett* **2010**, 419.

(119) Paton, R. S.; Maseras, F. *Org. Lett.* **2009**, *0*.

(120) *Isotope effects in chemistry and biology*; Boca Raton : Taylor & Francis, 2006.

(121) Persson, J. *F/ F and C/ C kinetic isotope effects in nucleophilic substitution reactions*; Uppsala : Acta Universitatis Upsaliensis, 1995.

(122) Pérez Bendito, D. *Kinetic methods in analytical chemistry*; Chichester, England : E. Horwood ; New York : Halsted Press, 1988.

(123) Brouard, M. *Reaction dynamics*; Oxford ; New York : Oxford University Press, 1998.

(124) Benko, D. A. Copyright (C) 2010 American Chemical Society (ACS). All Rights Reserved., 1979.

(125) Spies, M. A.; Toney, M. D. *J. Am. Chem. Soc.* **2007**, *129*, 10678.

(126) Bernasconi, C. F. *Investigation of rates and mechanisms of reactions*; New York : Wiley, 1986.

(127) Nieto-Oberhuber, C.; Lopez, S.; Echavarren, A. M. *J. Am. Chem. Soc.* **2005**, *127*, 6178.

(128) Tzeng, D.; Weber, W. P. *J. Org. Chem.* **1981**, *46*, 693.

(129) Matsumura, N.; Matsukawa, K.; Sakaguchi, Y.; Inoue, H. *Bull. Chem. Soc. Jpn.* **1982**, *55*, 1667.

(130) Li, H.; Widenhoefer, R. A. *Org. Lett.* **2009**, *11*, 2671.

(131) Zhang, Z.; Bender, C. F.; Widenhoefer, R. A. *J. Am. Chem. Soc.* **2007**, *129*, 14148.

(132) Qian, H.; Widenhoefer, R. A. *Org. Lett.* **2005**, *7*, 2635.

(133) Mizushima, E.; Hayashi, T.; Tanaka, M. *Org. Lett.* **2003**, *5*, 3349.

(134) Ackermann, L. *Organometallics* **2003**, *22*, 4367.

(135) Ackermann, L.; Bergman, R. G. *Org. Lett.* **2002**, *4*, 1475.

(136) Ackermann, L.; Kaspar, L. T.; Gschrei, C. J. *Org. Lett.* **2004**, *6*, 2515.

(137) Aikawa, K.; Kojima, M.; Mikami, K. *Angew. Chem., Int. Ed.* **2009**, *48*, 6073.

(138) Arredondo, V. M.; McDonald, F. E.; Marks, T. J. *Organometallics* **1999**, *18*, 1949.

(139) Bender, C. F.; Widenhoefer, R. A. *J. Am. Chem. Soc.* **2005**, *127*, 1070.

(140) Bender, C. F.; Widenhoefer, R. A. *Org. Lett.* **2006**, *8*, 5303.

(141) Besson, L.; Gore, J.; Cases, B. *Tetrahedron Lett.* **1995**, *36*, 3857.

(142) Bexrud, J. A.; Beard, J. D.; Leitch, D. C.; Schafer, L. L. *Org. Lett.* **2005**, *7*, 1959.

(143) Utsunomiya, M.; Hartwig, J. F. *J. Am. Chem. Soc.* **2004**, *126*, 2702.

(144) Yin, P.; Loh, T.-P. *Org. Lett.* **2009**, *11*, 3791.

(145) Bytschkov, I.; Doye, S. *Eur. J. Org. Chem.* **2003**, 935.

(146) Fukumoto, Y. *Yuki Gosei Kagaku Kyokaishi* **2009**, *67*, 735.

(147) Nobis, M.; Driessen-Holscher, B. *Angew. Chem., Int. Ed.* **2001**, *40*, 3983.

(148) WidenHoefer, R. A.; Han, X. *Eur. J. Org. Chem.* **2006**, 4555.

(149) Dey, N. K.; Hoque, M. E. U.; Kim, C. K.; Lee, B. S.; Lee, H. W. *J. Phys. Org. Chem.* **2009**, *22*, 425.

(150) Alonso, I.; Trillo, B.; Lopez, F.; Montserrat, S.; Ujaque, G.; Castedo, L.; Lledos, A.; Mascarenas, J. L. *J. Am. Chem. Soc.* **2009**, *131*, 13020.

(151) Trillo, B.; Lopez, F.; Montserrat, S.; Ujaque, G.; Castedo, L.; Lledos, A.; Mascarenas, J. L. *Chem. Eur. J.* **2009**, *15*, 3336.

(152) Lemiere, G.; Gandon, V.; Cariou, K.; Hours, A.; Fukuyama, T.; Dhimane, A.-L.; Fensterbank, L.; Malacria, M. *J. Am. Chem. Soc.* **2009**, *131*, 2993.

(153) Smolensky, E.; Kapon, M.; Eisen, M. S. *Organometallics* **2007**, *26*, 4510.

(154) Tobisch, S. *Chem. Eur. J.* **2007**, *13*, 4884.

(155) Stubbert, B. D.; Marks, T. J. *J. Am. Chem. Soc.* **2007**, *129*, 4253.

(156) Tobisch, S. *Dalton Trans.* **2006**, 4277.

(157) Tobisch, S. *Chem. Eur. J.* **2006**, *12*, 2520.

(158) Arredondo, V. M.; McDonald, F. E.; Marks, T. J. *Organometallics* **1999**, *18*, 1949.

(159) Zhong, H. A.; Widenhoefer, R. A. *Inorg. Chem.* **1997**, *36*, 2610.

(160) Li, G.; Liu, Y. *J. Org. Chem.*, *75*, 3526.

(161) Zhu, R.-X.; Zhang, D.-J.; Guo, J.-X.; Mu, J.-L.; Duan, C.-G.; Liu, C.-B. *J. Phys. Chem. A*, *114*, 4689.

(162) Yang, C.-Y.; Lin, G.-Y.; Liao, H.-Y.; Datta, S.; Liu, R.-S. *J. Org. Chem.* **2008**, *73*, 4907.

(163) Paton, R. S.; Maseras, F. *Org. Lett.* **2009**, *11*, 2237.

(164) Weber, D.; Tarselli, M. A.; Gagne, M. R. *Angew. Chem., Int. Ed.* **2009**, *48*, 5733.

(165) Kova¡cs, G.; Ujaque, G.; Lledos, A. *J. Am. Chem. Soc.* **2008**, *130*, 853.

(166) Bertrand, G.; Lavallo, V.; Frey, G. D.; Donnadieu, B.; Soleilhavoup, M. *Angew. Chem., Int. Ed.* **2009**, 47, 5224.

(167) Zeng, X.; Frey, G. D.; Kousar, S.; Bertrand, G. *Chem. Eur. J.* **2009**, *15*, 3056.

(168) La, L. R. L.; Brenzovich, W. E., Jr.; Benitez, D.; Tkatchouk, E.; Kelley, K.; Goddard, W. A., III; Toste, F. D. *Chem. Sci.*, *1*, 226.

(169) Widenhoefer, R. A.; Han, X. *Eur. J. Org. Chem.* **2006**, 4555.

(170) Nishina, N.; Yamamoto, Y. *Angew. Chem., Int. Ed.* **2006**, *45*, 3314.

(171) Miriyala, B.; Bhattacharyya, S.; Williamson, J. S. *Tetrahedron* **2004**, *60*, 1463.

(172) Schenck, T. G.; Bosnich, B. *J. Am. Chem. Soc.* **1985**, *107*, 2058.

(173) Katritzky, A. R.; Cheng, D.; Li, J. *J. Org. Chem.* **1998**, *63*, 3438.

(174) Barluenga, J.; Fernández, M. A.; Aznar, F.; Valdés, C. *Chem. Eur. J.* **2004**, *10*, 494.

(175) Deutsch, C.; Gockel, B.; Hoffmann-RoÌˆder, A.; Krause, N. *Synlett* **2007**, 1790.

(176) Kégl, T.; Kollár, L. *J. Mol. Cat. Chem.* **1997**, *122*, 95.

Biography

Alethea Nikeisha Duncan was born in Trinidad & Tobago on December 15, 1984. She was educated in the International Baccalaureate program at Coral Reef High School in Miami, FL. After graduating from high school she attended The Johns Hopkins University, where she majored in chemistry with a minor in Spanish. She relocated to North Carolina in 2005 to attend Duke University.

Education

2005-2011	Ph.D. in Organic Chemistry Department of Chemistry, Duke University, Durham, NC Advisor: Professor Ross A. Widenhoefer Dissertation: Gold(I)-Catalyzed Hydrofunctionalizations of Allenes with Nitrogen and Oxygen Nucleophiles
2002-2005	B.A. in Chemistry The Johns Hopkins University, Baltimore, MD

Honors and Awards

National Institute of Health Research Supplement to Promote Diversity in Health-Related Research, **2007-2010**
Dow Chemical Company's Building Engineering & Science Talent Symposium Awardee, **2010**
Duke University's Samuel Dubois Cook Society "Sammie" Award, **2010**
NOBCChE Advancing Science Scholar, **2009 & 2010**
Biotechnology Institute Minority Fellow **2010**
Julian Abele Graduate Student Leader of the Year, **2009**
Women in Science and Engineering Outstanding Woman Leader, **2008**

Publications and Presentations

"Gold(I)-Catalyzed Intermolecular Hydroamination of Allenes with Arylamines" Duncan, A. N. and Widenhoefer, R.A. Synthetic Letters, **2010** (3), 419-422.

"Gold(I)-Catalyzed Hydrofunctionalizations with Allenes" Duncan, A. N. and Widenhoefer, R.A. *Emory University Chemistry Department Special Seminar,* Atlanta, GA, April **2010**

"Scope and Mechanism of Gold(I)-Catalyzed Intermolecular Hydroamination of Allenes with Arylamines" Duncan, A. N. and Widenhoefer, R.A. *37th Annual Conference National Organization for the Advancement of Black Chemist and Chemical Engineers,* Atlanta, GA, April **2010**

"Scope and Mechanism of Gold(I)-Catalyzed Intermolecular Hydroamination of Allenes with Arylamines" Duncan, A. N. and Widenhoefer, R.A. *239th American Chemical Society National Meeting,* San Francisco, CA , March **2010**

"Gold(I)-Catalyzed Intermolecular Hydroamination of Allenes with Arylamines" Duncan, A. N. and Widenhoefer, R.A. *123rd NC American Chemical Society Sectional Conference,* Research Triangle Park, NC, September **2009**

"Kinetic Studies of Gold(I)-Catalyzed Intermolecular Hydroamination and Hydroalkoxylation with Allenes" Duncan, A. N. and Widenhoefer, R.A. *36th Annual Conference National Organization for the Advancement of Black Chemist and Chemical Engineers,* St. Louis, MO, April **2009**

"Kinetic Studies of Gold(I)-Catalyzed Intermolecular Hydroamination with Allenes" Duncan, A. N. and Widenhoefer, R.A. *Duke University Bouchet Society Fourth Annual Lecture and Poster Series,* Durham, NC, February **2009**

"Gold(I)-Catalyzed Dynamic Kinetic Enantioselective Intramolecular Hydroarylation of Allenes" *32nd Reaction Mechanisms Conference*, Chapel Hill, NC June **2008**

"Gold(I)-Catalyzed Intramolecular Enantioselective Hydroarylation of Allenes with Indoles" Duncan, A. N. and Widenhoefer, R.A. *Duke University Graduate Student Research Day*, Durham, NC, April **2008**

"Gold(I)-Catalyzed Intramolecular Enantioselective Hydroarylation of Allenes with Indoles" Duncan, A. N. and Widenhoefer, R. A., *Duke University Bouchet Society Third Annual Lecture and Poster Series* Durham, NC, February **2008**

"Gold(I)-Catalyzed Intramolecular Enantioselective Hydroarylation of Allenes with Indoles" Duncan, A. N. and Widenhoefer, R.A. *13th Conference for African American Researchers in Mathematical Sciences,* Boston, MA, June **2007**

"Gold(I)-Catalyzed Intramolecular Enantioselective Hydroarylation of Allenes with Indoles" *40th National Organic Symposium 2007,* Durham, NC, June **2007**

Society Memberships

American Chemical Society
National Organization for the Professional Advancement of Black Chemists and Chemical Engineers
Phi Lambda Upsilon